

Developing an optical sensor for the visualisation of pH gradients in marine sediments

Sonia Tariq

A thesis submitted in accordance with the requirements for the degree
of Doctor of Philosophy (PhD) from the University of East Anglia.

School of Chemistry, University of East Anglia.

July, 2015

© This copy of the thesis has been supplied on condition that anyone who consults it is understood to recognise that its copyright rests with the author and that use of any information derived there from must be in accordance with current UK Copyright Law. In addition, any quotation or extract must include full attribution.

I. Declaration

I declare that the work contained in this thesis submitted by me for the degree of Doctor of Philosophy is my work, except where due reference is made to other authors, and has not been previously submitted by me for a degree at this or any other university.

Sonia Tariq

II. Abstract

Many important biogeochemical processes that occur in marine sediments are intimately linked to pH dependent processes, but surprisingly little is known about the details of the pH profiles generated. This is mainly due to the difficulty of obtaining samples and measuring representative profiles. Such profiles have previously been determined using glass-membrane micro-electrodes, but this is slow and electrodes easily break in harsh sediments (insertion is “blind”). Profiles have also been measured using fluorescent dye-based sensors, but their handling needs special light sources and filters and sensor membrane preparation is quite complex, which has restricted its use to laboratory studies.

A simple optical pH sensor has been developed for this application by immobilising bromothymol blue in a PVC membrane. This device responds in a pH range suitable for marine sediments. The sensor is simple to use, the dye does not leach and it gives a visible colour readout so when photographed, the pictures can be used to extract Red Green Blue values and converting them to colour index values representing the sensor colour. This can be related to pH via a colour index v pH calibration using standard buffers or seawater by bubbling CO₂. The sensor responds reasonably quickly and can be used for multiple cycles.

Sensor strips have been attached to transparent plastic probes with a Nytran diffusion membrane added to provide a white background to stop interference from the colour of sediments. Preliminary tests have been carried out by inserting these probes in sediment cores (in the lab and aboard the RVs Endeavour, Discovery and Prince Madog), and also in the field at Stiffkey salt marsh, in order to measure vertical pH profiles. This has provided promising results. Seasonal profiles at Stiffkey have been taken, recording pH values ranging from 5-8. The sensors have been adapted for use with a Sediment Profile Imagery (SPI) system, to map the pH profile of marine sediments rapidly *in-situ* using various survey approaches.

III. Dedication

In the loving memory of my beloved husband

Abdur Rashid

IV. Table of contents

I. Declaration	i
II. Abstract	ii
III. Dedication	iii
IV. Table of contents	iv
V. List of figures	xii
VI. List of tables	xxviii
VII. Acknowledgement	xxxix

Chapter 1

Introduction	1
1.1 The importance of oceans	1
1.2 The importance of marine chemistry.....	1
1.3 Basic concepts	3
1.3.1 Acids and Bases	3
1.3.2 pH scale	4
1.3.3 Acid base indicators	5
1.4 pH of marine sediments and its importance	6
1.5 Degradation of Organic matter	9
1.5.1 Oxidative Mineralization	9
1.5.2 Reoxidation	9
1.5.3 Nitrification and Denitrification	10
1.5.4 Iron and Sulfate Reduction and Methanogenesis.....	10
1.5.5 Precipitation processes	11
1.5.6 Other reactions	11
1.6 Relation between pH and biogeochemical processes	12
1.7 Ocean acidification and its impact on sediment fauna	16

1.8 Sediment Profile Imagery	19
1.8.1 Construction of SPI cameras.....	19
1.8.2 Applications of SPI Cameras	21
1.9 Chemical sensors	22
1.9.1 Properties of a good sensor	23
1.10 Methods for measuring pH of marine sediments.....	23
1.10.1 Using a glass membrane pH electrode	24
1.10.2 Glass pH electrode	24
1.10.3 pH microelectrodes.....	26
1.10.4 Using pH sensitive fluorescent and indicator dyes	28
1.11 Knowledge gap and the aim of the project	34
1.12 Dye Immobilization techniques.....	36
1.12.1 Non-covalent Immobilization	36
1.12.2 Covalent Immobilization	37
1.13 The role of components in dye immobilization in a plasticised polymer membrane	38
1.13.1 Polymer.....	38
1.13.2 Counter ion	41
1.13.3 Wetting agent and Plasticizer	41
1.14 Standard methods of measuring pH of seawater.....	42
1.14.1 Measurement of pH by potentiometry	42
1.14.2 Measurement of pH by spectroscopy	43
1.15 Photographing optical sensor responses	44
1.16 References	47

Chapter 2

Developing a pH sensor.....	57
-----------------------------	----

2.1 Introduction	57
2.1.1 Selection of dyes	57
2.1.2 Materials and Methods	60
Phosphate buffers	60
2.1.3 Response of bromothymol blue in phosphate buffer	61
2.1.4 Response of neutral red in phosphate buffer	61
2.1.5 Dye immobilization in a membrane	62
2.2 Results and Discussions	64
2.2.1 The response of BTB in buffer solution	64
2.2.2 Response of neutral red in buffer solution	68
2.2.3 Dye immobilization using cellulose acetate	70
2.2.4 Response of BTB membrane in a series of phosphate buffer solutions.....	72
2.2.5 Response of neutral red membrane in phosphate buffer solution	73
2.3 Conclusions	75
2.4 References	75

Chapter 3

Optimization of a pH sensor.....	77
3.1 Introduction	77
3.2 Materials and Methods.....	77
3.3 Neutral red membrane optimization	77
3.3.1 Effect of varying the amount of counter ion and Dye	77
3.3.2 Effect of varying the amount of plasticizer and ethylene glycol.....	78
3.4 BTB membrane optimization	78
3.4.1 Using the ratio of components that worked well with neutral red	79
3.4.2 Trying a different counter ion for BTB membrane	79

3.4.3 Replacing the polymer	79
3.4.4 Increasing the amount of Plasticizer in PVC membranes	80
3.4.5 Changing the amount of dye and counter ion	80
3.5 PVC based BTB membranes	81
3.5.1 Investigating the pK _a Shift	81
3.5.2 Changing the dye due to pK _a shift	82
3.5.3 Tris Buffer	84
3.5.4 Cresol red immobilization	85
3.6 Results and Discussions	86
3.6.1 Neutral red membrane optimization.....	86
3.6.2 Effect of varying the amount of counter ion and dye.....	86
3.6.3 Effect of varying the amount of plasticizer and ethylene glycol.....	89
3.6.4 BTB membrane optimization	90
3.6.5 Cresol red Immobilization	107
3.6.6 Testing response of bromothymol blue membrane in salt solution ..	109
3.6.7 Response time of BTB membrane	110
3.7 Conclusions	112
3.8 References	113

Chapter 4

Sediment probe development and sensor characteristics	115
4.1 Introduction.....	115
4.2 Materials and Methods.....	115
4.2.1 Thickness of membrane	115
4.2.2 Adding a white background to the sensing membrane.....	116
4.2.3 Developing a sediment core probe	118
4.2.4 Photographing the probe	119

4.2.5	Enhancing the colour of the sensor.....	121
4.2.6	Response time with Nytran membrane.....	124
4.3	Characteristics of BTB membrane.....	124
4.3.1	Effect of Temperature on sensing membrane.....	124
4.3.2	Effect of salt on sensing membrane.....	128
4.3.3	The effect of light on the sensor.....	128
4.3.4	Effect of camera Flash.....	129
4.3.5	Storing Preference.....	129
4.3.6	Reusability.....	129
4.4	Results and discussions.....	129
4.4.1	Controlling the thickness of the membrane.....	129
4.4.2	White background.....	133
4.4.3	Photographing the probe.....	135
4.4.4	Enhancing the colour of the sensor.....	139
4.4.5	Thickness of membrane.....	142
4.4.6	Response time with Nytran.....	143
4.4.7	Response time with increased dye and Nytran.....	145
4.4.8	Effect of temperature on membrane.....	148
4.4.9	Effect of Salt on membrane.....	156
4.4.10	Effect of light.....	165
4.4.11	Effect of flash.....	167
4.4.12	Storing preference.....	168
4.4.13	Reusability.....	169
4.5	Conclusions.....	170
4.6	References.....	171

Chapter 5

Device calibration and first tests on a cruise	172
5.1 Introduction	172
5.2 Materials and Methods	172
5.2.1 Calibration using phosphate buffers	172
5.2.2 Calibration using agarose gel	173
5.2.3 Investigating the variability of probe response in calibration	175
5.2.4 Calibration in seawater	176
5.2.6 Automation of pH measuring technique	177
5.2.7 Application of the pH sensors in sediment cores during the Cefas Endeavor cruise	179
5.3 Results and Discussions	179
5.3.1 Calibration with phosphate buffers	179
5.3.2 Sediment core analysis	181
5.3.3 Improving the photographic conditions	183
5.3.4 Calibration using agarose gel	186
5.3.5 Investigating the variabilities	192
5.3.6 Calibration using seawater	196
5.3.7 Calibration at different temperatures	198
5.3.8 Cruise Trial (Cefas Endeavor cruise 'CEND 15113')	198
5.4 Conclusions	219
5.5 References	220
Chapter 6	
Seasonal pH profiles from Stiffkey salt marsh	221
6.1 Introduction	221
6.1.1 Study Site	222
6.2 Material and Methods	223

6.3 Results and discussions.....	225
6.3.1 Calibration for the summer pH profiles.....	225
6.3.2 Calibration for the autumn pH profiles	226
6.3.3 Calibration for the winter pH profiles	227
6.3.4 <i>Response Time of probe in the mud</i>	227
6.3.5 Reproducibility of the probe	230
6.3.6 Seasonal pH profiles.....	232
6.3.7 Seasonal pH profiles from the vegetation.....	233
6.3.8 Seasonal pH profiles from the pond.....	236
6.3.9 pH profiles at the creek in summer	239
6.3.10 pH profiles at the creek in autumn.....	241
6.4 Conclusions	244
6.4 References	245

Chapter 7

pH profiles from recovered cores and SPI trials	246
7.1 Introduction.....	246
7.2 Materials and Methods.....	246
7.3 Results and discussions	249
7.3.1 pH profiles of sediment cores from the Prince Madog cruise	249
7.3.2 SPI Trial from Prince Madog.....	258
7.3.3 pH profiles from Cefas March 2015 cruise (DY021):	260
7.3.4 Sediment Profile Imagery (SPI).....	268
7.3.5 Issues observed.....	271
7.4 Conclusions	274
7.5 References	275

Chapter 8

Summary and future work	276
8.1 Summary	276
8.2 Future work.....	280
8.3 References	280

V. List of figures

Figure 1.1 processes in the marine sediments.....	07
Figure 1.2 An example of typical pH profile of marine sediments. (a rough guide taken from cai <i>et al.</i> ,1999).. ..	15
Figure 1.3 pH profile of marine sediments (a rough pattern taken from Stahl <i>et al.</i> , 2006).....	16
Figure 1.4 Photograph of SPI taken at Cefas during an experiment, The SPI parts are labelled. The SPI faceplate is inserted in a bucket full of seawater. pH meter and temperature probe were used during an experiment and are not the parts of SPI.	20
Figure 1.5 Diagram of SPI camera showing how the sediments against the faceplate is photographed. The image reflects at 450 at the mirror.	21
Figure 1.6 Sensor diagram explaining how a sensor works.....	22
Figure 1.7 Design of a combination glass electrode.	25
Figure 1.8 Schematic showing how the sensors will be attached to the SPI faceplate.	36
Figure 1.9 Colour addition in RGB systems.	46
Figure 2.1 Acidic (yellow) and basic form (blue) of bromothymol blue showing the ionising group. A mixture of both species appears green (Klots <i>et al.</i> , 2011).	58
Figure 2.2 Different forms of phenol red (parent compound of bromothymol blue)...	59
Figure 2.3 Protonation reaction of neutral red showing the protonated form in the acid (red) and neutral form (yellow) in base.	60
Figure 2.4 BTB response with increasing pH (left to right pH: 5.8, 6.0, 6.2, 6.5, 6.6, 6.8, 7.0, 7.2, 7.4, 7.5, 7.8 and 8.0).	64

Figure 2.5 UV-Vis spectrum of Bromothymol blue.	64
Figure 2.6 RGB values measured with image J for BTB at pH values stated.....	66
Figure 2.7 Colour Index values plotted against pH obtained by applying the formula (a) (R-B)/G and (b) (R+B)/G.....	67
Figure 2.8 Neutral red response to increasing pH (left to right 5.8, 6.1, 6.27, 6.59, 6.64, 6.86, 7.06, 7.26, 7.54, 7.66, 7.99 and 8.13).	68
Figure 2.9 UV visible spectra for neutral red at pHs 5.8, 6.1, 6.27, 6.59, 6.64, 6.86, 7.06, 7.26, 7.54, 7.66, 7.99, 8.13).	68
Figure 2.10 Colour response of neutral red represented as RGB values vs pH.	70
Figure 2.11 (a) Membrane formulated using CTAB, (b) TOAB in phosphate buffer (pH8.13).	71
Figure 2.12 UV-vis spectrum of BTB membrane at pH 8.13(blue) and after reversing completely to 5.8 (red).....	71
Figure 2.13 Absorbance at 640nm Vs pH of BTB membrane in phosphate buffer (some of the membranes did not equilibrate completely).....	72
Figure 2.14 Image of neutral red membrane in a series of buffer solutions (pH from left to right: 5.82, 6.27, 6.86, 7.54, and 8.13) showing the leaching of dye.	73
Figure 2.15 Neutral red membrane spectrum in phosphate buffers at different pH values.....	74
Figure 3.1 Ionising group of cresol purple.	83
Figure 3.2 Ionising group of cresol red.	84
Figure 3.3 (a) membrane 1 (1:3) response, (b) membrane 2 response (1:2), (c) membrane 3 (1:1) response. pH: 5.82, 6.27, 6.86, 7.54, 8.13 from left to right.	87

Figure 3.4 UV-vis spectrum of (a) membrane 1 (1:3), (b) membrane 2 (1:2), (c) membrane 3 (1:1).	88
Figure 3.5 Response of membranes 1 (a) and 4 (b).	89
Figure 3.6 Neutral red membrane immobilised in PVC, slow response on same day.....	91
Figure 3.7 UV-Vis spectrum of PVC membrane containing neutral red dye.	91
Figure 3.8 (A): Thick membrane (70% plasticizer) (B): Thin membrane (70% plasticizer).....	93
Figure 3.9 UV-Vis spectrum of PVC membrane with 70% plasticizer (a) Thick membrane (b) thin membrane.	94
Figure 3.10 Equilibrium colours of neutral red membranes with different levels of plasticizers keeping the amount of other components the same. (a) 40% plasticizer, (b) 60% plasticizer, (c) 65% plasticizer, (d) 70% plasticizer, (e) 75% plasticizer and (f) 80% plasticizer.	95
Figure 3.11 UV-vis spectra of membranes with different levels of plasticizers. (a) 40% plasticizer, (b) 60% plasticizer, (c) 65% plasticizer, (d) 70% plasticizer, (e) 75% plasticizer and (f) 80% plasticizer.	96
Figure 3.12 Responses of membranes made with different dye: counter ion ratios. (a) 1:4, (b) 1:2, (c) 2:1, (d) 3:1, (e) 4:1, (f) 6:1.	98
Figure 3.13 UV-vis spectra of membranes with different counter ion ratios. (a) 1:4, (b) 1:2, (c) 2:1, (d) 3:1, (e) 4:1, (f) 6:1.	99
Figure 3.14 (a) Dye leaching in membrane 1. (b) Membrane 2 (all samples went blue).	100
Figure 3.15: Membrane 2 response, which remained blue in all samples.	101

Figure 3.16 (a) Response of membrane 1 (slightly green in acidic medium), (b) UV-vis spectrum of membrane 1, (c) Response of membrane 2 (all blue), (d) UV-vis spectrum of membrane 2.	102
Figure 3.17 Response of membrane in a series of citrate buffer solutions (pH from left to right: 2.6, 3.2, 4.2, 4.8 and 5.8).	104
Figure 3.18 Response of cresol red in buffer solutions (pH from left to right: 4.2, 4.8, 5.4, 5.8, 6.4, 6.7, 7.0 (citrate buffer), 7.4, 7.8, 8.2, 8.8, 9.0 (tris buffer).	105
Figure 3.19 UV visible spectrum of cresol red in buffer solutions of different pH from left to right: 4.2, 4.8, 5.4, 5.8, 6.4, 6.7, 7.0 (citrate buffer), 7.4, 7.8, 8.2, 8.8, 9.0 (tris buffer).	105
Figure 3.20 Response of cresol purple in Tris buffer solutions pH from left to right: (9.09, 8.51, 8.18, 7.94, 7.57, 7.32, 6.7)	106
Figure 3.21 UV-Vis spectrum of cresol purple at different pHs.	106
Figure 3.22 Cresol red membrane response in buffer pH from left to right 4.8, 5.4, 5.8, 6.4, 6.7, 7.0, 7.4, 7.7, 7.8, 8.2, 8.5, 8.8, 9.0, 9.2, 9.8.....	107
Figure 3.23 UV-vis spectrum of cresol red membrane at different pHs.	107
Figure 3.24 (a) Cresol red membrane response in saline buffer (pH: 5.82, 6.93, 7.68, 8.19, 8.88, and 9.42)	108
Figure 3.24 (b) UV-vis spectrum of cresol red membrane in saline buffer.	108
Figure 3.25 (a): (from left to right, pH of phosphate buffer: 5.9, 6.0, 6.8, 7.5, and 8.2) containing 0.5M NaCl. (b): From left to right pH: Citrate buffer 5.8, 6.4, 7.0, Tris buffer: 7.4, 7.8 containing 0.5M NaCl.	109
Figure 3.26 UV-vis spectrum of BTB membrane in saline buffer. (a) Phosphate buffer solutions of different pHs containing 0.5M NaCl. (b): Citrate buffer solutions of pH 5.8, 6.4, 7.0 and Tris buffer solutions of pH 7.4, 7.8 containing 0.5M NaCl.	110

Figure 3.27 Time scan of BTB membrane showing the response time for re-equilibration from one pH to another (pH intervals indicated in the legend).	111
Figure 4.1 Meter bars used to spread the membrane solution and control the thickness of membrane.	115
Figure 4.2 Illustration of adding white membrane on sensing membrane.	117
Figure 4.3 Probe schematic and a photograph of an actual probe. (Note: The slight apparent curvature is due to a barrelling aberration of the camera lens at its closest focal point setting.)	118
Figure 4.4 Image of polystyrene box used for photographing the probe.	119
Figure 4.5 Image of the light box showing flash inside and the camera fixed outside.	120
Figure 4.6 Image of the light box with LED lights attached.	120
Figure 4.7 Image of the device used to study the effect of temperature.	125
Figure 4.8 Experimental set up for temperature studies.	127
Figure 4.9 Improved sensor design with increased amount of dye and a white Nytran membrane behind.	127
Figure 4.10 Response of membrane made from (a) 40 μm metering bar (b) 24 μm metering bar (c) 12 μm metering bar, (d) 6 μm metering bar..	130
Figure 4.11 Absorbance Spectrum for membrane made from (a) 40 μm metering bar (b) 24 μm metering bar (c) 12 μm metering bar, (d) 6 μm metering bar.	131
Figure 4.12 Time scan (at 640nm) of membrane made from (a) 40 μm metering bar (b) 24 μm metering bar (c) 12 μm metering bar, (d) 6 μm metering bar.	132
Figure 4.13 Response of different opaque white membranes used.	135

Figure 4.14 The colour index of two standard colours chosen from the chart row below the probe stand.	135
Figure 4.15 (a) Colour indices of white slices in a column, (b) a row from the photograph of the light box within a photo and (c) the colour indices of white row of the light box in different photos.	136
Figure 4.16 The colour index values of white row along the box where the probe rests.	137
Figure 4.17 Comparison of lighting consistency before (red) and after (blue) adding extra LED lights in the corners of the light box.	137
Figure 4.18 photo taken using (a) battery and (b) mains.	138
Figure 4.19 membrane made from (a) 6 μm (b) 12 μm metering bars	140
Figure 4.20 Time scan of membrane made by switching the pH from 8.02 to 5.9 at 640nm from (a) 6 μm (b) 12 μm metering bars.	140
Figure 4.21 (a) Composition 4 compared with old composition. (b) Composition 5, homogenous and intense colour. (c) Composition 7, patchy and inhomogeneous....	141
Figure 4.22 Change from 7.7 to 5.9 and from 5.9 to 7.7 for membrane with composition 5 at 640nm.	142
Figure 4.23 Change from pH (a) 5.8 to 8, (b) 8 to 5.8	144
Figure 4.24 Change from pH (a) 7.7 to 5.9, (b) from pH 5.9 to 7.7	145
Figure 4.25 Response time with Nytran membrane and increased dye+ counter ion content.	146
Figure 4.26: Response time curve showing the equation used to calculate the time constant.	147

Figure 4.27 Change in colour index values with temperature increase.	148
Figure 4.28 Change in colour index values with temperature. pH was changing.	151
Figure 4.29 Change in colour index values with temperature at pH 7.27.	152
Figure 4.30 Change in colour index values with temperature at pH 7.27.	153
Figure 4.31 Effect of temperature on sea water while pH was changing.	153
Figure 4.32 Colour index vs. Temperature. pH was controlled using NaOH: at pH 7.97.	154
Figure 4.33 (R-B)/G vs. Temperature. pH was controlled using HCl: at pH 7.85(red),7.72(grey),7.47(yellow)	155
Figure 4.34 The colour response of membrane at salt concentrations 0.05M, 0.15M, 0.25M, 0.35M and 0.45M (from left to right) (a) at pH 7.3, (b) at pH 5.8.	156
Figure 4.35 UV visible spectrum of BTB membrane in 1:1 phosphate buffer and 1M NaCl solution (similar ionic strength to seawater).	157
Figure 4.36 Effect of salt on membrane at (a) pH 5.8 (b) 7.3.	158
Figure 4.37 The colour response of membrane at different salt concentrations from left to right: 0.20M, 0.21M, 0.22M, 0.23M, 0.24M, 0.26M, 0.27M, 0.28M, 0.29M, 0.30M (a) at pH 7.3 and (b) at pH 5.8.	159
Figure 4.38 Effect of salt on membrane at pH (a) 5.8 (b) 7.3.	160
Figure 4.39 UV-visible spectrum of membrane at pH 6.69, blue: 0.40M, red: 0.46M, grey: 0.48M, and yellow: 0.52M.	161
Figure 4.40 Colour index values at different salt concentrations.	162
Figure 4.41 UV visible spectrum of membrane in seawater. Blue: original seawater, red: 10% diluted sea water and green: 10% increased salt in seawater.	163
Figure 4.42 UV-vis spectrum at different dilutions.	164

Figure 4.43 Effect of dilution at pH 7.97 and temperature 22.1 ⁰ C on the extracted colour index values.	164
Figure 4.44 Effect of light on the sensor. (a) Day 2: response in the buffer (pH 7.7) in which probes were kept.(b) Day 2: Response in buffer 6.5 (c) Day 3: response in buffer pH 7.7 in which they were kept (d) : Day 3: response in buffer pH 6 (e) Day 4: Response in the buffer pH 7.7 in which they were kept, clear bleaching of dye.	166
Figure 4.45 (a): Image taken at the start of the experiment. (b): Image taken at the end of the experiment.	167
Figure 4.46 Colour index vs time in minutes.	168
Figure 4.47 The reusability of the sensing membrane kept in the acidic buffer pH 4.7 in a cuvette and wrapped with foil.	169
Figure 4.48 The reusability of the sensing membrane kept in basic buffer pH 7.8 in a cuvette and wrapped with foil.	169
Figure 5.1 (a) Figure of calibration stick showing the general design (b) photograph of the calibration sticks with different spacing and hole sizes.	173
Figure 5.2 Apparatus used for calibration.	174
Figure 5.3 Glass slides stuck together with agarose gel inside.	175
Figure 5.4 Experimental set up for calibration. (b) A closer view of glass device.	176
Figure 5.5 Result output from the R script showing the data as (a) a pH ‘heat map’ of the sensor area, (b) an average pH value across the strip and (c) box plot- white box: interquartile range (iqr), horizontal line: median value, vertical line: range of the data, individual points: potential outliers, which are identified as >2.5 iqr from the median.	178
Figure 5.6 Probes of three different designs.	179

Figure 5.7 Calibration graph of striped probe showing equation and R^2 value.	180
Figure 5.8 Calibration graph of normal probe showing linear equation and R^2 value.	180
Figure 5.9 Probes in the sediment core.	181
Figure 5.10 Photograph of the probe response taken in the lab without controlling light conditions.	182
Figure 5.11 pH vs depth profile of the sediment core.	183
Figure 5.12 Calibration graph after photographing in the polystyrene box.	184
Figure 5.13 Photo of probe after response taken in polystyrene box with an external flash inside.	185
Figure 5.14 pH vs depth profile of sediment core.	186
Figure 5.15 photo of probe used for calibration in a light box containing flash.	187
Figure 5.16 Calibration sticks and probes used for calibration.	187
Figure 5.17 Comparison of probes used in calibration by using different methods (For description of methods see pp173-175)	188
Figure 5.18: photo of probe calibrated using the aluminium apparatus.	188
Figure 5.19 Calibration probes showing the variability of colour wet or dry when protran is used. (a) Photographed wet (b) photographed dry.	189
Figure 5.20 Comparison of two probes (a) Protran (b) Nytran.	189
Figure 5.21 Calibration graph of two probes.	190
Figure 5.22 Calibration of two probes (a) using gel (b) buffer solutions.	191
Figure 5.23 Calibration graph for three probes.	195
Figure 5.24 Calibration in seawater.	196

Figure 5.25 Calibration of probes in seawater using the same composition of membrane which was used for calibration in phosphate buffer.	197
Figure 5.26 Calibration at three different temperatures.	198
Figure 5.27 Calibration for the cruise trial.	199
Figure 5.28 The pH profile at station 30 measured by probe and the actual probe (a) a false colour pH map generated by the software for the sensor area (b) an average pH value across the strip (c) box plot- white box: interquartile range (iqr), horizontal line: median value, vertical line: range of the data, individual points: potential outliers, which are identified as >2.5 iqr from the median. (d) The actual probe.....	201
Figure 5.29 (a) and (b) pH profile measured by microelectrode at station 30(profile1). (Source: Alida Rosales Villa), (c) pH vs depth profile measured by probe.	202
Figure 5.30 pH profile measured by probe at station 43 (a) a false colour pH map generated by the software for the sensor area (b) an average pH value across the strip (c) box plot- white box: interquartile range (iqr), horizontal line: median value, vertical line: range of the data, individual points: potential outliers, which are identified as >2.5 iqr from the median. (d) The actual probe.	204
Figure 5.31 (a) pH profile measured by microelectrode at station 43. (Source: Alida Rosales Villa). (b) pH profile measured by probe at station 43.	205
Figure 5.32 pH profile measured by probe at station 60 (a) a false colour pH map generated by the software for the sensor area (b) an average pH value across the strip (c) box plot- white box: interquartile range (iqr), horizontal line: median value, vertical line: range of the data, individual points: potential outliers, which are identified as >2.5 iqr from the median. (d) The actual probe.	207
Figure 5.33 pH profile measured by probe at station 68 (a) a false colour pH map generated by the software for the sensor area (b) an average pH value across the strip (c) box plot- white box: interquartile range (iqr), horizontal line: median value, vertical	

line: range of the data, individual points: potential outliers, which are identified as >2.5 iqr from the median. (d) The actual probe.	209
Figure 5.34 pH profile measured by probe at station 81 (a) a false colour pH map generated by the software for the sensor area (b) an average pH value across the strip (c) box plot- white box: interquartile range (iqr), horizontal line: median value, vertical line: range of the data, individual points: potential outliers, which are identified as >2.5 iqr from the median. (d) The actual probe.	210
Figure 5.35 pH profile measured by probe at station 101 (a) a false colour pH map generated by the software for the sensor area (b) an average pH value across the strip (c) box plot- white box: interquartile range (iqr), horizontal line: median value, vertical line: range of the data, individual points: potential outliers, which are identified as >2.5 iqr from the median. (d) The actual probe.	211
Figure 5.36 pH profile measured at station 101 by microelectrode (source: Alida Rosales Villa). (b) pH profile measured at station 101 by probe.	212
Figure 5.37 pH profile measured by probe at station 119 (a) a false colour pH map generated by the software for the sensor area (b) an average pH value across the strip (c) box plot- white box: interquartile range (iqr), horizontal line: median value, vertical line: range of the data, individual points: potential outliers, which are identified as >2.5 iqr from the median. (d) The actual probe.	214
Figure 5.38 pH profile measured by probe at station 127 (a) a false colour pH map generated by the software for the sensor area (b) an average pH value across the strip (c) box plot- white box: interquartile range (iqr), horizontal line: median value, vertical line: range of the data, individual points: potential outliers, which are identified as >2.5 iqr from the median. (d) The actual probe.	215
Figure 5.39 pH profile measured at station 127 by microelectrode (source: Alida Rosales Villa). (b) pH profile measured at station 127 by probe.	216

Figure 5.40 pH profile measured by probe at station 141 (a) a false colour pH map generated by the software for the sensor area (b) an average pH value across the strip (c) box plot- white box: interquartile range (iqr), horizontal line: median value, vertical line: range of the data, individual points: potential outliers, which are identified as >2.5 iqr from the median. (d) The actual probe.	218
Figure 6.1 (a) Map showing the location of the site. (b) Photos of the study sites: creek and pond.	222
Figure 6.2 Vegetation at the study site mainly found close to the pond. (a) Antriplex portulacoides, (b) Limonium vulgare.	223
Figure 6.3 Calibration graph for the probes used to collect the summer data (n=3)...	225
Figure 6.4 (a) Calibration graph for the probes used in the pond (b) Calibration graph for the probes used at the creek.	256
Figure 6.5 Calibration graph for the probes used in the pond and vegetation (n=3)...	227
Figure 6.6 Apparent pH plotted after different equilibration time intervals where 0 mm is the interface.	228
Figure 6.7 Actual probes taken at (a) 5min, (b) 10min, (c) 15min, (d) 30min, and (e) 60min.	228
Figure 6.8 Response time curve plotted by averaging the pH values from 40mm to 150mm in the profile given in figure 6.6 for the given time.	229
Figure 6.9 pH profiles from the same site using the same probe multiple times illustrating that the probe is reusable. The interface is marked as a line on each profile (a) Profile at first use, (b) profile at second use, (c) profile at third use.	230
Figure 6.10 Probes and pH meter in the vegetation near the pond.	233
Figure 6.11 Mean seasonal pH profiles in the vegetation near the pond at Stiffkey salt marshes (n=3, 4 and 6 for summer, autumn and winter).....	233
Figure 6.12 Mean pH in vegetation in autumn at 1m distance from the pond.....	234

Figure 6.13 Average pH profile of vegetation in winter measured by long probes (blue) and individual profiles (grey).....	235
Figure 6.14 Probes in the pond showing probe insertion, probe in-situ under the pond surface and probe removed and wiped ready for photography.	236
Figure 6.15 Seasonal pH profiles at the edge of the pond at Stiffkey saltmarshes showing mean pH profiles (n=3 for autumn and winter, n=2 for summer).	236
Figure 6.16 Seasonal pH profiles of pond at Stiffkey saltmarshes (n= 3, 13 and 5 for summer, autumn and winter where n is the number of profiles averaged).	237
Figure 6.17 pH profile of pond taken from long probe in winter.	238
Figure 6.18 Mean pH profiles at the creek at station (a) 1, (b) 2, (c) 3, (d) 4, (e) 5, (f) 6 and (g) 7. (n=2) (h) Photograph of the creek.	240
Figure 6.19 Mean pH profiles at the creek at station (a) 1, (b) 2, (c) 3, (d) 4, (e) 5, (f) 6 and (g) 7. (n=2) (h) Photograph of the creek.	242
Figure 7.1 (a) Experimental set up for SPI probe calibration, (b) closer view of bucket.	248
Figure 7.2 Calibration at 15 C ⁰ graph for the probes used in the Prince Madog cruise.	249
Figure 7.3 Calibration at 11 C ⁰ graph for the probes used in the Prince Madog cruise.	249
Figure 7.4 pH profile at station 32 and the actual probe (a) a false colour pH map generated by the software for the sensor area (b) an average pH value across the strip (c) box plot- white box: interquartile range (iqr), horizontal line: median value, vertical line: range of the data, individual points: potential outliers, which are identified as >2.5 iqr from the median. (d) The actual probe..	251
Figure 7.5 pH profile at station 34 and the actual probe (a) a false colour pH map generated by the software for the sensor area (b) an average pH value across the strip	

(c) box plot- white box: interquartile range (iqr), horizontal line: median value, vertical line: range of the data, individual points: potential outliers, which are identified as >2.5 iqr from the median. (d) The actual probe.252

Figure 7.6 pH profile at station 33 and the actual probe (a) a false colour pH map generated by the software for the sensor area (b) an average pH value across the strip (c) box plot- white box: interquartile range (iqr), horizontal line: median value, vertical line: range of the data, individual points: potential outliers, which are identified as >2.5 iqr from the median. (d) The actual probe..253

Figure 7.7 pH profile at station 35 and the actual probe (a) a false colour pH map generated by the software for the sensor area (b) an average pH value across the strip (c) box plot- white box: interquartile range (iqr), horizontal line: median value, vertical line: range of the data, individual points: potential outliers, which are identified as >2.5 iqr from the median. (d) The actual probe.....254

Figure 7.8 pH profile at station 37 and the actual probe(a) a false colour pH map generated by the software for the sensor area (b) an average pH value across the strip (c) box plot- white box: interquartile range (iqr), horizontal line: median value, vertical line: range of the data, individual points: potential outliers, which are identified as >2.5 iqr from the median. (d) The actual probe..255

Figure 7.9 pH profile at station A6 core2 subcore2 and the actual probe (a) a false colour pH map generated by the software for the sensor area (b) an average pH value across the strip (c) box plot- white box: interquartile range (iqr), horizontal line: median value, vertical line: range of the data, individual points: potential outliers, which are identified as >2.5 iqr from the median. (d) The actual probe..... 256

Figure 7.10 pH profile at station A6 core3 subcore2 and the actual probe (a) a false colour pH map generated by the software for the sensor area (b) an average pH value across the strip (c) box plot- white box: interquartile range (iqr), horizontal line: median value, vertical line: range of the data, individual points: potential outliers, which are identified as >2.5 iqr from the median. (d) The actual probe.257

Figure 7.11 pH profile at station A6 core4 subcore2 and the actual probe (a) a false colour pH map generated by the software for the sensor area (b) an average pH value across the strip (c) box plot- white box: interquartile range (iqr), horizontal line: median value, vertical line: range of the data, individual points: potential outliers, which are identified as >2.5 iqr from the median. (d) The actual probe..	258
Figure 7.12 SPI images with the attached pH probes from brief sediment insertion during the Prince Madog cruise .	259
Figure 7.13 Calibration graph for probes used in the recovered sediment cores.....	260
Figure 7.14 SPI calibration graph from in-situ calibration using SPI system.....	260
Figure 7.15 Map showing the location of the sites covered during the cruise.....	262
Figure 7.16 Two pH profiles of station Box H taken from the same core using two probes.	264
Figure 7.17 Two pH profiles of station spatial 031 taken from the same core using two probes. Blue line represents the sediment water interface.	265
Figure 7.18 Two pH profiles of station spatial 035 taken from the same core using two probes.	266
Figure 7.19 Average pH profiles of sand, sandy mud and muddy sand.	267
Figure 7.20 pH profile of mud at station spatial 001.	267
Figure 7.21 Equilibration time series of (a) fresh probe and (b) used probe using SPI.	269
Figure 7.22 pH profiles at different stations using SPI.	270
Figure 7.23 pH profiles at the same station where station B was at 5m distance, C at 10m, D at 15m and E at 20m from A taken by SPI.	271
Figure 7.24 Images of the used probes showing the white patches due to aging.....	272

Figure 7.25 A closer view of the probe in the microscope.272

Figure 7.26 SPI-image, showing the mud dragged into the probe slot and hid the probe.

.....273

VI. List of tables

Table 1.1 Processes in marine sediments and their effect on pH. (Soetaert <i>et al.</i> , 2007)	14
Table 1.2 Types of polymers, their properties and use in sensors.	41
Table 2.1 Amount and function of the membrane components.	62
Table 2.2 Amount and function of the membrane components.	63
Table 2.3 RGB values taken from ImageJ for the photographs of BTB membranes equilibrated in buffers of varying pH.	65
Table 2.4 RGB values of neutral red response taken from photographs using ImageJ...	69
Table 3.1 Composition of membranes containing different amounts of dye and counter ion.....	77
Table 3.2 Composition of membranes containing different amounts of ethylene glycol and plasticizer.	78
Table 3.3 Composition of membrane.	79
Table 3.4 Composition of PVC membrane.	80
Table 3.5 Composition of membranes containing different amounts of dye and counter ion.	80
Table 3.6 Composition of BTB membranes containing different amounts of dye and counter ion.	81
Table 3.7 Composition of membrane used to check the pK_a shift.	82
Table 3.8 Composition of cresol red membrane.	85
Table 3.9 Composition of BTB membrane used for testing the response in salt solution.	86

Table 3.10 Composition of membranes containing different counter ions.	103
Table 4.1 Different compositions of membrane tried to enhance the colour of the sensor.	123
Table 4.2 Composition of membrane used to study the temperature effect.	124
Table 4.3 Composition of membrane with increased dye.	126
Table 4.4 Comparison of white membranes.	133
Table 4.5 Colour index values of probe photographed using mains and battery.	139
Table 4.6 RGB values at different temperatures. pH changed by changing temperature.	148
Table 4.7 pH and colour index values at different temperatures.	150
Table 4.8 pH and colour index values at different temperatures.	151
Table 4.9 pH and colour index values at different temperatures.	152
Table 5.1 Composition of sensing membrane used for calibration.	175
Table 5.2 Calculation of pH using the equation from the calibration graph.	182
Table 5.3 Validation of pH calculation.	184
Table 5.4 Calculation of pH with depth in the sediment core from probe photo.	185
Table 5.5 Colour index values at same pH on a calibration probe.	189
Table 5.6 Comparison of probes at same pH for calibration.	190
Table 5.7 RGB values and colour index values for three probes at pH 5.8 including values with in a photograph and in five different photographs.	193
Table 5.8 Mean colour index values of three probes at pH different pH values, standard deviations and standard error of means.	194

Table 5.9 Important measurements during the cruise (source: Alida Rosales Villa) Salinity is defined as ‘ The total amount of solid material in grams contained in one kilogram of seawater when all the carbonate has been converted to oxide, the bromine and iodine replaced by chlorine, and all organic matter completely oxidised’ (As cited in: Williams and Sherwood, 1994).	200
Table 5.10 RGB values of dark and yellow patches on the sensing probe.	208
Table 6.1 pH, temperature and conductivity measured at pond, creek and vegetation in Stiffkey salt marsh.	232
Table 7.1 Temperature observed at different stations. (Source: Claire Powel, Cefas).	250
Table 7.2 Location of stations and their temperature (Source: Briony Silburn, Cefas).	263

VII. Acknowledgement

I would like to take this golden opportunity to thank my primary supervisor, Dr Andrew Mayes for his expert guidance, enthusiastic encouragement, and useful critiques and advise that made this project successful. I greatly appreciate his efforts and hard work without which it was impossible to achieve the goals of this project. An additional thanks goes for his moral support, understanding my difficult circumstances and boosting my energy up during my very bad time. I am blessed to have a supervisor like him. A special thanks goes to my secondary supervisor, Dr Silke Kröger (Cefas) whose hard work and input in the project made the deployment of the sensors in different cruises possible. I would like to thank both of them for helping me get additional funding both at the start, middle and at the end of my PhD. My deepest appreciation goes to my secondary supervisor Dr Tim Jickells (UEA, Env) for his useful advises throughout the journey. I would like to thank him for convincing his student to use my sensors during the cruise.

A special thanks goes to Alida Rosales, Dr Claire Powel and Briony Silburn for using the sensors during the cruise and trying them on the SPI. I would like to thank Alida Rosales for providing her microelectrode pH profiles that made the comparison of profiles taken from the probes possible.

I would like to thank David Stephens (Cefas) for creating the automated R script that made the photograph analysis very quick and easy. Not forgetting Ruth Parker, Nigel Lyman, David Sivyer for their contribution in the project. I would like to thank Dr Julian Andrews for introducing us to Stiffkey salt marshes. I would like to thank Dr Julia Butt for her advice regarding redox sensors and Colin Lockwood to train me for the glove box. Dr David Russel, Maria and Susan are greatly acknowledged for letting me use the lab and UV-Vis spectrophotometer. I would like to thank Lisa (lab technician) for donating sea water.

Many thanks to Lasbela University of agriculture, water and marine sciences uthal, Pakistan and higher education commission for funding my PhD. Cefas, UEA, Funds for female graduates and British council is whole heartedly thanked for additional funds. I would like to thank Dean's office specially Jane Amos and Wendy Bainham for giving

nursery fee discount. I am blessed to have a very helpful research group and would like to appreciate their help and moral support. Thank you Dr. Paul, Dr. Laili Che Rose, Dr. Abdirahman, Beccy, Dr. Miguel and Dr. Pilar Fernandez.

I would like to thank all my colleagues from Lasbela University of agriculture, water and marine sciences specially the Vice Chancellor, Dr Dost Muhammad Baloch, Pro V.C Dr. Gul Hassan Baloch, Additional registrar, Mr Ammanullah Roonjah, Mr Kamran Saeed, Mr Abdul Qadir Roonjah, Dr Nasir Abbas, Dr Aslam Buzdar, Zaffarullah Jatak, Waseem Hashmi (HEC) and all the members of scholarship committee for arranging additional funds from HEC for the fourth year of PhD. Not forgetting my colleagues studying in U.K, Ms. Kalsoom Jaffer, Mr. Raza Bazai, Dr. Gulawar, Dr. Jalal Faiz, Dr. Dolat Khan and Dr Habibul Hassan for their moral support.

I am grateful to all my friends, Mehrnaz ,Saanya, Aya, Farhana, Sumera, Dr. Nayab Ahmed, Noor Armylisa, Nadwa, Faiza, Tahani, Xiao Yang, Rhoda, Eliot, Trevor, James, James, Qi, Robin, Ellion, Mercedes, Salma, Maimoona, Safia Bano, and all my friends, colleagues, all the Muslim and Pakistani community in Norwich . A big thank you to Mr and Mrs Ulfat Rasool for babysitting my son and making it possible for me to attend my husband's funeral. A big thank you to my parents, Tariq Mehmood and Shagufta Sheeren and my brother, Mohammed Ahsan and cousin sister Ayesha for their love and support throughout the journey. I am very grateful to my beloved son, Ayaan Rashid whose existence and unconditional love kept me strong and made this journey possible. Not forgetting his father and my husband, Late Abdur Rashid who supported me in my first year of Ph.D. His extra ordinary love, respect and care is appreciated. It was very hard without you my love but I did it. I would like to thank my grandfather Mohammed Sadiq for being my guarantor to get the funding. Thanks to Dr. Ayaz Khan Malghani and Gohram for their support. All my uncles (Zaffar, Azhar, Tahir, Talat, Zubair and Tufail), aunts, cousins and in laws are acknowledged. A special thanks goes to Dr. Khalaf Alenezi who I respect a lot for his support, help and advice. Finally I would like to thank those friends who have hurt me and did not help me when I needed them the most (they know who they are). This has made me realise my hidden strengths and I came up even stronger to achieve my goals.

Chapter 1

Introduction

1.1 The importance of oceans

71% of the earth's surface is covered by the world's oceans and the total volume is around $1.35 \times 10^8 \text{ km}^3$. The Pacific Ocean, which is the largest and the deepest ocean and constitutes about 50.1% of the world's ocean, covers one third of the surface of the earth. The Atlantic and the Indian oceans make 29.4% and 20.5% of the world ocean. (Kenish, 2001). Marine science is a vast subject and attracts scientist from geology, chemistry, biology, physics and meteorology often working together to solve complex problems and understand inter-related systems. For many scientists who are interested in oceanography, knowledge of marine geochemistry is required. (Chester and Jickells, 2012)

1.2 The importance of marine chemistry

Understanding marine chemistry is important because it underpins major global cycles such as the carbon, nitrogen and water cycles. Dissolved oxygen regulates biogeochemical cycles such as the carbon, sulphur and nitrogen cycles (Yingst and Rhoads, 1980). Nitrogen flows between the land, sea, atmosphere and sediments. Human activities have brought changes in the nitrogen cycle by adding more nitrogen to the land for agriculture purposes which has provided more food but on the other hand it has also caused eutrophication, hypoxia, harmful algal blooms, smog, acid rain, and loss of stratospheric ozone. Carbon is the key element of life on earth. The carbon cycle includes all life forms on earth as well as the inorganic carbon reservoir and the link between them. Elemental carbon occurs mainly in the form of graphite and diamond. In the ocean carbon is found in dissolved form such as carbonate and bicarbonate ions or as carbonic acid. Carbonate minerals are found in the lithosphere and carbon is present as a gas form in the atmosphere as carbon dioxide, carbon monoxide or methane. Assimilation of carbon by photosynthesis produces $(\text{CH}_2\text{O})_n$ in the form of sugars. In the ocean, carbon is present in different forms such as dissolved inorganic carbon (DIC), dissolved organic carbon, particulate organic carbon and in the

form of marine biota. Primary production by photosynthesising marine algae is the major source of organic carbon in the oceans.

Sulfur is a key nutrient to life for example, it provides structural integrity to protein-containing tissues via S-S cross-linking. Sulfur in its sulfate form is the second most abundant anion in rivers and seawater. Sulfur is also responsible for acid rain. Sulfur is found as a free sulfur ion in ocean and in the form of evaporate minerals in sedimentary rock such as gypsum. Sulfate reducing bacteria metabolise sulfur to produce H_2S which reacts with iron to form pyrite. Thus Sulfur is found in gaseous, aerosol, aqueous, soil, mineral, and biological forms.

Phosphorus is the tenth most abundant element on earth. It is found in minerals such as apatite. Apatite is also formed by organisms as part of the structure of teeth, bones and scales. After the organism dies, these components are accumulated in sediments or soil. In general, many of phosphorite deposits are of marine origin. The biogenic matter produced in the water settles to the sediments and its decomposition releases phosphate to the seawater and pore water which forms large deposits of phosphorus (Butcher *et al.*, (Ed.), 2009). Thus C, N, P and S cycles play an important role in the environment and are connected to oceans, therefore studying marine chemistry is important.

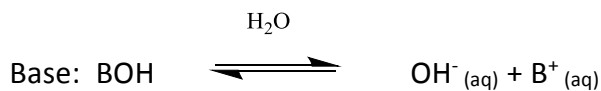
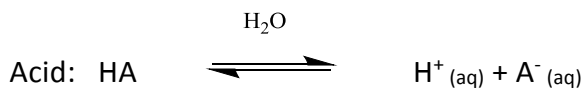
Not only is sea water chemistry important but also the marine sediment chemistry is equally important. There are many biological processes taking place in marine sediments that cause chemical changes in the sediments. The colour of marine sediments changes with redox changes so it is a useful parameter to depict the biological activities in sediments. Brown colour of sediments suggests that there is oxygen deposition while where brown colour disappears, it indicates there is a biological activity so oxygen is being consumed thus reduction is taking place. (Lyle, 1983). The parameters that could be measured as indicators of these processes are pH, redox changes, free metals, carbon, nitrogen, sulphur, phosphorus, organic carbon content and mineral composition.

pH of marine sediments is an important parameter to understand different biological processes such as heterotrophic respiration, chemoautotrophic activity, photosynthesis, precipitation, and dissolution of calcium carbonate. All of these processes are directly linked to pH. (e.g., Revsbech *et al.* 1983, Cai *et al.* 1995, Reimers *et al.* 1996).

1.3 Basic concepts

1.3.1 Acids and Bases

Svante Arrhenius defined acids and bases in 1887. According to the definition, acids are substances that dissociate in water and give hydrogen ions (H^+) while bases are substances that dissociate in water and give hydroxide ions (OH^-). Representing acid with a general formula HA and base with BOH, the following reactions represent the Arrhenius definition for acid and base.



The hydrogen ions produced by dissociation of acid do not remain as individual ions but get attracted to polar water molecules and form hydronium ions.

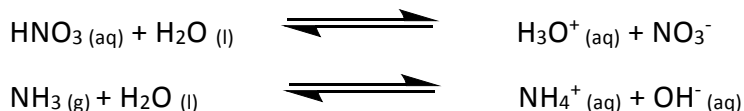


The hydronium ions may form $H_5O_2^+$ or $H_7O_3^+$ with the water molecules. Thus in aqueous solution, the hydrogen ion is generally a hydronium ion. According to the Arrhenius definition, the acids contain hydrogen ion and bases contain hydroxide ions but in the case of ammonia, which is a base, this definition fails to explain.



As seen in the equation, the ammonia does not contain hydroxide ions, but rather removes a proton from the water to generate hydroxide ions.

The Arrhenius definition is only applicable in aqueous solutions, which is another limitation. Thus an English chemist Thomas Lowry and a Danish chemist Johannes Brønsted independently proposed a broader definition for acids and bases in 1923. According to them an acid is a proton donor and a base is a proton acceptor. Thus acid and base interact with each other rather than behaving as individual species.



Where water is an amphoteric substance and acts as a base when acid is added and acts as an acid when base is added. NO_3^- produced is a base and hydronium ion is an acid. Here, HNO_3 and NO_3^- are termed as acid and conjugate base.

In the same year, Lewis defined acids as lone pair acceptors and bases as a lone pair donors. However, to understand the properties of acids and bases in their broadest sense, all three definitions need to be considered. (Myers, 2003)

1.3.2 pH scale

Water, being amphoteric, can donate protons to the base and act as an acid or accept protons from an acid and form hydroxide ions when it acts as a base. Thus water dissociates into a small amount of ions producing both hydronium and hydroxide ions.



At 25°C the concentration of both hydronium and hydroxide ions is $1.0 \times 10^{-7}\text{M}$. Putting this definition in perspective, two molecules of water in every billion molecules dissociate. The equilibrium constant K_w (ion product constant) equals the product of hydrogen and hydroxide ion concentrations.

$$K_w = [\text{H}^+][\text{OH}^-] = (1.0 \times 10^{-7}\text{M})(1.0 \times 10^{-7}\text{M}) = 1.0 \times 10^{-14}\text{M}$$

This equation is applicable to both water and aqueous solutions. Because ionic concentration is so small and the negative exponents make it more tedious to deal with, a Danish biochemist, Søren Peer Lauritz Sørensen introduced the concept of pH (abbreviation for a French word '*pouvoir hydrogène*', meaning power of hydrogen) in 1909 to express the hydrogen ion concentration. The pH of a solution is given by

$$\text{pH} = -\log_{10} [\text{H}^+]$$

Where brackets represent the molar concentration. In an acidic solution, the hydrogen ion concentration increases above $1.0 \times 10^{-7}\text{M}$ and the pH value becomes small while in a basic solution, the hydrogen ions decrease below $1.0 \times 10^{-7}\text{M}$ and the pH value increases. As pH is expressed as a base 10 logarithm, so a unit change in pH represents a change in ion concentration of a factor of ten for example, a solution with pH 5 has 100 times higher concentration of hydronium ions than a solution of pH 7. (Myers, 2003)

1.3.3 Acid base indicators

Indicators may be used to determine whether a solution is acidic or basic for example: litmus. Indicators change their colour as the pH changes and the range of pH that can be detected depends on the pK value of the indicator. The indicator exhibits different coloured forms in acidic and basic medium, which exist in equilibrium. The hydrogen ion concentration plays an important role in the equilibrium, thus the colour changes depending on the concentration of the hydrogen ions.

If the red form of litmus is represented by the formula HIn and the blue form by In^- , then the following dissociation reaction takes place



In basic solution, $[\text{H}^+]$ is very low and the equilibrium is shifted to the right and the indicator is converted to its basic form. In the case of litmus it is blue. In acidic solution, the $[\text{H}^+]$ is large and the equilibrium is shifted to the left so the indicator (litmus in this case) converts into the red form. The amounts of the two forms of indicator can be

calculated as a function of hydrogen ion concentration. The equilibrium expression for the equation above is given below

$$[\text{H}^+] [\text{In}^-] / [\text{HIn}] = K_{\text{In}}$$

Where K_{In} is the equilibrium constant for indicator.

By rearranging the equation to: $[\text{HIn}] / [\text{In}^-] = [\text{H}^+] / K_{\text{In}}$

The relationship between the ratios of the two forms of indicator with $[\text{H}^+]$ can be explained. When the two forms are present in equal amounts, the $[\text{HIn}] / [\text{In}^-]$ is 1 and the $[\text{H}^+] = K_{\text{In}}$. The value of the constant is therefore equal to the hydrogen ion concentration and the change in the colour of indicator is half completed and the pH value is the pK_a of the indicator. If the pH is decreased by one unit, $[\text{H}^+]$ becomes ten times the K_{In} making the ratio $[\text{HIn}] / [\text{In}^-]$ equal to 10. This means at a pH unit 1 less than the pK value of the indicator, the acidic form dominates over basic form by the ratio 10:1 so 91% of indicator is in the acidic form and 9% in basic form (Pauling, 1970). Conversely, at a pH 1 unit above the pK_a 91% is in the basic form. The range $pK_a \pm 1$ thus defines the useful working range of a typical indicator, since there will be little visible colour change beyond this part.

1.4 pH of marine sediments and its importance

To understand how pH can be interpreted to help understand the chemistry of marine sediments, it is important to understand the chemical processes taking place in the top marine sediments. The physical, biological and chemical processes occurring in the top several hundred meters of marine sediments are termed as early diagenesis. Early diagenesis involves benthic bacterial activity on organic matter which is the source of energy for them and the amount of organic matter present can be responsible for benthic production. (Henrichs, 1992). A simple zonation of marine sediments was described by Froelich *et al.* (1979) based on grouping the chemical processes occurring in that zone as oxic, suboxic and anoxic while a broader zonation was described by Berner splitting the anoxic zone into sulfidic and methanic zones. (Berner, 1981)

In organic diagenesis, the marine organic matter is depleted by different oxidants starting from the oxidant that releases the maximum free energy. Once it has been completely used by the bacteria, a second oxidant is used. The preference of oxidant depends on the free energy produced, this process continues until all the matter has been depleted or all the oxidants have been used (Froelich *et al.*, 1979). The processes in the sediments zones (often termed as early diagenesis) are explained in detail as well as summarised in the figure 1.1 (Gattuso and Hansson, 2011).

Water column

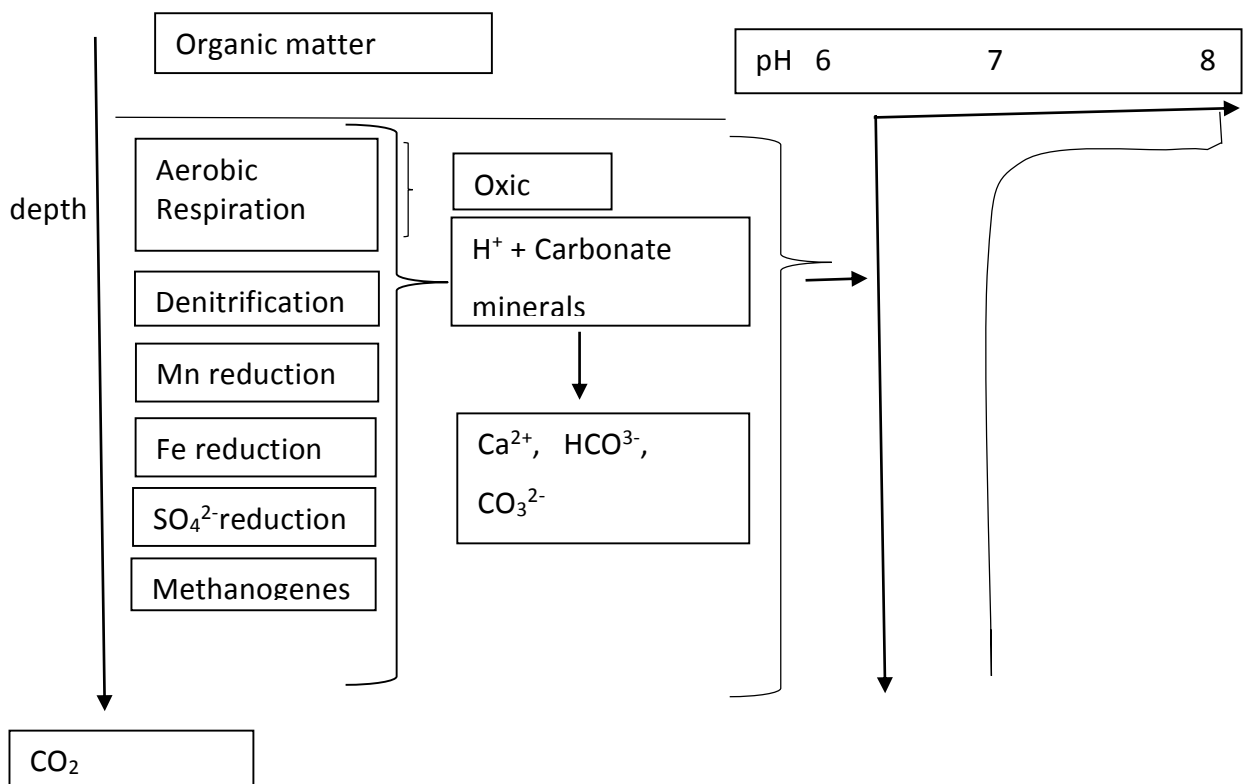
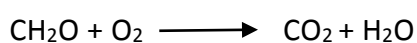
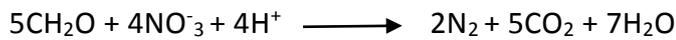


Figure 1.1: processes in the marine sediments.

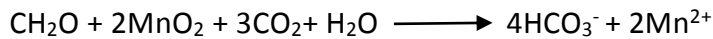
In the oxic zone, aerobic respiration takes place. Oxygen is used during aerobic respiration, releasing carbon dioxide and water. This results in a decline in pH as the production of ammonia and phosphate that increase pH has lower molar concentration than the CO₂ being produced. The reaction is given below:



When oxygen has been consumed, in the suboxic zone, during denitrification (nitrate reduction), nitrate is used as an oxidant and reduced to nitrogen gas.



When nitrate has been used, manganese reduction takes place.



Iron reduction follows the manganese reduction in suboxic zone.



Anoxic zones undergo sulfate reduction and use CO_2 in methanogenesis. (Gattuso and Hansson, 2011)



The iron and manganese species precipitate following reduction (Froelich *et al.*, 1979). It is noteworthy that all the processes except methanogenesis produce CO_2 or carbonic acid and thus are responsible for a decline in the pH of sediments. In addition to these processes, other microbial processes like nitrification, which uses ammonia and produces nitric acid, result in a pH decline too (Soetaert *et al.*, 2007).



Soetaert *et al.* have calculated that excluding the CO_2 production responsible for the decline in the pH, the other microbial processes affect the acid base equilibria by only 0.001 of a pH unit per mole of the substrate oxidised or reduced. Hence oxidation of organic carbon by the various processes above is the predominant factor changing pH, hence measuring pH provides a proxy for carbon oxidising activity. (Soetaert *et al.*, 2007)

The penetration of electron acceptors like oxygen in the sediment depth is critical in driving production of hydrogen ions and the rate of depletion of organic matter and

depends on the sediment properties such as porosity and supply of organic matter (Westrich and Berner 1984). Aller and Yingst (1978) have pointed out that although the processes discussed above dominate in the depth profile, the burrows of macro fauna and their walls allow increased O₂ penetration and thus have a different pH environment from the surrounding sediments.

1.5 Degradation of Organic matter

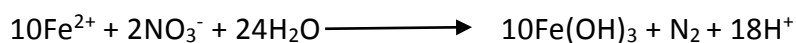
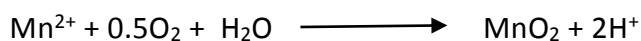
The degradation of organic matter is a complicated process and involves lots of reactions. However, we are interested in the reactions that are regulated by pH or have an effect on the pH. The following reactions are directly related to the pH of the sediments and therefore are of great importance and interest.

1.5.1 Oxidic Mineralization

The organic matter in the sea bottom comes from the primary producers and is mainly phytoplankton cells, zooplankton exuvia and faecal pellets. The organic particles, when they arrive at the sea bottom, have a different composition than in the surface water because of bacterial attack and organic nitrogen and phosphorus depletion in the detritus. Further mineralization takes place by the benthic microorganisms in the sediments that feed on the detritus by consuming oxygen in the oxic zone (Jørgensen, 1982).

1.5.2 Reoxidation

Oxidic mineralization of organic matter produces reduced substances (Fe²⁺, Mn²⁺, NH₄⁺ and S²⁻) by consuming oxygen, that can subsequently be re-oxidised. The following equations explain the re-oxidation processes (Soetaert *et al.*, 2007).





The Manganese oxides are reduced to Mn^{2+} just below the oxic zone and either travel back to the surface in the water or get re-oxidised in the oxic zone consuming oxygen and releasing H^+ . Many pelagic red clays have manganese and iron nodules thus the surface sediments are rich in manganese (Jørgensen *ibid*).

1.5.3 Nitrification and Denitrification

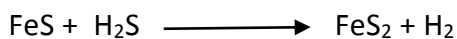
Ammonium is produced by the oxic mineralisation. Ammonium oxidation leads to nitrate production by diffusion of the ammonium upwards in the oxic zone while downwards in the sediments nitrate is consumed by denitrifying bacteria to N_2 . Nitrite, NO_2 and N_2O are the intermediates during the denitrification process (Jørgensen *ibid*)

1.5.4 Iron and Sulfate Reduction and Methanogenesis

Iron in the surface sediment is in the form of oxyhydroxides and is reduced to ferrous ions below the nitrate zone. The iron reduction may take place by H_2S , in the presence or absence of bacteria, or respiration or fermentation may use the iron as electron acceptor (Jørgensen *ibid*). The processes involving nitrate, nitrite, manganese, or iron as oxidants are called suboxic diagenesis (Froelich *et al.*, 1979). The redox potential below this zone becomes very low and favours sulphate reduction also termed as the sulfidic zone, and is typically three or four fold thicker than the oxic zone. In most coastal sediments, which are organic-rich, sulfate may be consumed a few mm below the surface, but typically it is present for a few meters depth. It is interesting that sulphate has been traced down to several hundred metres depth in the pelagic sediments while it is not reduced at all in the red clays and calcareous oozes of the deep sea. Anaerobic diagenesis ends up with the accumulation of methane in the porewater below the sulfidic zone. (Claypool and Kaplan, 1974; Martens and Berner, 1974). Methanogenesis does not occur at sulfidic zones as the methanogenic bacteria cannot compete with the sulfidic ones and therefore it occurs only when sulphate had been reduced. (Jørgensen, *ibid*)

1.5.5 Precipitation processes

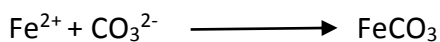
The following precipitation reactions, occurring in marine sediments, are of great interest as they are directly related to pH. One of the reactions is iron sulphide production either by ironoxyhydride or by the reduced iron which leads to pyrite (FeS_2) formation (Soetaert *et al.*, 2007).



Manganese and iron carbonate minerals are formed from the dissolved metal ions and tend to decrease the pH while formation of gypsum ($\text{CaSO}_4 \cdot 2\text{H}_2\text{O}$) has no effect on pH unless the pH is very low (Soetaert *et al.*, 2007). The argument is about the fact that the carbonate mineralisation in the equation below happens in the accessible pH range of sediments hence removal of conjugate base by precipitation increases ionisation and H^+ production.

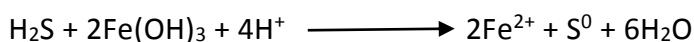


Whereas at normal pH conditions only SO_4^{2-} is present and its removal does not decrease pH but at low pH, H^+ ion production decreases pH.



1.5.6 Other reactions

The iron and manganese oxides are reduced by H_2S and tend to increase the pH of the sediment due to S^0 formation (Soetaert *et al.*, 2007).





The buffering capacity of sea sediments that involves carbonate dissolution and macrofauna bioturbation is also important to be considered. This is discussed later in the ocean acidification section.

1.6 Relation between pH and biogeochemical processes

The pH regulates most of the biogeochemical processes and is in turn affected by these processes. Table 1.1 summarises the results from Soetaert *et al.* (2007) that explain the effect of processes on sediment pH.

Process	Effect on pH	Reason
Photosynthesis	Increase in pH	Consumes CO_2 , Some algae use bicarbonate rather than CO_2 thus a proton is consumed or a hydroxide ion is produced and pH increases.
Aerobic respiration	Decrease in pH	CO_2 is released. $\text{CH}_2\text{O} + \text{O}_2 \longrightarrow \text{CO}_2 + \text{H}_2\text{O}$
Ammonium production	Increase in pH	Protons are consumed $\text{NH}_3 + \text{H}^+ \rightleftharpoons \text{NH}_4^+$
Nitrification	Decrease in pH	Production of nitric acid $\text{NH}_3 + 2\text{O}_2 \longrightarrow \text{HNO}_3 + \text{H}_2\text{O}$
Carbonate dissolution	Increase in pH	Releases excessive negative carbonate that

		<p>consumes H^+ to form HCO_3^-.</p> $CaCO_3 \Rightarrow CO_3^{2-} + Ca^{2+}$
Re-oxidation and calcification	Decrease in pH	<p>Re-oxidation produces protons</p> <p>Calcification uses excess negative charge.</p> $CO_3^{2-} + Ca^{2+} \Rightarrow CaCO_3$
Denitrification	pH dependant (at low pH, denitrification increases the pH)	At low pH, nitrate is reduced to NO_2 , N_2O and N_2 .
Fe and Mn reduction	Increase in pH	<p>The protons consumed are far more than the protons released in DIC (dissolved inorganic carbon) production.</p> <p>When H_2S is used it produces S^0</p>
Sulphate reduction	pH dependant (favours low pH)	At low pH, sulphate is consumed and thus pH is increased.
Production of DIC	Decrease in pH	Releases protons
FeS formation	Increase in pH if iron hydroxide is used,	Consumption of Fe^{2+} and production of hydrogen

	decrease in pH if Fe^{2+} is used.	ions decreases pH. S^0 production increases pH.
FeS_2 (pyrite) formation	Increase in pH	S^0 production increases pH.
Iron and manganese Carbonate precipitation	Decrease in pH	Consumption of Fe^{2+} and Mn^{2+} and release of protons.

Table 1.1: Processes in marine sediments and their effect on pH. (Soetaert *et al.*, 2007)

The pH is highly dependent on the microbial activity, which depends on the supply of organic matter and nutrients. The building of permanent or semi-permanent burrows by microorganisms has a large effect on pH. These burrows increase the surface area between the overlying water and the reduced sediments thus allowing the transport of organic matter and solutes into and out of the sediments which enhances the degradation process and reduces the pH. Burrow ventilation can add oxygen to anoxic sediments and can reduce pH (Gattuso and Hansson, 2011).

A typical pH profile of marine sediments is given in figure 1.2.

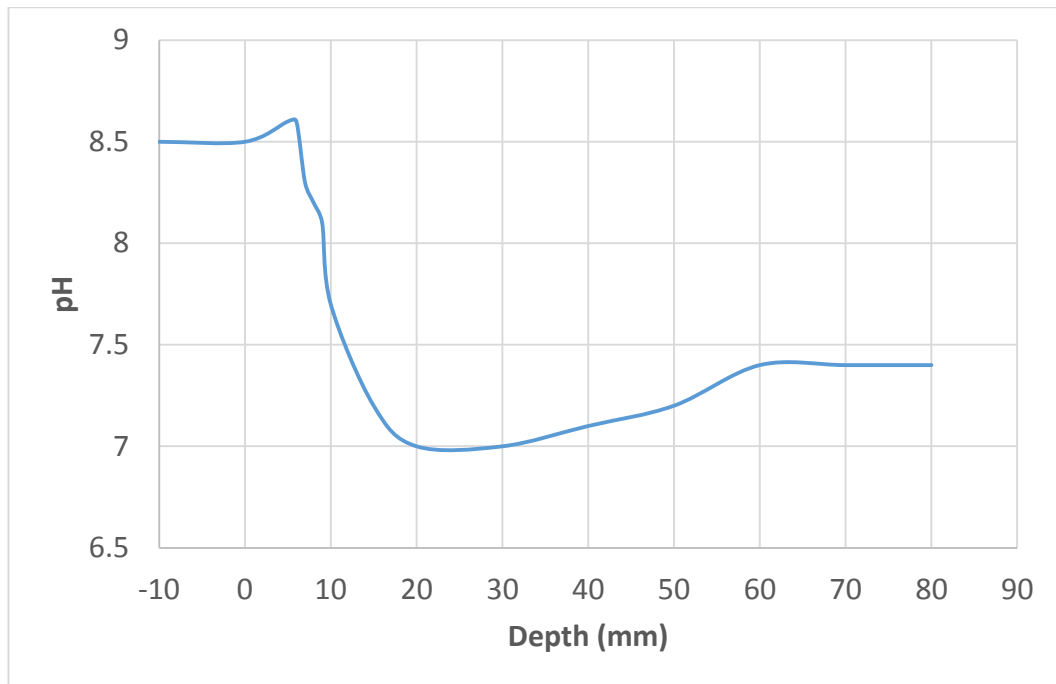


Figure 1.2: An example of typical pH profile of marine sediments. (a rough guide taken from cai *et al.*, 1999).

In a typical pH profile of the marine sediment a sharp decline in pH just below the sediment-water interface is often observed due to the oxic mineralization and oxic re-oxidation of reduced ammonium, Fe^{2+} , Mn^{2+} , sulphide and methane. The pH reaches its minimum value where the oxic-anoxic zones meet. (Revsbech *et al.*, 1983, Archer *et al.*, 1989, Cai *et al.*, 2000, Stahl *et al.*, 2006). Then, a combined effect of Fe and Mn-oxide reduction increases the pH (Wenzhofer *et al.*, 2001). The figure 1.3 summarises the processes indicated by pH.

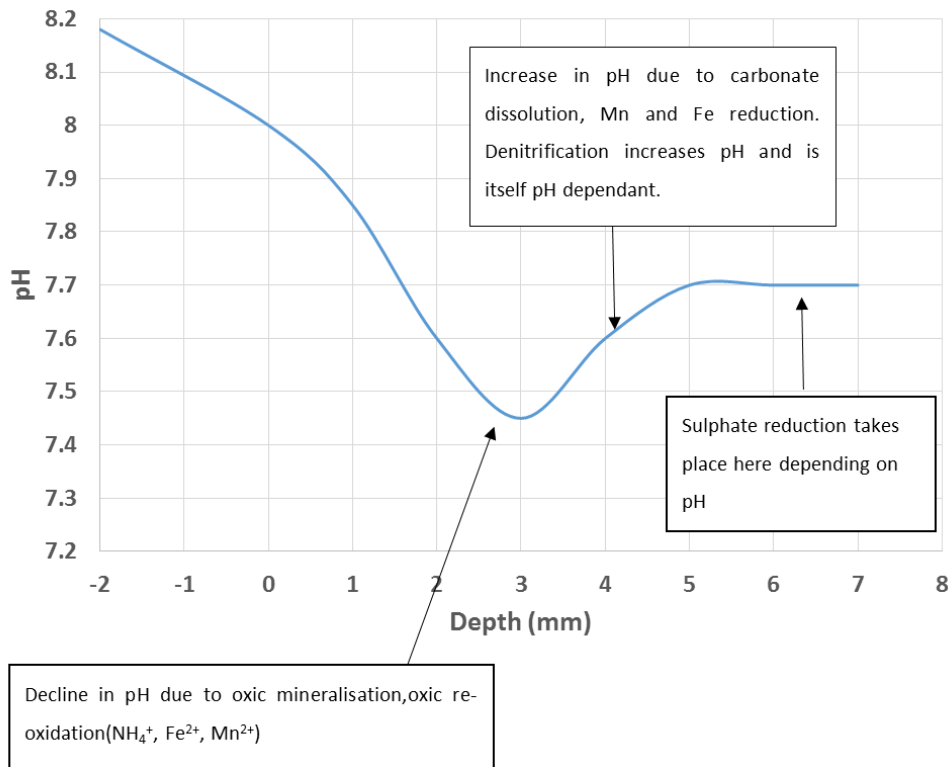


Figure 1.3: pH profile of marine sediments (a rough pattern taken from Stahl *et al.*, 2006).

1.7 Ocean acidification and its impact on sediment fauna

The decrease in the pH of the ocean by uptake of CO_2 over an extended period is referred to as ocean acidification. This could happen due to addition or removal of chemical substances from the ocean which is natural or caused by human activity known as anthropogenic ocean acidification. The seawater dissolves CO_2 and carbonate chemistry of seawater changes. The concentration of bicarbonate and dissolved inorganic carbon increases and pH decreases. As the concentration of hydrogen ions is proportional to the concentration of bicarbonate and carbonate ratio so when it increases, pH decreases. However the supply of CO_2 in the sediment is buffered by the macrofauna bioturbation which is responsible for dissolution of CaCO_3 thus sustaining the redox reactions by preventing an increase in total alkalinity and production of hydrogen ions. Burdige *et al.*, in 2008 showed that sea grasses produce O_2 directly into the sediments and increase mineralisation favouring an increased dissolution of CaCO_3 but the sea grass foliage decreased the bottom water flow thus resulting in the uptake of O_2 from the sediments. These two opposite processes compete and the dominance of one process over the other depends on the density of

the sea grass and the carbonate dissolution from O_2 coming from sea grass dominates at densities above $0.5m^2$ of leaf area per m^2 of seafloor. The photosynthesis of microphytobenthic communities also introduces O_2 and is responsible for carbonate dissolution that increases total alkalinity which determines the carbonate and bicarbonate concentration. The increased bicarbonate concentration due to carbonate dissolution may reprecipitate as a different mineral for example, aragonite dissolution resulting in calcite precipitation (Burdige *et al.*, 2008). Thus any pH changes coming from seawater into the sea sediments are partly buffered by the dissolution process.

Based on the observations that the pH of sediments is lower than the minimum pH in the surface waters of the sea and the sediments have a better buffering capacity, it is assumed that infaunal organisms may be more tolerant to ocean acidification than the ones that live in the water column or on the surface of the sediments but this assumption is based on their tolerance to hypoxia and anoxia and not hypercapnia (increased amount of CO_2) however more evidence is required before it can be concluded confidently that they can tolerate hypercapnia. Reipschläger *et al.*, 1997 and Pörtner *et al.*, 1998 and 2000 showed that short term hypercapnia ($10000 \mu atm$ CO_2 level) caused metabolic depression in *Sipunculus nudus*, a sipunculid worm as the body fluid acidifies. However Wood *et al.* (2008, 2010) showed that the infaunal brittlestar, *Amphiura filiformis* shows reduction in oxygen uptake when exposed to hypercapnia. A few infaunal species may survive in acidic environments, for example Dashfield *et al.* (2008) showed that *Echinocardium cordatum* showed no mortality in acidified sediments of pH 7.5. Widdicombe *et al.* (2009) reported that capitellid worms were tolerant to pH less than 6 for over a month. Same was reported for *Neries virens* by Batten and Bamber (1996) and Widdicombe and Needham (2007). However these few observations cannot be generalised for all the infauna because different species have different capability to tolerate changed CO_2 levels at different stages of their life cycle and it depends on the time period of the exposure to the hypercapnia. Dupont and Thorndyke (2009) showed that the larvae are more sensitive to any changes in pH than the adults. Some infaunal organisms may be living at the very limit of their

tolerance to CO₂ and just a small change in pH could affect their survival and functioning.

According to the literature, hypercapnia does not affect the burrowing activity of some infaunal organisms. Widdicombe and Needham (2007) showed that there was no effect on burrowing activity when *N. Virens*, a polychaete worm, was exposed to pH 7.21-7.30 for five weeks but according to some early studies by Batten and Bamber (1996) very low pH less than 6.5 can disrupt the burrowing activity. Wood *et al.* (2009) showed that bioturbation of *Amphiura filiformis* is not affected at a pH of 7.7-7.3 for 40 days. Dales *et al.* (1970) observed that the respiratory irrigation of polychaetes *Hyalinoecia tubicola* and *Diopatra cuprea* was not affected by a low pH of 7.5. Ries *et al.* (2009) showed that at a low pH, for *Mya arenaria* and *Argopecten irradians*, the rate of calcification ceases and Wood *et al.* (2008, 2010) observed that in *A. filliformis*, arm regeneration increases at low pH and leads to muscle wastage after 40 days. (Gattuso and Hansson, *ibid*)

Thus, human activities have increased CO₂ levels in the environment which has been taken up by the ocean as a sink. This has caused decreased pH of ocean water and is referred to as ocean acidification. This has affected the life in the sea water and may also have affected the life in the sea sediments, some of these effects have been evidenced in the micro fauna and discussed in this section. However very little is known about the marine sediment's pH and thus more knowledge is required before it is concluded that ocean acidification has affected the life and processes in the marine sediments. The important parameter which can describe and can lead to a successful conclusion is pH of the marine sediments; therefore it is important to measure the pH profiles of marine sediments.

1.8 Sediment Profile Imagery

Sediment Profile Imagery (SPI) is a method of quick survey and marine sediment monitoring (Curtis, 2004). It was first developed by Roads and Cande in 1971 to explore the *in-situ* processes between sediment and water. Quantitative studies of marine sediments are usually carried out by taking samples and sieving the sediments during which lots of important information is lost. It is also quite a time consuming process. In contrast SPI analyzes rapidly and conserves the depth/structure information (Rosenberg *et al.*, 2003). SPI is a special technique to view into the marine sediments approximately up to 25-30 cm deep from the sediment surface. One can achieve qualitative and quantitative data on the physical, biological and chemical characteristics of marine sediments precisely without losing any information (Diaz and Trefry, 2006). SPI works by taking *in situ* images of the marine sediments to collect information rapidly. It is reliable in a way that the changes in the sediments can be traced at the time they occur. It works like an inverted periscope which captures *in-situ* cross sectional images of sediment. Some varieties of SPI system contain time lapse cameras to collect series of photographs and some have coring devices to take physical samples of the sediments.

1.8.1 Construction of SPI cameras

A SPI camera consists of a camera mounted on a wedge shaped prism with a faceplate and an internal light source provided by the flash strobe. A mirror is mounted at the back of the prism at a 45 degree angle so the vertical sediment-water profile is reflected up to the camera (Figure 1.4). Distilled water is filled in the prism to minimise unwanted reflections and minimise pressure changes. Turbidity of the water does not affect the outcome as the object being photographed is against the faceplate. A SPI camera can either be handheld or operated through cables from a research vessel.

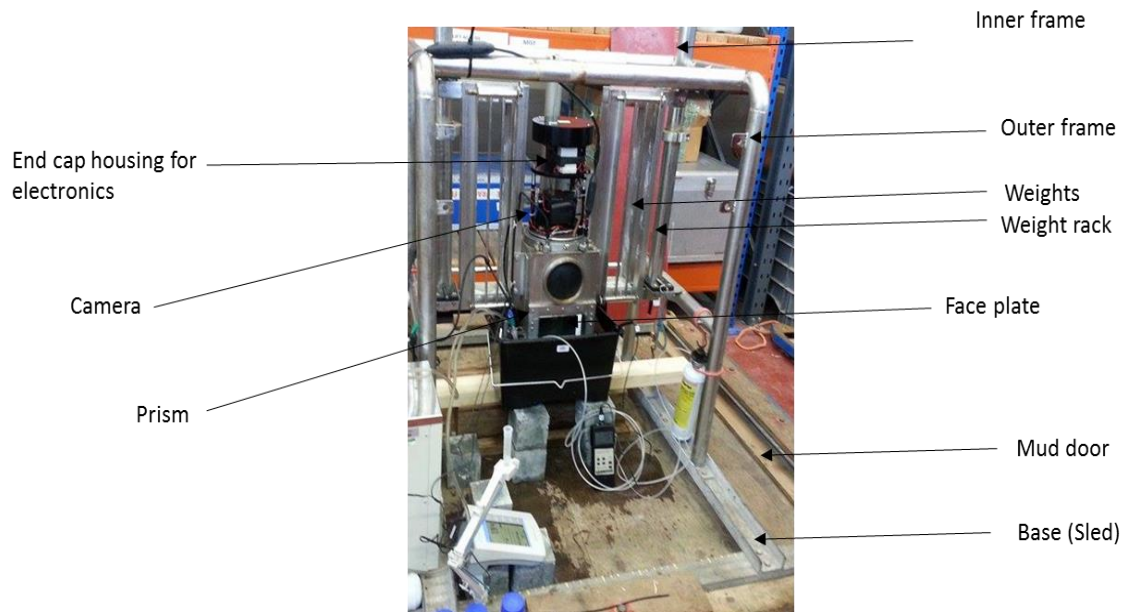


Figure 1.4: Photograph of SPI taken at Cefas during an experiment, The SPI parts are labelled. The SPI faceplate is inserted in a bucket full of seawater. pH meter and temperature probe were used during an experiment and are not the parts of SPI.

The systems operated through boats have a moveable camera mounted on the frame which can be operated by producing tension on the winch wire. As the camera is lowered, the tension on the winch wire keeps the prism in the up position and releases to the down position as soon as the frame touches the bottom. The prism penetrates into the sediment, the trigger activates a time delay on the release of the camera shutter and the photograph is taken when the prism comes to rest (Figure 1.5). The photographs can then be analysed with image analysis software.

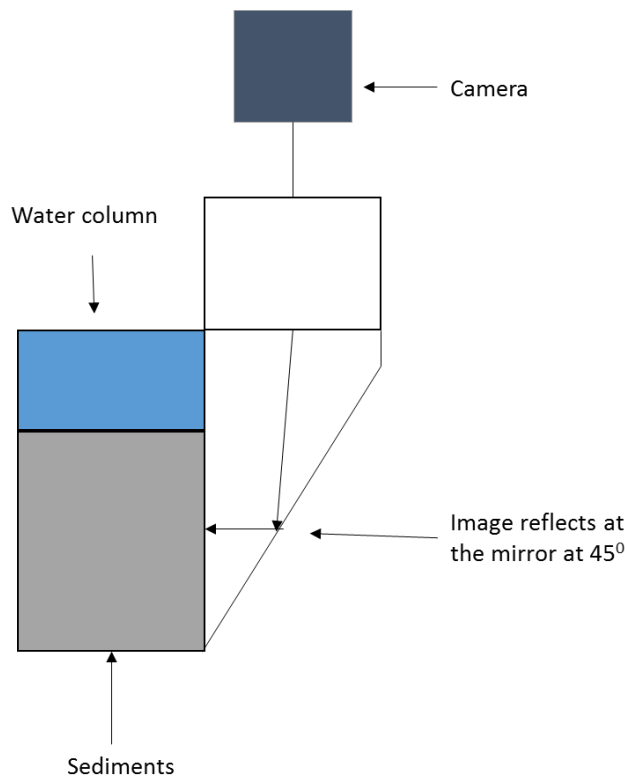


Figure 1.5: Diagram of SPI camera showing how the sediments against the faceplate is photographed. The image reflects at 45° at the mirror.

1.8.2 Applications of SPI Cameras

SPI cameras can be used to quantify over 20 physical, chemical and biological parameters such as prism penetration, sediment grain size, mud clasts, redox area, pH sediment surface relief, methane gas vesicles, surface pelletal layer, apparent faunal dominants, voids, burrows, worm tubes, microbial aggregation, dredged material etc. It can be used for sewage sludge disposal site studies, assessment of low dissolved oxygen, dredged material disposal sites, aquaculture impact assessment, Industrial discharge impact assessment, oil platform impact assessment, sediment quality surveys and identification of pollution sites (Curtis, 2004). A few specific examples of application include; the use of SPI to determine the effects of trawling on benthic habitats (Nilsson and Rosenberg, 2003; Rosenberg *et al.*, 2003; Smith *et al.*, 2003), fish farm impacts (Karakassis *et al.*, 2002; O'Connor *et al.*, 1989), assessing macrobenthic communities at dredge disposal sites (Birchenough *et al.*, submitted) and using SPI for time-lapse analysis of animal sediment relationships (Solan and Kennedy, 2002).

If the SPI camera could be combined with additional sensing capability that was robust and could simply quantify additional sediment parameters then the power and range of application for SPI cameras could be increased further.

1.9 Chemical sensors

The IUPAC has defined a chemical sensors as “A chemical sensor is a device that transforms chemical information, ranging from the concentration of a specific sample component to total composition analysis, into a useful analytical signal. The chemical information, mentioned above, may originate from a chemical reaction of the analyte or from a physical property of the system investigated.” (Hulanicki *et al.*, 1991)

Chemical sensors consist of two parts: a receptor and a transducer. The **receptor** part of a sensor converts the chemical information into a form of energy which may be measured by the transducer.

The **transducer** has the ability to transform the energy containing chemical information into a signal. (Hulanicki *et al.*, 1991)

Janata (2010) defines chemical sensing as a process of getting information of chemical composition of a system immediately. He further states that in this process a chemical species and its sensor interact with each other to give an amplified signal. Thus, the process of chemical sensing comprises two steps:

1. Recognition of chemical species (obtain a signal)
2. Detection/amplification of signal by some physical transducer

For instance, measurement of pH with a glass electrode identifies hydronium ion to give a signal which is then measured by a pH meter, which acts as a physical transducer converting it into an analogue mV reading which appears on a pH meter display. (Janata, 2010).

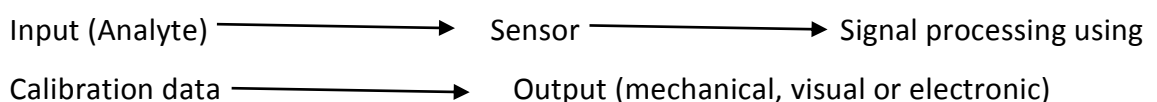


Figure 1.6: Sensor diagram explaining how a sensor works .

1.9.1 Properties of a good sensor

In the literature, the following properties of a good sensor have been mentioned:

- It should be accurate.
- It should not be very expensive.
- It should be easy to utilize.
- It should give a rapid response, thus it should save time. (Janata, Ibid)

Other than the properties mentioned above, a good sensor should be robust so that it can be used under adverse conditions and it should be specific for a particular chemical species so the other chemicals do not interfere.

Interaction between chemical species and sensor can be of two types.

- a) Surface interaction
- b) Bulk interaction

In surface interaction, the species under consideration adsorbs on the surface whereas in the bulk interaction, the species under consideration distributes itself between sample and sensor and gets absorbed. The interaction depends upon the size of the molecule. Large molecules like proteins may adsorb on the surface while smaller ones may absorb and undergo bulk interaction. The '**Ruggedness**' is a property of a sensor being reliable in adverse conditions and the '**Reversibility**' means the ability of the sensor to respond when there is a change in chemical concentration. A sensor is reversible if it responds to change in the concentration of a chemical species. (Janata, Ibid)

1.10 Methods for measuring pH of marine sediments

Although pH of the marine water column has been measured with great care for many years, surprisingly little attention has been given to the measurement of pH of marine sediments. The following review explains different methods of measuring pH of marine sediments.

1.10.1 Using a glass membrane pH electrode

Glass membrane pH electrodes can be used if marine sediments are brought into the lab but by bringing them into the lab one cannot measure the rapid pH changes that may occur in marine sediments. Bringing the sediments into the lab can change the conditions and thus change the actual pH of sediments. It is useful to determine pH *in-situ* so as to monitor rapid pH changes. Previously glass membrane pH electrodes have been used to determine the pH of marine sediments, as is detailed below.

1.10.2 Glass pH electrode

Glass pH electrodes are sensitive to the hydrogen ions. The pH electrode has a glass shaft with a thin glass membrane at the end (sensitive part). The electrode contains an internal solution and an internal electrode. Generally silver chloride is used as the material for an internal electrode and potassium chloride maintained at pH 7 is used as an internal solution. A reference electrode consists of a liquid junction, internal solution, internal solution filter port, a tube to support the reference electrode, and an internal electrode (silver chloride or mercurous chloride). Potassium chloride is used as an internal solution. The liquid junction contacts the test solution with the internal solution. A temperature compensation device is also required because the electromotive force can vary depending on the temperature. The glass electrode, reference electrode and temperature-compensation device are often combined together in a combination electrode to make the pH measurements easy by inserting a single probe in the test solution (horiba website). Figure 1.7 shows a typical design of a glass electrode.

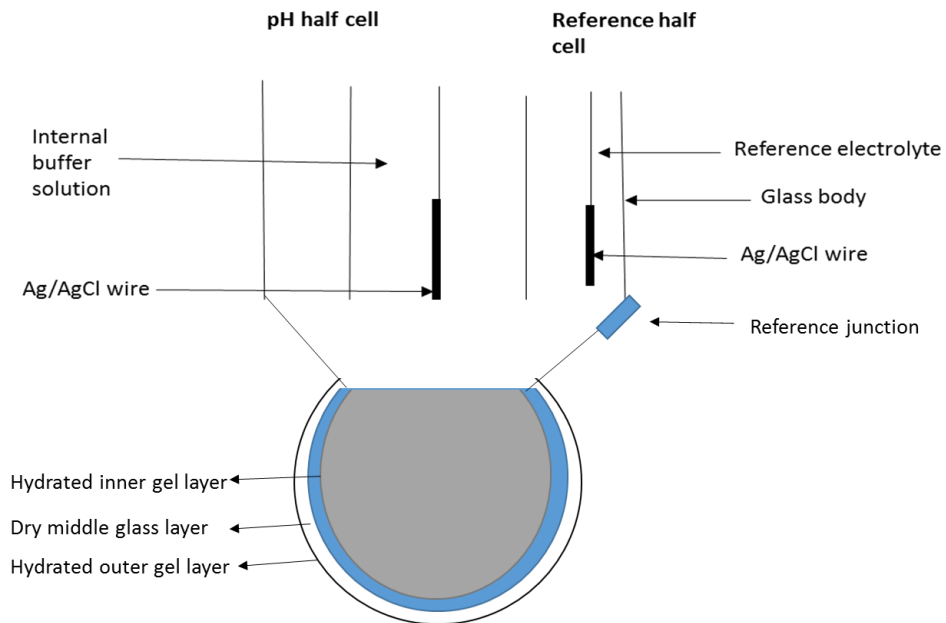


Figure 1.7: Design of a combination glass electrode.

The principle of measuring pH from glass electrode is that the reference electrode has a constant potential. The potential difference is caused between the reference electrode and the glass electrode when the glass electrode that is sensitive to hydrogen ions comes in contact with a sample solution and results in an electromotive force that can be measured. The potential is a linear function explained by the Nernst equation given below:

$$E = E_c + (2.3 \times RT \div nF) \times \log [H^+]$$

Where E= measured potential, R= gas constant, n=ionic charge, E_c = cell potential under standard conditions, T= temperature in degrees Kelvin and F= Faraday constant.

When the glass electrode that is sensitive to hydrogen ions comes in contact with a solution, a gel layer is formed and hydrogen ions flow inside or outside the glass electrode depending on the nature of the sample solution. In case of acidic solution, the hydrogen ions move inside and in case of alkaline solution, the hydrogen ions move outside from the electrode thus causing a potential difference between the glass and the reference electrode. (Tolido, 2013)

Joris M. Gieskes and W. Carl Rogers determined the pH of interstitial waters of marine sediments in 1973 using a pH electrode and found alkalinity by titration (Gieskes and Rogers, 1973). E. Gomez *et al.* used a WTW pH meter to measure the pH of sediments.

Sampling was done using a hand corer. The top layer was taken and stored in a plastic flask at 4 °C in saturated bisulfite solution to prevent oxygen interference (Gomez *et al.*, 1999).

R.B Philip measured pH of marine sediments with a VWR-brand portable pH meter on site when he was observing the effect of low pH on biological species. He collected samples in a small basket, centrifuged sediments for 10 minutes and decanted water. (R.B Philip, 1999. Dashfield *et al.* used a WTW pH meter to measure the pH profile by taking samples of sediment, sieving and adding the most abundant species of microorganism in it (Dashfield *et al.*, 2008).

Standard pH electrodes have a glass bulb diameter in millimetres and do not have high spatial resolution therefore they cannot be used to measure pH changes in small areas. Microelectrodes have been developed to resolve this problem. They reach into the sediments allowing less disturbance in the sediments and giving high resolution micro profiles. (Cai and Reimers, 1993)

1.10.3 pH microelectrodes

The microelectrodes are miniature versions of standard glass membrane electrodes and have a much smaller diameter of the sensing part (in μm) for high spatial resolution.

David *et al.* used microelectrodes in 1989 (David *et al.* 1989). Cai *et al.* in 1993 developed a pH microelectrode by using the technique described by Hincke (1967) and modifying the pH bulb and fitting a piece of silicone rubber tubing along the shaft. They used it for *in-situ* measurement of marine sediment pH. The pH microelectrodes were stable and fast and gave a near-Nernst response slope. (Cai *et al.*, 1993). Reimers *et al.* used the same electrode prepared by Cai *et al.* (1993) for *in-situ* pH measurement, though they reported problems with the difficulty in measuring i.e. breakage etc. (Reimers *et al.*, 1996). Komada *et al.* prepared the same electrode as Cai (1993) and measured pH profiles in the laboratory before and after incubating sediments (Komada *et al.*, 1998).

pH microelectrodes have a short life time, small tip diameter (<1 μm), high resistance and are fragile so they break very easily in a harsh environment. In order to resolve these problems, microelectrodes have been modified by adding a polymer based liquid membrane that makes the tip stronger for application in the harsh environment of sediments (Zhao and Cai, 1999).

pH microelectrodes were modified by Zhao and Cai by adding a pvc liquid membrane on the tip of the microelectrode and making a larger tip. This electrode was prepared specially for hard environment like sediments where electrodes can break. The liquid membrane solution contained 10% tridodecylamine, 1% potassium tetrakis(4-chlorophenyl)borate (KT4CIPB) and 89% 2-nitrophenyloctyl ether (2-NPOE) and 33% PVC dissolved in excess THF and by adding phosphate buffer of pH 7. These electrodes were stable up to a month and the tip was stronger than the classic ones which had no polymeric membrane tip. Response time was 4 s. The sediments were taken from estuarine areas and were stored in an incubator at 22 °C and measurements were taken after a few weeks. They found that microelectrodes should have a 10 μm tip and a polymer membrane so the liquid does not drain and the tip does not break (Zhao and Cai, 1999). The same pH meter was used for measuring the pH of marine sediments by Cai *et al.* in 1999 and 2000. The sediments were collected and incubated in the laboratory for 1-3 weeks and then the overlying water was replaced by the water taken from the same site. The results were compared with a glass mini electrode which measured smaller pH changes than the microelectrode (Cai *et al.*, 1999 and 2000).

Cefas (Center of environment, fisheries and aquaculture science) have used Unisense pH microelectrodes for profiling studies mostly with recovered sediment cores on research cruises. The results of this work have not yet been published (Greenwood *et al.*, 2015).

Although microelectrodes have been effective for pH profiling, optical sensing is another alternative for sediment pH profiling because optical sensors have more robust design than glass electrodes and due to the fact that they are less sensitive to

electrical noise, and can exhibit lower drift. Whereas dealing with glass electrodes is tedious and, their breakage and signal instability is frustrating (Stahl *et al.*, 2006).

1.10.4 Using pH sensitive fluorescent and indicator dyes

This technique has been used by a number of groups, even though it needs special experimental requirements and may be difficult to apply during a cruise.

Zhu *et al.* in 2005 used fluorescent foil optode made from HPTS (8-hydroxy-1, 3,6-pyrenetrisulfonic acid trisodium salt) immobilised in a Polyvinyl chloride (PVC) membrane to measure pH of marine sediments. The sensor was insensitive to oxygen, temperature and intensity of light. Its pH range was 5.5-8.6. Response time was 4 minutes from pH 8 to 6 and 6 minutes from pH 6 to 8 and its properties remained the same for at least 200 pH cycles. A camera was used to record the fluorescence. Sampling was done by taking sediments from the site and storing in a glass tank in the dark. Bottom water from the sampling site was added into it. Samples, which were taken from a site where a large number of *Nereis succinea* were present, were introduced with the same species. The foil was attached to the tank and fluorescent spectra were taken. For calibration, a pH meter was used. The optode could be stored for a year if refrigerated. (Zhu *et al.*, 2005)

The same dye HPTS was used by Zhu *et al.* in 2006(a) but by immobilising it into a different polymer to measure the pH two dimensionally in bioturbated marine sediments. The dye was covalently immobilised on the surface of a polyvinyl alcohol membrane. The membrane was supported by a clear polyester sheet. The membrane showed a single emission band at 540nm and dual excitation bands at 428 nm and 506 nm. As the pH increased, the emission followed by the excitation at 428 nm (acid form) decreased and emission from excitation at 506 nm (base form) increased. The dye responded in the range of 5.8-8.6. The optode was excited by two LED lights with respective irradiation maxima at 420 nm and 500 nm. The emitted luminescent light was imaged by a digital camera. An emission filter (540 nm) was mounted between the lens and the camera. The response was insensitive to dissolved oxygen but sensitive to ionic strength thus pK_a increased with decreasing salinity. Sediment cores were obtained and brought to the laboratory. Sediments were sieved. A glass walled

microcosm was wrapped with the sensor foil inside and was then inserted in the sediments, then seawater was added to the sediments. These samples were kept in the dark but they lost some fauna. To check the pH variation with faunal burrowing activity, the common species which is usually found at the sampling site (*Nereis succinea*) was added and the pH fluorescence and photographs were taken every day for many weeks. The images were processed using software (image pro plus and Maxim DL image processing software). For comparison, a pH meter with a glass membrane electrode was used.

The fluorescent dye response time was 1 minute for a 90% signal response from pH 6-8. However, it can take up to 2 minutes for full equilibrium. Reversibility took 5 minutes to equilibrate completely for 2 pH units change. It was stable for hundreds of cycles.

The sensor had the following qualities:

- It could be stored for 1 year at room temperature and for three years in the refrigerator.
- It gave bright green fluorescence at 540nm with dual excitation at wavelengths 428 nm and 506 nm
- The response time of the optode is dependent on temperature. The response time for the optode itself was 4 minutes but for *in situ* measurements in the sea and sediments it became longer because the temperature decreased in the depth of the sediments. The observed response time was 15 minutes. (Zhu *et al.*, 2006 (a))

Hulth, *et al.* developed a pH sensor using HPTS by immobilising it into cellulose acetate in a foil made of PVC. The foil was then spread on the water lying on the sediments and the pH was measured by scanning the response using a CCD camera. The sensor was used to scan two dimensional hydrogen ion concentration (Hulth, *et al.*, 2002). Hakonen *et al.* in 2007 also used the same fluorescent HPTS for measuring the pH of marine sediments. They suggested that an alternative to HPTS is 6, 8-dihydroxypyrene-1, 3-disulfonic acid (DHPDS) which can be used as a sensor to determine pH between 6 and 9. The method of sampling was quite similar to the above strategy. They collected sediments in an Olausson box-corer, sieved the sediments while being wet

and transferred to a microcosm where they added natural sea water and a species called *T.sarsi* for 7 days. The sensor was made using the method of Hulth, *et al.* (2002). The sediments were also photographed. Calibration was done using a standard pH meter.

Stahl *et al.* used an optical fluorescent pH membrane which was based on a hydrogel (proton permeable) matrix incorporating 2', 7'-dihexyl-5(6)-N-octadecyl-carboxamidofluorescein ethyl ester (DHFAE) which is a lipophilic pH indicator, to determine the pH of marine sediments. They used ruthenium (II)-Tris-4, 7-diphenyl-1, 10-phenanthroline [Ru (dpp)₃]-incorporated nanoparticles as a reference standard. For the synthesis of DHFAE they followed Schröder *et al.* (2005). The pH optode sensor was attached to the glass of a small aquarium with tape and a sample of sediments was then added. The measurement was taken by exciting the fluorophore/ phosphor using a green LED light (λ_{\max} 530) and the emission of the sensor was recorded using a CCD camera. For determination of pH of each sample, two images were taken, one before excitation and the other after excitation i.e. one when the LED is on and the other when LED is off and the ratio of the two images is taken to infer the pH of the sample. The sediment samples were taken in squared frames from a shallow water site. The sediments were kept in the aquarium adding water from the sampling site for 1 day. A 24 hour day and night natural cycle was applied. During the day measurements, the external light was turned off when taking the image and the path between camera and the optode sensor was shaded black. The sensor can detect the pH range of 7.3-9.3 (the pK_a of the dye is 8.3) which is suitable for some marine conditions. The sensors are stable up to months when kept in darkness and have response time of <200 s between pH 7.6-8.3. The light had a negative effect on the performance of the sensor because the pH indicator photo bleached, which caused a negative drift in the signal ratio at higher pH. They found that during a 24h cycle, the pH varied from ~7.3 during night time to >8.3 in day time along the sediment water interface. However the pH shifted from ~7.8 in the night time to ~8.3 in the day time due to strong diurnal benthic variation in the overlying water. This was same at the depth of the sediments where the polychaetes ventilated the burrows. Although the

sensor had a good range for detecting pH in marine sediments, it has the following limitations when making *in situ* measurements:

- When images are taken in light exposed environments, photo-degradation of the pH indicator and sensitivity to ambient light is a major problem.
- The slow response time can be a problem in measuring the pH of environments having rapid fluctuating pH. (Stahl *et al.* , 2006)

Schröder *et al.* made pH fluorosensors for the marine system in 2005. They used carboxyfluorescein derivatives 2', 7'-dihexyl-5(6)-N-octadecylcarboxamidofluorescein (DHFA) and 2', 7'-dihexyl-5(6)-N-octadecyl-carboxamidofluoresceinethyl ester (DHFAE) as a fluorescent dye immobilised in a membrane made with polyurethane hydrogel. Sensors have a pH range matching the marine environment (7.2-9.2) but the pH in marine sediment can be below 7 (Zhao *et al.*, 1999). Response time was 90s for a 1 fold pH change (Schröder *et al.*, 2005). The sensor was better than HPTS because of its broader pH sensing range and less effect of salt changes.

Yanzhen *et al.* developed a SPI instrument called CHEM-SPI having a fluorosensor foil attached to it. They used it for vertical measurement of pH, O₂ and *p* CO₂. The pH was measured as follows.

The guillotine pressure vessels had the following components:

- Stepper-Driven LED wheel for excitation
- Stepper-Driven emission filter wheel
- Digital canon camera (SLR)

A 7-watt 415 nm LED and a 1-watt 505 nm LED were used for measuring pH as LED428 and 506 were not available, which would have been optimal for the 8-hydroxy-1, 3, 6-pyrenetrisulfonic acid tri sodium salt (HPTS). Two other LEDs i.e. 1-watt white LED was used for visible images and short pass filters (480 SWP, 520 SWP) were mounted on the 470 nm and 505 nm LEDs to reduce the background interference. To control the electronic components, a computer on ship was used. The digital camera was set as per requirement. To measure the pH, the sensing foil was mounted to the imaging window. For the preparation of the pH sensing foil they followed Zhu *et al.* (2005). The

fluorescent dye used for the pH measurement was 8-hydroxy-1, 3, 6-pyrenetrisulfonic acid tri sodium salt (HPTS) which was immobilised on the polyvinyl alcohol membrane on a polyester sheet. For accurate measurement of pH, calibration was done with the buffers having a salinity of 27, which is the condition *in-situ*. The buffers had pH values of 8.183, 6.868, and 6.048. For taking images, the buffers taken as a thin film were incorporated in between the sensing foil and the polyester sheet and the edges were thermally fused that created sealed and flexible thin film standard sheets. These were then mounted into the surface of the optical pressure window in the form of strips. The sensor foils were also attached to the pressure window. A layer of sea water was added in between the foil and window so that the bubbles do not interfere while taking the images. The pH was measured and the photographs were taken at regular intervals which were then converted into TIFF and JPEG and analysed in the image processing software.

The pH decreased down the sediment. This is because the organic matter was being degraded by the consumption of oxygen and release of CO₂ and organic acids were produced, resulting in a decrease in the pH (lower than 6.6 from 0.5 to 3cm depth). The oxidation of hydrogen sulphide, ammonium and ferrous ion into their acids further dropped the pH. The macrofauna activity reduces the pH. The pH dropped from 8 to 7 at depth of 0.5cm and drops to 6.2 at 1-1.5cm and the pH increased to 7.2 at the depth of 7cm. This increase is because of undisturbed marine sediments. In the spring the minimum pH observed was 6.2 while in winter it remained homogeneous (7.5-7.8). The overall range of the pH in Long Island Sound marine deposits was 6-8. (Yanzhen *et al.*, 2011).

Larsen *et al.* used HPTS as a fluorescent dye for measuring pH of marine sediments and modified the work by using a photographic technique. Sensors were photographed after exciting them with LEDs. They used Raw images and the calibration was done by taking the ratio between blue and red images which gave a sigmoid curve. ImageJ and another image processing software (available from the authors) were used for image analysis. Samples were analysed in an aquarium. (Larsen *et al.*, 2011)

Schröder *et al.* proposed a method for 2D pH mapping which includes a CCD camera, LED as an excitation source and a sensing membrane as optical transducer. The optode contains a lipophilic fluorescein derivative and platinum (II) mesotetrakis(pentafluorophenyl)porphyrin immobilised in a hydrogel mixture. Depending on the pH indicator used, pH 6-8 or 7-9 can be measured. Images were taken and these RAW images were used in image processing software to get the pH information. The sensor matrix polymer was prepared by dissolving the D4 hydrogel sample in a water/ethanol mixture, the pH indicator solution was added into the matrix to form a final cocktail. Titanium oxide was added into it to enhance the light scattering within the sensing layer. The solution was stirred for 12 h and then it was spread on the Mylar polyester foil to form the sensing membrane. (Schröder *et al.*, 2007)

Borisov *et al.* developed fluorescent poly (styrene-block-vinylpyrrolidone) Nano beads as an optical pH sensor. They stained the Nano beads with lipophilic pH indicators which were based on fluoresceins and 1-hydroxypyrene-3, 6, 8-trisulfonate. The desired pK_a value can be achieved by changing the substituent on the pH indicator. The sensor has pK_a values ranging from 5.6 to 7.7 and they claimed it could be applied to marine systems however practical evidence has not been shown (Borisov *et al.*, 2009).

Masuda *et al.* developed a pH indicator based immobilised gel sheet. The indicator, bromothymol blue was immobilised in a gel sheet which was made from a solution (TUPR-5, Kansai Paint, Japan) whose main constituent is polyethylene glycol. To this solution, 1% (v/v) photo initiator (PIR-1, Kansai paint, Japan) was added and then the solution was placed between two slides and was exposed to UV light of 365 nm for 10 seconds. The cover slide was removed carefully and the gel was immersed in the dye solution. After 24 hours, it was washed with some standard buffer solution. The calibration and the pH measurements were taken by photographing the response and using software to get YCrCb where Y is the brightness, Cr is red-difference and Cb is blue difference chroma (signal used in picture to convey the colour information separately from the accompanying luma (brightness) signal). RGB information

acquired by a CCD is influenced by the brightness. To reduce the brightness it was converted into YCrCb by using equations. (Masuda *et al.*, 2009)

1.11 Knowledge gap and the aim of the project

The pH of a marine sediment, as discussed previously, is an important parameter associated with the biogeochemistry of marine sediments but little is known about the pH profiles of marine sediments. This is due to the problems in the measurements of the pH profiles as discussed before in the literature review. pH glass electrodes have low resolution and are not useful for marine sediments and microelectrodes are expensive and break in the sediments as the insertion is blind and you never know what you are going to hit. The profiles can only be measured up to 50mm in the sediments using microelectrodes. Fluorescent based optical sensors require illumination and a fluorimeter or optical filter setup, making the process complicated and in some cases preparation of the sensing membrane takes a long time. The aim of the project is to make optical pH sensors that will be robust and will be very simple to manufacture and easy to use *in-situ* during a cruise. These sensors will be able to be applied to the accessible sea sites or salt marshes and will also be able to attach to SPI and the SPI will take the images of the responding sensor. Figure 1.8 shows how the sensors will be attached to the SPI faceplate. The SPI will take images of the sensor after its response to the pH. The Images will be processed using computer software to get the colour information, through which the pH will be determined using a calibration plot. The following schematic explains the methodology.

Develop a robust optical pH sensor for marine sediments



Calibrate it by taking Images in the lab under different pH conditions



Process images in software to get colour information, convert this into a calibration equation



Take measurements with SPI or in the sediment cores and take Images



Process the images in software and use the calibration equation to convert colour information into pH values

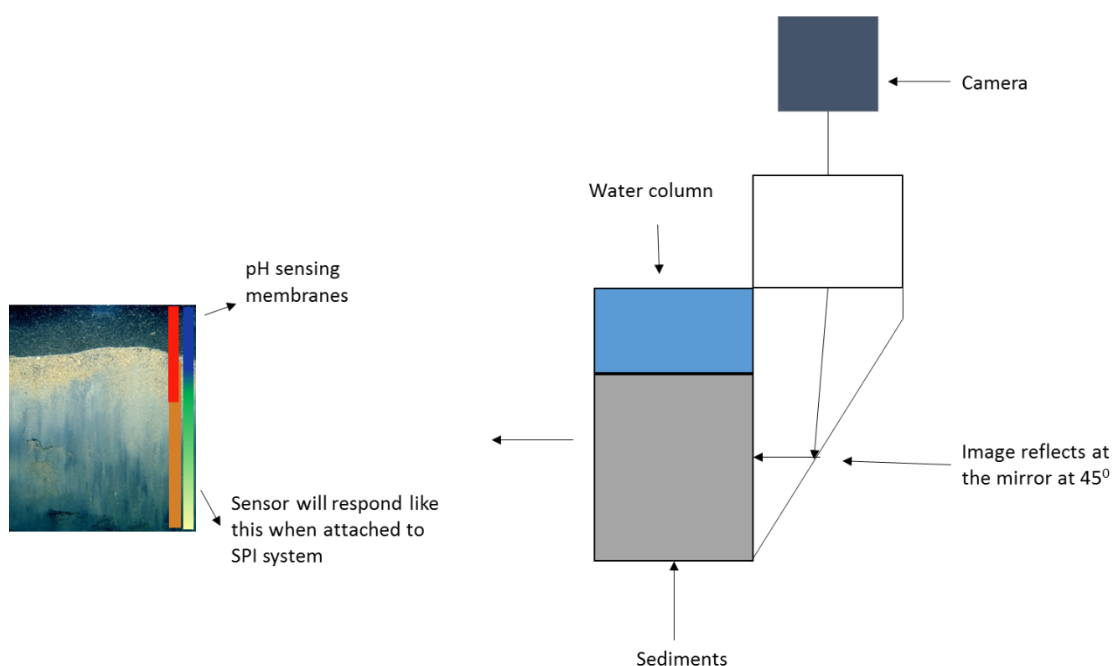


Figure 1.8: Schematic showing how the sensors will be attached to the SPI faceplate.

1.12 Dye Immobilization techniques

The immobilization technique can be non-covalent (mechanical, electrostatic, hydrophobic, sol-gel) or covalent.

1.12.1 Non-covalent Immobilization

(a) Hydrophobic interactions

Most of the dyes useful as pH indicators are at least partially water soluble and if dissolved in a lipophilic polymer, they tend to leach out. Thus all components are made lipophilic to make them soluble in a hydrophobic polymer and insoluble in the sample solution. This can be achieved by ion pairing. The water soluble dye and the water soluble ionic surfactant of opposite charge are dissolved separately in water and then both the solutions are mixed to obtain a precipitate that is polymer soluble. This may be good for dyes as many have large aromatic (conjugated) structures to give the visible colour and this is quite hydrophobic favouring retention in a hydrophobic membrane.

(b) Physical immobilization and Electrostatic immobilization

Mechanical or physical immobilization involves adsorption and including the dye in polymer spheres from which they cannot escape and dissolution in the solvents containing polymer. Although the technique is simple, the dye may wash out.

Electrostatic immobilization can be favourable if the polymer contains charged groups like sulfo, it can bind to a dye with the opposite charge. The indicators are either cations or anions and thus can be immobilized using this approach. Positively or negatively charged dyes can be ion-paired with the polymer of the opposite charge.

(c) Sol gel technique

The sol gel technique includes preparation of a glass in which dye can be incorporated. In a sol gel process inorganic matrices are formed via three steps. The components of the sol gel include precursors (e.g. tetramethoxysilane), water, acid or base as a catalyst, indicator and a solvent. Mixing them causes hydrolysis of ester, silanol-ester condensation and silanol-silanol condensation of the precursor. In the first step, "sol" is formed which is a colloidal suspension of solid particles in the liquid. Colloids have a diameter of 1-100 nm. The colloidal particles and condensed silica link to form a "gel" after a certain period (ageing). After the sol-gel transition, the solvent is removed. If solvent is removed by evaporation, "xerogels" are formed and if removed by supercritical evacuation, the product is an "aerogel". Sol-gel is ion-permeable and thus is very popular for sensor applications.

1.12.2 Covalent Immobilization

Chemical (Covalent) immobilization binds the dye firmly via a covalent bond to the polymer backbone thus it does not wash out. There is no leaching, crystallization or evaporation of components but the methods are very tedious. Reactive groups must be present on both dye and polymer and at least one must be activated for the chemical reaction. Often obtaining the indicator chemistry and polymers with functional groups requires a lot of effort. The chemical modification of dye can make it less selective and sensitive to the analyte. Two different ways are used for covalent immobilization. A reactive dye can bind to the reactive polymer or the reactive dye can be converted to a monomer and polymerised with other monomers to form the dye

polymer. Many reactive indicator dyes are available with isothiocyanate groups, sulfonyl chloride groups, succinimidyl groups, vinylsulfonyl groups and can be covalently attached to amino-PVC or other amino polymers. (Dakin and Culshaw (Eds.), 1997, J Mohr, 2006).

1.13 The role of components in dye immobilization in a plasticised polymer membrane

The physical entrapment of the dye (chromoionophore) in a polymer matrix involves a polymer, counter ion or ion-balance reagent, wetting agent and plasticizer. Once an appropriate dye has been chosen to sense a targeted specie, polymer chemistry plays an important role in developing the sensing membrane.

1.13.1 Polymer

Polymers, which are usually optically inert, are used as a solid support on which the indicator dyes are immobilized and also, they provide selective permeability for species of interest and thus reject some others. For optical use, polymer material has to fulfil some requirements such as the dye and all components should dissolve well along with the polymer and should not wash out. The polymer should be permeable for the analyte allowing it to diffuse fast. No crystallisation of indicator should occur in the polymer. It should be stable against ambient light, chemicals (acids and bases). It should be nontoxic. The choice of polymer can affect the response of the sensor. Some polymers like polystyrene and polyester display fluorescence under UV excitation but poly vinyl chlorides and poly vinyl alcohols are generally non-fluorescent. Many different types of polymers have been reported for optical use that can be used to immobilise the dye in different ways. Some of them are listed in the table 1.2.

Type of polymer	Examples	Properties	Applications
1. Lipophilic polymers	<p>Examples of lipophilic polymers are Poly (vinyl chloride), poly (methyl methacrylate), polystyrene derivatives, poly(vinyl acetate).</p> <p>Non polar lipophilic polymers are poly (ethylene vinyl acetate), poly (hexylmethacrylate), poly (dimethyl siloxane) and cis-polybutadiene</p>	<p>Polar lipophilic polymers have high glass transition temperature and are brittle. They require plasticizer to make them soft and more permeable.</p> <p>Nonpolar lipophilic polymers do not require plasticizers but are not good solvent for dyes and analytes. PVC is soluble in THF and cyclopentanone. Poly(methyl methacrylate), polystyrene and poly(vinyl acetate) are also soluble in ethyl acetate, ethylmethylketone or dichloromethane.</p>	Suitable for immobilisation of hydrophobic dyes.
2. Hydrophilic polymers	<p>Poly HEMA/HEA/HPA/HPMA , poly acrylamides, carbohydrates such as dextran, agarose etc.</p> <p>The acrylates and acrylamides can also be</p>	<p>In such a polymer matrix, ions can diffuse freely but the water intake causes swelling of the polymer leading to a change in the optical</p>	Suitable for immobilisation through covalent bonding and

	copolymerised with the monomers to introduce positive or negative charge.	properties of the sensor.	through co-polymerization.
3. Ionic polymers	Nafion, polystyrene sulfonates, triethylammonium methylcellulose, polyaniline, phosphine, polyallylamine.	These polymers have large dissociable groups.	Used for ion exchange chromatography and to exchange their counter ions with indicator ions.
4. Polymers used in sol-gel glass (the components are mixed to form a sol (colloids) that after a certain time form a gel).	Silicates, titanates can be doped with other components.	Sol gel is ion permeable and can be used in chemical sensing.	pH and ionic strength sensing(Lee and Asher,2000), oxygen sensing(Aubonn <i>et al.</i> , 2003),

Table 1.2: Types of polymers, their properties and use in sensors.

Plasticized PVC can be used for ion sensing (also pH sensing) which otherwise is not possible. PVC has been successfully used for optical sensing such as sulphur dioxide sensing (Alves *et al.*, 2005), copper (Ganjali, 2012), alcohol (Lau. *et al.*, 1999), mercury (II) (Mahajan *et al.*, 2013), strontium (Zamani *et al.*, 2008) etc. The useful plasticizers are dioctyl-phthalate, nitro-phenyl-octyl-ether, trioctyl-phosphate and similar long chain esters and ethers. Cellulose acetate has also been used in these immobilization

techniques. (Dakin and Culshaw (eds), 1997, Mohr, 2006). It is less hydrophobic than PVC.

1.13.2 Counter ion

The addition of a counter ion (with respect to the dye) in the matrix leads to an ionic balance to maintain the electroneutrality of the membrane by free exchange of the metal ions with protons during a pH change. For example, in the case of the basic pH dye congo red (L), tetraphenylborate Na^+R^- acts as a counter ion and forms a lipophilic complex with the hydrophilic protonated form (LH^+) of the dye and the reagent does not wash out.



While with bromothymol blue which is acidic, and a quaternary ammonium counterion ($\text{R}-\text{N}^+\text{R}_3$ shown here as R^+ is used in this case to maintain the electroneutrality.



After the deprotonation of the dye due to increasing pH, the counter ion forms a lipophilic complex $[\text{L}^-\text{R}^+]$ with hydrophilic anionic form and prevents the dye from leaching. (Wróblewski, *et al.*, 1998).

1.13.3 Wetting agent and Plasticizer

The wetting agent, e.g. ethylene glycol, enhances the hydrophilicity of the membrane. Once the solvent (in which all the components are dissolved) evaporates, the ethylene glycol may be miscible with the water or during conditioning may exchange with the water molecules. It also helps in speeding up the response. Hydrophilic plasticizers can decrease the response time. (Wróblewski, *et al.*, 1998). Polymers with high glass transition temperatures (T_g) are brittle and due to their high density of polymer chains, the ions cannot diffuse easily in the polymer matrix thus affecting the sensing capability. This problem can be solved by adding a plasticizer that makes the polymer flexible and allows the ion exchange. The response time of sensors can be affected by changing the type or amount of plasticizer. Some of the lipophilic plasticizers are bis(2-

ethylhexyl)sebacate, dibutyl sebacate, tris(2-ethylhexyl)phosphate and tris(2-ethylhexyl trimellitate) (Mohr, 2006). Phthalates (dioctyl phthalate, dibutyl phthalate) have also been widely used as plasticizers.

1.14 Standard methods of measuring pH of seawater

pH is a measure of activity of the hydrogen ions in a *dilute* or pure solution but in natural waters that have a salinity more than 5, the convention used to define chemical activity does not accurately estimate activity coefficients. pH of sea water therefore is measured on a concentration scale. Three concentration scales can be used to measure the pH- the free, total or seawater pH scale for which three different scale units are used which are molarity (mol L^{-1}), molality ($\text{mol Kg}_{\text{H}_2\text{O}}^{-1}$) or molinity ($\text{mol Kg}_{\text{soln}}^{-1}$). The free proton concentration is defined as: $\text{pH}_F = -\log \{[\text{H}^+]\}$

The total proton concentration is defined as

$$\text{pH}_T \approx -\log\{[\text{H}^+] + [\text{HSO}_4^-]\}$$

And the seawater proton concentration as

$$\text{pH}_{\text{SWS}} \approx -\log\{[\text{H}^+] + [\text{HSO}_4^-] + [\text{HF}]\}.$$

pH of seawater can be traced by the electrical potential of HCl in artificial sea water by the standard hydrogen and silver-silver chloride electrodes if calibrated properly. The pH of the real seawater cannot be measured by this method due to interference of fluoride and bromide ions with silver ions in the silver-silver chloride half-cell. Therefore as a standard, artificial seawater buffer solutions are used to measure the pH by spectroscopic or potentiometric methods.

1.14.1 Measurement of pH by potentiometry

In this method, hydrogen sensitive glass/reference electrodes calibrated using a seawater buffer are used to measure the pH of the seawater. The total hydrogen ion concentration includes the contribution from the medium ion sulfate and is defined as

$$\begin{aligned} [\text{H}^+] &= [\text{H}^+]_F (1+S_T/K_s) \\ &\approx [\text{H}^+]_F + [\text{HSO}_4^-] \end{aligned}$$

Where H_F is the free hydrogen ion concentration in seawater, S_T is the total sulfate concentration and K_s is the acid dissociation constant for HSO_4^- .

The operational pH is defined by the following expression

$$pH(X) = pH(S) + \frac{E_s - E_x}{RT \ln 10 / F}$$

Since buffers are made in the synthetic sea water thus there is minimum residual liquid junction error. The values of pH have been assigned to buffers made in synthetic seawater by doing measurements using cells without a liquid junction. (Dickson *et al.*, 2007)

1.14.2 Measurement of pH by spectroscopy

pH is determined by adding an indicator dye to seawater. For the sulfonephthalein indicators such as cresol purple, the following dissociation reaction takes place in seawater where I represents the indicator dye.



So the pH can be determined as follows

$$pH = pK[HI^-] + \log_{10} \frac{[I^{2-}]}{[HI^-]}$$

Since different forms of dye give different absorption spectra thus $[I^{2-}]/[HI^-]$ can be determined.

At an individual wavelength, λ , the measured absorbance in a cell with a path length, l , is given by the Beer–Lambert law as

$$\frac{A_\lambda}{l} = \varepsilon_\lambda(HI^-)[HI^-] + \varepsilon_\lambda(I^{2-})[I^{2-}] + B_\lambda + e$$

Where B_λ is the background absorbance of the sample and e is an error term due to instrumental noise. Provided that the values of the extinction coefficients: $\varepsilon_\lambda(HI^-)$ and $\varepsilon_\lambda(HI^{2-})$ have been measured as a function of wavelength, absorbance measurements made at two or more wavelengths can be used to estimate the ratio $[I^{2-}]/[HI^-]$.

If only two wavelengths are used and the background can be eliminated by a subtractive procedure, assuming no instrumental error, the equation can be rearranged to give

$$\frac{[I^{2-}]}{[HI^{-}]} = \frac{\frac{A_1}{A_2} - \frac{\epsilon_1(HI^{-})}{\epsilon_2(HI^{-})}}{\frac{\epsilon_1(I^{2-})}{\epsilon_2(HI^{-})} - \left(\frac{A_1}{A_2}\right) \epsilon_2(I^{2-})/\epsilon_2(HI^{-})}$$

Where number 1 and 2 are the wavelengths chosen. For the best sensitivity, the wavelengths corresponding to the absorbance maxima of the base (I^{2-}) and acid (HI^{-}) forms are used. The “ ϵ ” terms are the extinction coefficients of the specified species at wavelength 1 and 2.

For taking the measurement, the sample cell is warmed to 25 °C in a thermostated compartment. For *m*-cresol purple, the absorbance of cell plus seawater is measured at wavelengths 730 nm (non-absorbing wavelength), 578 nm (absorption maxima of the base form of dye) and 434 nm (absorption maxima of acid form of dye). About 0.05-1 cm³ of 2 mmol dm³ dye is added and shaken to mix the dye with sea water. The absorbances at the three wavelengths are measured again. The absorbances measured for the background (without dye) are subtracted from the absorbances measured with the dye. The absorbance measured at a nonabsorbing wavelength is used to monitor any baseline shift due to error in repositioning the cell. The measured shift is subtracted from the background corrected absorbances at wavelength 1 and 2 to get the final corrected absorbance for each wavelength

$$pH = pK_2 + \log_{10} \left(\frac{\frac{A_1}{A_2} - \frac{\epsilon_1(HI^{-})}{\epsilon_2(HI^{-})}}{\frac{\epsilon_1(I^{2-})}{\epsilon_2(HI^{-})} - \left(\frac{A_1}{A_2}\right) \epsilon_2(I^{2-})/\epsilon_2(HI^{-})} \right)$$

Where pK_2 is the acid dissociation constant for the species HI^{-} and A_1 and A_2 are the corrected absorbances, at the wavelengths corresponding to the absorbance maxima of the base and acid forms. (Waters, 2012 and Dickson *et al.*, 2007)

1.15 Photographing optical sensor responses

Digital cameras have become very inexpensive and most people have a camera in their smartphones. There is much interest in using camera as a universal transducer for all

types of chemical and biosensors for medical, industrial and environmental applications. Spectrophotometers cannot be used in some cases to measure the absorbance and response of the optical sensors due to size, cost, power, stability or other factors. However, in such cases the response of optical sensors might be photographed and the colour in the photographs can be translated into a mathematical value thus making it possible to convert the colour information into a calibrated sensor response.

The colour in photographs can be mathematically defined by the Red Green and Blue values which are known as the primaries in additive devices which in this case is a camera. In such devices, the colours are generated when the light sources that have different wavelengths are combined. By varying the intensities of these three primaries, any colour can be produced. For example the following colours are produced by combining the primaries.

Blue +Green= Cyan

Red +Blue= Magenta

Red +Green=Yellow

Red +Green +Blue= White (Trussell *et al.*, 2005)

Figure 1.9 explains the combination of colours.

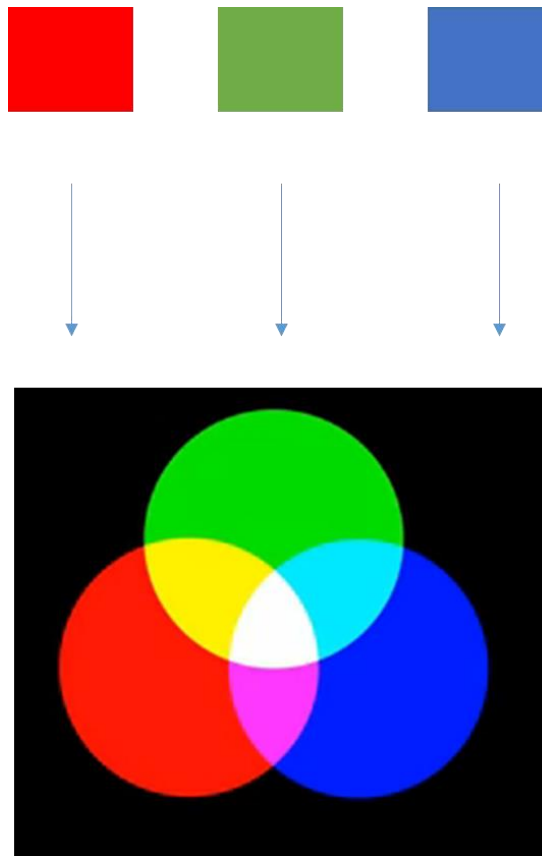


Figure 1.9: Colour addition in RGB systems.

Photographing the optical sensor response and getting results by analysing the photos using suitable software has previously been used for measurement of $p\text{CO}_2$ distribution in marine sediments (Zhu *et al.*, 2006 (b)), diagenetic studies of marine sediments using a pH fluorosensor (Hulth *et al.*, 2002); measuring the pH of marine sediments (Stahl *et al.*, 2006); oxygen and pH measurements from the Images of fluorosensor response (Larsen *et al.*, 2011 and Schröder *et al.*, 2007). An instrument CHEM-SPI has been previously developed by attaching the fluorosensors to the SPI to determine the pH of marine sediments using the Imaging approach (Fan *et al.*, 2011). These have been described in more detail previously in methods of measuring pH using fluorescent dyes.

While there is great enthusiasm for using the imaging approach to record the optical sensor's response, it turns out that it is much more difficult to apply it practically than it would at first appear due to variabilities in cameras, inability to control the auto settings, image processing, user variation, positioning of camera, positioning of sensor

and ill-defined lighting conditions. For this reason there have been few examples of simple absorbed or reflected colour measuring sensors in chemical measurements. Fluorescent systems relying on dual or multi-wavelength ratiometric methods have been more successful since they circumvent some of these problems. This produces other complications, however.

The key aim of this project was to develop robust optical pH sensors that can be photographed. To investigate any variabilities arising due to photographic technique and to solve these problems as much as possible to make the measurements reliable. Thus making it possible to translate the colour information in photographs into a pH value.

1.16 References

Aller, R. C. 1978 Experimental studies of changes produced by deposit feeders on pore water, sediment, and overlying water chemistry. *American Journal of Science* **278**, 1185–234.

Alves, F. L., Jr, M. R., Gimenez, I. F. & Alves, O. L. 2005 An organopalladium-pvc membrane for sulphur dioxide optical sensing. *Sensors and Aquators B: Chemical* **107**, 47-52.

Archer, D., Emerson, S. & Reimers, C. 1989 Dissolution of calcite in deep-sea sediments: pH and O₂ microelectrode results. *Geochimica et Cosmochimica acta* **53**, 2831-2845.

Aubonnet, S., Barry, H. F., Buelzingsloewen, C. V., Sebattie, J. M. & MacCraith, B. D. 2003 Photo-patternable optical chemical sensors based on hybrid sol-gel materials. *Electronics Letters* **39**, 913.

Bates, R. G. & Guggenheim, E. A. 1960 Report on the standardization of pH and related terminology. *Pure and Applied Chemistry* **1**, 163–168.

Batten, S. D. & Bamber, R. N. 1996 The effects of acidified seawater on the polychaete *Nereis virens* Sars, 1835. *Marine Pollution Bulletin* **32**, 283–287.

Berner, R. A. 1981 A new geochemical classification of sedimentary environments. *Journal of Sedimentary Petrology* **51**, 359-365.

Birchenough, S. N. R., Boyd, S. E., Coggan, R. A., Limpenny, D.S., Meadows, W. J. & Rees, H. L. 2006 Lights, Camera, Acoustics: Assessing macrobenthic communities at a dredged material disposal site off the north east coast of the UK. *Journal of Marine Systems* **62**, 204-216.

Borisov, S. M., Herrod, D. L., & Klimant, I. 2009 Fluorescent poly (styrene-block-vinylpyrrolidone) nanobeads for optical sensing of pH. *Sensors and Aquators B: Chemical* **139**, 52-58.

Burdige, D. J., Zimmerman, R. C. & Hu, X. P. 2008 Rates of carbonate dissolution in permeable sediments estimated from pore-water profiles: the role of sea grasses. *Limnology and Oceanography* **53**, 549–565.

Butcher, S. S., Charlson, R. J., Orians, G. H. & Wolfe, G. V. (Eds.) (1992). *Global biogeochemical cycles*. San Diego: Academic press limited. pp239-304.

Cai, W., Reimers, C. E. 1993 The development of pH and pCO₂, microelectrodes for studying the carbonate chemistry of pore waters near the sediment-water interface. *Limnology and Oceanography* **38**, 1762-1773.

Cai, W., Reimers, C. E. & Shaw. T. 1995 Microelectrode studies of organic carbon degradation and calcite dissolution at a California Continental rise site. *Geochimica et Cosmochimica Acta* **59**, 497–511.

Cai, W. & Reimers, C. E. 1999 The development of pH and pCO₂, microelectrodes for studying the carbonate chemistry of pore waters near the sediment-water interface. *Limnology and Oceanography* **38**, 1762-1773

Claypool, G. E., & Kaplan, I. R. (1974). *Natural Gases in Marine Sediments*. New York: Plenum Press. pp99-140.

Curtis, M. 2005 Review of Standards & Protocols for sediment Profile Imagery. *MESH-Action2.1*.

Dakin, J. & Culshaw, B. (Eds.) (1997). *Optical Fiber Sensors*. Vol.4. London: Boston-Artech House. pp53-107.

Dales, R. P., Mangum, C. P., & Tichy, J. C. 1970 Effects of changes in oxygen and carbon dioxide concentrations on ventilation rhythms in onuphid polychaetes. *Journal of the Marine Biological Association of the United Kingdom* **50**, 365–380.

Dashfield, S. L., Somerfield, P. J., Widdicombe, S., Austen, M. C. & Malcolm, N. 2008 Impacts of ocean acidification and burrowing urchins on within-sediment pH profiles and subtidal nematode communities. *Journal of Experimental Marine Biology and Ecology* **365**, 46–52

David, A., Emerson, S. & Reimers, C. 1989 Dissolution of calcite in deep-sea sediments: pH and O₂, microelectrode results. *Geochimica et Cosmochimica Acta* **53**, 2831-2845

Diaz, R. J. & Trefry, J. H. 2006 Comparison of sediment profile image data with profiles of oxygen and Eh from sediment cores. *Journal of Marine System* **62**, 164-172

Dickson, A. G. 1990 Standard potential of the reaction: $\text{AgCl}_{(s)} + 1/2\text{H}_2_{(g)} = \text{Ag}_{(s)} + \text{HCl}_{(aq)}$, and the standard acidity constant of the ion HSO_4^- in synthetic seawater from 273.15 to 318.15 K. *Journal of Chemical Thermodynamics* **22**, 113–127.

Dickson, A. G. 1993 The measurement of sea water pH. *Marine Chemistry* **44**, 131–142.

Dickson, A. G., Sabine, C. L., & Christian, J. R., (Eds.) (2007). *Guide to best practices for ocean CO₂ measurements*: PICES special publication 3, p191

Dupont, S. & Thorndyke, M. C. 2009 Impact of CO₂ -driven ocean acidification on invertebrate's early life history– what we know, what we need to know and what we can do. *Biogeosciences Discussion* **6**, 3109–3131.

Fan, Y., Zhu, Q., Aller, C. R. & Rhoads, C. D. 2011 An in situ multispectral imaging system for planar optodes in sediments: Examples of high-resolution seasonal patterns of pH. *Aquatic Geochemistry* **17**, 457-471.

Froelich, P. N., Klinkhammer, G. P., Bender, M. L., Luedtke, N. A., Heath, G. R., Cullen, D., Daulphin, P., Hammond, D., Hartman, B. & Maynard, V. 1979. Early oxidation of organic matter in pelagic sediments of the equatorial atlantic: suboxic diagenesis. *Geochimica Acta* **43**, 1075-1090.

Ganjali, M. R., Ghalfarloo, A., Faridbod, F. & Norouzi, P. 2012 Copper selective PVC membrane sensor. *International Journal of Electrochemical Science* **7**, 3706-3716.

Gattuso, J. P. & Hansson, L. (Eds.) (2011). *Ocean acidification*. Oxford: Oxford university press. pp176-187.

Gieskes, M. J., & Rogers, W. C. 1973 Alkalinity determination in interstitial waters of marine sediments. *Journal of sedimentary petrology* **43**, 272-277.

Gomez, E., Durillon, C., Rofes, G. & Picot, B. 1999 Phosphate adsorption and release from sediments of brackish lagoon: pH, O₂ and loading influence. *Water Research* **33**, 2437-2447.

Greenwood, N., Pearce, D., Parker, R., Kröger, S., Sivyer, D., Silburn, B & Powell, C. 2015 Assessing the spatial and temporal variability in carbon parameters in UK shelf seas. Poster presented at NERC UK Ocean Acidification programme science meetings.

Hakonen, A., Hulth, S., Dufour, S. 2010 Analytical performance during ratiometric long-term imaging of pH in bioturbated sediments. *Talanta* **81**, 1393–1401.

Hulanicki, A., Glab, S., Ingman, F., 1991 Chemical sensors definitions and classification. *Pure and Applied Chemistry* **63**, 1247-1250.

Henrichs, S. M. 1992 Early diagenesis of organic matter in marine sediments: progress and perplexity. *Marine Chemistry* **39**, 119-149.

Hulth, S., Aller, R. C., Engström, P. & Selander, E. 2002 A pH plate fluorosensor (optode) for early diagenetic studies of marine sediments. *Limnology and Oceanography* **47**, 212–220.

Janata, J. (2010). *principles of chemical sensors*. 2nd ed. U.S: Springer. pp1-2. Jørgensen, B.B The major biogeochemical cycles and their interactions. B. B., *scope* **21**.

Karakassis, I., Tsapakis, M., Smith, C. J. & Rumohr, H. 2002 Fish farming in the Mediterranean studied through sediment profiling imagery. *Marine Ecology Progress Series* **227**, 125-133.

Kenish, J. M. (2001). *practical handbook of marine science*. 3rd ed. U.S: CRC press. p1.

Komada, T., Reimers, C. E. & Boehme, S. E. 1998 Dissolved inorganic carbon profiles and fluxes determined using pH and PCO₂ microelectrodes. *Limnology and Oceanography* **43**, 769-781.

Lau, R. C., Choi, M. M, Lu, J. 1999 Alcohol sensing membrane based on immobilised ruthenium (ii) complex in carboxylated PVC and surface covalently bonded alcohol oxidase. *Talanta* **48**, 321-331.

Larsen, M., Borisov, S. M., Grunwald, B., Klimant, I. & Glud, R. N. 2011 A simple and inexpensive high resolution colour ratiometric planar optode imaging approach: application to oxygen and pH sensing. *Limnology and Oceanography-Methods* **9**, 348–360.

Lee, K. & Asher, S. A., 2000 Photonic crystal chemical sensors: pH and ionic strength. *Journal of the American society* **122**, 9564-9537.

Lyle, M. 1983 The brown-green colour transition in marine sediments: a marker of the Fe(III)-Fe(II) redox boundary. *Limnology and Oceanography* **28**, 1026-1033.

Mahajan, R. K., Kamal, A., Kumar, N., Bhala, V. & Kumar, M. 2013 Selective sensing of mercury(ii) using PVC based membranes incorporating recently synthesized 1,3-alternate thiacalix[4] crown ionophore. *Environmental Science and Pollution Research* **20**, 3086-3097.

Martens, C. S., & Berner, R. A. 1974 Methane production in the interstitial waters of sulphate depleted marine sediments. *Science* **185**, 1167-1169.

Masuda, T., Maruyama, H., Arai, F., Anada, T., Fukuda, T. & Suzuki, O. 2009 Development of a pH indicator immobilized-gel-sheet for microenvironment analysis. *Micro-nanomechatronics and human science, 2009. MHS 2009. International symposium on*, 362-367.

Mohr, G. J. (2009). *Polymers for optical sensors*. (Ed: Baldini, F., Chester, A. N., Homola, J. & Martellucci, S.) Netherlands: Springer. p298.

Millero, F. J, Zhang, J. Z , Fiol, S., Sotolongo, S., Roy, R. N., Lee, K., & Mane, S. 1993 The use of buffers to measure the pH of seawater. *Marine Chemistry* **44**, 143–152.

Millero, F. J., DiTrollo, B. Suarez, A. F. & Lando, G. 2009 Spectroscopic measurements of the pH in NaCl brines. *Geochimica et Cosmochimica Acta* **73**, 3109–3114.

Myers, R. (2003). *The basics of chemistry*. Westport, CT: Greenwood press. pp156-161.

Nilsson, H. C., Rosenberg, R., 2003. Effects on marine sedimentary habitats of experimental trawling analysed by sediment profile imagery. *Journal of Experimental Marine Biology and Ecology* **285-286**, 453-463.

O'Connor, B. D. S., Costelloe, J., Keegan, B. F. & Rhoads, D. C. 1989. The use of REMOTS technology in monitoring coastal enrichment resulting from mariculture. *Marine Pollution Bulletin* **20**, 384-390.

Pauling, L. (1970). *General chemistry*. San Francisco: W.H. freeman and company. pp486-487

Philp, R. B., 1999 Cadmium content of the marine sponge *Microciona prolifera*, other sponges, water and sediment from the eastern Florida panhandle: possible effects on *Microciona* cell aggregation and potential roles of low pH and low salinity. *Comparative Biochemistry and Physiology Part C* **124** , 41–49

Pörtner, H. O., Reipschläger, A., & Heisler, N. 1998 Acid-base regulation, metabolism and energetics in *Sipunculus nudus* as a function of ambient carbon dioxide level. *Journal of Experimental Biology* **201**, 43–55.

Pörtner, H. O., Bock, C., & Reipschläger, A. 2000 Modulation of the cost of pH regulation during metabolic depression: a P-NMR study in invertebrate (*Sipunculus nudus*) isolated muscle. *Journal of Experimental Biology* **203**, 2417–28.

Ohline, S. M., Reid, M. R, Husheer, S. L, Currie, K. I & Hunter, K. A. 2007 Spectrophotometric determination of pH in seawater off taiaroa head, otago, new zealand: Full spectrum modelling and prediction of pCO₂ levels. *Marine Chemistry* **107**, 143–155.

Reimers, C. E., Ruttenberg, K. C., Kanfield, D. E., Christiasen, M. B. & Martin, J. B. 1996 Porewater pH and authigenic phases formed in the

uppermost sediments of the Santa Barbara Basin. *Geochimica et Cosmochimica Acta* **60**, 4037-4057

Reipschlager, A., Nilsson, G. E. & Portner, H. O. 1997 A role for adenosine in metabolic depression in the marine invertebrate *Sipunculus nudus*. *American Journal of Physiology* **272**, 350–356.

Ries, J. B., Cohen, A. L. & McCorkle, D. C. 2009 Marine calcifiers exhibit mixed responses to CO₂-induced ocean acidification. *Geology* **37**, 1131–1134.

Revsbech, N. P., Ward, D. M., 1983. Oxygen microelectrode that is insensitive to medium chemical composition: use in an acidic microbial mat dominated by *Cyanidium caldarium*, *Applied and Environmental Microbiology* **45**, 755-759.

Chester, R. & Jickells, T. (2012) *Marine geochemistry*. U.K: John Wiley and Son Ltd. p1.

Rosenberg, R., Grémare, A., Amouroux, J. M. & Nilsson, H. C. 2003 Benthic habitats in the northwest Mediterranean characterised by sedimentary organics, benthic macrofauna and sediment profile images. *Estuarine, Coastal and Shelf Science* **57**, 297-311.

Rosenberg, R., Nilsson, H.C., Grémare, A. & Amouroux, J. 2003 Effects of demersal trawling on marine sedimentary habitats analysed by sediment profile imagery. *Journal of Experimental Marine Biology and Ecology* **285-286**, 465-477

Schröder, C. R., Weidgans, B. M. & Klimant, I. 2005 pH Fluorosensors for use in marine systems. *The Royal Society of Chemistry* **130**, 907–916.

Schröder, R. C., Polerecky, L., & Klimant, I. 2007 Time-resolved pH/pCO₂ mapping with luminescent hybrid sensors. *Analytical chemistry* **79**, 60-70.

Smith, C. J., Rumohr, H., Karakassis, I. & Papadopoulou, K. N. 2003 Analysing the impact of bottom trawls on sedimentary seabeds with sediment profile imagery. *Journal of Experimental Marine Biology and Ecology* **285-286**, 479-496.

Soetaert, K., Hoffmann, A. F., Middelburg, J. J., Meysman, F. J. R. & Greenwood, J. 2007 The effect of biogeochemical processes on pH. *Marine chemistry*. **105**, 30-51.

Solan, M. & Kennedy, R. 2002 Observation and quantification of in situ animal-sediment relations using time-lapse sediment profile imagery (t-SPI). *Marine Ecology Progress Series* **228**, 179-191.

Stahl, H., Glud, A., Schroder, C. R., Kliment, I., Tengberg, A., Glud, R. N., 2006 Time resolved pH imaging in marine sediments using luminescent planar optode. *Limnology and Oceanography: Methods* **4**, 336–345.

Toledo, M., 2013 A guide to pH measurements-The theory and practice of pH applications.

Trussell, H. J, Saber, E., & Vrhel, M. 2005 Colour image processing basics and special issue overview. *IEEE signal processing magazine* **22**, 14-22.

Waters, Jason F., 2012. Measurement of Seawater pH: A Theoretical and Analytical Investigation. *Open Access Dissertations* Paper 908.

Widdicombe, S., Dashfield, S. L., McNeill, C. L., Needham, H. R., Beesley, A. M., Øxnevad, S., Clarke, K. R. & Berge, J. A. 2009 Effects of CO₂ induced seawater acidification on infaunal diversity and sediment nutrient fluxes. *Marine Ecology Progress Series* **379**, 59–75.

Wenzhofer, F., Adler, M., Kohls, O., Hensen, C., Strotmann, B., Boehme, S. & Schulz, H. D. 2001 Calcite dissolution driven by benthic mineralization in the deepsea: In situ measurements of Ca²⁺, pH, pCO₂ and O₂. *Geochimica et Cosmochimica Acta* **65**, 2677–2690.

Westrich, J. T., & Berner, R. A. 1984 The role of sedimentary organic matter in bacterial sulfate reduction: The G model tested, *Limnology and Oceanography* **29**, 236-249.

Widdicombe, S. & Needham, H. R. 2007 Impact of CO₂ -induced seawater acidification on the burrowing activity of *Nereis virens* and sediment nutrient flux. *Marine Ecology Progress Series* **341**, 111–122.

Wroblewski, W., Rozniecka, E., Dybko, A. & Brzożka, Z. 1998 Cellulose based bulk pH optomembranes. *Sensors and Actuators* **48**, 471–475.

Wolaver, T. G., Zieman, J. & Kjerfve, B. 1986 Factors affecting short-term variability in sediment pH as a function of marsh elevation in a Virginia mesohaline marsh. *Journal of Experimental Marine Biology and ecology* **101**, 227-237.

Wood, H. L., Spicer, J. I. & Widdicombe, S. 2008 Ocean acidification may increase calcification rates, but at a cost. *Proceedings of the Royal Society B: Biological Sciences* **275**, 1767–73.

Wood, H. L., Widdicombe, S. & Spicer, J. I. 2009 The influence of hypercapnia and macrofauna on sediment nutrient exchange? *Biogeosciences* **6**, 2015–24.

Wood, H. L., Spicer, J. I., Lowe, D. M., & Widdicombe, S. 2010 Interaction of ocean acidification and temperature: the high cost of survival in the brittlestar *Ophiura ophiura*. *Marine Biology* **157**, 2001–13.

www.horiba.com/application/material-property-characterization/water-analysis/water-quality-electrochemistry-instrumentation/the-story-of-ph-and-water-quality/the-basis-of-ph/measuring-ph-using-a-glass-electrode/?L=23moist=18651moist=5744moist=5742moist=23209

www.mbhes.com/improvements_in_ph_measurement.htm

Yanzhen, F, Qingzhi, Z., Aller, R. C. & Rhoads, D. C. 2011 An In Situ Multispectral Imaging System for Planar Optodes in Sediments: Examples of High-Resolution Seasonal Patterns of pH. *Aquatic Geochemistry* **17**, 457 - 471.

Yao, W., & Byrne, R. H., 1998. Simplified seawater alkalinity analysis: Use of linear array spectrometers. *Deep Sea Research Part I: Oceanographic Research Papers*. **45**, 1383–1392.

Yingst, J. Y. & Rhoads, D.C. (1980) *Marine benthic dynamics*. (Ed: Tenore, K.R. & Coull, B. C.). Columbia: University of South Carolina Press. pp407-421.

Zamari, H. A., Ganjali, M. R., Norouzi, P. & Adib, M. 2008 *Materials science and engineering:C* **28**, 157-163.

Zhao, P. & Cai, W. 1999. pH polymeric membrane microelectrodes based on neutral carriers and their application in aquatic environments. *Analytica Chimica Acta* **395**, 285-291.

Zhao, C. W. & Yongchen, P. W., 2000 pH and pCO₂ microelectrode measurements and the diffusive behaviour of carbon dioxide species in coastal marine sediments. *Journal of Marine Chemistry* **70**, 133-148.

Zhu, Q. Z., Aller, R. C. & Fan, Y. 2005 High-performance planar pH fluorosensor for two-dimensional pH measurements in marine sediment and water. *Environmental Science and Technology Journal* **39**, 8906–8911.

Zhu, Q. Z., Aller, R. C. & Fan, Y. 2006 (a). Two dimensional pH distribution and dynamics in bioturbated marine sediments. *Geochimica Et Cosmochimica Acta*. **70**, 4933–4949.

Zhu, Q., Aller, C. R & Fan. Y. 2006 (b) A new ratiometric, planar fluorosensor for measuring high resolution, two-dimensional pCO₂ distributions in marine sediments. *Marine chemistry* **101**, 40-53

Chapter 2

Developing a pH sensor

2.1 Introduction

2.1.1 Selection of dyes

Likely pH values in marine sediments are in the approximate range 6-8, hence an indicator dye with a pK_a of about 7 would be ideal to give maximum sensitivity to change over the required range. The indicator must have a clear and easily visualised colour change over this range to allow for photographic monitoring. Bromothymol blue (pK_a : 7) and neutral red (pK_a : 6.7) were chosen as appropriate dyes for making marine pH sensing membranes. Both sense the pH in the range that is required for marine monitoring. Neutral red gives red and orange colours in acidic and basic media while bromothymol blue gives a better range of yellow, green and blue from acidic to basic media. There are many other dyes that have similar pK_a values for example bromoxylene blue, acid Alizarin violet N, aurin, benzaurin and calcein, but they were rejected because their structure suggested that they could also respond to redox changes thus possibly interfering with the pH sensing capability of the membrane under the variable redox conditions in a marine sediment. Calcein chelates metals and its fluorescence is highly sensitive to Ca^{2+} and Mg^{2+} at alkaline pH. It has been used for detecting Ca^{2+} and Mg^{2+} (Ntailianas and Whitney, 1964). Some other dyes become colourless in either acidic or basic medium which is not ideal for photographing. Many fluorescent dyes are capable of sensing the appropriate pH range but they need special experimental designs and lighting, which is difficult to handle and detracts from the simplicity of a visual colourimetric change. The structure and properties of selected dyes are summarised below.

(a) Bromothymol blue

Bromothymol blue, also known as Dibromothymolsulfonephthalein was first isolated in a colourless form by Orndorff and Cornwell (Orndorff and Cornwell, 1926). They thought it was a derivative of the lactone form. Its quinoid hydrated form is coloured and upon heating it converts back to its colourless form. The crystals are dark coloured

and contain two water of crystallisation. They pulverize to form a red coloured powder. It is soluble in water, ether, methyl alcohol and ethyl alcohol but it is less soluble in benzene, toluene and xylene. (Kolthoff, 2007)

Chemical/Dye Class: Sulfonephthalein

Molecular Formula: $C_{27}H_{28}Br_2O_5S$

Molecular Weight: 624.38

pH Range: 6.0 –7.6

Colour Change at pH: Yellow (6.0) to blue (7.6)

pK_a : 7.05 (± 0.05)

Physical Form: Light pink or cream coloured powder

Solubility: Sparingly soluble in water, benzene; soluble in ethanol, ether; insoluble in petroleum ether

UV-Visible (λ_{max}): 420 nm, 435 nm, 620 nm (Sabnis, 2007)

Structure:

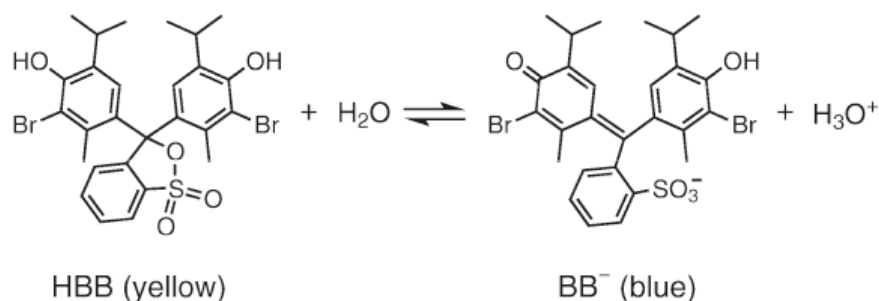


Figure 2.1: Acidic (yellow) and basic form (blue) of bromothymol blue showing the ionising group. A mixture of both species appears green (Klots *et al*, 2011).

Bromothymol blue belongs to a class of indicators known as ‘sulphonephthalein’. Phenol red (pK_a 8 at 20 °C) is the parent compound of this class. Figure 2.1 shows different forms of bromothymol blue and figure 2.2 shows different forms of phenol red (parent compound).

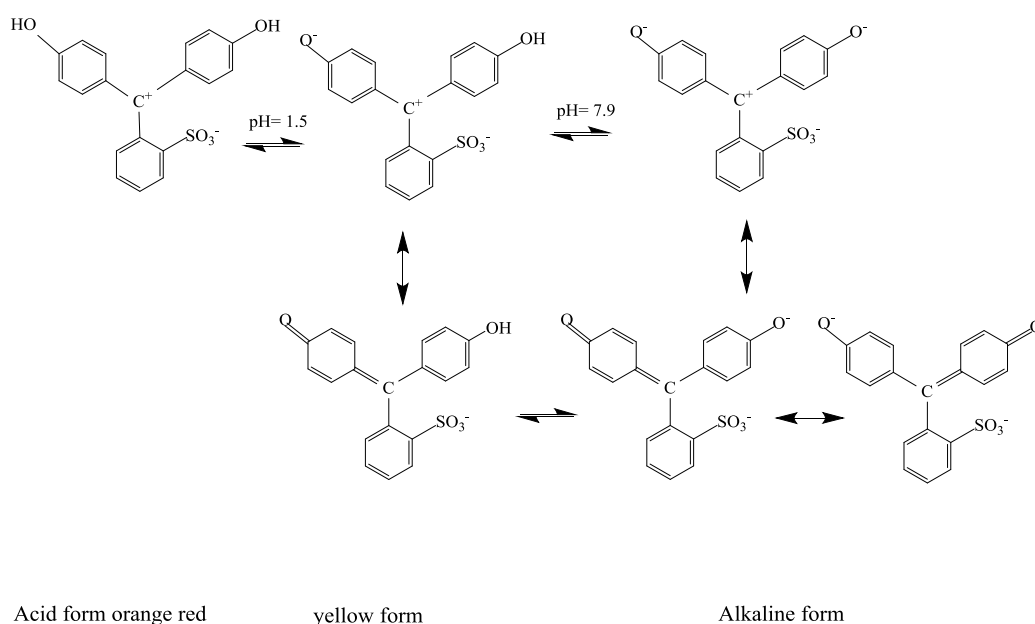


Figure 2.2: Different forms of phenol red (parent compound of bromothymol blue).

In phenol red, an asymmetrical structure is formed from a symmetrical structure by splitting off of a proton. The splitting off of a second proton again forms a symmetrical structure. The gradual dissociation is caused by the charge which remains on the molecule after the first proton gets dissociated. The oxygen group formed is a better donor for the central carbon atom than the hydroxyl group, therefore a one-sided quinonoid structure is formed. The dark red colour (alkaline form) is formed after the dissociation of a second proton and two alternative quinonoid ring systems represent it. The symmetrical structures are more stable than the asymmetrical ones and their light absorbance shifts towards the longer wavelength. Halogen substitution influences the proton binding capacity of the acid form and also the wavelength of the absorption maximum of the colour. The halogen substitution in the phenolic ring shifts the pH transition interval to the lower pH values therefore bromothymol blue has lower pK_a value than its parent compound. (Bishop, 1972). Bromothymol blue might be responsive to redox reactions but no evidence has been reported before.

(b) Neutral red

Chemical/Dye Class: Miscellaneous, Azine

Molecular Formula: $C_{15}H_{16}N_4 \cdot HCl$

Molecular Weight: 288.78

pH Range: 6.8–8.0

Colour Change at pH: Red (6.8) to yellow (8.0)

pK_a 6.7

Physical Form: Dark green or brownish-black powder

Solubility: Soluble in water, ethanol; practically insoluble in xylene

UV-Visible (λ_{max}): 540 nm, 533 nm, 544 nm, 529 nm, 454 nm (Sabnis, 2007)

Structure:

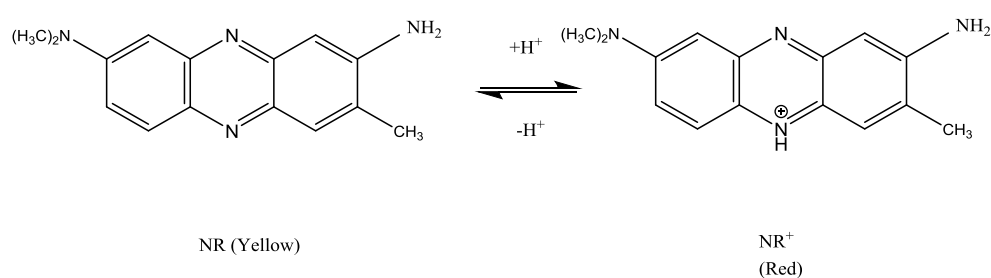


Figure 2.3 Protonation reaction of neutral red showing the protonated form in the acid (red) and neutral form (yellow) in base.

The protonation neutral red results in a positive charge on nitrogen and it appears red in acid solution. Neutral red can be sensitive to redox changes. Its redox potential at pH 7 is -0.34 volt and at pH 5 it is -0.20 volt. (Swan and Felton, 1957) It was used for immobilisation and optimisation in the beginning of this work, however later, only bromothymol blue was used.

2.1.2 Materials and Methods

Phosphate buffers

To check the response of bromothymol blue as a pH dye, Sørensen's phosphate buffers of pH values ranging 5.8 to 8.1 were prepared.

Stock solutions: A: 0.05 M $\text{NaH}_2\text{PO}_4 \cdot 2\text{H}_2\text{O}$ B: 0.05 M $\text{Na}_2\text{HPO}_4 \cdot 12\text{H}_2\text{O}$

The two stock solutions were mixed with appropriate volumes to get 12 solutions of different pH values (Dawson, 1986). The pH was measured using a Fisher Scientific AB15 pH meter with glass membrane and a temperature probe.

2.1.3 Response of bromothymol blue in phosphate buffer

1 mM bromothymol blue solution was made by mixing 62.4 mg of bromothymol blue in water to make volume 100 ml, 0.5 ml of 0.05M Na₂HPO₄.12H₂O was added to aid dissolution. The phosphate buffers made as explained above were taken in 12 cuvettes. One ml of buffer solution and 1 ml of dye solution were taken per cuvette and the solutions analysed in a UV visible Hitachi U-3000 spectrophotometer. 1 ml of buffer and 1 ml of distilled water was taken as a reference. Wavelength was scanned between 350 nm and 800 nm. The stock dye sample had too high absorbance so it was further diluted by five folds.

The cuvettes were also photographed with a camera (Canon EOS 600D) using the automatic mode setting on the camera and analysed using “Image j” software (Rasband, 1997-2014) to extract Red Green Blue (RGB) values from the area representing the dye solution. To do this, the image was opened in ImageJ. The section of the photo to be measured was selected using the rectangle tool and the selection was scaled to one pixel (height: 1, width: 1) by choosing the scale option from the ‘Image’ drop down menu. This opens the image selection in a new window that averages the selected area into a unit pixel. This makes the area constant each time a new selection is made. By clicking the ‘plugin’ drop down menu and ‘Analyse’, the RGB values can be measured. The results were saved as an excel file by clicking ‘save as’ on the results window. The same basic procedure was used to extract all RGB colour values from selected photo areas during this work.

2.1.4 Response of neutral red in phosphate buffer

The experiment was repeated using neutral red as a dye. 1 mM dye solution was made without adding the phosphate buffer, then further diluted 10 folds (i.e. 0.1 mM). The response was observed in 12 phosphate buffer solutions. Samples were photographed and measured in the UV-visible spectrophotometer. The photos were used with ImageJ to extract the RGB values from the colour response at each pH value.

2.1.5 Dye immobilization in a membrane

(a) Bromothymol blue (BTB) immobilization

The dye was immobilised in cellulose acetate. The following were dissolved in 3 mL tetrahydrofuran in a screw-top vial. 0.02 M of the dye were taken and 0.05 M of Cetyl trimethyl ammonium bromide were taken.

Component	Amount	Function
Bromothymol Blue	12.5 mg	Dye
Cetyl trimethyl ammonium bromide(CTAB) or Tetraoctyl ammonium bromide (TOAB)	20 mg 44 mg	Counter ion
Cellulose acetate	74 mg	Polymer
Bis(2-ethyl hexyl) sebacate	56 mg	Plasticizer
Ethylene Glycol	37.5 mg	Wetting agent
THF	3 mL	Solvent

Table 2.1: Amount and function of the membrane components.

The mixture was dissolved using a combination of sonication, heating in hot water and magnetic stirring. The molar ratio of dye: counter ion was 1: 2.5. 0.02 moles of dye and 0.05 moles of CTAB were taken. When the counter ion was changed, the molar ratio of dye: counter ion was 1:7.14 and 0.14 moles of TOAB were taken.

(b) Membrane formation

250 μ L solution was spread on a polyester plastic sheet (photocopier transparency sheet bought from local store) and on microscopic glass slides using a homemade wire wrapped metering bar. The membrane was formed after drying, which adhered onto the plastic as it dried and the plastic was cut into small pieces and put into 12 cuvettes containing 1 mL water+ 1 mL phosphate buffer solutions of pH: 5.82, 6.11, 6.27, 6.59, 6.64, 6.86, 7.06, 7.26, 7.54, 7.066, 7.99 and 8.13. The UV-Vis spectra were measured with the light passing through the membrane. The membranes were also photographed *in-situ* in the buffers.

(c) Neutral red immobilization

The same composition of solution was used as for BTB but the counter ion was replaced with Sodium tetra phenyl borate due to the positive charge of the dye. Initially, 1: 1.36 ratio (dye: counter ion) was taken. A glass slide was used to spread the solution. This gave a more homogeneous layer of membrane than the metering bar. The membrane pieces were kept in phosphate buffer solution of pH 8.13 and 5.8. The experiment was repeated by taking 1: 3.94 (dye: counter ion ratio). The composition given in table 2.2 was used.

Component	Amount	Function
Neutral red	5.8 mg	Dye
Sodium tetraphenylborate	27 mg	Counter ion
Cellulose acetate	74 mg	Polymer
Bis(2-ethyl hexyl) sebacate	56 mg	Plasticizer
Ethylene Glycol	37.5 mg	Wetting agent
THF	3 mL	Solvent

Table 2.2: Amount and function of the membrane components.

Five phosphate buffer solutions of pH 5.82, 6.25, 6.86, 7.54 and 8.13 were taken in five cuvettes each containing a piece of membrane. The response was photographed and the UV-vis spectrum was measured.

2.2 Results and Discussions

2.2.1 The response of BTB in buffer solution

Bromothymol Blue (BTB) showed good variation of colour with increasing pH, yellow in acidic solution, green in neutral and blue in basic medium (figure 2.4).



Figure 2.4: BTB response with increasing pH (left to right pH: 5.8, 6.0, 6.2, 6.5, 6.6, 6.8, 7.0, 7.2, 7.4, 7.5, 7.8 and 8.0)

Figure 2.5 shows the UV spectrum of bromothymol blue at different pHs.

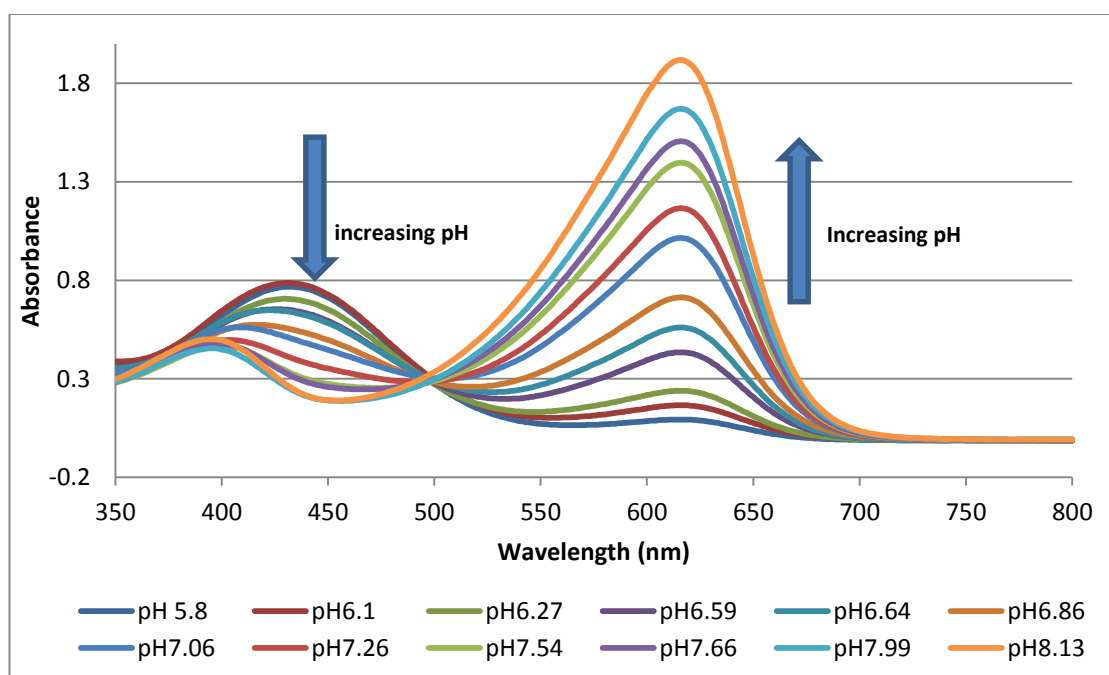


Figure 2.5: UV-Vis spectrum of Bromothymol blue.

Figure 2.5 shows two peaks, At pH 5.8 the spectrum has one higher peak with λ_{max} 438 nm. On increasing pH, intensity at 438 nm drops and peak appears with λ_{max} 620nm.

RGB values after analysing in Image J are listed in table 2.3.

pH	Red	Green	Blue
5.8	137	141	37
6.11	117	131	35
6.27	117	141	55
6.59	86	122	60
6.64	75	112	79
6.86	62	100	89
7.06	51	83	88
7.26	46	80	101
7.54	55	82	118
7.66	51	76	117
7.99	46	70	124
8.13	40	62	114

Table 2.3: RGB values taken from ImageJ for the photographs of BTB membranes equilibrated in buffers of varying pH

The values given in table 3 were plotted in a bar graph to compare and visualise the response (figure 2.6).

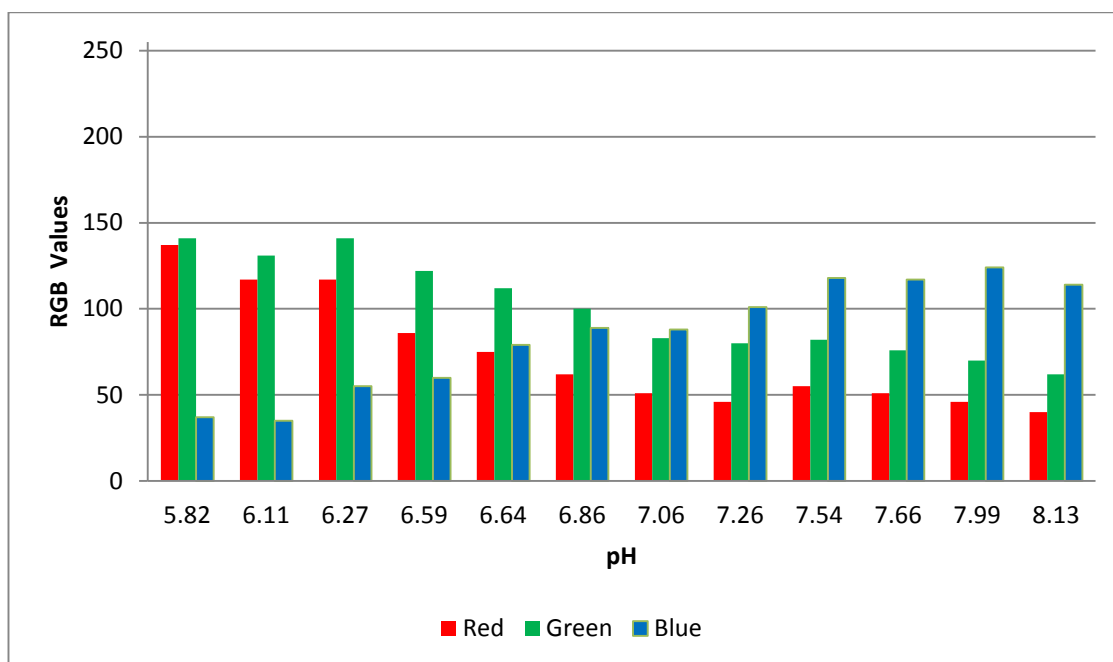


Figure 2.6: RGB values measured with image J for BTB at pH values stated.

Figure 2.6 clearly shows higher green values at first and then lower green values as the blue value increases with high pH and the colour changes from yellow to green and then blue. There is more green and red in the acidic samples that look yellow because red and green add up to give yellow. In the middle of the graph, where the pH is close to neutral, the red value goes down and green and blue add up to give green shades where green is either equal to the blue or more than blue. As green and blue add up to give Cyan, the colour in basic solution becomes blue. When green and blue add up, red significantly goes down so the yellow colour vanishes and depending on the values of green or blue the colour in the photograph looks either green or blue i.e. higher green values give a green colour and higher blue values give a blue colour.

It can be seen in figure 2.6 that the blue and red values vary more than the red value. Therefore to convert three values into a single number that would define the colour, a single mathematical formula can be used keeping blue and red in the nominator (As they are varying more than green) and the green value in the denominator to normalise. Two simple formulas $(R-B)/G$ and $(R+B)/G$ were used to get a single value called the colour index value which defined the colour. The red green and blue values

are given in the table 2.3. The colour index values were plotted against the pH values in figure 2.7.

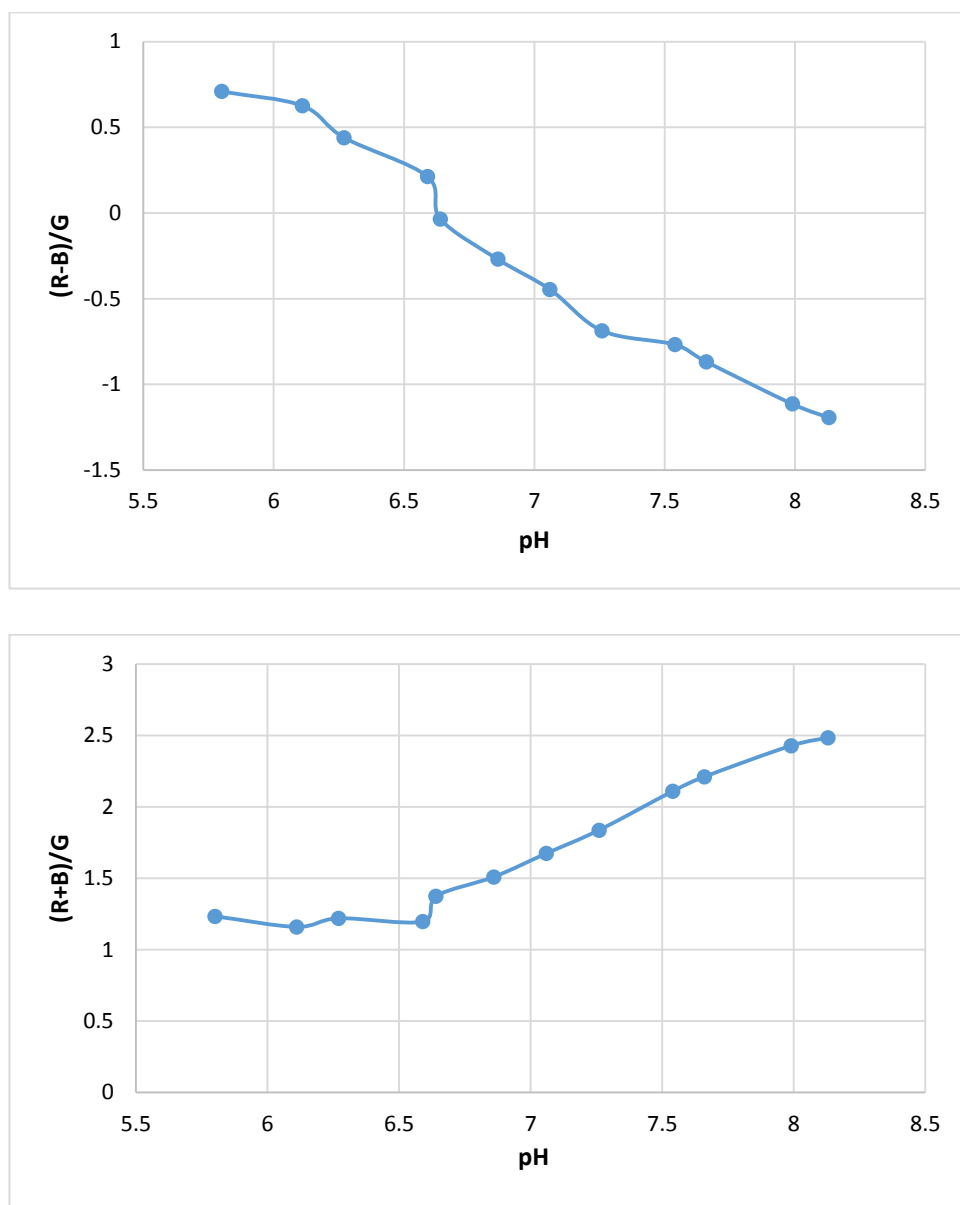


Figure 2.7: (a) Colour Index values plotted against pH obtained by applying the formula (a) $(R-B)/G$ and (b) $(R+B)/G$.

As seen in figure 2.7a and b, the trend is completely opposite when the red and blue values are subtracted or added. Colour index values decrease with increasing pH when red and blue values are subtracted and increase when they are added. Both the graphs define the colour change well. However the formula $(R-B)/G$ was used in this work to define the colour index.

2.2.2 Response of neutral red in buffer solution

Neutral red shows a good colour response between red and orange. It is red in acidic medium and orange in basic medium. (Figure 2.8)

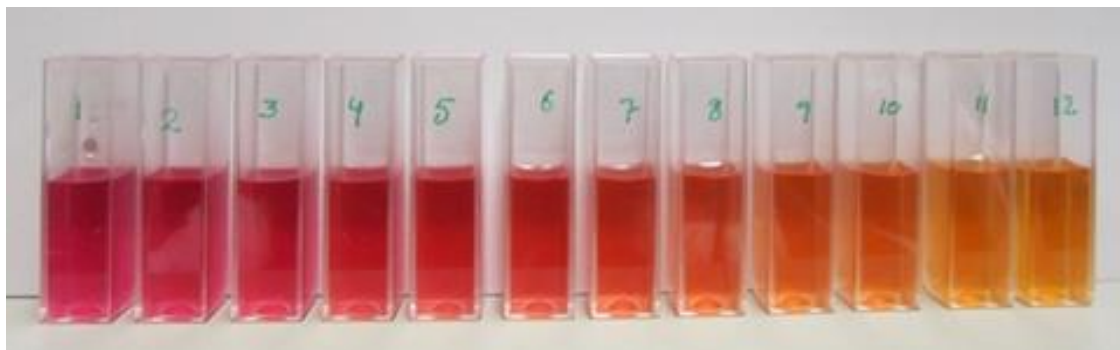


Figure 2.8: Neutral red response to increasing pH (left to right 5.8, 6.1, 6.27, 6.59, 6.64, 6.86, 7.06, 7.26, 7.54, 7.66, 7.99 and 8.13)

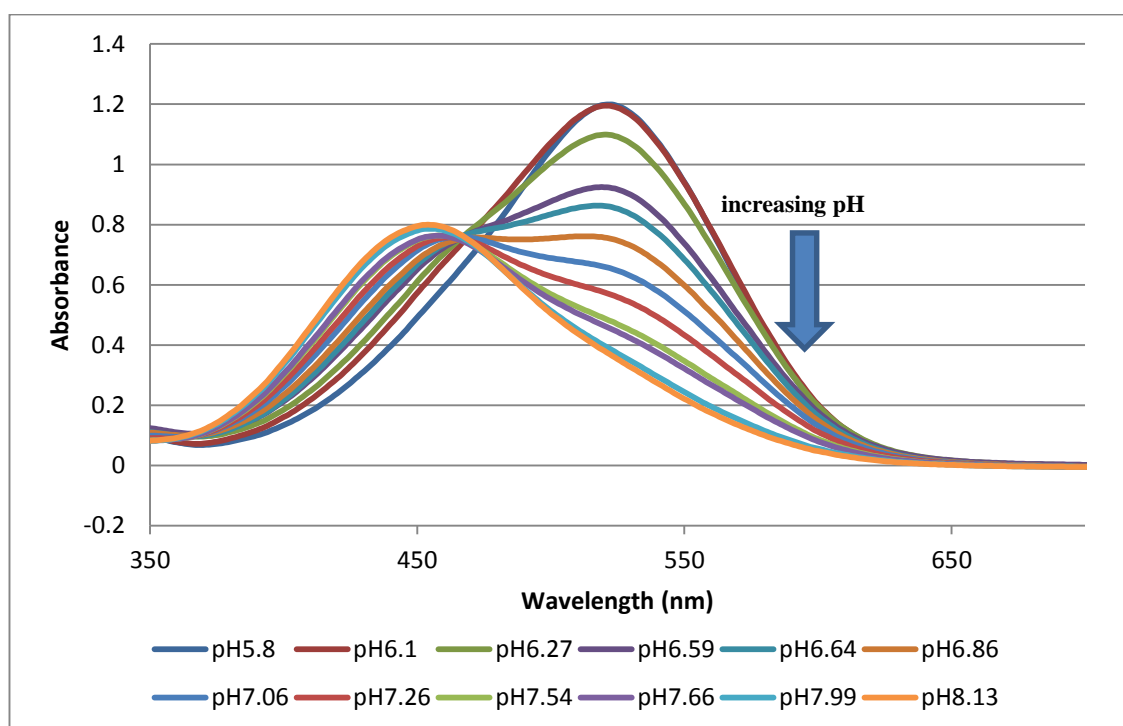


Figure 2.9: UV visible spectra for neutral red at pHs 5.8, 6.1, 6.27, 6.59, 6.64, 6.86, 7.06, 7.26, 7.54, 7.66, 7.99, 8.13)

In acidic buffer the dye has a red colour which gives a peak at wavelength 523 nm but the peak gradually disappears as the pH increases and the dye becomes orange which gives a peak at 470 nm.

The red green and blue values were taken from ImageJ. Table 2.4 and the figure 2.10 shows the RGB values with increasing pH.

pH	Red	Green	Blue
5.8	164	32	58
6.1	168	42	61
6.27	172	39	53
6.59	171	29	36
6.64	169	30	33
6.86	175	37	31
7.06	180	48	33
7.26	184	63	40
7.54	184	65	24
7.66	176	63	19
7.99	182	82	17
8.13	175	82	15

Table 2.4: RGB values of neutral red response taken from photographs using ImageJ.

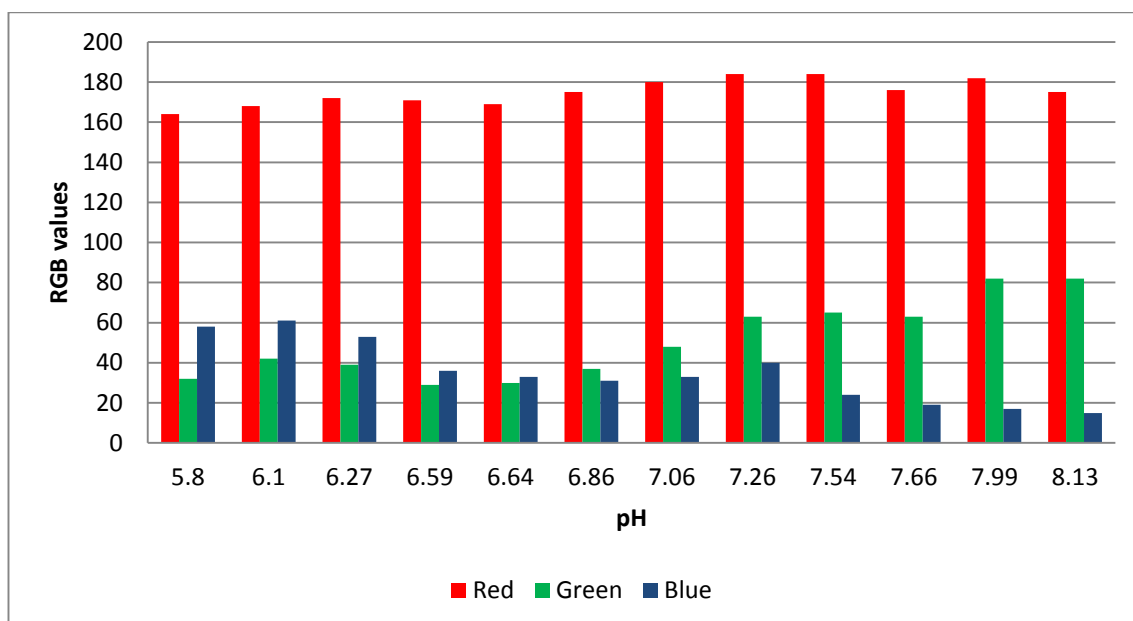


Figure 2.10: Colour response of neutral red represented as RGB values vs pH

Since neutral red is red in acidic solution, we expect the red and blue values to be higher at this point because red and blue add up to give magenta while at the right hand side of the graph the blue value decreases and the green raises up as the colour changes to orange. Since orange is close to yellow colour and green and red add up to give yellow colour, Figure 2.10 explains it very well.

2.2.3 Dye immobilization using cellulose acetate

(a) Bromothymol blue Immobilization

For this formulation (table 2.1), it was difficult to get all the components dissolved and the CTAB precipitated within the membrane formulation solution once the solution cooled down. This made the membrane inhomogeneous. The response was limited to certain spots within the membrane. Glass is not a good base to spread the membranes on because the membrane did not adhere well and peeled off when inserted into solutions. CTAB was replaced with tetraoctyl ammonium bromide (TOAB), which gave a nice homogenous membrane and there was no issue of precipitation as there was with CTAB when inserted in buffer (figure 2.11). The membrane responded quickly the first time it was exposed to buffer but did not reverse quickly when the buffer in the cuvette containing the membrane was changed.

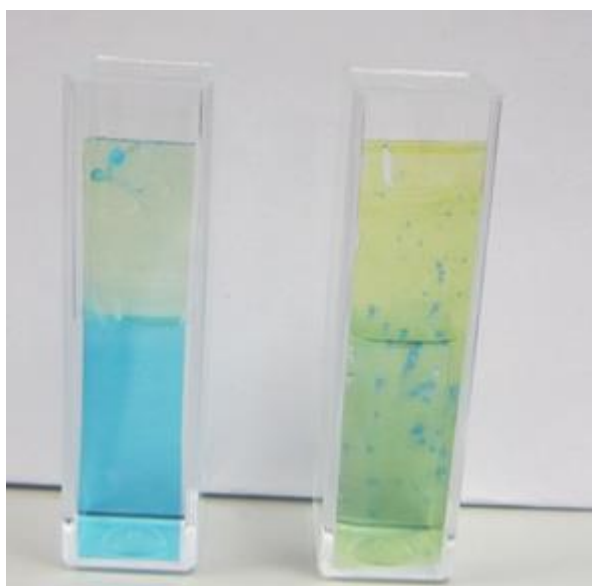


Figure 2.11: Membrane formulated using CTAB (Right) and TOAB (left) in phosphate buffer (pH8.13)

The UV-vis spectrum of the sensing membrane formulated using TOAB is given in figure 2.12. There is a peak at 640 nm. There is a slight shift of wavelength after immobilising the dye. A free dye spectrum has a peak at 620 nm. The buffer in the same cuvette was changed from pH 8.13 to pH 5.82 and a time scan was taken at a fixed wavelength of 640nm. The response was extremely slow. The membrane responded and converted from blue to yellow in 10 days. The spectrum was taken again once it reversed completely.

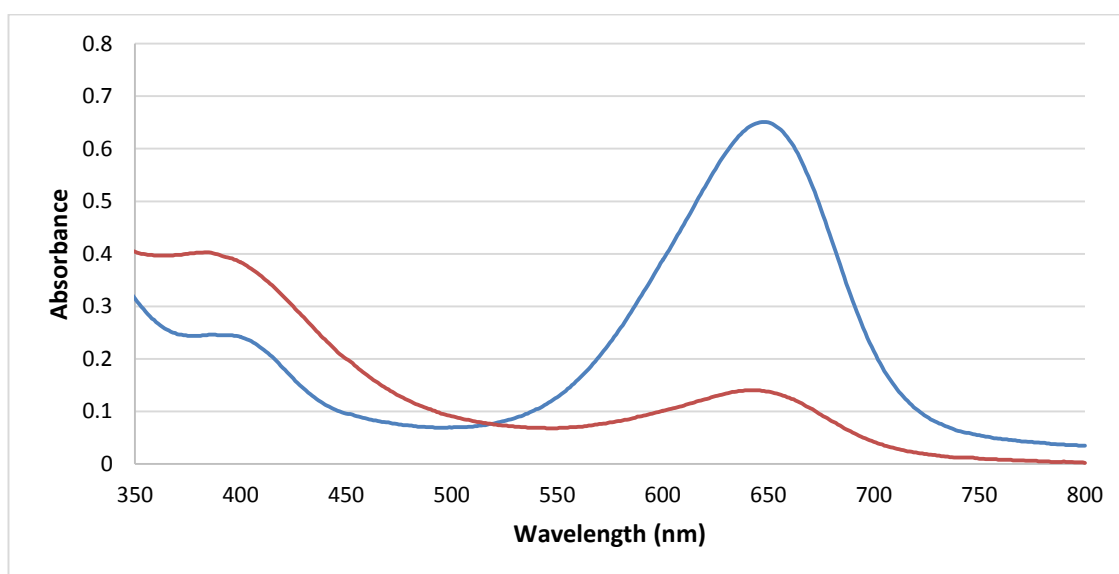


Figure 2.12: UV-vis spectrum of BTB membrane at pH 8.13(blue) and after reversing completely to 5.8 (red)

As indicated in figure 2.12, the absorbance decreased at 640 nm from 0.63 to 0.17 and increased at 400 nm, consistent with the spectral changes expected in going from basic to more acidic indicator colour, but the extremely slow response was not anticipated and the absorbance peak at 640 nm was not completely lost.

2.2.4 Response of BTB membrane in a series of phosphate buffer solutions

When TOAB was used as a counter ion and the response of the membrane was studied in a series of phosphate buffer solutions. It was surprising that the membranes appeared blue in all the solutions regardless of whether the solution was acidic or basic. It should have been yellow in the acidic solution, green in neutral and blue in acidic solution. The cuvettes were covered with parafilm and left for two days. The colour changed from blue to green. On the fourth day, the spectra were measured when the membrane seemed to have been equilibrated.

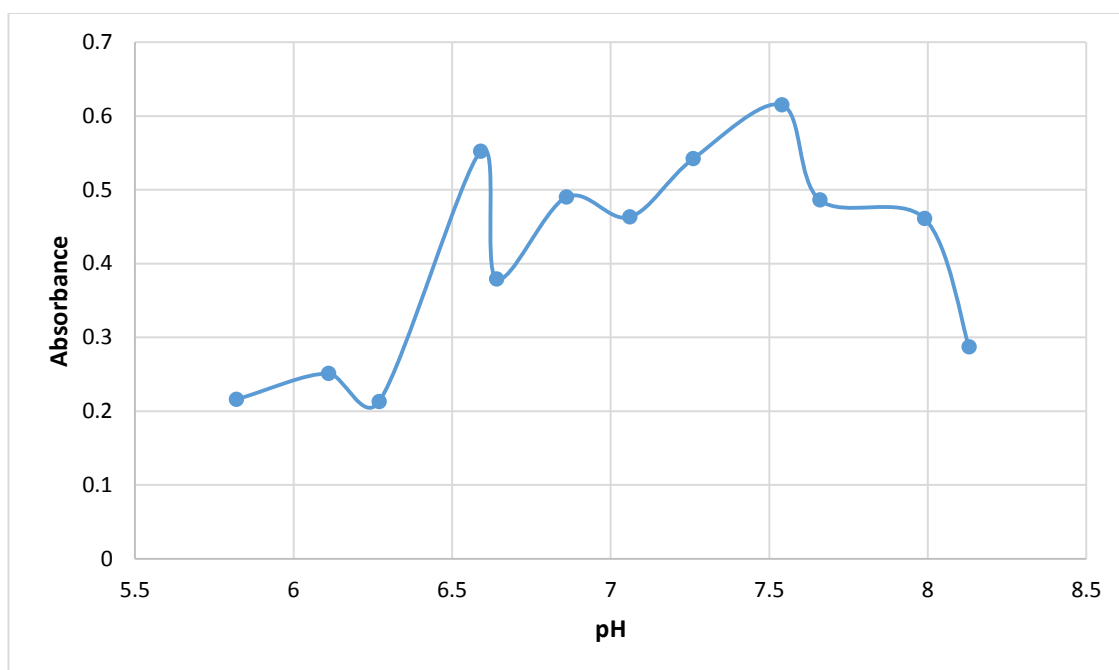


Figure 2.13: Absorbance at 640nm Vs pH of BTB membrane in phosphate buffer (some of the membranes did not equilibrate completely).

Since all the membranes had not equilibrated completely, a clear trend of increasing absorbance with increasing pH cannot be seen in some of the membranes (figure 2.13).

2.2.5 Response of neutral red membrane in phosphate buffer solution

The membrane did not respond quickly. It was left for a day. It was observed next day that the dye had leached out. The membrane was checked in some fresh buffer solution to see if the dye continued to leach out. It was observed that the dye continued to leach out. The experiment was repeated by taking 1: 3.94 ratios of dye: sodium tetraphenyl borate but the response was still slow. After two days the membrane was photographed and spectra were measured, but the membrane still had not equilibrated completely. There was less leaching of dye as compared to the first experiment where 1: 1.36 ratio of dye: sodium tetraphenyl borate were taken.

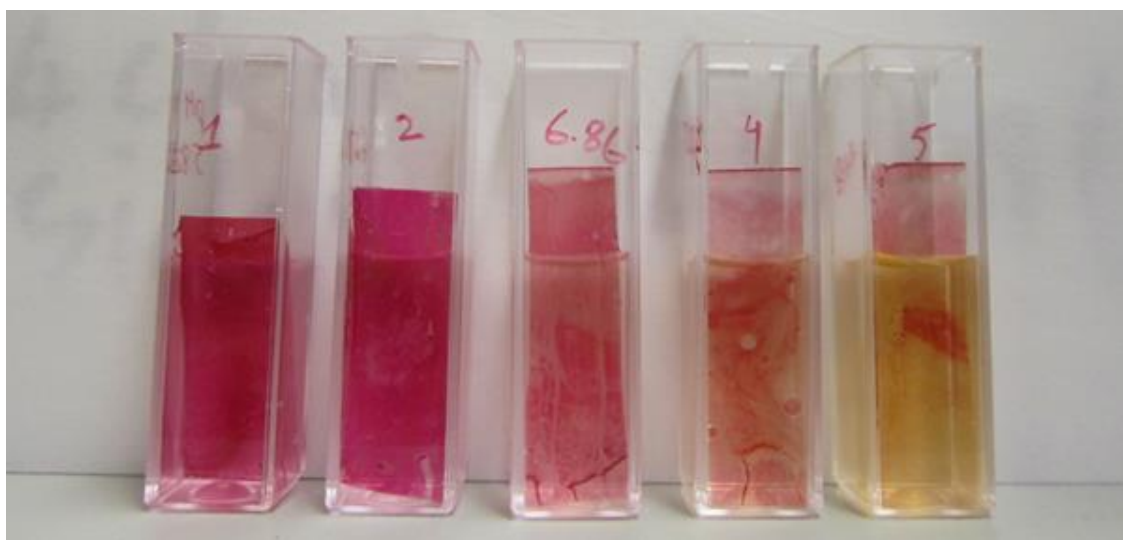


Figure 2.14: Image of neutral red membrane in a series of buffer solutions (pH from left to right: 5.82, 6.27, 6.86, 7.54, and 8.13) showing the leaching of dye.

The leaching of dye can be observed in photograph (figure 2.14). The UV-vis spectrum of neutral red membrane is shown in figure 2.15.

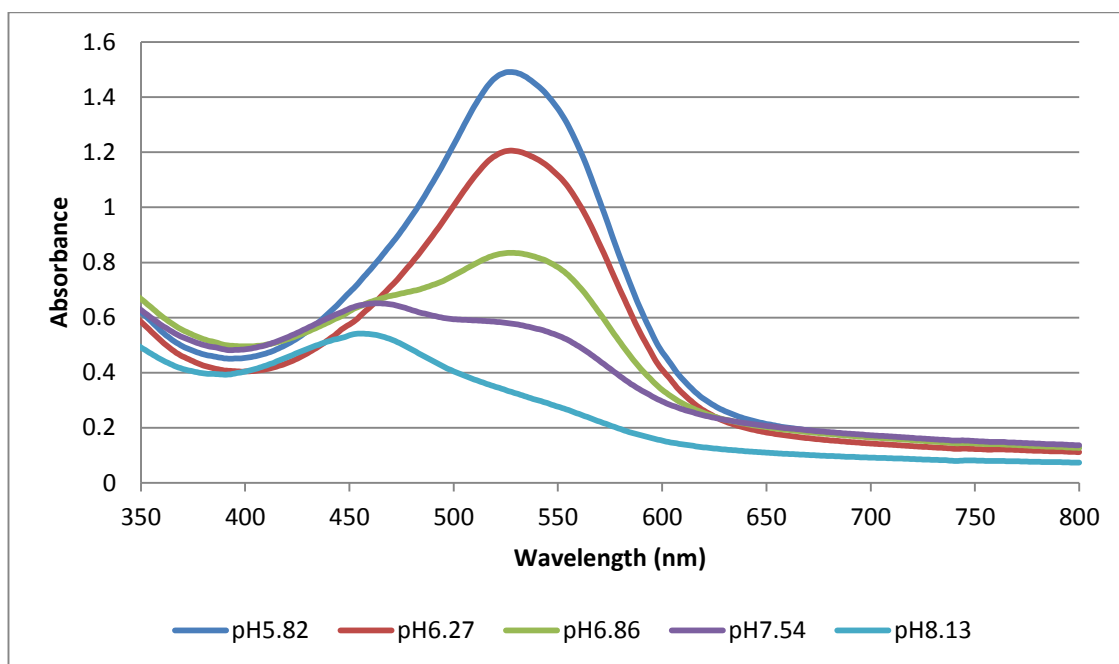


Figure 2.15: Neutral red membrane spectrum in phosphate buffers at different pH values.

The peak shifted from 523 nm (in the free dye solution) to 530 nm (membrane) for acidic buffer but the spectrum changed in the expected way and showed the difference in absorbance due to pH response, but this could be because of the free dye that leached out of the membrane, so the membrane needed to be optimised to improve response time and prevent dye leaching.

2.3 Conclusions

The following conclusions can be drawn:

- Suitable dyes have been selected for marine pH monitoring, which have pK_a values giving colour changes in the pH range that is expected in the marine environment.
- The spectra and the colour properties of the dyes have been obtained.
- The dyes have been immobilised in cellulose acetate but the membrane still needs to be optimised for a fast reversibility and the dye leaching has to be controlled.
- A computer software package, ImageJ, has been chosen to extract the colour information.
- The colour information from the photos has been taken successfully in the form of RGB values but it still needs a method to plot the RGB information against pH, so that pH can be inferred from the extracted RGB values.

2.4 References

Bishop, E. (Ed.) (1972). *Indicators*. New York: Pergamon press. pp99-103. Dawson, R. M. C. , Elliot, D. C., Elliot, W. H., Jones, K. M. (1986). *Data for biochemical research*. 3rd ed. Oxford: Clarendon press oxford. p432.

Klotz, E., Doyle, R., Gross, E. & Mattson, B. 2011 The equilibrium constant for bromothymol blue: A general chemistry laboratory experiment using spectroscopy. *Journal of chemical education* **88**, 637-639.

Kolthoff, I. M. (1937). *Acid-base indicators*. 3rd ed. New York: The Macmillan Company. p128.

Ntailianas, H. A. & Whitney, R. M. 1964 Calcein as an indicator for the determination of total calcium and magnesium and calcium alone in the same aliquot of milk. *Journal of dairy science* **47**, 19-27

Orndorff, W. R. & Cornwell, T. K. 1926 Thymolsulfonephthalein, the intermediate acid, 4'-hydroxy-3'-isopropyl-6'-methyl-benzoyl-benzene-2-

sulfonic acid and some of their derivatives. *Journal of the American Society* **48**, 981-993.

Rasband, W. S., ImageJ (version: 141o), U. S. *National Institutes of Health, Bethesda, Maryland, USA*, <http://imagej.nih.gov/ij/>, 1997-2014.

Sabnis, R. W. (2007). *Handbook of acid-base indicators*. U.S: Taylor & Francis Inc. p54.

Sabnis, R. W. (2007). *Handbook of acid-base indicators*. U.S: Taylor & Francis Inc. p60.

Swan, G. A. & Felton, D. G. (1957). *Phenazines*. New york and London: Interscience publishers. pp112-114.

Wróblewski, W., Roźniecka, E., Dybko, A. & Brzózka 1998 Cellulose based bulk pH optomembranes. *Sensors and aquators B* **48**, 471-475.

Chapter 3

Optimization of a pH sensor

3.1 Introduction

A pH sensing membrane immobilised in cellulose acetate was successfully developed. The membrane has to be optimised for a fast reversibility and less leaching of dye. This chapter discusses different attempts made in order to optimise the sensing membrane by changing the amounts of the components of membrane and/or changing the components.

3.2 Materials and Methods

The neutral red and bromothymol blue membranes were optimized by changing the ratio of the membrane solution components and observing their effect on the membrane to improve the response.

3.3 Neutral red membrane optimization

The effect of changing the ratio of different components was studied. The amount of dye, counter ion, ethylene glycol and plasticizer were varied and the effect was studied.

3.3.1 Effect of varying the amount of counter ion and Dye

The previous composition of membrane had a dye to counter ion ratio of 1: 4.6 (w/w). Three different membranes were made with the following ratios keeping the amount of other components the same. The composition of membranes indicating different amounts of dye and counter ion are given in table 3.1.

Dye : NaTPB (w/w)	Amount of dye	Amount of NaTPB
1:3	8.2 mg	24.6 mg
1:2	10.93 mg	21.87 mg
1:1	16.4 mg	16.4 mg

Table 3.1: Composition of membranes containing different amounts of dye and counter ion.

The response of membranes was compared by putting them in five buffer solutions of pH 5.82, 6.27, 6.86, 7.54 and 8.13. They were left for a day and the UV-vis spectrum was taken after they responded. The spectra were measured using a Hitachi 3000 spectrophotometer in all the experiments below unless stated. The response was also photographed.

3.3.2 Effect of varying the amount of plasticizer and ethylene glycol

The ratio of plasticizer i.e. bis-2 ethylhexyl sebacate) and ethylene glycol was varied and the effect was studied keeping the dye and counter ion ratio 1:1 since it worked well in the previous experiment. The previous ratio was 1:1.5 (Ethylene glycol: plasticizer). The following ratios were taken to make the membranes and test the response in buffer solutions of pH 7.99. (Table 3.2). The responses were compared.

Ethylene glycol: Bis-2(ethylhexyl sebacate)	Amount of Ethylene glycol	Amount of Bis-2(ethylhexyl sebacate)
1:1	46.75 mg	46.75 mg
1:2	31.2 mg	62.4 mg
1:3	23.37 mg	70.11 mg
2:1	62.4 mg	31.2 mg
3:1	70.11 mg	37.37 mg
1.5:1	56 mg	37.5 mg

Table 3.2: composition of membranes containing different amounts of ethylene glycol and plasticizer.

The membranes were compared by putting them in five phosphate buffer solutions of pH 5.82, 6.27, 6.86, 7.54 and 8.13.

3.4 BTB membrane optimization

Since the neutral red membrane response had improved a lot as a result of optimisation, the same ratio was used to make a BTB membrane and to check the response.

3.4.1 Using the ratio of components that worked well with neutral red

The best ratios of dye: counter ion (1:1) w/w and ethylene glycol and plasticizer (2:1) w/w that worked well with the neutral red membrane were used for optimizing the BTB membrane. The following composition was used to form the membrane (Table 3.3).

Component	Amount
Bromothymol blue	28.25 mg
Tetraoctyl ammonium bromide	28.25 mg
Cellulose acetate	74 mg
Ethylene glycol	62.4 mg
Bis-2(ethylhexyl sebacate)	31.2 mg
THF	4 mL

Table 3.3: Composition of membrane.

The response was checked in 5 phosphate buffer solutions of pH 5.9, 6.0, 6.8, 7.5 and 8.2.

3.4.2 Trying a different counter ion for BTB membrane

Tetraoctyl ammonium bromide was replaced by tetrabutyl ammonium bromide. Two membranes were made. One with the old ratio and replacing the 0.8mmoles of TOAB with tetrabutyl ammonium bromide and the other one with the best ratio that worked well with the neutral red stated in table 3.3.

3.4.3 Replacing the polymer

To improve the response and to control the leaching of dye, the Cellulose acetate was replaced by polyvinyl chloride, maintaining the best ratio of components and neutral red was taken as a dye. Ethylene glycol was not added at all in PVC-based membranes since it is too polar to act as an effective plasticizer. The following composition given in table 3.4 was taken.

Component	Amount
Neutral red	16.4 mg
NaTPB	16.4 mg
PVC	74 mg
Bis-2(ethylhexyl sebacate)	31.2 mg
THF	3 mL

Table 3.4: Composition of PVC membrane.

3.4.4 Increasing the amount of Plasticizer in PVC membranes

The plasticizer used in previous experiments was 22.6% of total components. Six different membranes were prepared having 40% (142.72 mg), 60% (214.08 mg), 65% (231.92 mg), 70% (250 mg), 75% (267.6 mg) and 80% (285.44 mg) plasticizer. The response was observed by photography and by recording UV/Vis spectra.

3.4.5 Changing the amount of dye and counter ion

The ratio of dye and counter ion was changed. Six types of membranes were made each with a different dye to counter ion ratio but keeping the plasticizer at 70% (250mg) as this amount worked well. The following compositions were taken.

Membrane	Dye : NaTPB	Amount of neutral red	Amount of NaTPB
1	1:4.6	5.8 mg	27 mg
2	1:2	10.93 mg	21.87 mg
3	2:1	21.87 mg	10.93 mg
4	3:1	24.6 mg	8.2 mg
5	4:1	26.24 mg	6.56 mg
6	6:1	28.11 mg	4.7 mg

Table 3.5: Composition of membranes containing different amounts of dye and counter ion.

The solution was spread using a glass slide that made a thinner membrane at the bottom and thicker on the top of the transparency sheet. Thinner parts of the membrane sheet were taken as they responded quickly and the response was photographed and the spectrum was taken.

3.5 PVC based BTB membranes

Two different BTB membranes were made. One with the ratio that worked well with neutral red i.e. 3:1 dye: counter ion and 70% plasticizer while the other contained an inverted ratio 1:4 dye: counter ion but keeping the plasticizer at 70%. The two membranes had the compositions shown in table 3.6.

Component	Amount taken for membrane 1	Amount taken for membrane2
BTB	24.6 mg	12.5 mg
TOAB	8.2 mg	44 mg
PVC	74 mg	74 mg
Bis-2(ethylhexyl sebacate)	250 mg	250 mg
THF	3 mL	3 mL

Table 3.6: Composition of BTB membranes containing different amounts of dye and counter ion.

The response was photographed in 5 Phosphate buffers and the UV/VIS spectra were recorded.

3.5.1 Investigating the pK_a Shift

Since the apparent pK_a value for BTB shifted downwards in a PVC plasticized membrane, the pH response was investigated in citrate buffer at more acidic pH values to check how far the pK_a value shifted. It was hoped that this would help in choosing a dye with an appropriate higher pK_a value than bromothymol blue so if it were plasticized and its pK_a value shifted down in the same way, it would still remain in the region of interest. Citrate buffer was made in the range pH 2.7 to 7.0 using a standard recipe from "Data for biochemical research" (Dawson, 1986).

A fresh membrane was made using the composition given in table 3.7.

Component	Amount
BTB	6.25 mg
TOAB	25 mg
PVC	74 mg
THF	3 mL
Bis-2(ethylhexyl sebacate)	250 mg

Table 3.7: Composition of membrane used to check the pK_a shift.

Five buffers of pH (2.6, 3.2, 4.2, 4.8, and 5.8) were selected and the response was noted.

3.5.2 Changing the dye due to pK_a shift

Since the pK_a value of bromothymol blue shifted down by about 1 pH unit, two new dyes, cresol red and cresol purple were selected, which have pK_a values slightly higher than bromothymol blue.

(a) *m*-Cresol purple

Cresol Purple, also known as metacresolsulfonephthalein, always has a dark colour, which is indicative of the quinoid structure. It has a yellow to purple transformation of colour from pH 7.4-9.0. The crystals are green but when pulverized produce a dark red powder. It is slightly soluble in water, readily soluble in methyl alcohol, ethyl alcohol, glacial acetic acid and insoluble in carbon tetrachloride, benzene and ether. Cresol purple has the following structure and characteristics: (I.M. Kolthoff, 2007).

Chemical/Dye Class: Sulphonephthalein

Molecular Formula: $C_{21}H_{18}O_5S$

Molecular Weight: 382.43

pH Range: 7.4–9.0

Color Change at pH: yellow (7.4) to purple (9.0)

pK_a : 8.32

Physical Form: Olive green powder

Solubility: slightly soluble in water and ethanol and soluble in methanol

UV-Visible (λ_{max}): 579 nm, 371 nm at pH 9 (Sabnis, 2007)

Structure:

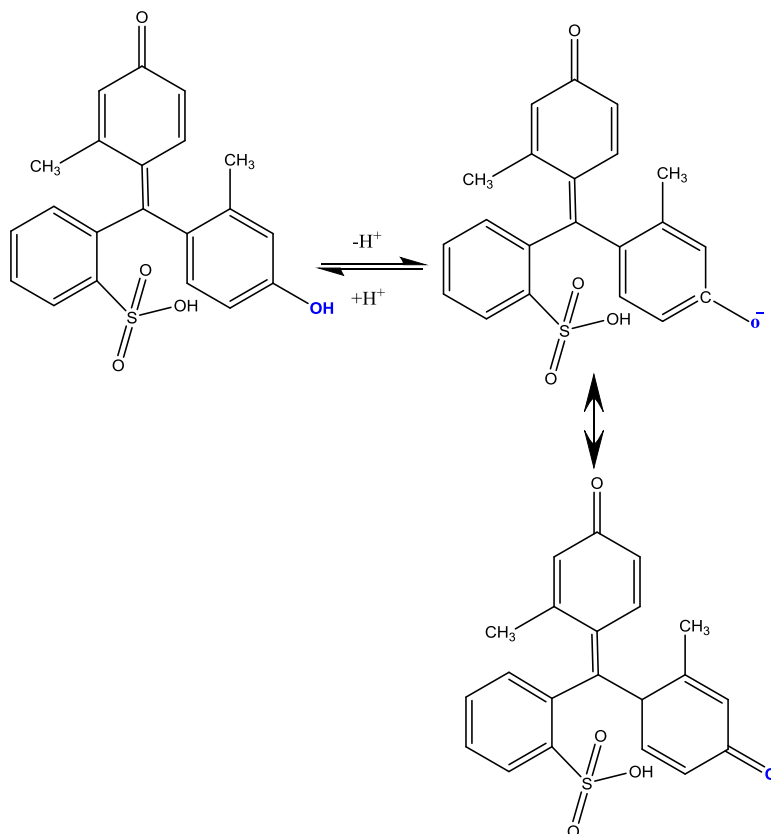


Figure 3.1: Ionising group of cresol purple.

(b) *o*-Cresol red

Chemical/Dye Class: Sulphonephthalein

Molecular Formula: C₂₁H₁₈O₅S

Molecular Weight: 382.43

pH Range: 7.0–8.8

Color Change at pH: yellow (7.0) to reddish purple (8.8)

pK_a: 8.32

Physical Form: Reddish brown powder

Solubility: slightly soluble in water and ethanol and soluble in methanol

UV-Visible (λ_{max}): 570 nm, 367 nm, at pH 8.8 and 432 nm at pH 7 (Sabnis, 2007:105)

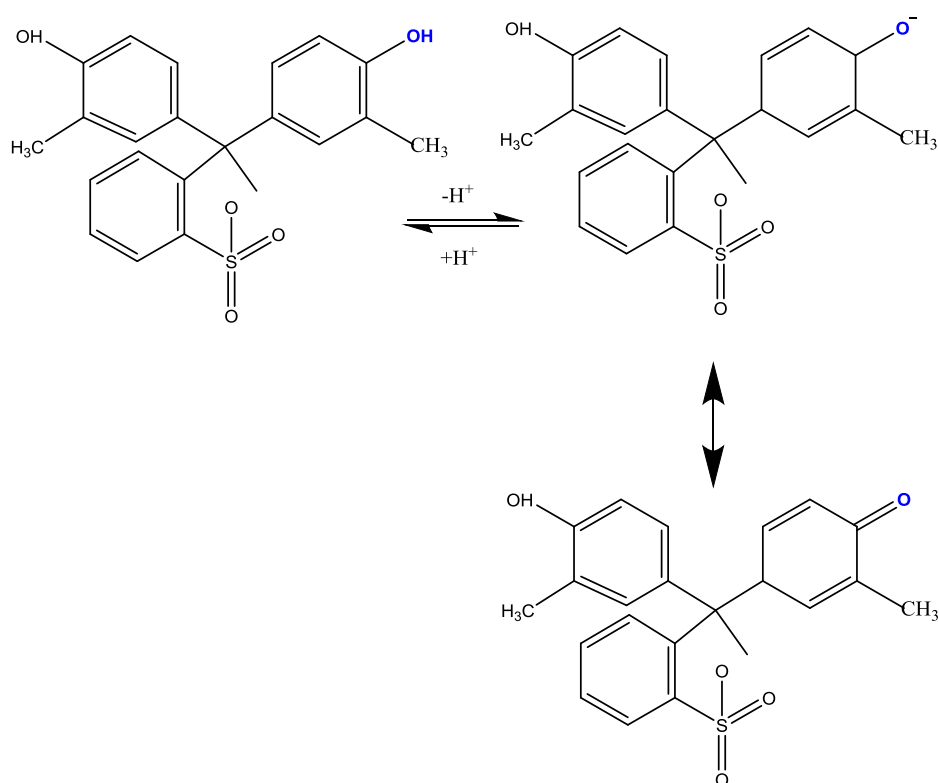
Structure:

Figure 3.2: Ionising group of cresol red.

3.5.3 Tris Buffer

0.1 M Tris (hydroxymethyl) aminomethane buffer solutions of pH ranging from (7.1-8.9) was made using standard recipes to check the response at high pH. (Dawson. RMC, 1986).

A 0.02 mM solution of cresol red and a 0.5mM solution of cresol purple were made. The response was photographed and measured in a UV-Vis spectrophotometer. The following buffers were taken for cresol red:

Citrate buffer of pH 4.2, 4.8, 5.4, 5.8, 6.4, 6.7, 7.0 and

Tris buffer of pH 7.4, 7.8, 8.2, 8.8, and 9.0.

1 mL of dye solution and 1 mL of buffer were mixed in a cuvette. Photographs were taken and UV/Vis spectra were recorded. For cresol purple, Tris buffer of pH 6.7, 7.32, 7.57, 7.94, 8.18, 8.51, 9.09 were taken. 2mL of buffer solution was mixed with 1 mL of

dye solution to get decent spectra. Spectra were measured using a Hitachi 3010 spectrophotometer.

3.5.4 Cresol red immobilization

Cresol red was immobilised in a similar way to the BTB immobilisation by taking the composition that worked well for response with BTB but shifted the pK_a down. The following composition of table 3.8 was taken:

Component	Amount
Cresol red	24.6 mg
Tetraoctyl ammonium bromide	44 mg
PVC	74 mg
Bis-2 (ethylhexy sebacate)	250 mg
THF	3 mL

Table 3.8: composition of cresol red membrane.

The response was measured in 15 buffer solutions using a UV/Vis spectrophotometer. The following buffer solutions were taken and 1 mL of buffer and 1 mL water were taken in the cuvette.

Citrate buffer of pH: 4.8, 5.4, 5.8, 6.4, 6.7, 7.0

Tris buffer of pH: 7.4, 7.7, 7.8, 8.2, 8.5, 8.8, 9.0, 9.2, and 9.8

(a) Testing the response in salt solution

Sea water contains about 0.5 M NaCl so 1 M NaCl solution was made and 1mL of this solution plus 1mL buffer solution was taken which makes the final concentration of NaCl 0.5 M and the response was photographed and measured in the UV-spectrophotometer. The cresol red membrane's response was observed using citrate buffers (pH 5.82, 6.93) and Tris buffers (pH: 7.68, 8.19, 8.88, and 9.42). The BTB membrane was made using the composition of table 3.9.

Component	Amount
BTB	12.5 mg
TOAB	44 mg
PVC	74 mg
Bis-2 (ethylhexy sebacate)	250 mg
THF	3 mL

Table 3.9: composition of BTB membrane used for testing the response in salt solution.

The response was checked in a series of phosphate buffer solutions (pH5.9, 6.0, 6.8, 7.5, 8.2), Citrate buffers (pH 5.8, 6.4, 7.0) and Tris buffer (pH7.4, 7.8). The response was photographed and spectra recorded with UV/vis spectrophotometer.

3.6 Results and Discussions

3.6.1 Neutral red membrane optimization

By changing the composition of the membrane, the following results were obtained.

3.6.2 Effect of varying the amount of counter ion and dye

A range of counter ion to dye ratios (1:3, 1:2, 1:1) were tried in an attempt to optimise the response of the membrane. The best and the fastest membrane was membrane 3 with the ratio 1:1 neutral red to NaTPB. It was dissolved in slightly more solvent (3.5 mL) while the other two were dissolved in 3 mL of tetrahydrofuran. All the membranes still showed dye leaching however.

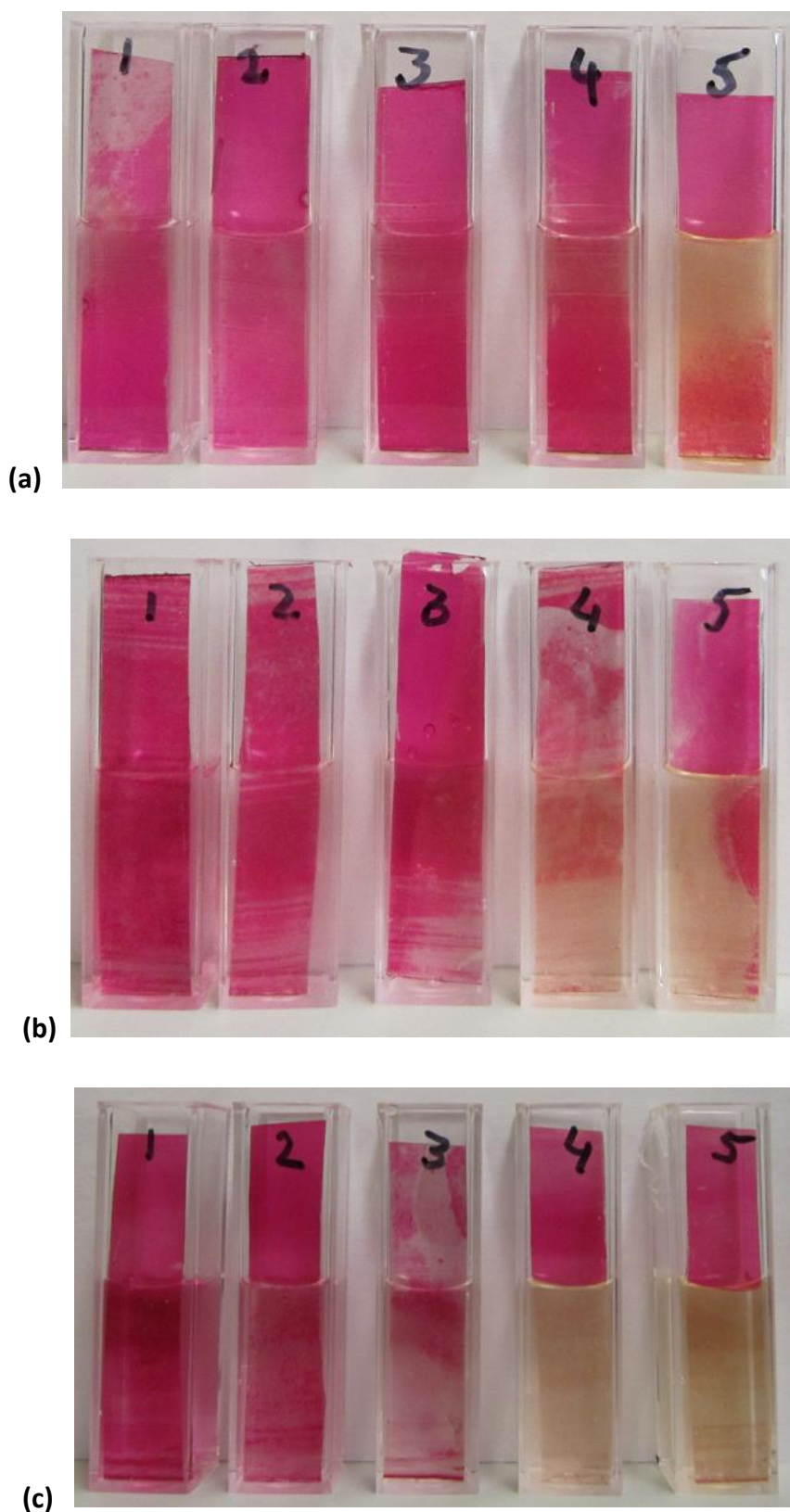


Figure 3.3: Neutral red membrane containing NaTPB as a counter ion. Response of (a) membrane 1 (1:3), (b) membrane 2 (1:2), (c) membrane 3 (1:1). pH: 5.82, 6.27, 6.86, 7.54, 8.13 from left to right.

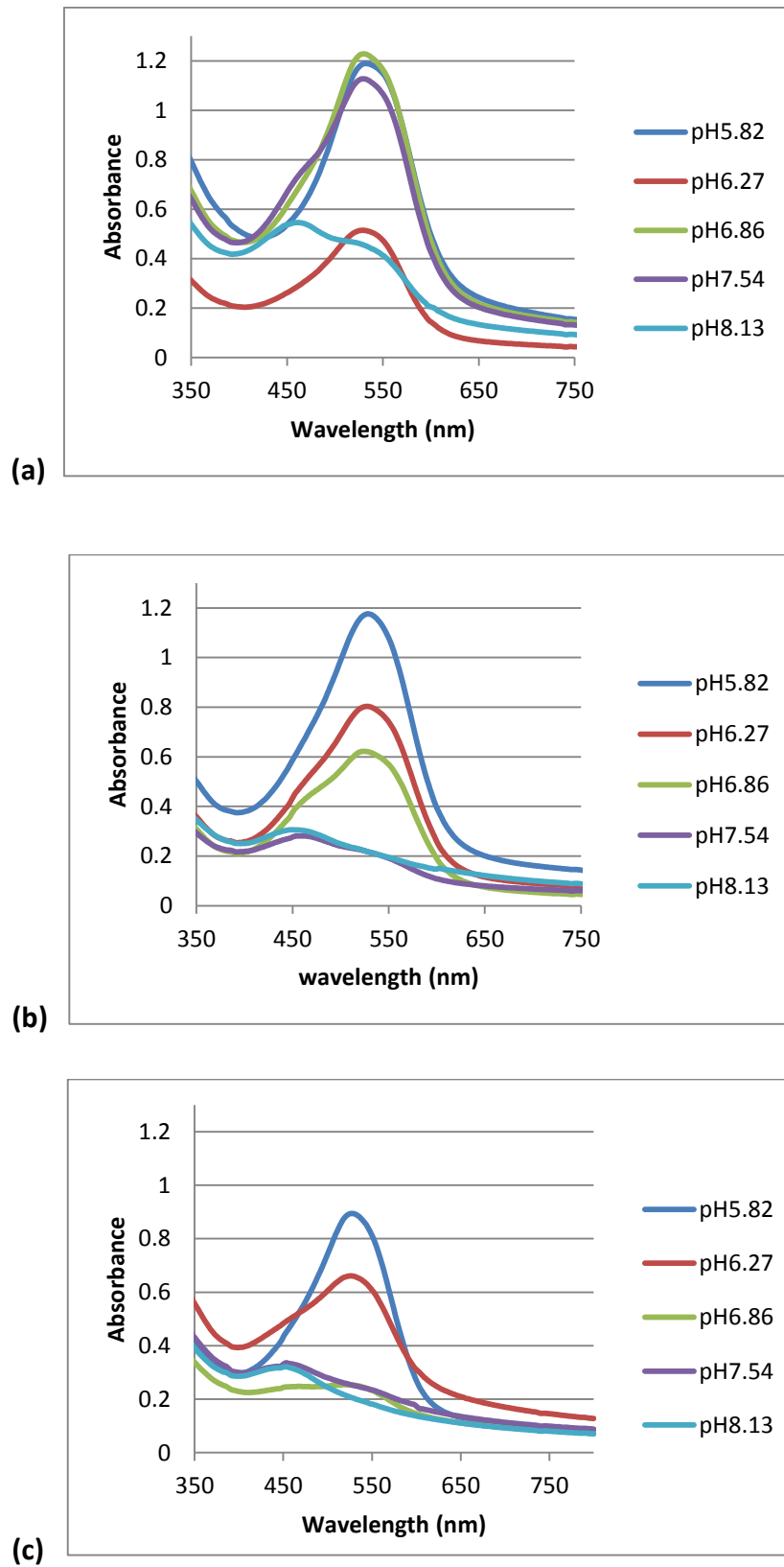


Figure 3.4: UV-vis spectrum of neutral red membrane containing NaTPB (a) membrane 1 (1:3), (b) membrane 2 (1:2), (c) membrane 3 (1:1).

The spectra of membranes 2 and 3 show peaks corresponding to the orange colour in the basic test medium (pH: 7.54 and 8.13) but membrane 2 took a bit longer than membrane 3 to equilibrate and, as can be seen in Figure 3.3b, there are still red areas in cuvettes 4 and 5 which did not equilibrate to orange completely although the membrane is in basic buffer. The spectrum of membrane 1 shows one peak in the orange region but the membrane put in buffer pH 7.54 did not equilibrate to the orange colour so the peak is still in the red region. Therefore it was concluded that the membrane 3 has the best composition of counter ion and dye.

3.6.3 Effect of varying the amount of plasticizer and ethylene glycol

The ratio of plasticizer, Bis-2 (ethylhexyl sebacate) and ethylene glycol was varied and the effect was studied. Membrane 1 (1:1) and membrane 4 (2:1) responded quicker than all other membranes (figure 3.5). Both of them responded in 10 minutes. Membrane 1 split into two colours orange and red as seen in figure 3.5a. The membranes in cuvettes 4 and 5 have an orange region on the top and are still red below. This means membrane 1 had equilibrated on the top but was still equilibrating at the bottom while membrane 4 was homogeneous and had equilibrated. This suggests that the 2:1 ratio is superior. The response time was noted manually. It took 45 minutes to reverse from 5.8 to 7.9.

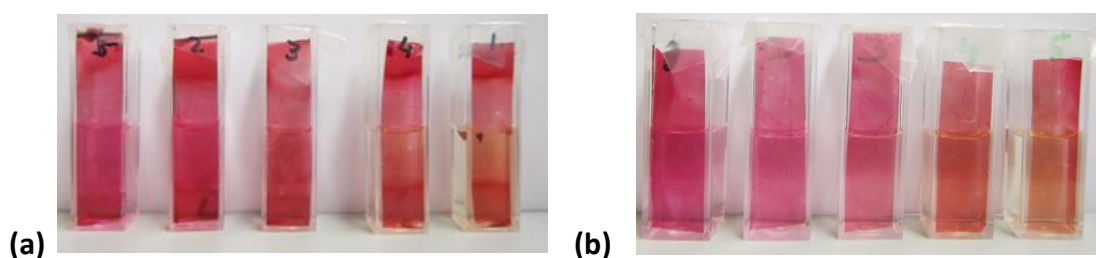


Figure 3.5: Response of neutral red membranes (a) 1 with plasticizer and ethylene glycol ratio (1:1) and (b) with plasticizer and ethylene glycol ratio 4 (2:1).

3.6.4 BTB membrane optimization

(a) Using the ratio of components that worked well with neutral red

The best composition found from the neutral red studies was taken as the starting point for BTB optimisation. The response was very slow. The cuvettes were wrapped with parafilm and left over the weekend. The response was very slow and after 72 h, only the membrane kept in the most basic buffer (pH:8.2) changed to green but had not completely equilibrated since it should be blue in basic solution. The ratio of components that works well for neutral red membrane does not work at all for the bromothymol blue membrane. The membrane made with the best ratio that worked well for neutral red could not retain the dye in it and the dye leached out.

(b) Trying a different counter ion for BTB membranes

Tetrabutyl ammonium bromide was used instead of tetraoctyl ammonium bromide and with a 1:4 dye to counter ion ratio. The samples 4 and 5 became green after 10 minutes but did not reach the expected blue colour which means they were still equilibrating. The concentration that worked well with neutral red was taken and it was observed that the dye leached out so this is clearly not an effective composition for BTB.

(c) Changing the polymer

PVC has been previously used extensively for ion selective electrodes and optical ion binding sensors in sensing different metals and ions for example, zinc (Gorton *et al.* 1977 and Gupta *et al.* 2001), Nickel (II) (Mousavi *et al.*, 2000), phosphate (Wroblewski *et al.*, 2013), Pb(II) (Gupta *et al.* 2006), mercury(II) (Fakhari *et al.* 1997) and many more. Gorton *et al.* made a zinc sensing PVC membrane containing 8% ligand (zinc salt of di-n-octylphenylphosphoric acid (HDOPP)), 62% solvent (di-octylphenylphosphonate (DOPP-n) and 30% PVC. (Gorton *et al.*, 1977) Mousavi *et al.* made a nickel (II) ISEs PVC membrane using 1,10-dibenzyl-1, 10-diaza-18-crown-6 (DbzDA18C6) as a neutral carrier. Wroblewski *et al.* prepared plasticised PVC based membranes that contained uranyl salophene derivatives. They studied the effect of different components of membranes on phosphate sensing and reported that the uranyl salophene III (without ortho-substituents) in PVC/o-nitrophenyl octylether (o-NPOE) membrane having 20

mol% of tetradecylammonium bromide (TDAB) has the highest sensitivity for phosphate (Wroblewski *et al.*, 2013).

Since PVC has been used previously for plasticized dye based sensors, cellulose acetate was replaced by PVC using neutral red as a dye. It was observed that PVC membranes were better than cellulose acetate membranes as they were more homogeneous and the dye did not leach out at all. The response time, however, was not as good as cellulose acetate membranes. The membranes were kept in buffer solutions and observed next day. It showed a good colour range and had equilibrated (figure 3.6 and 3.7).

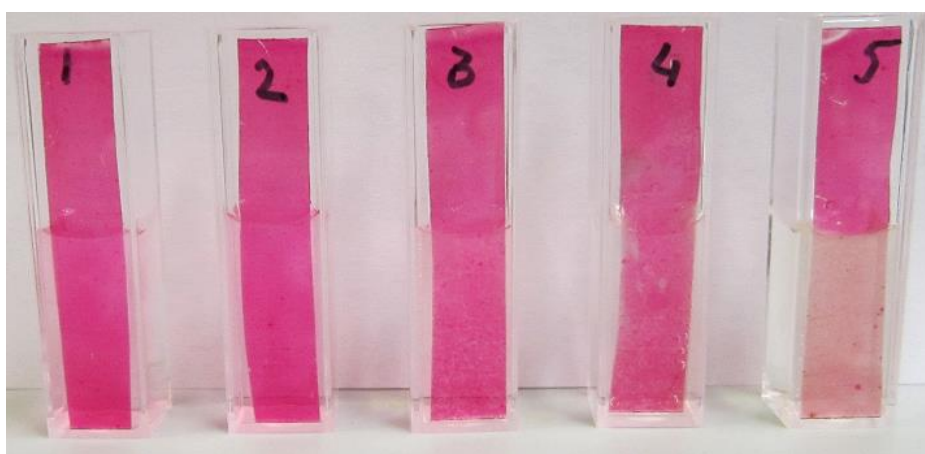


Figure 3.6: Neutral red membrane immobilised in PVC containing NaTPB as a counter ion, slow response on same day.

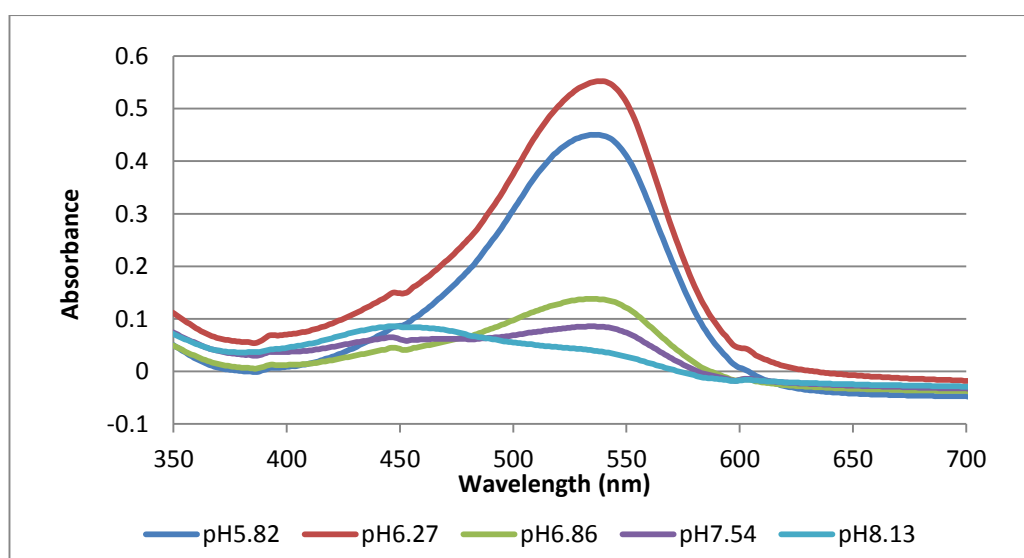


Figure 3.7: UV-Vis spectrum of PVC membrane containing neutral red dye.

The UV-vis spectrum for neutral red membrane is quite similar to the spectrum of free dye in buffer solution (chapter 2). The peak at 523 nm is observed in the spectrum of free dye and the absorbance decreases as the pH increases in the case of the free dye spectrum but in PVC membrane the peak has shifted slightly to 539 nm and the absorbance decreases by increasing pH just like the spectrum of the free dye except that we see lower absorbance at pH 5.82 than at pH 6.27 which could be because the membrane in buffer 5.82 had not equilibrated yet to reach the maximum absorbance. Another difference is that at pH 7.54, a free dye turns orange but in plasticised membrane it was still red and turned orange at slightly higher pH 8.13, this can also be seen in the spectrum where we expect the peak to rise at 450 nm and disappear at 539nm but it is still there and this can be because the pK_a has shifted up (figure 3.7). Further experiments were carried out in an attempt to speed up the response time and conclude whether the pK_a had shifted or the membrane was still equilibrating.

(d) Increasing the amount of plasticizer in PVC membranes

The amount of plasticizer was increased to make the membrane softer and more mobile. To get a faster response, a range of plasticizer composition from 40% to 80% was tested. The membrane with the fastest response was the one with 70% plasticizer. It responded in 10 minutes. As the membranes were made by spreading the solution on transparency sheet using a glass slide, the top portion of the membrane was thicker than the bottom (more liquid on the top resulted in thicker membrane and in the bottom, the solution almost runs out and gives thinner membranes). It was observed that the thinner membranes responded faster than the thicker ones as expected for a diffusion-controlled process (figure 3.8, 3.9 and 3.10).

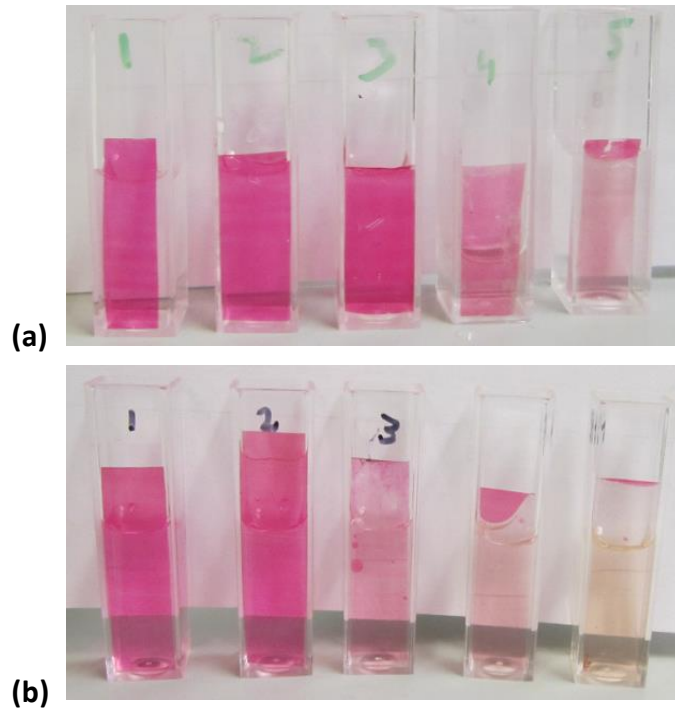


Figure 3.8: Neutral red membrane in phosphate buffer solutions pH left to right in the cuvettes: 5.82, 6.27, 6.86, 7.54 and 8.13(a): Thick membrane (70% plasticizer) (b): Thin membrane (70% plasticizer).

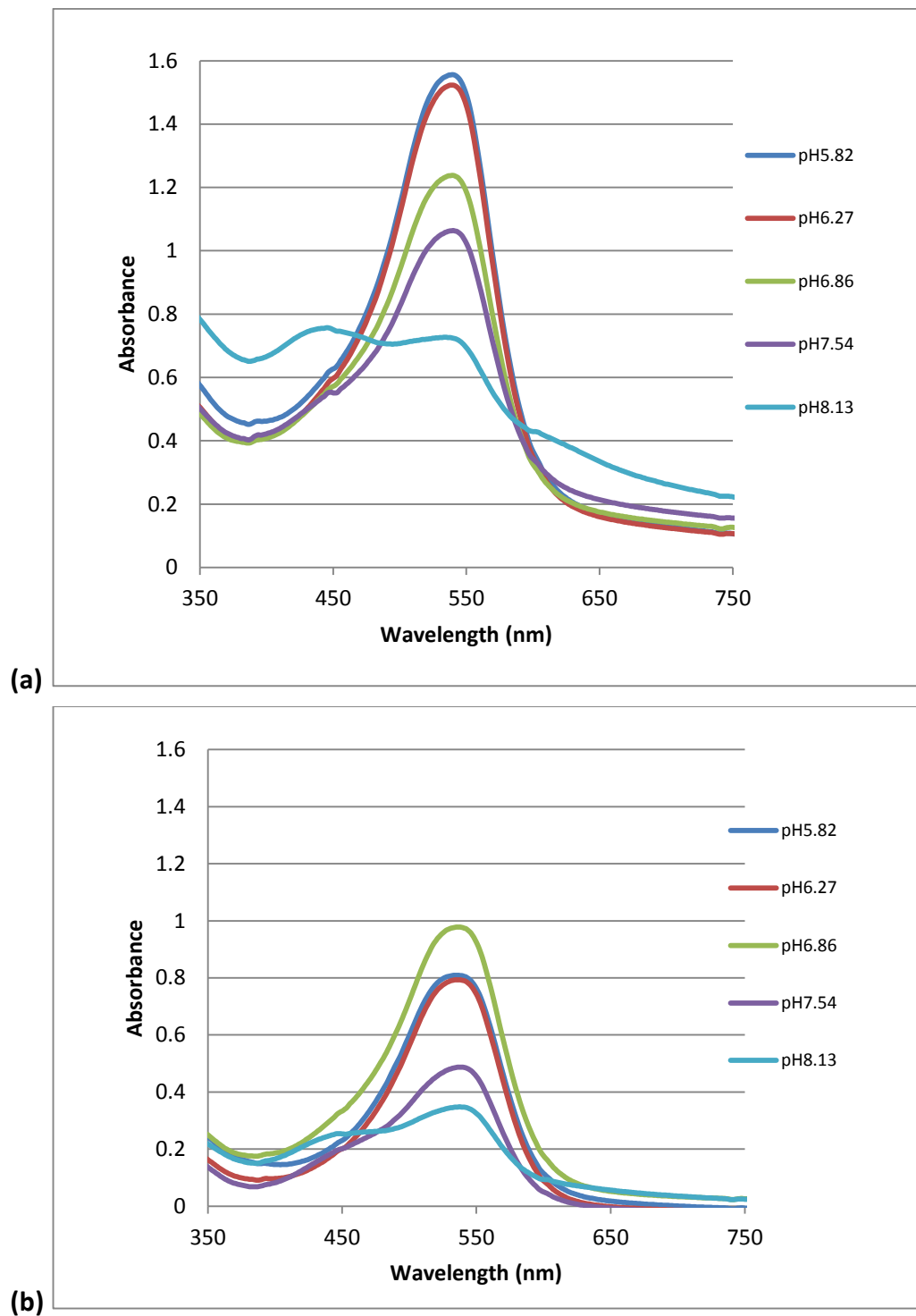


Figure 3.9: UV-Vis spectrum of neutral red membrane plasticized in PVC with 70% plasticizer (a) Thick membrane (b) Thin membrane

Since the thicker membrane contains more dye, its absorbance is higher than that of the thinner membrane. In the spectrum of the thinner membrane, the absorbance for

pH 6.86 is more than that of pH 6.27 and 5.82 which could be because of the membrane inhomogeneity since the decrease in pH should lead to a decrease of the absorbance at 539 nm.

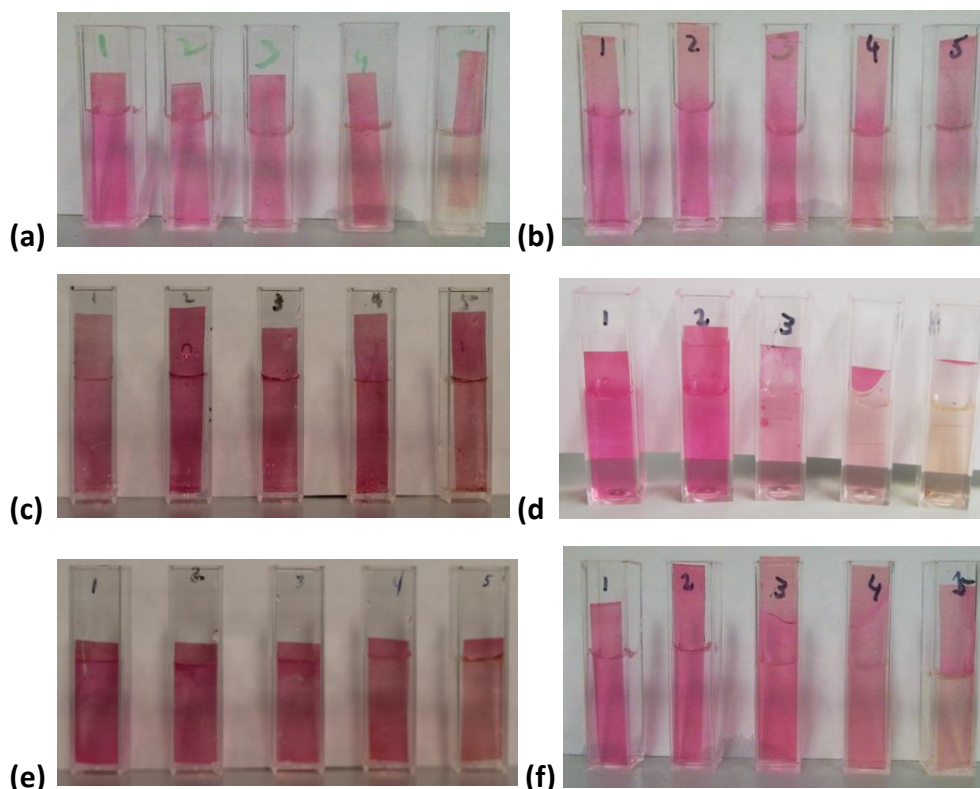


Figure 3.10: Equilibrium colours of neutral red membranes with different levels of plasticizers keeping the amount of other components the same. (a) 40% plasticizer, (b) 60% plasticizer, (c) 65% plasticizer, (d) 70% plasticizer, (e) 75% plasticizer and (f) 80% plasticizer.

Comparing the images in figure 3.10, 80% plasticizer in the membrane seems to make the membrane good in response but not any better than 70% plasticizer in the membrane. The cuvettes numbered '4' and '5' should be orange as the solution in them is basic but they are not, whereas in the 70% plasticizer samples, there is a clear change in the colour in the basic medium. 70% plasticizer makes the membranes softer and

enhances the mobility of ions thus speeding up the response time. Therefore it was concluded that 70% plasticizer should be taken.

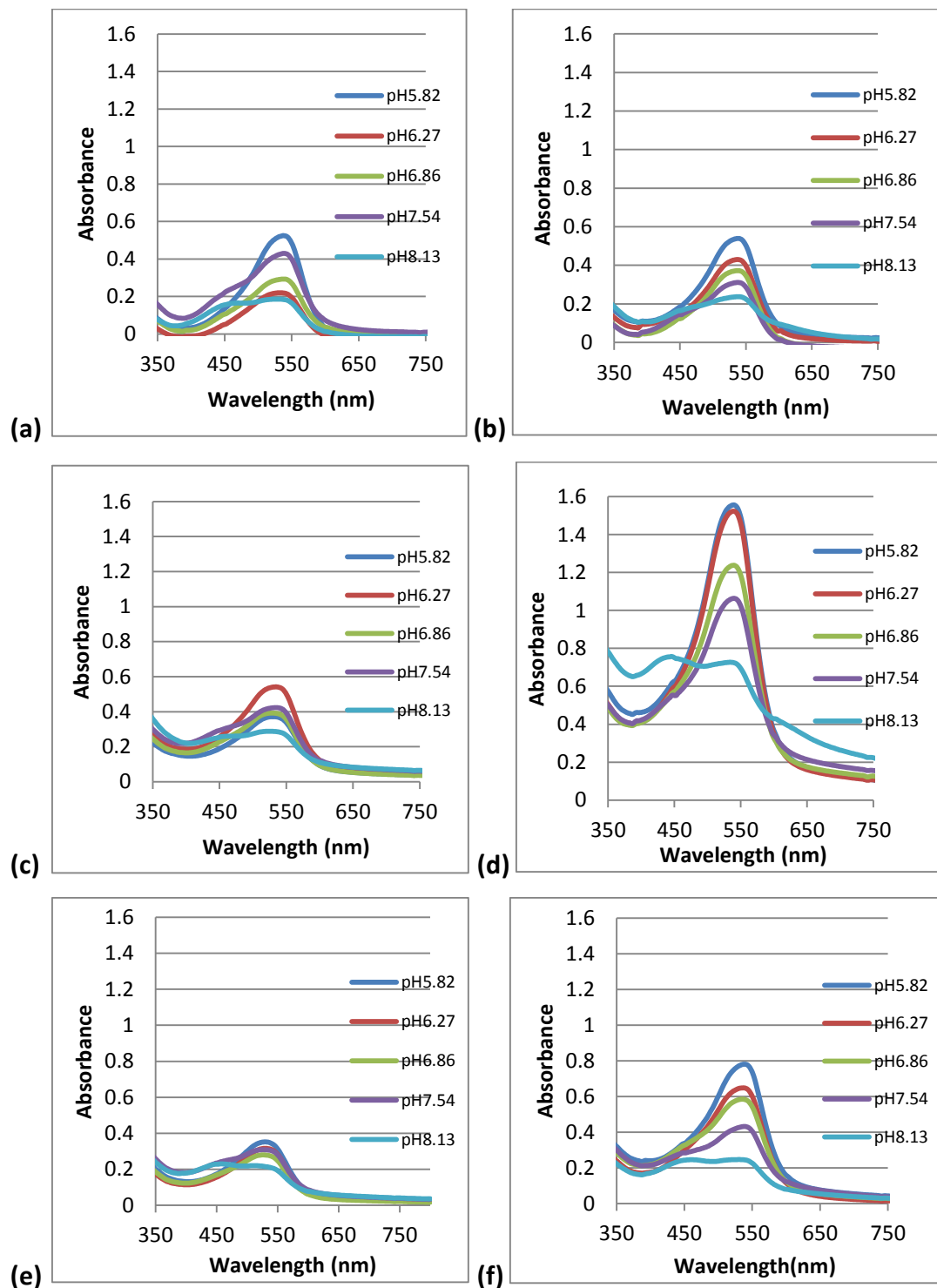


Figure 3.11: UV-vis spectra of neutral red membranes with different levels of plasticizers. (a) 40% plasticizer, (b) 60% plasticizer, (c) 65% plasticizer, (d) 70% plasticizer, (e) 75% plasticizer and (f) 80% plasticizer.

Figure 3.11a does not show a regular progressive change of the dye so it had not equilibrated therefore 40% plasticizer is not good. Figure 3.11c and 3.11e show that the membrane was still equilibrating because the change in colour should decrease the absorbance but increased absorbance has been seen in some cases which was not expected. Figure 3.11b (60%), 3.11d (70%) and 3.11f (80%) shows the expected pattern of dropping of peak with increasing pH. Out of them 70% plasticizer makes the membrane very soft without making it too thin for colour detection and gives decent colour in the photographs while the 80% plasticizer makes it very thin and the intensity of colour decreases. 60% plasticizer does not make the membrane soft enough so it was rejected. 65% and 75% plasticizers were tried later after playing with the composition of membrane. The best ratio of dye and counter ion was chosen to test 65% and 75% plasticizers. The amounts of dye and counter ion taken for 65% and 75% were 24.6 mg and 8.2m g. The dye taken was more than it was taken for other percentages of plasticizer but the absorbance decreased. Therefore it was concluded that 70% plasticizer should be taken.

Coating membranes on glass was also tried. The solution was spread on a glass plate. The membranes stuck to the glass while the cellulose acetate based membranes did not remain on the glass and peeled off when inserted into solution.

(e) Changing the amount of dye and counter ion

Membranes were made with a wide range of dye: counter ion ratios from (1:4 to 6:1) keeping the plasticizer 70%. The responses are shown in the figure 3.12. The images were taken after an hour when all membranes seemed to have responded. The membrane with 3:1, 4:1 and 6:1 ratios showed good response but the best membrane that showed the fastest response was the membrane with ratio 3:1. It also reversed in the least time i.e. 10 minutes from 5.9 to 8.2 (red to orange). The colour change was noted by eye using a stopwatch.

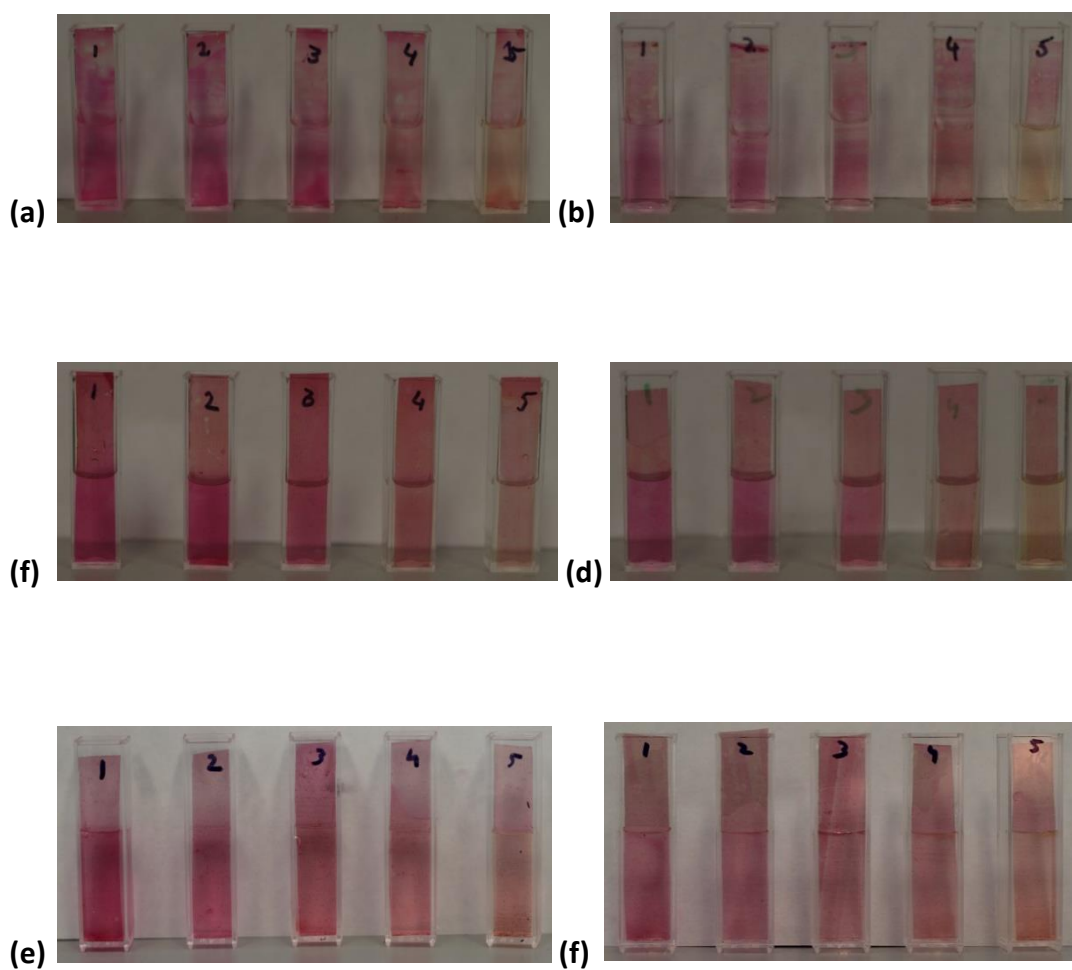


Figure 3.12: Responses of neutral red membranes made with different ratios of dye: counter ion. (a) 1:4, (b) 1:2, (c) 2:1, (d) 3:1, (e) 4:1, (f) 6:1.

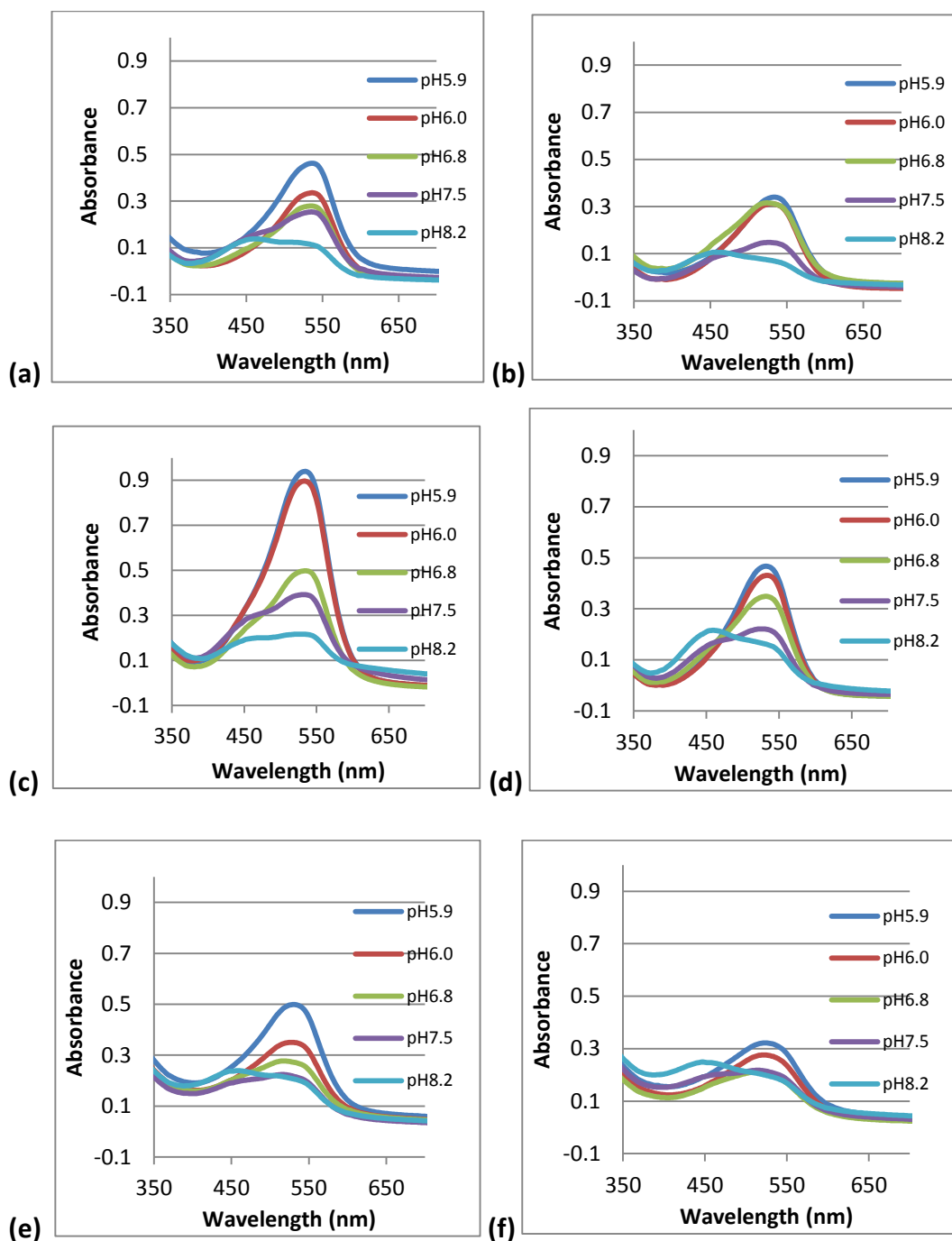


Figure 3.13: UV-vis spectra of neutral red membranes with different counter ion ratios. (a) 1:4, (b) 1:2, (c) 2:1, (d) 3:1, (e) 4:1, (f) 6:1.

All the membranes show more or less the same spectrum except that the orange peak is clearer for membrane with 3:1 ratio and because it shows a clear and fast optical response, therefore this ratio was taken as the best ratio. In summary, 70% plasticizer and a 3:1 dye to counter ion ratio respectively make an effective sensing membrane with a clear and reasonably rapid response.

(f) Using the best composition for BTB membrane

The ratio of counter ion and dye that worked well for neutral red (3:1) did not work well for bromothymol blue and the dye leached out from membrane 1 when it was dipped in buffer. Therefore the spectrum showed the properties of the free dye and is not shown here and the figure 3.14a also reflects the free dye. Membrane 2 (1:4) was better because it retained the dye and it responded as soon as it was dipped in the solution. The response was very fast and the membrane was very homogeneous, unlike cellulose acetate membranes where precipitated material caused inhomogeneity in the layer. The only problem was that the membrane gave the same colour in all the buffer solutions (pH 5.9, 6.0, 6.8, 7.5, 8.2). The colour remained blue regardless of the solution being neutral or acidic. The figure 3.14 below illustrates the response. This is in sharp contrast to the behaviour of free dye in solution, which showed the expected yellow to green to blue transitions over this pH range (membrane 1 in the figure 3.14 shows the colour range for free dye because the dye leached).

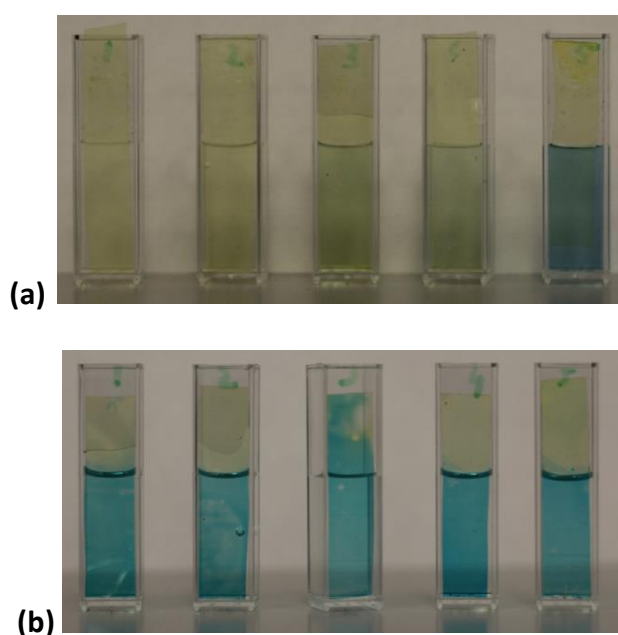


Figure 3.14: Response of PVC based BTB membrane containing TOAB as a counter ion. All samples went blue (a) Dye leaching in membrane 1 (3:1) (b) Membrane 2 (1:4) where ratios are between dye and counter ion.

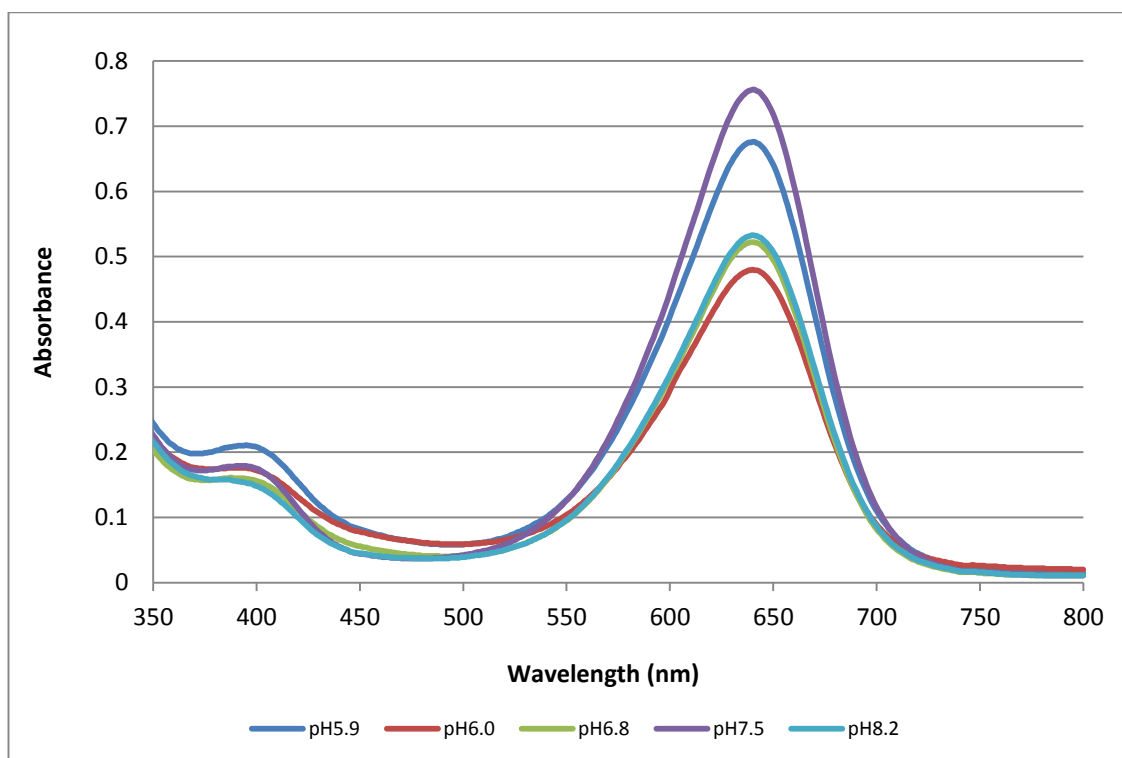


Figure 3.15: UV visible spectrum of BTB membrane .Membrane 2 response, which remained blue in all samples.

The spectrum in figure 3.15 confirms the visual observation. In yellow samples (acid response), the peak at 640 nm vanishes and the peak at 400 nm rises but as all the samples remained blue, therefore the only peak observed was at 640 nm.

To investigate what had happened, the amount of dye was increased and two membranes were made. Membrane 1 had a dye and counter ion ratio of 1:3 (8.2 mg: 24.6 mg) and membrane 2, 1:2 (10.93 mg: 21.87 mg). Membrane 2 responded quickly and gave the same colour in all the buffer solutions (Figure 3.16c) and membrane 1 had a slight difference of colour but the response was very slow (Figure 3.16a).

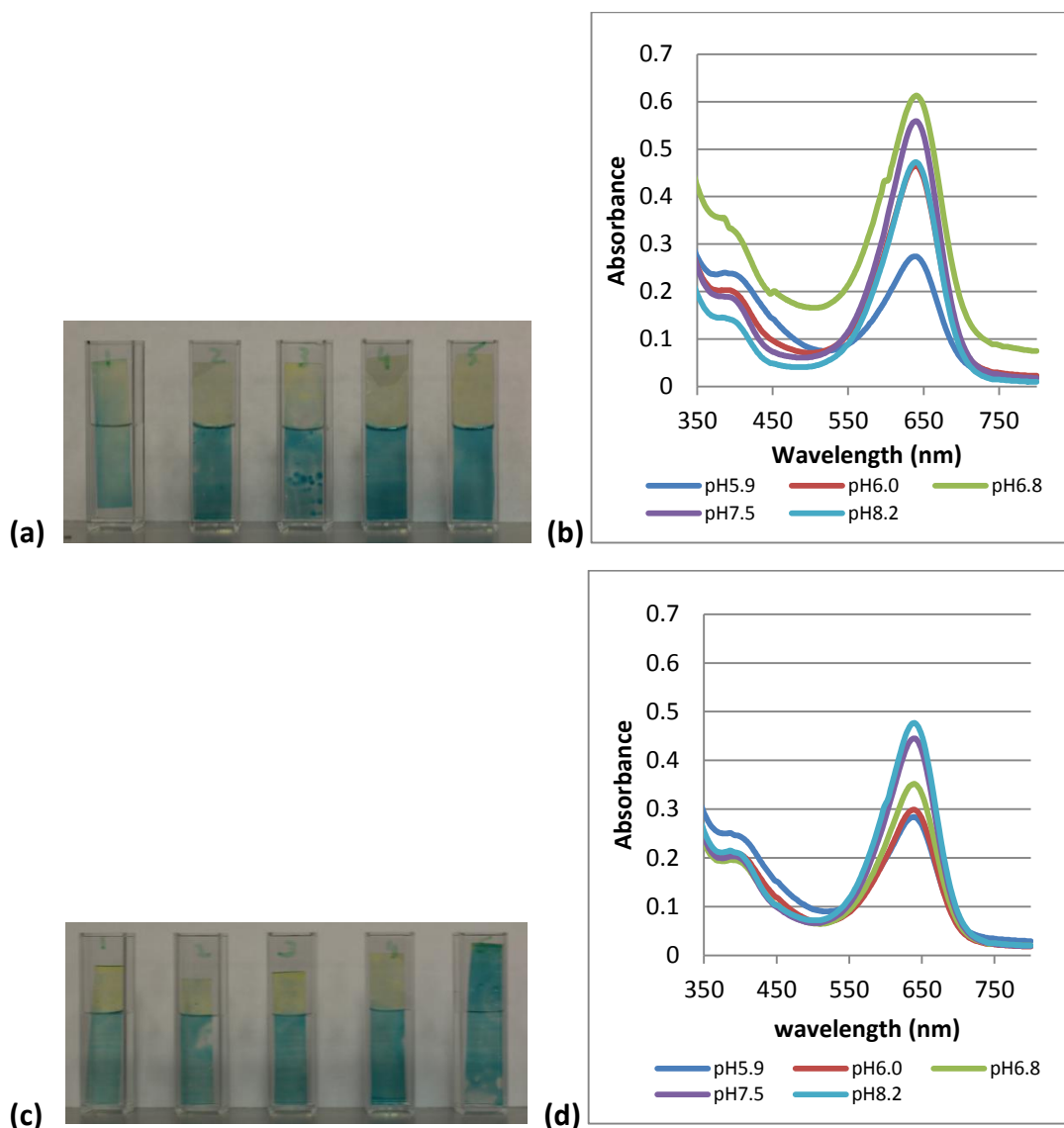


Figure 3.16: BTB membrane (a) Response of membrane 1 (slightly green in acidic medium), (b) UV-vis spectrum of membrane 1, (c) Response of membrane 2 (all blue), (d) UV-vis spectrum of membrane 2.

The spectrum of membrane 1 and membrane 2 turned blue in all the buffer solutions and the spectrum also showed peaks only in the blue region. This suggested that the pK_a value of the dye may have shifted to a lower value and that is why it remained blue over the whole pH range (5.9-8.2) measured. To confirm this, membrane was tested in very acidic solution i.e. 0.1 M HCl (pH: 1). the membrane turned yellow which confirms that it is still responsive and suggests that the pK_a shift hypothesis is probably correct. The bromothymol blue, when placed in the hydrophobic environment of a PVC membrane, shifts its pK_a value below the usual value of (7.0, 7.1). This is not unusual and it has been observed that the spectral properties of dyes can change when

immobilised. For example the spectrum of thiazole yellow changes when it is immobilised. (Safavi.A, Abdullahi.H 1998).

(g) Changing the counter ion to try to resolve the pK_a shift problem

CTAB and Tetrabutyl ammonium bromide were tried as counter ion.

Two membranes were made using the composition given in table 3.10.

Component	Amount taken for membrane 1	Amount taken for membrane2
BTB	12.5 mg	6.25 mg
CTAB	29 mg	Not taken
Tetrabutyl ammonium bromide	Not taken	25 mg
PVC	74 mg	74 mg
Bis-2 (ethylhexyl sebacate)	250 mg	250 mg
THF	3 mL	3 mL

Table 3.10: composition of membranes containing different counter ions.

When the response was checked, the dye leached out from both membranes. CTAB precipitated in the membrane and made it inhomogeneous. It did not respond in water and stayed yellow but responded in basic solution and gave a blue colour. Membranes with TBAB showed extensive dye leaching and the membrane itself did not respond at all.

(h) Investigating the pK_a Shift

A new series of citrate test buffer was made up covering the range 2.6 to 5.8. These were used to test the response of BTB membranes. The membrane went yellow in pH 2.6, 3.2, 4.2 and 4.8 but went green at pH 5.8.

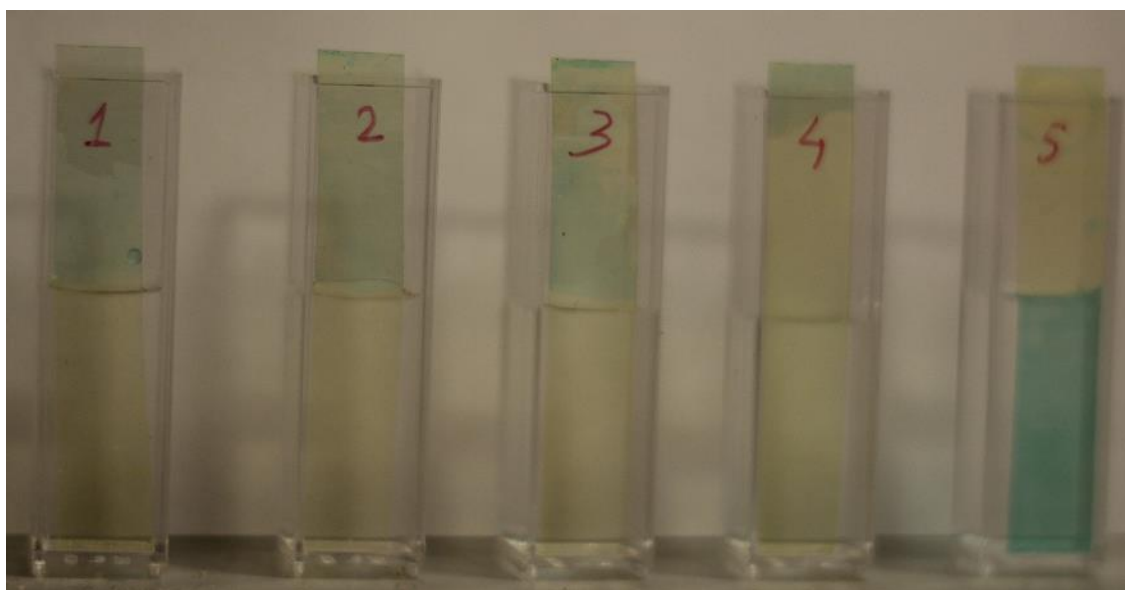


Figure 3.17: Response of membrane in a series of citrate buffer solutions (pH from left to right: 2.6, 3.2, 4.2, 4.8 and 5.8).

Free dye becomes green at pH 7 but in the immobilised form it becomes green at pH 5.8, which means that in plasticized form, the pH value had shifted down by about 1 pH unit. Dyes may change their properties when immobilised. For instance fluorescein, has a pK_a shift to higher values (pK_a up to 0.73 units) compared to the pK_a found in solution when immobilised. Cajlakovic *et al.* (2002). This problem could be solved by changing the dye. A dye with a pK_a value of 8 might be expected to respond in the region around pH 7 when plasticized (assuming a similar response to the membrane microenvironment). For this purpose, either cresol purple or cresol red should be suitable.

(i) Changing the dye due to pK_a shift

Cresol red is yellow below pH 7, at pH 7; it is light brown and dark brown at 7.4. It becomes brownish violet at higher pH from 7.8 to 8.2 and violet at 8.8 and 9. Cresol purple is yellow below 7.4 and goes brown between 7.8-8.2 while at very high pH 8.8-9, it is purple.

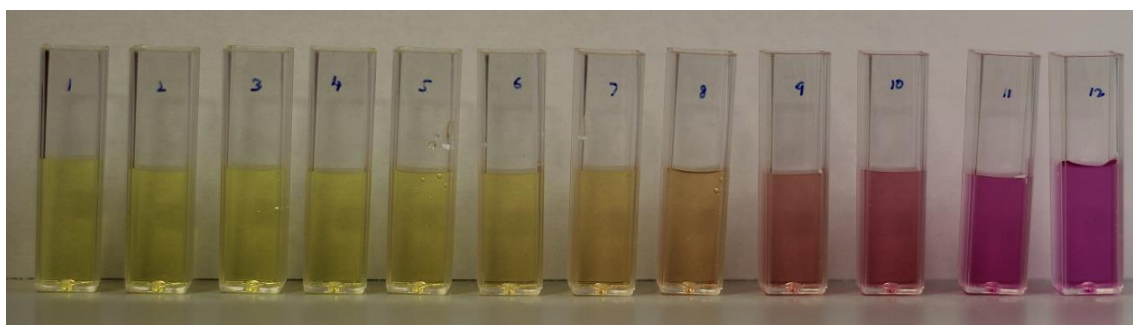


Figure 3.18: Response of cresol red in buffer solutions (pH from left to right: 4.2, 4.8, 5.4, 5.8, 6.4, 6.7, 7.0 (citrate buffer), 7.4, 7.8, 8.2, 8.8, 9.0 (tris buffer)).

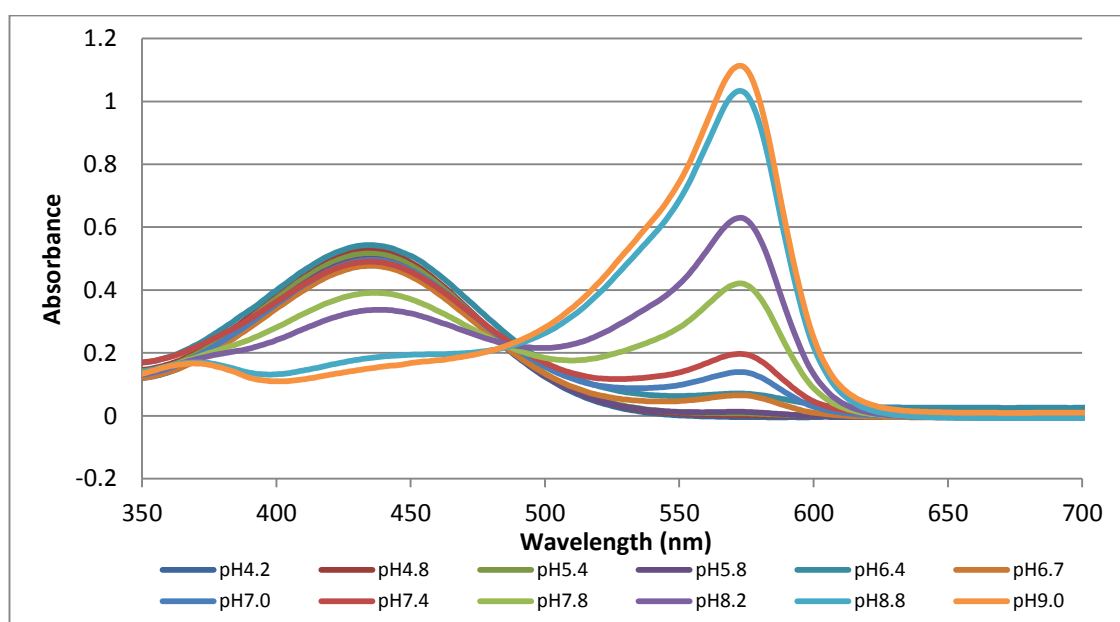


Figure 3.19: UV visible spectrum of cresol red in buffer solutions of different pH from left to right: 4.2, 4.8, 5.4, 5.8, 6.4, 6.7, 7.0 (citrate buffer), 7.4, 7.8, 8.2, 8.8, 9.0 (tris buffer).

The absorption spectrum shows two peaks, one at 574 nm and the other at 432 nm. The peak at 574 nm decreases with decreasing pH while the peak at 432 nm increases. There is an isosbestic point at about 490 nm. “An isosbestic point is a wavelength where the absorbance of two light-absorbing forms are equal. The isosbestic point is useful in both quantitative and qualitative work. Where a clear isosbestic point occurs during a reaction, it is taken as evidence that only two species are involved.” (Scott.RA and Lukehart.CM (Ed.), 2007)



Figure 3.20: Response of cresol purple in Tris buffer solutions pH from left to right: (9.09, 8.51, 8.18, 7.94, 7.57, 7.32, 6.7)

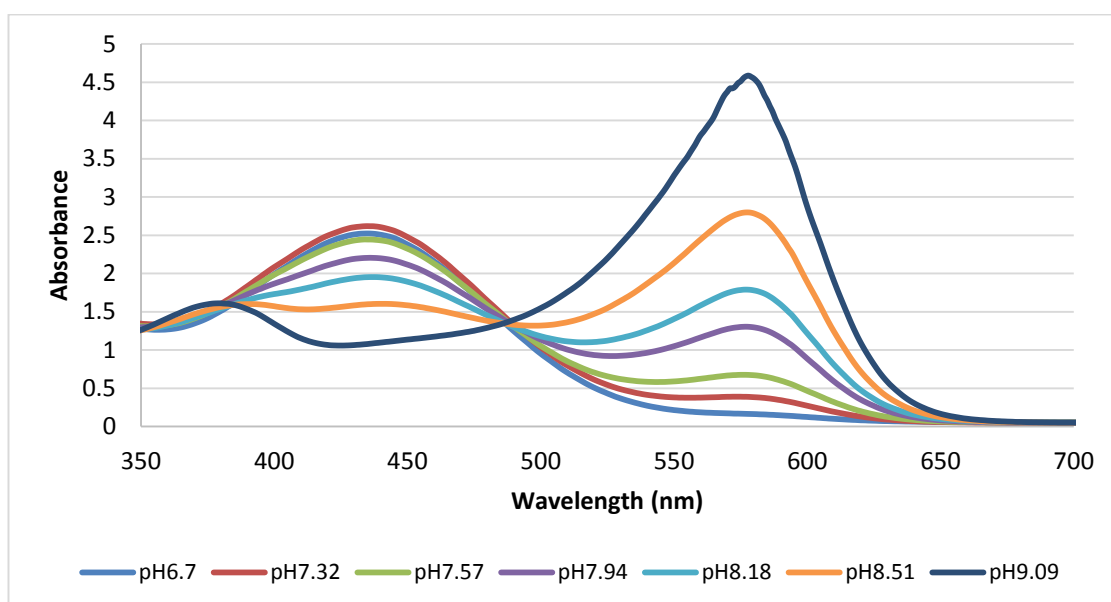


Figure 3.21: UV-Vis spectrum of cresol purple at different pHs.

The peak at 580 nm decreases with decreasing pH and vanishes and the peak appears at 439 nm in acidic medium. There is a clear isosbestic point at 488 nm.

3.6.5 Cresol red Immobilization

The membrane showed a fast response equilibrating in 2 minutes. Although the apparent pK_a shifted down by about 0.3 pH units, it responds in the region of interest.

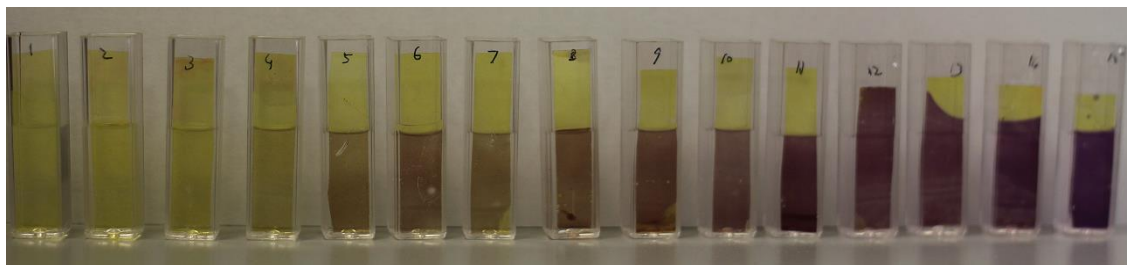


Figure 3.22: Cresol red membrane response in buffer pH from left to right 4.8, 5.4, 5.8, 6.4, 6.7, 7.0, 7.4, 7.7, 7.8, 8.2, 8.5, 8.8, 9.0, 9.2, 9.8

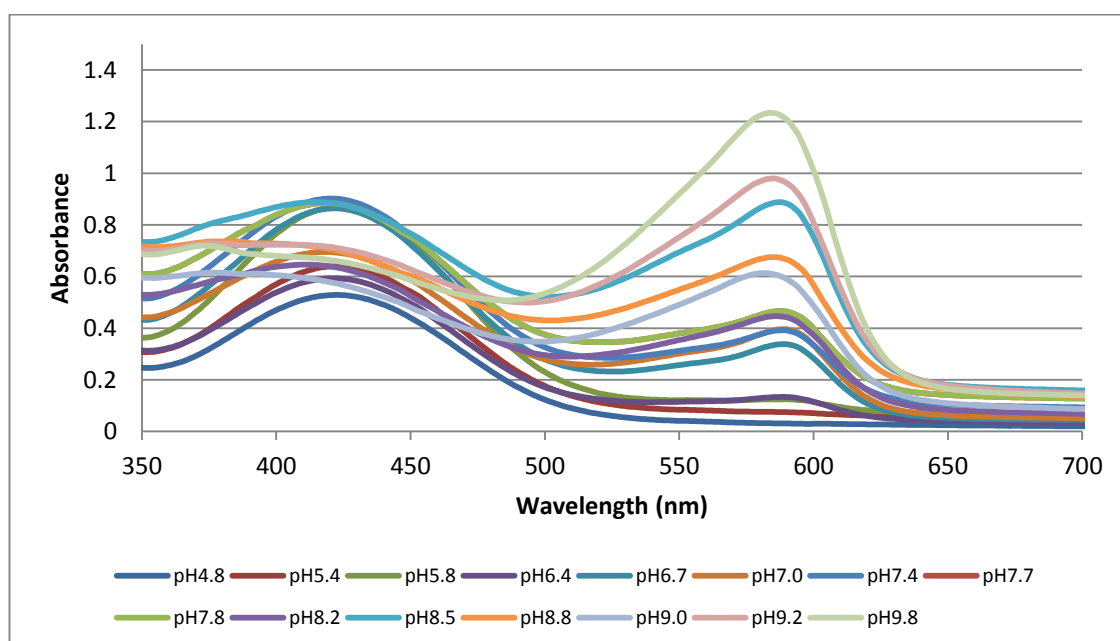


Figure 3.23: UV-vis spectrum of cresol red membrane at different pHs.

It is interesting that the immobilised cresol red membrane behaves differently than a free dye. Figure 3.22 shows that in basic medium cresol red membrane turned purple where as a free dye turns red. The dye behaves differently when immobilised in PVC and its spectroscopic properties change. The peak at 574 nm observed in figure 3.19 has moved slightly to 588 nm in figure 3.23 and the peak at 432 nm in figure 3.19 has moved to 424 nm in figure 3.23. From basic to acidic pH, the peak position (wavelength) changes too.

(a) Testing response of cresol red membrane in salt solution

The response of membranes was checked in 0.5 M NaCl solution of buffers of different pHs. In salt water, the pK_a value shifted up by about a 1 pH unit. There was only a few seconds delay in the response time as compared to the response in non-salt solution.



Figure 3.24(a) : Cresol red membrane response in saline buffer (pH: 5.82, 6.93, 7.68, 8.19, 8.88, and 9.42)

Previously it went light brown at pH 6.7 and in saline water it went light brown at 7.68 which means, the pK_a has come back to its original value in salt conditions. The spectra in figure 3.24 also show that the peak at 574 nm rises at pH 7.68 (light brown) and below this, the membrane remains yellow so the peak vanishes. In presence of salt, immobilised cresol red behaves like a free dye and went red in basic buffer.

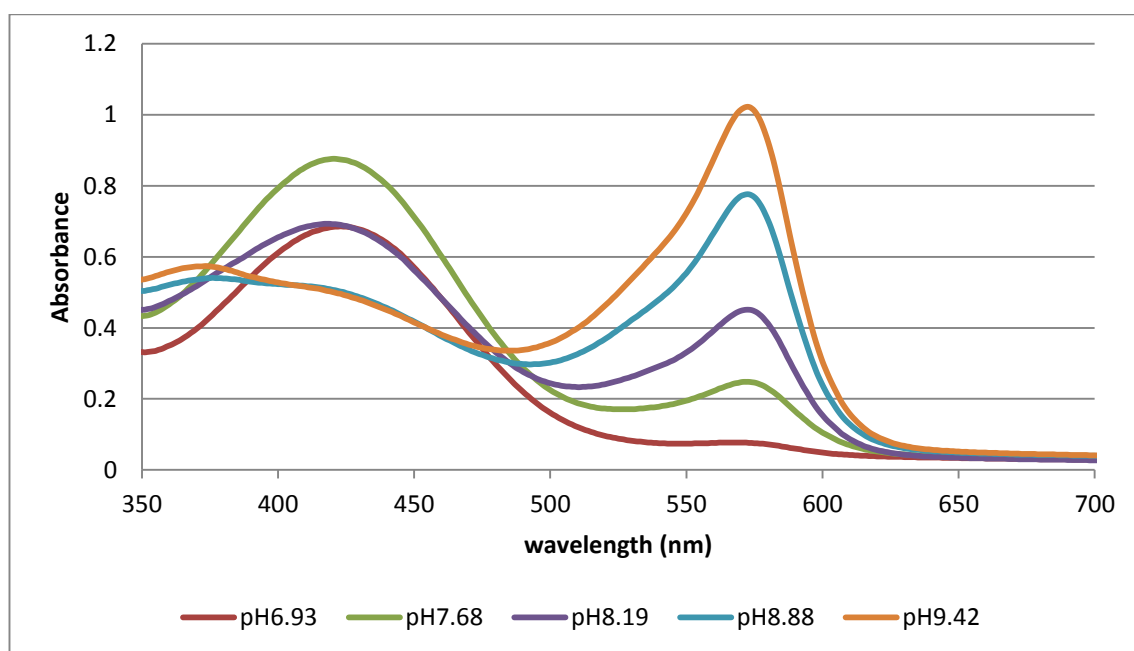


Figure 3.24 (b) : UV-vis spectrum of cresol red membrane in saline buffer.

This is not surprising as according to the literature, the colour range of organic dyes used as indicators is affected by foreign salts. (E. Bishop, 1972). Since in plasticized

membranes, the apparent pK_a shifts down but shifts up again when used in a salt solution, bromothymol blue should respond in the pH range of interest in salt water. Therefore bromothymol blue could be tested in salt water, and if the pK_a value shifts up again then it will respond in the pH range required for marine measurements and should be suitable for the envisaged application after all, which would be beneficial because of its strong and clear colour changes.

3.6.6 Testing response of bromothymol blue membrane in salt solution

The BTB membrane was tested in buffers containing 0.5 M NaCl-an ionic strength similar to natural seawater and its apparent pK_a value shifted back to its original value. The membrane responded within 1 minute. There was no leaching of dye and the colour response was as expected from free solution experiments. The membrane reverses within seconds from basic to acidic response (7.8-5.8), showing rapid kinetics and full reversibility.

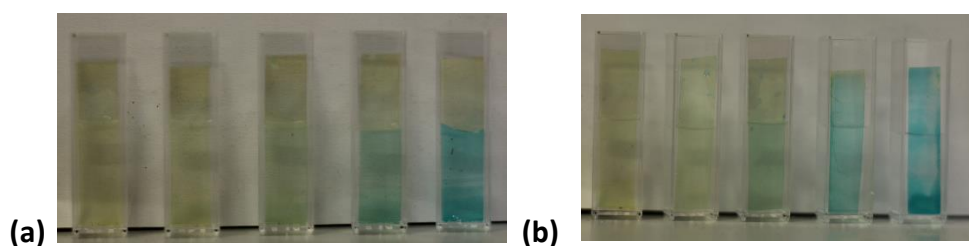


Figure 3.25 (a): (from left to right, pH of phosphate buffer: 5.9, 6.0, 6.8, 7.5, and 8.2) containing 0.5 M NaCl. (b): From left to right pH: Citrate buffer 5.8, 6.4, 7.0, Tris buffer: 7.4, 7.8 containing 0.5 M NaCl.

Figure 3.25 shows that the pK_a value of immobilised bromothymol blue shifted back to its original value making it appear yellow in acidic medium, green at neutral pH and blue in basic medium, which in the absence of salt otherwise appears blue in all samples.

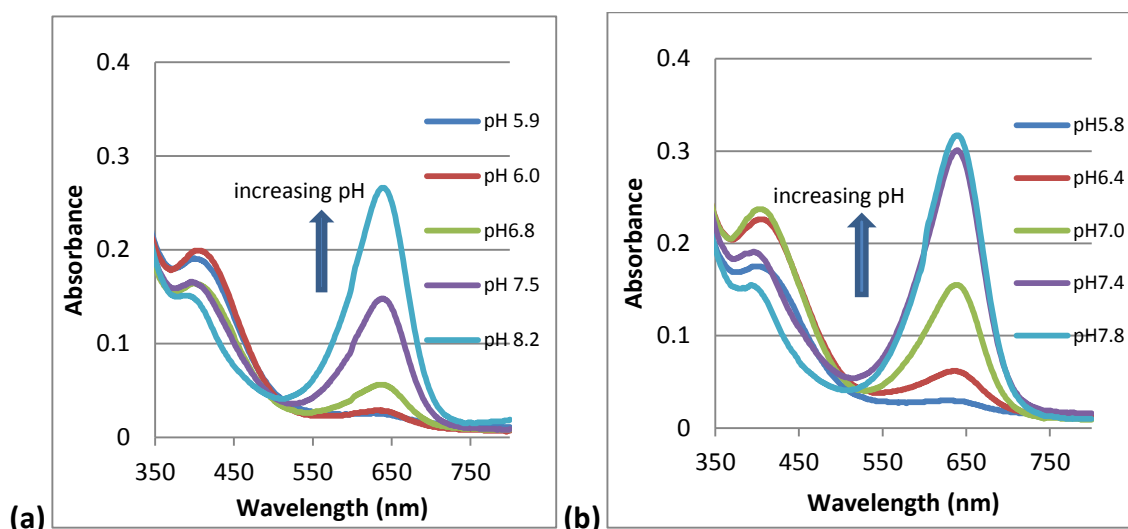


Figure 3.26: UV-vis spectrum of BTB membrane in saline buffer. (a) Phosphate buffer solutions of different pHs containing 0.5 M NaCl. (b): Citrate buffer solutions of pH 5.8, 6.4, 7.0 and Tris buffer solutions of pH 7.4, 7.8 containing 0.5 M NaCl.

Figure 3.26 shows the spectra of BTB membrane in the 0.5 M NaCl solution of buffers at different pHs. The buffers used for testing were citrate and Tris buffers. Citrate buffer solutions of pH 5.8, 6.4, 7.0 and Tris buffer solutions of pH 7.4, 7.8 containing 0.5M NaCl were used. Citrate (low pHs) and tris (high pHs) buffer solutions were used along with phosphate buffers separately to cover a wide range of pHs, in order to monitor the pK_a shift that may occur in the presence of salt, but the membrane responded in the range expected from the free dye. That is why the spectrum was recorded only in the range where the colour change was observed. The peaks in the spectra above increase by increasing pH so the absorbance in the red region increases when pH is increased, making the membrane appear blue. This behaviour of membrane is similar to the free dye in buffers without added salt.

3.6.7 Response time of BTB membrane

To investigate the rate of response to change of pH, samples of membrane equilibrated in one buffer had the buffer switched to one of a different pH. The time to equilibrate was followed in a UV-vis spectrophotometer at a fixed wavelength of 639nm (λ_{max} for BTB in membrane).

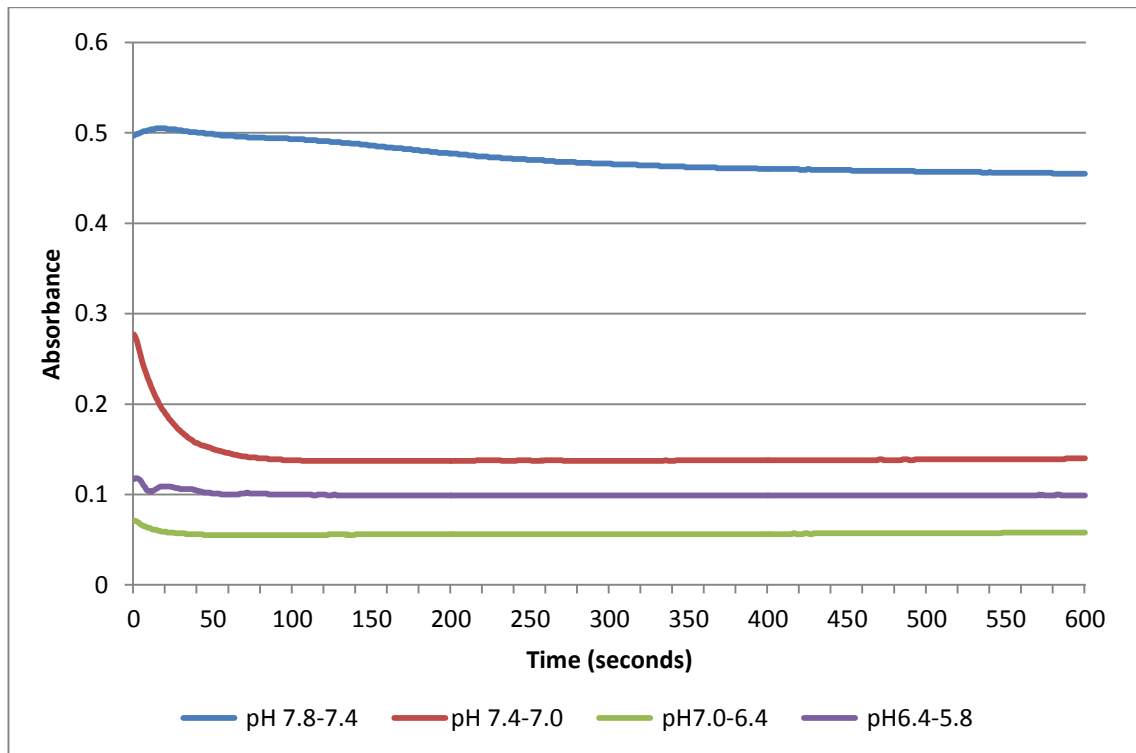


Figure 3.27: Time scan of BTB membrane showing the response time for re-equilibration from one pH to another (pH intervals indicated in the legend).

As seen in figure 3.27, during the first cycle, conversion from pH 7.8 to 7.4 took about 6 minutes. It was observed that the membrane response was a bit slow in the beginning but it became faster from the second cycle onwards. Probably, it is slow because when the membrane is made by spreading the solution, the components of membrane are scattered and not well organised for faster diffusion of H^+ ions but once the membrane is conditioned in aqueous solution, the components arrange themselves and the diffusion becomes fast which decreases the response time.

The membranes equilibrated in about 100 seconds.

3.7 Conclusions

- PVC based sensing membranes are better than the cellulose acetate membranes because there is less dye leaching, fast ion diffusion, more homogeneity and no precipitation in the membrane.
- The composition of the membrane sometimes needs to be optimised for fast response if the dye is changed depending on the nature of acidic or basic dyes and counter ions. For example when the effective composition of membranes for neutral red (having a positively charged counter ion) was used in the case of bromothymol blue (which is a positively charged dye and the counter ion was negatively charged), the membrane response was very slow. However, the same composition is effective for the dyes that are positively charged keeping the counter ion the same. For example: bromothymol blue and cresol red are both positively charged and the same composition forms effective membranes.
- The spectral properties and the pK_a values of pH dyes may change after the dye has been plasticised in a PVC membrane but are also dependent on the presence or absence of salt. For example: bromothymol blue and cresol red.
- PVC based pH sensing membranes containing bromothymol blue as a dye have been developed and optimised for rapid response. The effective composition of BTB membrane solution that will be used in future is: BTB: 12.5 mg, TOAB: 44 mg, PVC: 74 mg, Bis-2 (ethylhexyl sebacate): 250 mg and THF: 3 mL. The solution was spread on a transparency sheet and left to dry, after drying, the sheet can be cut into pieces and the UV-vis spectrum can be measured.
- The pK_a value of plasticized bromothymol blue is highly dependent on the presence or absence of salt and shifts about 1 pH unit down in the absence of salt but shifts back to its original value of pK_a 7.0 in the presence of 0.5 M NaCl salt. This is favourable for application in the marine environment but it also hints to a cross-sensitivity on salinity. Knowing that the salinity in sea doesn't change drastically other than at estuaries, the sensor should perform well in marine environment. However, this may be a problem at estuaries.
- The membrane is homogeneous and shows no leaching of dye. The response time is about 100 s after being conditioned once.

3.8 References

- Bishop, E. (1972). *Indicators*. Rushcutters Bay: Pergamon Press. pp 50-55.
- Cajlakovic, M., Lobnik, A. & Werner, T. 2002 Stability of new optical pH sensing material based on cross-linked poly (viny alcohol) copolymer. *Analytica Chimica Acta* **455**, 207-213.
- Dawson, R. M. C., Elliot, D. C., Elliot, W. H., Jones, K. M. (1986). *Data for biochemical research*. Oxford: Clarendon press oxford, 3rd edition. p432.
- Fakhari, A. R., Ganjali, M. R. & Shamsipur, M. 1997 Pvc-based hexathia-18-crown-6-tetraone sensor for mercury (II) ions. *Analytical Chemical Journal* **69**, 3693–3696.
- Gorton, L. & Fiedler, U., 1977 A zinc-sensitive polymeric membrane electrode. *Analytica Chimica Acta* **90**, 233–236.
- Gupta, V. K., Kumar, A. & Mangla, R., 2001 Protoporphyrin IX dimethyl ester as active material in PVC matrix membranes for the fabrication of zinc (II) selective sensor. *Sensors Actuators B* **76**, 617–23.
- Gupta, V. K., Jain, A. K. & Kumar, P. 2006 PVC-based membranes of *N, N'*-dibenzyl-1, 4, 10, 13-tetraoxa-7, 16-diazacyclooctadecane as Pb(II)-selective sensor. *Sensors and aquators B: chemical* **120** , 259-265.
- <http://www.sigmaaldrich.com/catalog/product/sial/857890?lang=en®ion=GB>
- Kolthoff, I. M. (1936). *Acid-base indicators*. New York: The Macmillan Company. p130.
- Mousavi, M. F., Alizadeh, N., Shamsipur, M. & Zohari, N. 2000 A new PVC-based 1, 10-dibenzyl-1, 10-diaza-18-crown-6 selective electrode for detecting nickel II ion. *Sensors Actuators* **66**, 98–100.
- Sabnis, R. W. (2007). *Handbook of acid-base indicators*. U.S: Taylor & Francis Inc. p102.
- Sabnis, R. W. (2007). *Handbook of acid-base indicators*. U.S: Taylor & Francis Inc. p105.

Safavi, A. & Abdullahi, A., 1998 Optical sensors for high pH values. *Analytica chimica acta* **367**, 167-173.

Scott, R. A. & Lukehart, C.M. (Eds.), (2007). *Applications of physical methods to inorganic and bioinorganic chemistry*. Hoboken, NJ: John wiley and sons Ltd, p271.

Wróblewski, W., Wojciechowski, K., Dybko, A., Brzoźka, Z., Egberink, R. J. M., Snellink-Ruehl, B. H. M. & Reinhoudt, D. N., 2000. Uranyl salophenes as ionophores for phosphate-selective electrodes. *Sensors Actuators B* **68**, 313–318.

Chapter 4

Sediment probe development and sensor characteristics

4.1 Introduction

The PVC based pH sensing membranes containing bromothymol blue as a dye had been developed and optimised. The next step was to control the thickness of the membrane to produce the membranes with the same thickness each time they were prepared and to develop a robust sensing probe that can be applied in the sediment without damaging the membrane. This chapter discusses the development of the sediment probe, response time of the sensor, techniques for photographing the sensor (controlling lighting and positioning of the camera) and the characteristics of the sensor.

4.2 Materials and Methods

4.2.1 Thickness of membrane

To control the thickness of the membrane, metering bars were bought from RK printcoat instruments Ltd. Litlington, Royston, Herts SG8 0QZ United Kingdom. The meter bars are made by winding stainless steel wire precisely on a stainless steel rod which results in a pattern of identical shaped grooves. These grooves then control the wet thickness. Meter bars are shown in figure 4.1 (RK website).



Figure 4.1: Meter bars used to spread the membrane solution and control the thickness of membrane.

The membrane was made using four different metering bars. 50 μL solution was taken to spread. Four types of membranes having a nominal wet thickness of 6 μm , 12 μm ,

24 μm and 40 μm were made. Each type of membrane was dipped in five buffers (pH: 5.9, 6.5, 7.1, 7.5, 8.0) and the response was compared. The 20 samples were analysed in a UV-visible spectrophotometer (Hitachi U-3010) for their absorption spectra and were photographed. Time scans were done to check the response time for each type of membrane when switched from pH 5.9 to 8.02. The membranes were conditioned before the time scan in phosphate buffer solutions of pH 5.9 and 8.02. 1 ml artificial sea water and 1 ml buffer solution was taken in the cuvette.

The following metering bars were used:

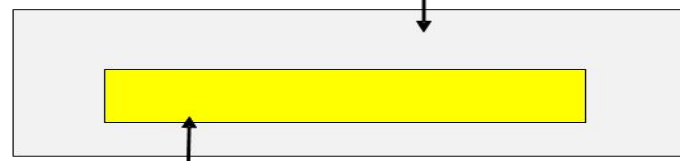
1. Yellow 6 μm
2. Red 12 μm
3. Green 24 μm
4. Black 40 μm

The indicated thickness is the target wet film thickness left after coating. The final dry thickness depends on the solid content of the spread solution. The actual thickness for the final concentration of the membrane will be discussed later in this chapter. Membranes made from yellow and red metering bar were conditioned twice in phosphate buffer solutions of pH 5.9 and 8.02 while the membranes made from green and black metering bars were conditioned once in phosphate buffers of pH 5.9 and 8.02.

4.2.2 Adding a white background to the sensing membrane

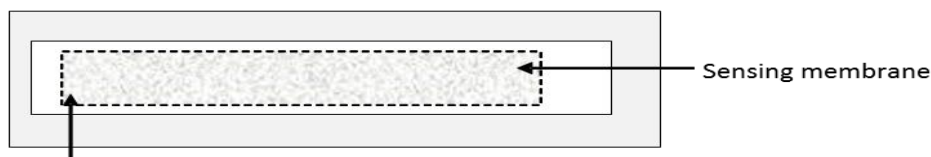
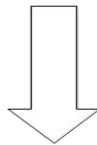
As marine sediments are typically dark and variable, their colour could interfere with the colour of the sensing membrane. Efforts were made to add a white background to stop colour interference. Figure 4.2 illustrates how the white membrane was stuck above the sensing membrane.

Double sided adhesive tape (bought from a local shop) stuck on transparency sheet



Sensing membrane

Adding white membrane



White membrane stuck above the sensing membrane.

Figure 4.2: Illustration of adding white membrane on sensing membrane.

The following white membranes were tested by assembling them as shown in figure 4.2.

1. Nylon based membranes:

- i. Nylon transfer Membrane /Nytran (Schleicher and Schuell)
- ii. Nytran 0.45 μm (Schleicher & Schuell)
- iii. Biobond Nylon membrane 0.45 μm (sigma)
- iv. Nytran N2 0.2 μm (Whatman)
- v. Nytran N45 (Whatman)

2. Cellulose based membranes:

- i. RC 59 membrane filter (Regenerated Cellulose membrane filters, 0.6 μm), (Schleicher and Schuell)
- ii. SMWP 02500 (Mixed cellulose Ester membranes,5 μm), (Millipore)
- iii. RAWP 02500 (Mixed cellulose Ester membranes, 1.2 μm), (Millipore)

3. Nitrocellulose membranes:

- i. Protran BA 83 (Nitrocellulose membranes)
- ii. Protran BA 83 0.2 (Whatman)
- iii. Protran BA 85 0.2 (Whatman)

- iv. Whatman membrane filters Cellulose Nitrate
- 4. Other membranes:
 - i. PVDF Transfer membrane /Westran (These are polyvinylidene fluoride membranes of 0.2 μ m pore size), (Schleicher and Schuell)

Other than the membranes named above, Sadolin Superdec Satin opaque wood protection (super white) paint as a white background was also tried. This paint forms a breathable microporous layer, which it was thought might allow water/H⁺ exchange. The paint was applied on the membrane and the membrane was tested in buffer after the paint dried.

4.2.3 Developing a sediment core probe

The membrane film was stuck to polystyrene or poly (methyl methacrylate) sticks using double sided adhesive tape. The nylon membrane (Nytran) was attached on it. Two such sensing probes were made. The new design made the sensor robust and it can be used in harsh conditions like marine sediments. The design also makes pH profiling possible. A mm scale was printed on transparency sheet and was stuck next to the sensing membrane to allow the insertion depth to be measured and to provide a depth measurement on photographs. Figure 4.3 illustrates the design of the probe.

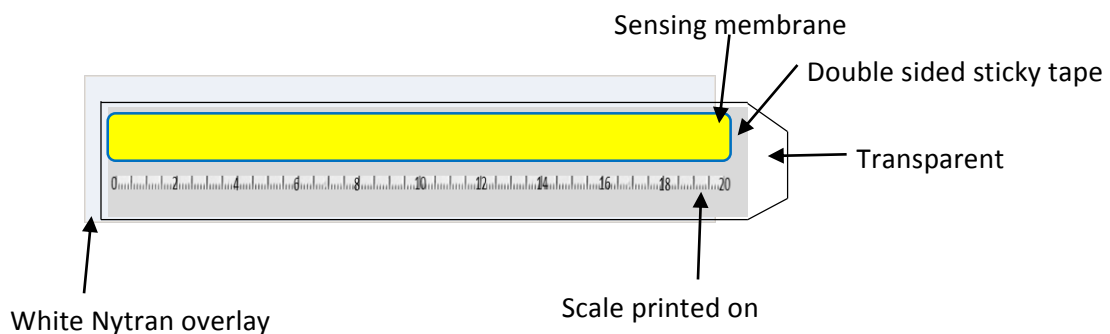


Figure 4.3: Probe schematic and a photograph of an actual probe. (Note: The slight apparent curvature is due to a barrelling distortion of the camera lens at its closest focal point setting.)

The black lines along the sides of the sensor strip were drawn in Microsoft power point and laser printed on transparency sheet. The membrane solution was spread on the back side of this transparency sheet to avoid the solvent disrupting the fused laser toner. This feature was added later to assist with automated edge detection during data analysis.

4.2.4 Photographing the probe

Initially the probe was photographed in natural light but it was observed that the lighting conditions are critical and variations can change the RGB values. A polystyrene box (dimensions: 39 cm ×29 cm) with a flash gun in it was therefore used to photograph the probes (figure 4.4). The camera was fixed in a hole made in the lid of the box. A second small hole was used to allow the built in camera flash light to enter the box and trigger the remote flash (Nissin digital, speedlite Di266).



Figure 4.4: Image of polystyrene box used for photographing the probe.

This set up still had some problems because when the lid of the box was opened to replace the probe, the camera position changed. A wooden box built from 6mm MDF painted with white Saddin superdec microporous matt/satin paint was constructed to keep the camera (Canon EOS 600D and Sandisk SD card) and the probe at the same position each time the probe was photographed (figure 4.5). The box contained a slotted shelf for the probe and the camera was fixed on the box. The flash gun (Nissin digital speedlite Di466) was kept inside the box and synchronised with a cable attached to the hot shoe of the camera.

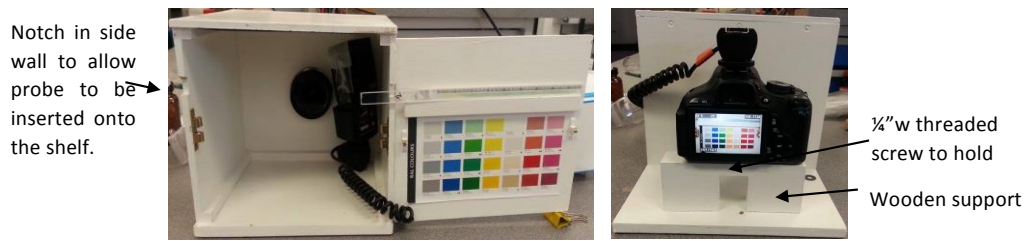


Figure 4.5: Image of the light box showing flash inside and the camera fixed outside.

Although this improved the photographic conditions, the lighting inside was still not consistent. The flash gun was operated using batteries and depending on the power and use of batteries, the lighting faded. There were also problems with flash positioning and reflection which caused bright spots in the box. Many different positions were tested, along with addition of frosted diffusers on the flash gun but even with these, no consistent and uniform lighting could be achieved. This was assessed by checking the uniformity of the white lines between the colour blocks on the attached paint chart using ImageJ.

In order to improve lighting uniformity, the flash was replaced with 54 large high power 12 V warm white LED chips which are splash proof and good for use in the sites close to the water (figure 4.6).

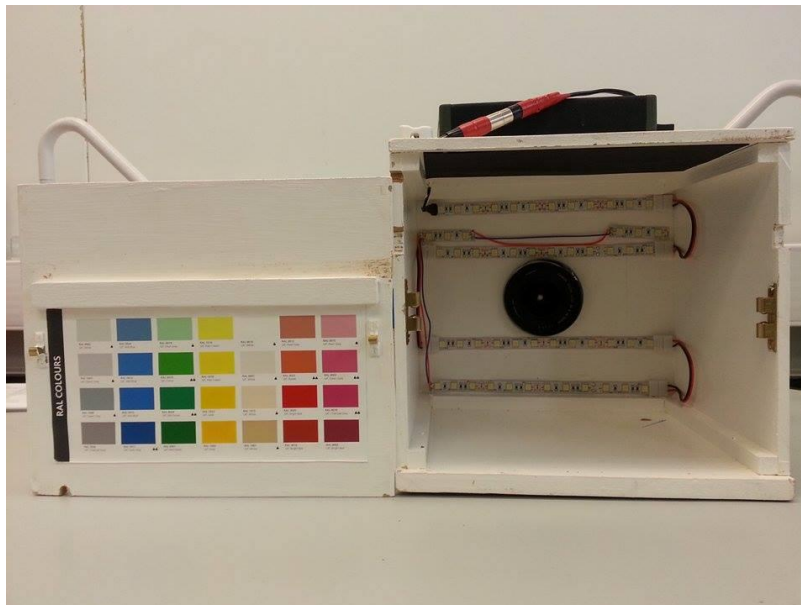


Figure 4.6: Image of the light box with LED lights attached.

The LED lights can be operated by either using the mains or the Lithium ion battery (Tracer Lithium polymer power pack/BP2544) attached to the box. The LEDs in the box had power of 13W so the current they would consume should be:

$$I=P/v = 13/12= 1.08 \text{ Amp}$$

Lithium polymer technology gives a very flat discharge curve which means if lights are being powered by the battery, they will remain bright for a minimum of 3-4 hours of continuous operation before brightness starts to dim. So a battery capacity of 8 Ah theoretically runs 8h and should be good for 30-60 minutes of intermittent use. The battery is resistant to water and is good for field work. The battery is connected to the LEDs using a connector, mini XLR plugs and socket bought from CPC/onecall and a 2A/240V inline switch bought from CPC/onecall.

Initially the box contained only four rows of LEDs (48). To check whether the lighting along the probe was consistent or not, the probe was dipped in NaOH solution and then moved along the shelf of the box and photographed at different points. Later 4 more LEDs were added in the corners of the box to make the lighting uniform along the line of the probe and correct the intensity drop-off near the edges.

To compare the photos taken using the mains and the battery, the probe was dipped in seawater (taken from Lowestoft) and was photographed 5 times using mains and five times using the battery and camera settings: Manual, 04", F22, ISO 100, Daylight mode, Exposure: 0, Zoom 24, focus: manual. This should confirm whether or not the lighting remains the same by using two different power supplies.

4.2.5 Enhancing the colour of the sensor

In order to obtain a bright colour in the photos for better colour analysis in the software, different approaches were tried such as increasing the amount of the dye and counter ion, decreasing the solvent and using a metering bar that gives thicker membranes. The following compositions tried are listed in table 4.1.

Composition	Composition of membrane	Comments
1	Same composition (BTB: 12.5 mg, Tetraoctyl ammonium bromide: 44 mg, PVC: 74 mg, THF: 1 mL, Plasticizer: 250 mg). The amount of solvent was lowered to 1 mL.	The membranes were made using 6 μm and 12 μm metering bars. 1 mL solution was taken when spread with 12 μm metering bar and 250 μL when using the 6 μm metering bar (Thicker membranes require more solution). The membranes response times were monitored in a spectrophotometer.
2	The amount of the dye and the counter ion was doubled and the amount of solvent was lowered to half. BTB: 25 mg, Tetraoctyl ammonium bromide: 88mg, PVC: 74 mg, THF: 1.5 mL, Plasticizer: 250 mg.	The 6 μm metering bar was used and 250 μL solution was spread on transparency sheet.
3	The amount of the dye and the counter ion was doubled and the amount of solvent was lowered 1 mL. BTB: 25 mg, Tetraoctyl ammonium bromide: 88 mg, PVC: 74 mg, THF: 1 mL, Plasticizer: 250 mg	6 μm metering bar was used and 250 μL solution was spread on transparency sheet.
4	The amount of the dye and the counter ion was increased four times and the	6 μm metering bar was used and 250 μL solution was spread on transparency sheet.

	amount of solvent was kept 3 mL. BTB: 50 mg, Tetraoctyl ammonium bromide: 176 mg, PVC: 74 mg, THF: 3 mL, Plasticizer: 250 mg	
5	The amount of the dye and the counter ion was increased four times and the amount of solvent lowered to half. BTB: 50 mg, Tetraoctyl ammonium bromide: 176 mg, PVC: 74 mg, THF: 1.5 mL, Plasticizer: 250 mg	6 μm metering bar was used and 250 μL solution was spread on transparency sheet.
6	The amount of the dye and the counter ion was increased six times and the amount of solvent was kept 3mL. BTB: 75 mg, Tetraoctyl ammonium bromide: 264mg, PVC: 74mg, THF: 3 mL, Plasticizer: 250 mg	6 μm metering bar was used and 250 μL solution was spread on transparency sheet.
7	The amount of the dye and the counter ion was increased eight times and the amount of solvent was kept 3mL. BTB: 100 mg, Tetraoctyl ammonium bromide: 352 mg, PVC: 74 mg, THF: 3 mL, Plasticizer: 250 mg	6 μm metering bar was used and 250 μL solution was spread on transparency sheet.

Table 4.1: Different compositions of membrane tried to enhance the colour of the sensor.

4.2.6 Response time with Nytran membrane

The sensing layer was made with a Nytran membrane overlay and the response was photographed every 15 seconds for 15 minutes after switching the pH from pH 8 to pH 5.8 and vice versa. 1 mL of artificial sea water and 1mL of buffer was taken in the cuvette. The experiment was repeated thrice to see the pattern. The photographs were taken every 15 seconds for 5 minutes and then every 30 seconds for 10 minutes from pH 5.8 to 7.8 and vice versa. The response time was checked by repeating the experiment with the increased dye content. The change was recorded from pH 5.9 to 7.7 in a phosphate buffer containing 0.5 M sodium chloride using a spectrophotometer and also by photographing every 15 sec for 5 minutes and then every minute for 25 minutes. The experiment was again repeated thrice and the means were plotted against the time.

4.3 Characteristics of BTB membrane

The effect of the following parameters was studied.

4.3.1 Effect of Temperature on sensing membrane

The effect of temperature on the membrane was studied using a sensing membrane with the following composition:

Components of membrane	Amount
Bromothymol Blue	12.5 mg
Tetraoctylammonium bromide	44 mg
Polyvinyl Chloride	74 mg
Tetrahydrofuran	3 ml
Bis(2ethylhexyl)sebacate	250 mg

Table 4.2: Composition of membrane used to study the temperature effect.

250 µl solution was taken and spread on a transparency sheet using the 6 µm metering bar. The sheet was left until it dried. The sheet was cut into square pieces. A piece of sensing membrane was conditioned in phosphate buffer pH 6.2 and pH 7.6.

Experimental set up

A circulating water bath was connected to a custom-built (M.Myles, UEA) glass device which was designed specially to hold the membrane inside (figure 4.7). It comprised a jacketed beaker with a flat glass window fused into it where the membrane could be attached and photographed without distortion. The glass device contained phosphate buffer (pH 5.93) with 0.5 M NaCl solution to make the amount of salt similar to sea water. A magnetic stirrer was used to stir and a thermometer was used to monitor the temperature of the buffer solution. A pH meter was used to monitor the pH of the solution. It was calibrated before monitoring the pH. The camera was fixed in front of the device. The water bath was at 26 °C . The photographs were taken at every temperature in a darkened room using a halogen desk lamp as the light source. The experiment was repeated by setting up the bath at a lower temperature and shooting photographs at each higher temperature as it was warmed up. The experiment was repeated again by using a phosphate buffer of pH 7.30.

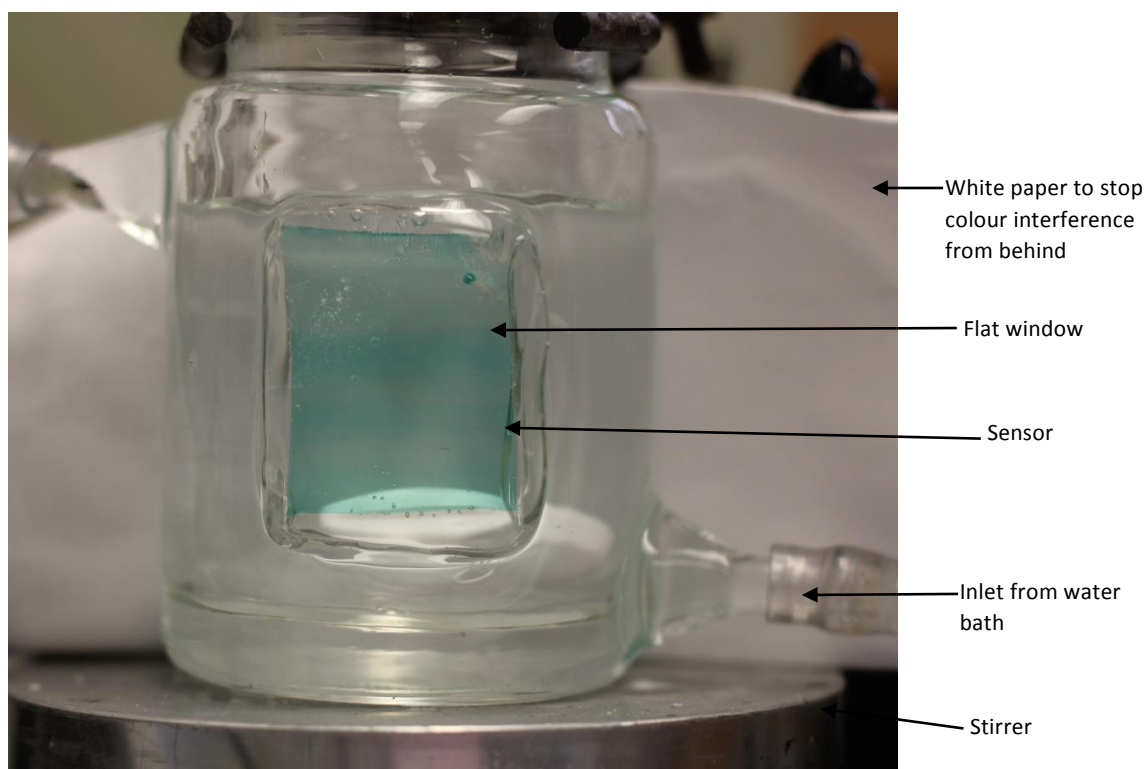


Figure 4.7: Image of the device used to study the effect of temperature.

Using ImageJ to analyse the photographs

The RGB values from the photographs were extracted using ImageJ. The photos were opened in ImageJ. The homogenous rectangle area from the sensor was selected. The area was then scaled to 1*1 pixels from the drop down menu in the 'Image' tab. This averages the area selected and makes sure that the area analysed in each photo is of the same pixels. From the 'plugin' tab, 'analyse' and then 'measure RGB' was selected. The results pop up in the result window. RGB values were converted into a single value using the formula $(R-B)/G$ and plotted against the temperature

Improving the sensor and the lighting conditions

The amount of dye was increased. The following membrane composition was used:

Components of membrane	Amount
Bromothymol Blue	50 mg
Tetraoctylammonium bromide	176 mg
Polyvinyl Chloride	74 mg
Tetrahydro Furan	3 ml
Bis2ethylhexyl sebacate	250 mg

Table 4.3: Composition of membrane with increased dye.

The sensing membrane was stuck to the double sided tape and the Nytran white membrane was stuck above covering the whole sensor. It was then pressed to remove all the air bubbles. The sensor was stuck to the glass window and the temperature effect was observed. The sensor was photographed in the dark room and the camera was fixed to a box. A desk lamp was used as a light source during photography. A black card was kept behind the device to get a better and clearer photograph of the sensor which had a nytran membrane as a backing material. Phosphate buffer pH 7.15 was used. The experiment was repeated using seawater.

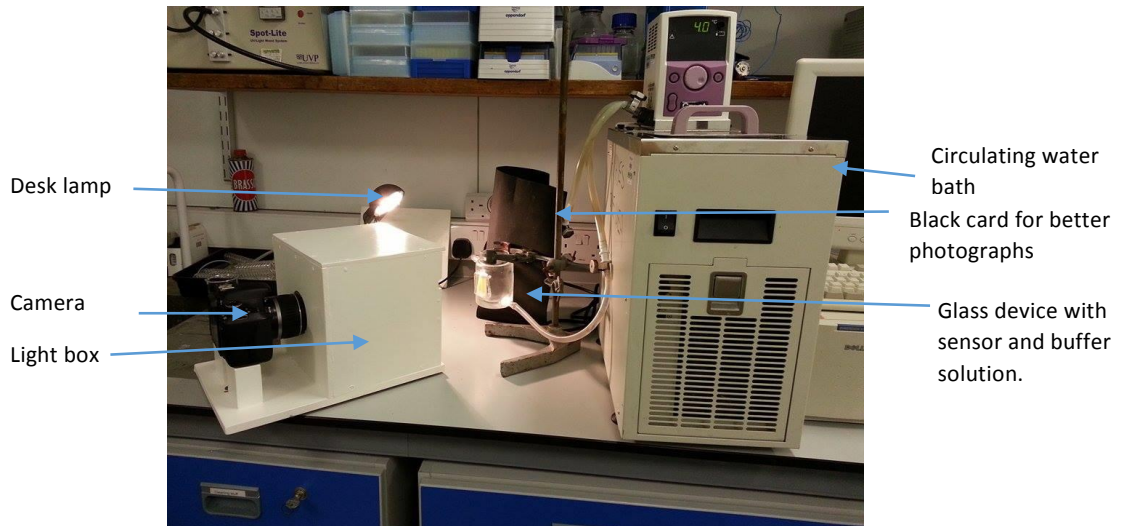


Figure 4.8: Experimental set up for temperature studies.

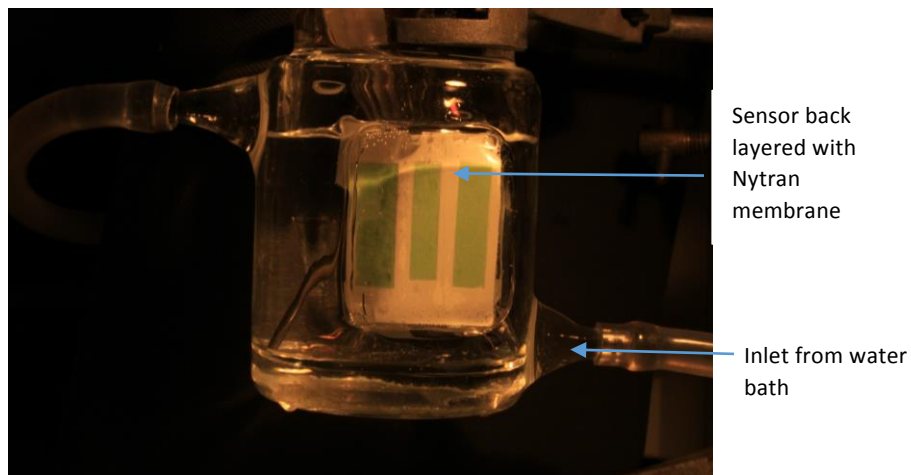


Figure 4.9: Improved sensor design with increased amount of dye and a white Nytran membrane behind.

Controlling the pH of the buffer

Since the pH of the phosphate buffer decreased with increasing temperature, the experiment was repeated with the pH adjusted using 1 M and 0.5 M sodium hydroxide drop wise to maintain the pH at each temperature. The same experiment was repeated but setting the water bath at a higher temperature and reducing the temperature and using 0.5 M HCl drop wise. The change was then photographed. The experiment was repeated using sea water. The pH of sea water (California Norfolk, NR29) was controlled (details of pH values during different experiments are discussed in results

and discussion section) using 0.125 M NaOH and 0.125 M HCl due to its lower buffering strength.

4.3.2 Effect of salt on sensing membrane

The sensing membrane was tested in 5 different NaCl concentrations i.e. 0.1 M, 0.3 M, 0.5 M, 0.7 M, and 0.9 M keeping the buffer and pH the same to check the effect of high ionic strength and observe whether or not the response was stable under these conditions. The strips of membrane were taken in a cuvette. 1 ml of buffer and 1 ml of salt water was added into the cuvette which makes the final concentration 0.05 M, 0.15 M, 0.25 M, 0.35 M, and 0.45 M in NaCl. The phosphate buffers tested had pH 5.8 and 7.3. All the samples were measured in a UV visible spectrophotometer and were also photographed. As the NaCl concentration in sea water is approximately 0.5M, the membrane was further tested in different concentrations that are more or less close and equal to the concentration of NaCl in sea water i.e. 0.40 M, 0.42 M, 0.44 M, 0.50 M, 0.52 M, 0.54 M, 0.56 M, 0.58 M, 0.60 M in a buffer of pH 6.6. A few low concentrations (0.20 M, 0.21 M, 0.22 M, 0.23 M, 0.24 M, 0.26 M, 0.27 M, 0.28 M, 0.29 M, and 0.30 M) of salt were also tested to observe any changes occurring due to difference in salt concentrations. The buffers tested had pH 5.8 and 7.3. All the samples were photographed and their absorption spectra were recorded in the UV-visible spectrophotometer.

4.3.3 The effect of light on the sensor

While trying to take spectra of the sensor with a white membrane attached to it using a fibre optic reflection spectrometer, it was observed that the high intensity light rapidly bleached the dye in the membrane so it became necessary to investigate if light affects the sensor. Two sensing probes were made using Nytran as a white background. The probes were conditioned once in acidic buffer and then in basic buffer before use. Two beakers were taken. Both contained buffer (pH: 7.7) and NaCl salt (0.5 M). One of the probes was kept in the dark while the other was kept in sunlight for 4 days. Every day, the response was checked and probes were photographed.

4.3.4 Effect of camera Flash

To investigate if the flash bleaches the dye or not, two probes were made. One of them was dipped in basic buffer and the other one was taken as a dry probe. Both the probes were photographed in the polystyrene box using the flash on maximum power every 5 minutes for 2 hours and 15 minutes (27 flash exposures, which would represent multiple re-uses of the sensor).

4.3.5 Storing Preference

The probes were tested for storing them in acid, base and buffer. Four probes were made. One of them was kept dry, the second in phosphate buffer (pH: 7), the third in 0.5 M HCl and the fourth in 0.5 M NaOH. The response was observed optically after 1 and 2 hours and the next day.

4.3.6 Reusability

The reusability of the membrane was checked by storing the sensing membrane in phosphate acidic (4.7) and basic (7.8) buffer in cuvettes and covering them with kitchen foil, the response was checked every hour for five hours after transfer into phosphate buffer pH 6.5. The response was analysed in the UV-Vis spectrophotometer.

4.4 Results and discussions

4.4.1 Controlling the thickness of the membrane

The membrane prepared from the 6 μm metering bar was thin and had low absorbance. The one prepared from the 40 μm bar responded slowly and increased the response time of the membrane. The one prepared from the 12 μm metering bar was good in response, absorbance and photographs. The images, UV-vis spectrum and the time scan of membranes made from different metering bars are shown in figure 4.10.

Note: Membranes made from 6 μm and 12 μm metering bars were conditioned twice while those made from 24 μm and 40 μm metering bars were conditioned once.

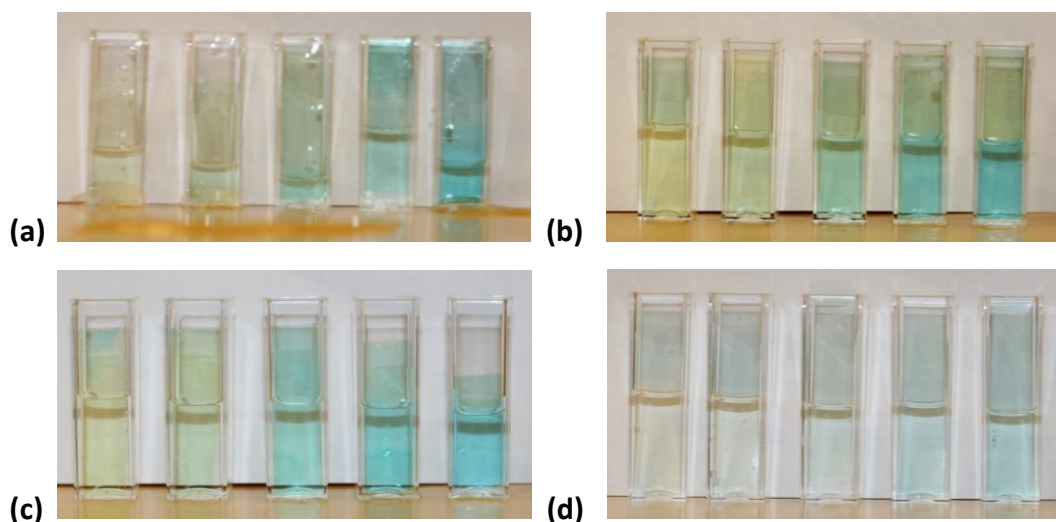


Figure 4.10: Response of BTB membrane made from (a) 40 μm metering bar (b) 24 μm metering bar (c) 12 μm metering bar, (d) 6 μm metering bar.

The 6 μm metering bar produced a very thin membrane that did not give a clear colour that could be photographed easily. The 12 μm metering bar kept the response rapid and produced a membrane that gave a decent colour intensity that could be photographed. 40 μm and 24 μm metering bars gave films with slower responses, therefore the 12 μm metering bar should be used. The thickness was controlled by using the metering bar so a homogenous sheet of membrane is obtained on the transparency sheet.

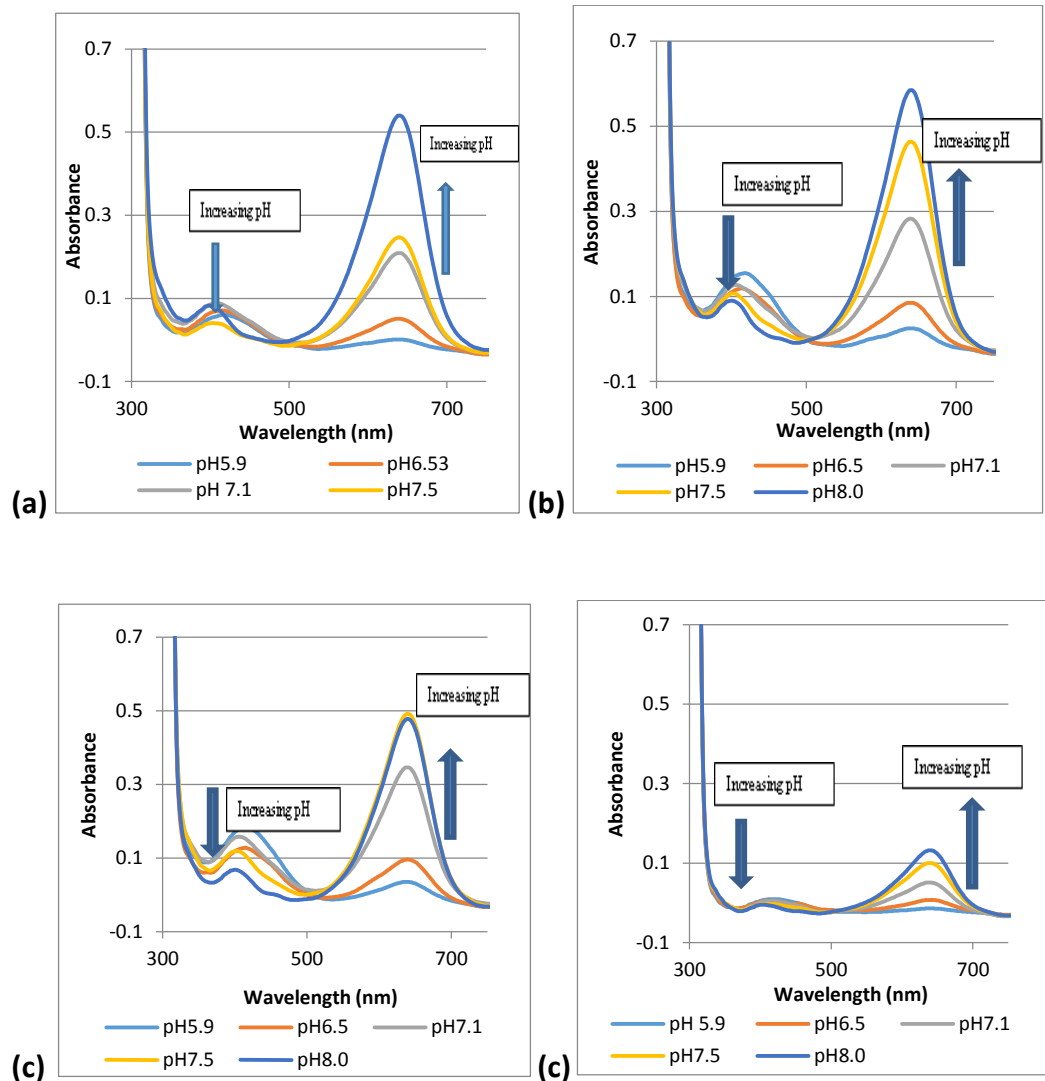


Figure 4.11: Absorbance Spectrum for BTB membrane made from (a) 40 μm metering bar (b) 24 μm metering bar (c) 12 μm metering bar, (d) 6 μm metering bar.

The spectra of films made from all the metering bars show the change in the colour with pH but as the sensor will be photographed *in-situ* in the marine sediments or as a probe, the membrane with a proper thickness that gives a clear colour response which can be photographed is preferred. The one made with the 12 μm metering bar gave suitable absorbance values.

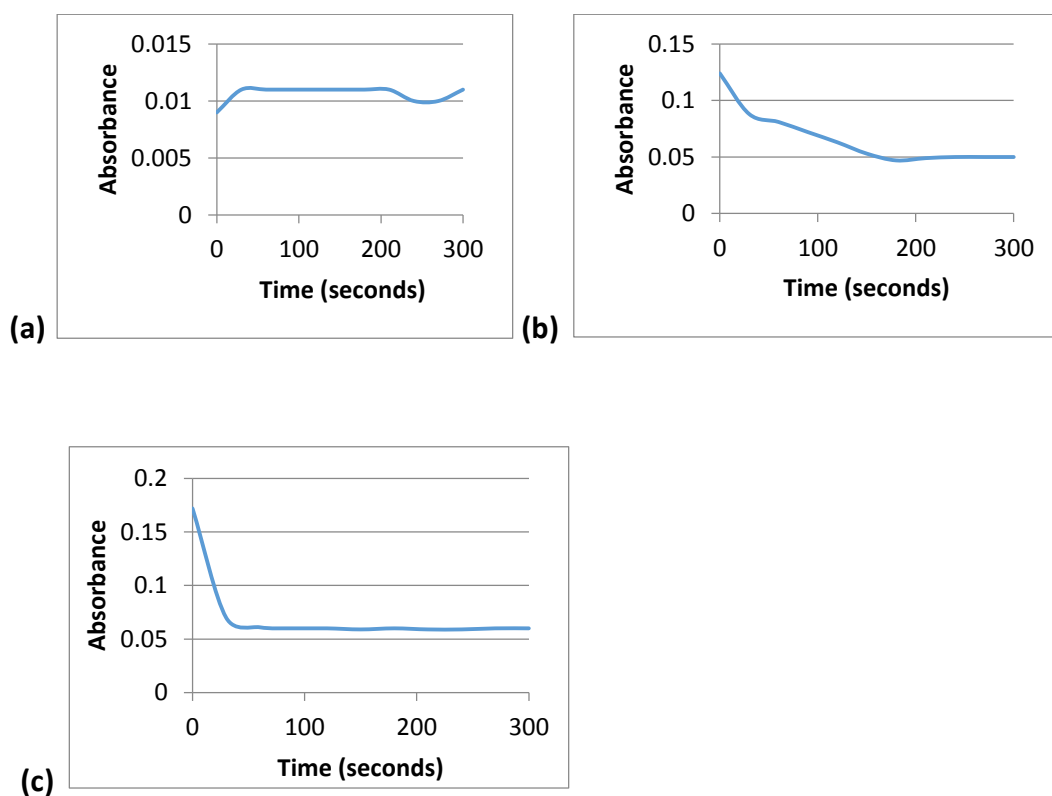


Figure 4.12: Time scan (at 640 nm) of BTB membrane made from (a) 40 μm metering bar (b) 24 μm metering bar (c) 12 μm metering bar by switching the pH from 5.9 to 8.02

The time scan of the membrane made with the 6 μm metering bar could not be recorded because the change was very rapid and the response was completed in the time it took to switch the buffer.

4.4.2 White background

The response characteristics of the various white membranes tested are summarised in table 4.4.

Name	Material	Response characteristics		
		Physical strength	Opacity/whiteness	Speed of response
PVDF	Polyvinylidene fluoride	Robust	Opaque	Slow
RC 59	Regenerated Cellulose nitrate	Robust	Less Opaque than Nytran	fast
Whatmann Cellulose nitrate	Cellulose nitrate	Very soft, tears while assembling	Less opaque than Nytran	Slow

Table 4.4: Comparison of white membranes.

SMWP	Mixed cellulose Ester	robust	Translucent	Fast
RAWP	Mixed cellulose Ester	Very soft, tears while assembling	Translucent	Slow
Nytran	Nylon	Robust	Opaque	Fast
Protran BA 83	Nitrocellulose	Robust	Opaque but less opaque than Nytran	Fast

Table 4.4: Comparison of white membranes.

PVDF transfer membrane (Westran) slows down the response. RC 59 did not remain opaque once used and the colour of sediment would still interfere. The Sadolin Superdec Satin prolonged the response time and membrane did not respond even after 20 minutes. Whatmann membrane (cellulose nitrate) filters slowed down the response and the membrane was very soft and tears while attaching it to the sensing membrane. SMWP did not remain opaque once used and did not stop colour interference and the response was also very slow. RAWP was too soft and tore and did not remain opaque once used either. Nytran was robust and remained opaque. Protran BA 83 was good in response but the opacity was less than Nytran. Nytran 0.45 (Sheicher & Schuell), Biobond Nylon membrane (Sigma), Nytran N2 (Whatmann) and Nytran N24 (Whatmann) responded similarly and were all opaque. Protran 83 was faster in response but Nytran was the best as a balance between opacity and response

time. Nytran (0.45 μm) was thus chosen as a background membrane to stop interference of colour.

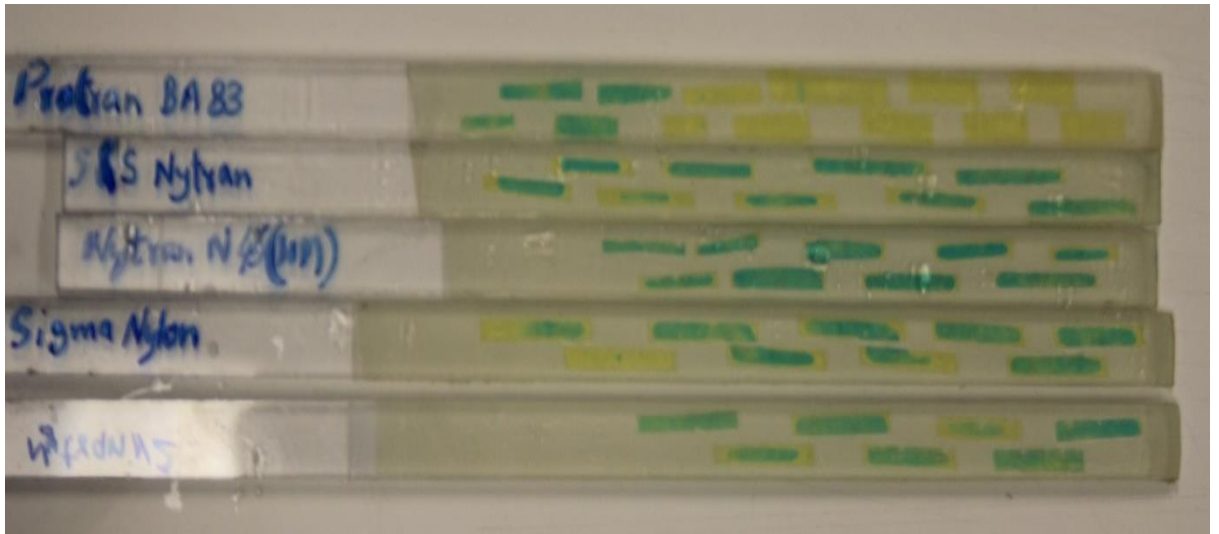


Figure 4.13: Response of different opaque white membranes used.

4.4.3 Photographing the probe

In a wooden dark box, with an external flash, a standard colour from the Image was taken and the colour index, which is obtained from RGB values by using the formula $(R-B)/G$, was measured in about 18 photos to see the variability in the lighting conditions.

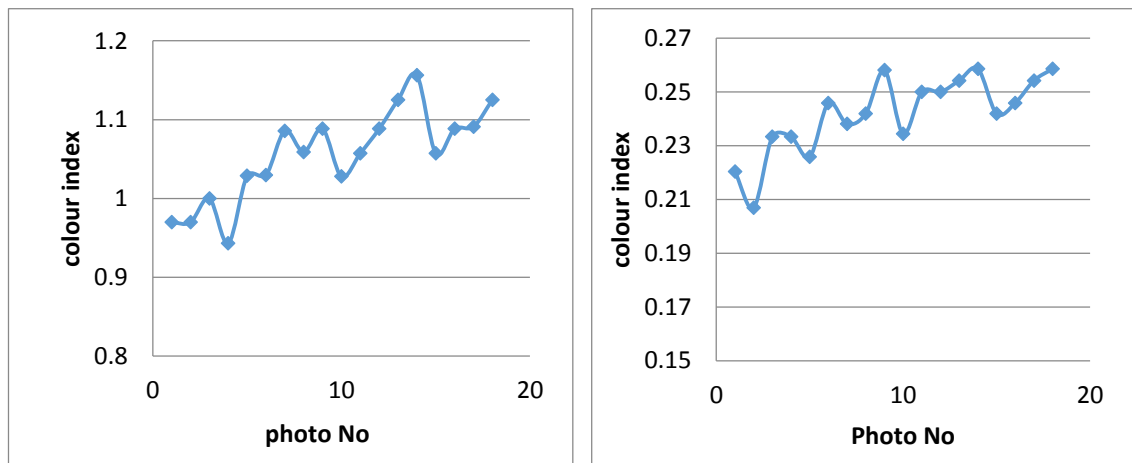


Figure 4.14: The colour index of two standard colours chosen from the chart row below the probe stand.

Both the charts show some variability although the same standard colour from the chart was taken. This means there is some lighting inconsistency. This can be double checked by taking white slices along the row and column within a photo and the same white piece in different photos.

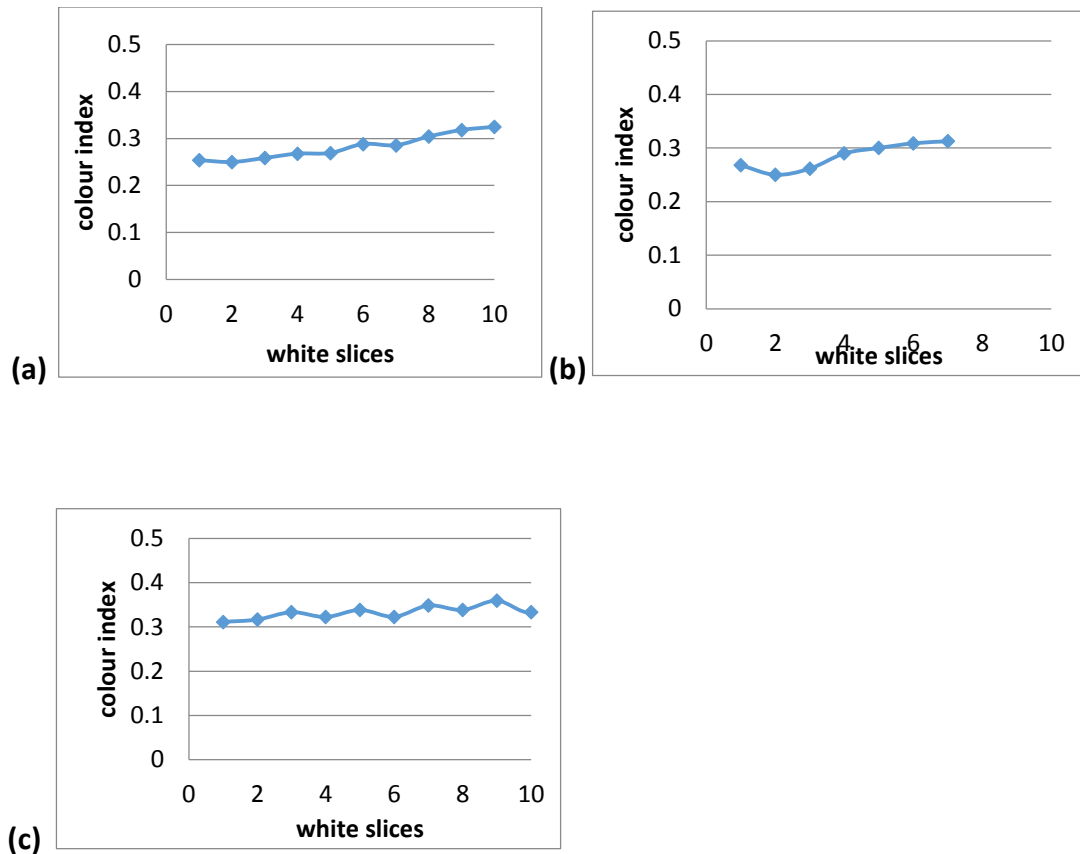


Figure 4.15: (a) Colour indices of white slices in a column with in a photograph, (b) a row from the photograph of the light box within a photograph and (c) the colour indices of white row of the light box in different photographs.

This means there was lighting inconsistency in the dark box due to the external flash. In an attempt to improve this, the flash was replaced with an array of white LED lights and the white row below the shelf in the photograph was analysed in imagej to extract the RGB values and plot the colour index against different points in the box to check if it had improved the lighting consistency.

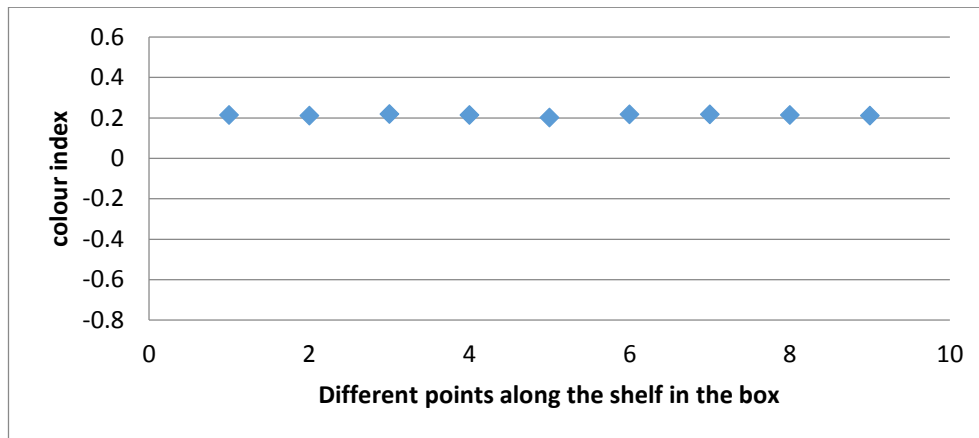


Figure 4.16: The colour index values of white row along the box where the probe rests.

In an attempt to improve lighting on the probe, the probe was dipped in NaOH solution and photographed by moving it along the shelf in the box with four rows of LED lights and the same portion of the probe was used to extract RGB values at each point. The colour indices $((R-B)/G)$ were plotted against the different points in the box to check the lighting consistency along the probe. There was still some inconsistency in the light along the line of the probe in the box. The colour index values were less in the corners which means the lighting was less there so some more LED lights were added into the corners to adjust the lighting and make it consistent. A probe was photographed after it had responded before and after adding the LED lights by moving it along the shelf.

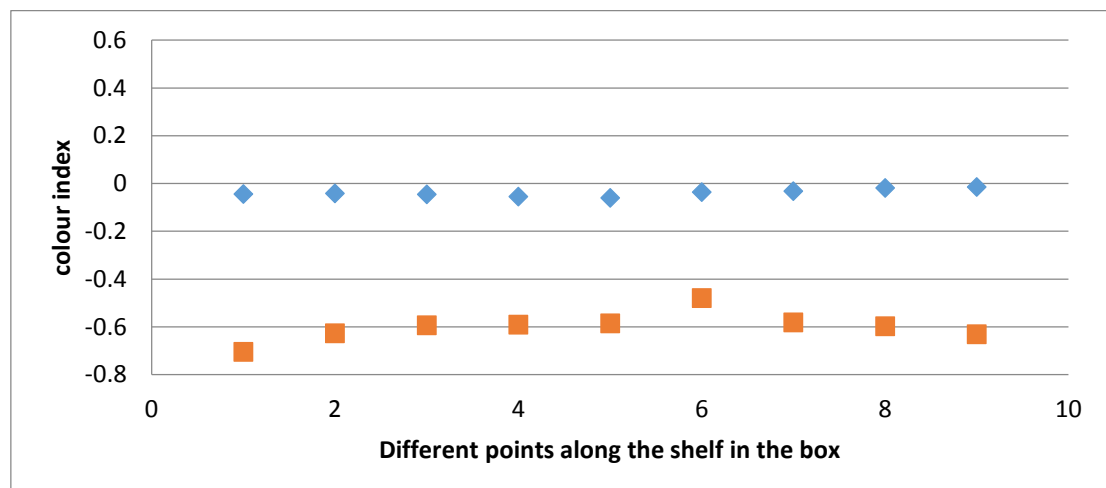


Figure 4.17: Comparison of lighting consistency before (red) and after (blue) adding extra LED lights in the corners of the light box.

As seen in figure 4.17, the lighting consistency has improved a lot and it looks more or less consistent after addition of extra LEDs. Both the graphs were transposed to see the difference. The colour index values were negative before adding the extra LED lights because the probe was used in NaOH solution which is very basic and the second time the probe was used in a phosphate buffer. However, the important thing to be noticed is how consistent the colour index values are along the shelf in the light box rather than how different they are in two experiments. The graph was plotted scaled to the typical colour index values of calibration (discussed in next chapter) to see how much error it may introduce. The standard deviation of the colour index values has dropped from 0.056 (before adding extra LED lights) to 0.015 (after adding LEDs) which is about 1% of the total index value range of calibration graph (1.4units). It was deemed that this was an acceptable error due to lighting variability.

Comparison of photographs taken using mains and battery power for the lighting

A Probe was dipped in seawater taken from Lowestoft and photographed five times using mains and battery as the power source for the LED lights.

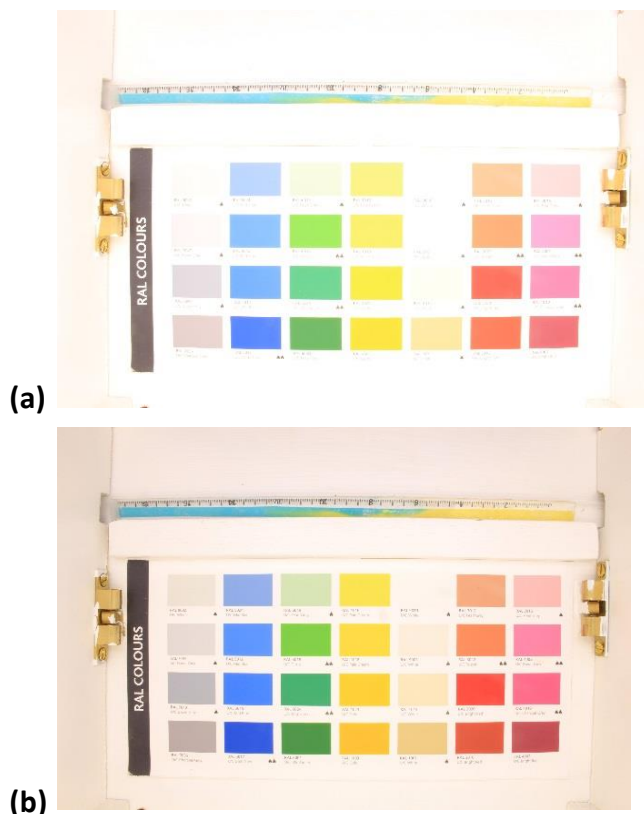


Figure 4.18: photo taken using (a) battery and (b) mains.

As seen in figure 4.18 and table 4.5, the photos taken using the battery were brighter than the ones taken using the mains.

Photo No	Colour index Values (Battery)	Colour index values (Mains)
1	-0.44	-0.59
2	-0.44	-0.59
3	-0.43	-0.60
4	-0.44	-0.59
5	-0.43	-0.59
Mean	-0.436	-0.592
SD	0.0054	0.0045

Table 4.5: Colour index values of probe photographed using mains and battery.

The colour index values of the photos taken using battery have higher values than the ones taken using mains but the values remain the same from photo to photo for the battery or mains with almost identical (small) SD values, which demonstrates the consistency of the lighting. The camera settings should be changed to get decent photos using the battery during field work. Moreover, the probe calibration should also be done using the battery with the same camera settings. The following camera settings were found by trial and error to give appropriate colour and brightness.

Using the mains: Manual, 0"4, F22, ISO 100, Daylight, Zoom between 18 and 24, focus manually.

Using the battery: Manual, 1/8 S, F22, ISO 100, Day light, Zoom between 18 and 24, focus manually.

4.4.4 *Enhancing the colour of the sensor*

In an attempt to obtain a bright colour in the photos for better colour analysis in the software, different approaches were tried such as increasing the amount of the dye and counter ion, decreasing the solvent and using a metering bar that gives thicker membrane. The following results were obtained.

1. The decrease in the solvent to 1 mL increased the response time. The membranes made from the 12 μm metering bar were darker in colour than the ones made by the 6 μm metering bar.

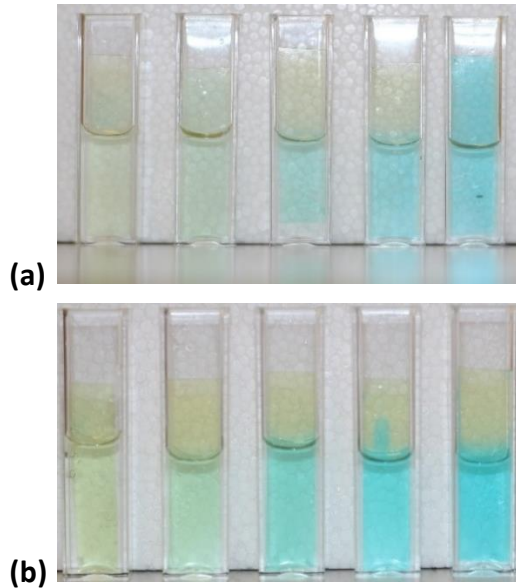


Figure 4.19: (a) membrane made from 6 μm metering bar (b) red metering bar.

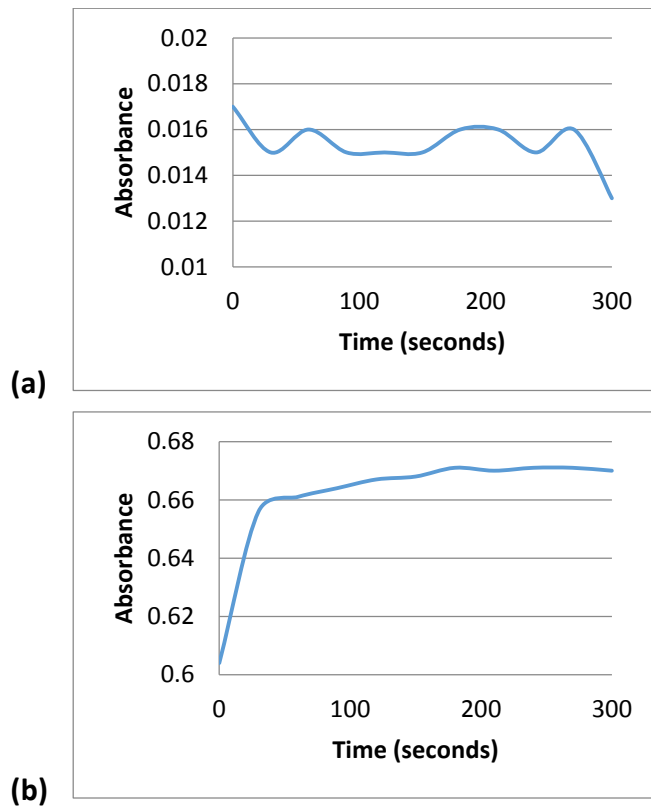


Figure 4.20: (a) Time scan of membrane made from 6 μm and, (b) 12 μm metering bars by switching the pH from 8.02 to 5.9 at 640nm.

Both the membranes were still equilibrating even at 5 minutes which has prolonged the response time. Compositions 2 and 5 produced homogeneous membrane with fast response but composition 5 had more dye and more intense colour in it therefore this composition was adopted as a final membrane composition.

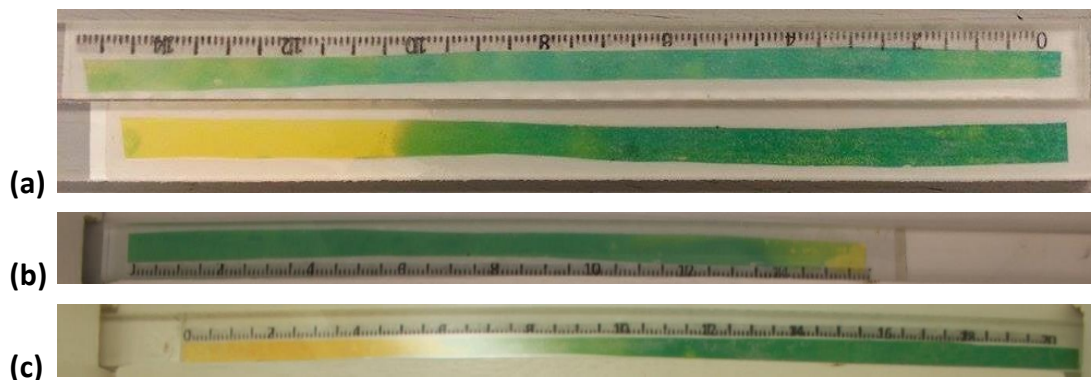


Figure 4.21: (a) composition 4 compared with old composition. (b) Composition 5, homogenous and intense colour. (c) Composition 7, patchy and inhomogeneous.

Composition 3 made the membrane very thick due to low solvent content and was very slow in response. Composition 4 made the membrane inhomogeneous and compositions 6 and 7 were not selected because when the solution was spread on transparency sheet, after drying, it made a patchy membrane with lots of spaces in between (presumably a surface tension problem causing the film to break up into droplets as it dries). The best composition was 5 (BTB: 50 mg, Tetraoctyl ammonium bromide: 176 mg, PVC: 74 mg, THF: 1.5 mL, Plasticizer: 250 mg). The solution should be spread using the yellow metering bar that gives a wet thickness of 6 μ . The membrane responds in seconds without a nytran membrane and the change in the spectrum could not be recorded because the membrane had already equilibrated before the spectrophotometer started recording the change as seen in figure 4.22. The absorbance around 0.1 is the change that has already occurred from pH 5.9 to 7.7 and the absorbance around 0.8 is the change that has already occurred from pH 7.7 to 5.9.

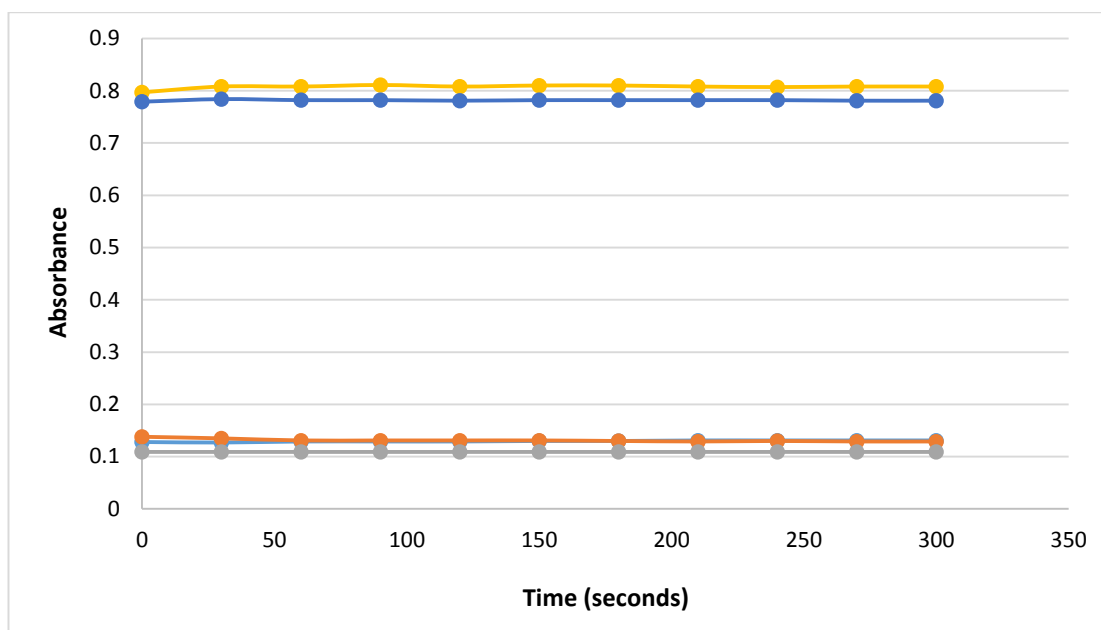


Figure 4.22: The change from 7.7 to 5.9 and from 5.9 to 7.7 for membrane with composition 5 at 640nm.

4.4.5 Thickness of membrane

The thickness of the sensing membrane depends on the solid content of the solution. The thickness of membrane for the solution made using the final concentration was calculated as follows. Membrane solution (3 mL) was made by doubling the amount of all the contents to obtain more solution i.e. 2× (BTB: 50 mg, Tetraoctyl ammonium bromide: 176 mg, PVC: 74 mg, THF: 1.5 mL, Plasticizer: 250 mg). Since 250 μL is spread on a transparency sheet, this volume from the membrane solution was weighed in a balance to get the weight which was 207.01 mg.

$$\text{Density} = \text{Weight}/\text{Volume} = 207.01 \text{ mg}/0.250 \text{ mL} = 828.04 \text{ mg/mL or } 828 \text{ mg/cm}^3$$

$$\text{Density} = 0.828 \text{ mg/mm}^3$$

$$\text{Thickness} = \text{Volume}/ \text{Area}$$

Where Volume = Weight/ Density. So,

$$\text{Thickness} = \text{Weight}/ \text{Density} \times \text{Area of transparency sheet}$$

$$\text{Thickness} = 207.01/0.82804 \text{ mg/mm}^3 \times (210 \times 297) \text{ mm}^2 = 0.0040 \text{ mm or } 4.0 \mu\text{m}.$$

The wet thickness of the film is thus 4.0 μm . The dry film thickness can be calculated using the percentage volume of solute in a solvent.

$$\% \text{ Volume} = \text{volume of solute (mL)} / \text{volume of solution (mL)} \times 100$$

Volume of solute can be calculated as follows

$$\text{Weight of solute} = 100 \text{ mg (dye)} + 352 \text{ mg (TOAB)} + 500 \text{ mg (plasticizer)} + 148 \text{ mg (PVC)} = 1100 \text{ mg}$$

$$\text{Volume of solute} = \text{Weight of solute} / \text{density}$$

$$\text{Volume of solute} = 1100 \text{ mg} / 828.04 = 1.328 \text{ mL}$$

$$\% \text{ volume} = 1.328 \text{ mL} / 3 \text{ mL} \times 100 = 44.3\%$$

Dry film thickness is about 44.3% of the wet film thickness. Thus

$$44.3/100 \times 4 = 1.78 \mu\text{m}$$

4.4.6 Response time with Nytran

Figure 4.23 shows the colour index values extracted from photos plotted against time in seconds following pH shifts by repeating the experiment. The graphs show the results from 3 repeats of the same pH shift with the same membrane.

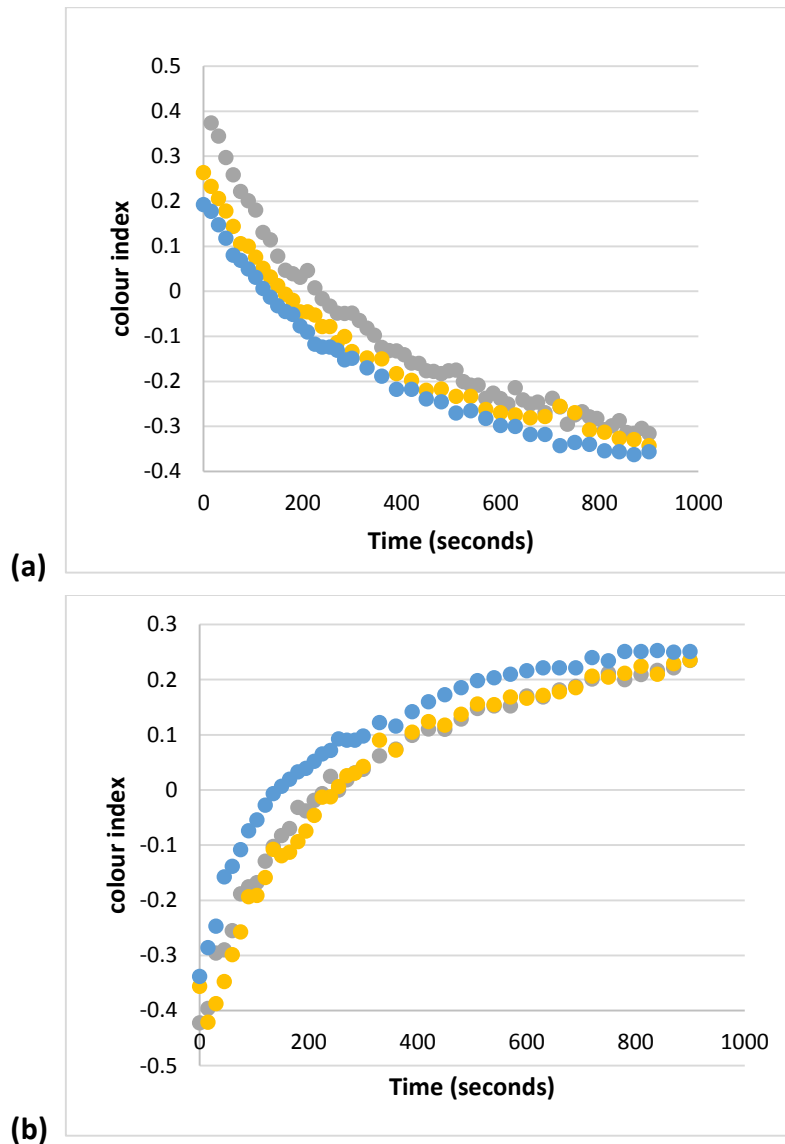


Figure 4.23: (a) change from pH 5.8 to 8. (b) and 8 to 5.8.

The membranes seem to be still equilibrating at 15 minutes so it would be interesting to record the change for 30 minutes to see the membrane completely equilibrated. It can also be noted, since the same membrane was used multiple times, that dye bleaching has resulted in a decrease in the colour index values at each cycle so at pH 8, the colour index value at first was -0.42 which in the next cycle was -0.33. This could be because of dye bleaching but more likely because the membrane had still not fully equilibrated before being switched back.

4.4.7 Response time with increased dye and Nytran

Since the composition of the membrane was changed and more dye and counter ion were added and the amount of solvent was decreased to get a stronger colour in the photos, it may have changed the response time. Thinner membranes were made by using the 6 μm metering bar, however, as the solid content had increased, this may have compensated the other changes. The response time was measured again by photographing the change from 7.7 to 5.9 and vice versa using the same membrane. The membrane was photographed in the dark room using a tungsten light source.

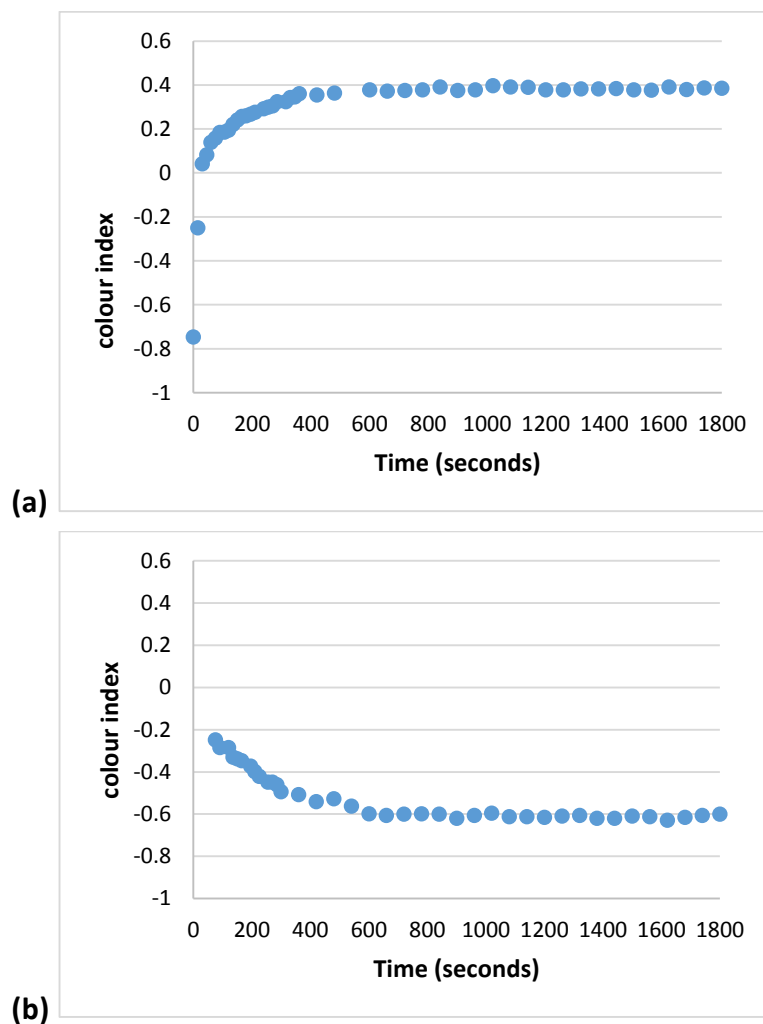


Figure 4.24: Change from (a) pH 7.7 to 5.9, (b) from pH 5.9 to 7.7.

It can be seen from the figure 4.24 that the membrane response time has improved compared with the data in figure 4.23 and the membrane equilibrates by 15 minutes. Although the colour index value at pH 7.7 in the beginning was -0.8 but in second cycle,

it only arrived to -0.6 and got equilibrated. This is probably because the tungsten lamp was kept very close to the membrane, therefore the sensor was somewhat bleached.

To get rid of this problem, the experiment was repeated thrice and each time a fresh membrane was taken. The means were plotted against the time in seconds and are shown in figure 4.25.

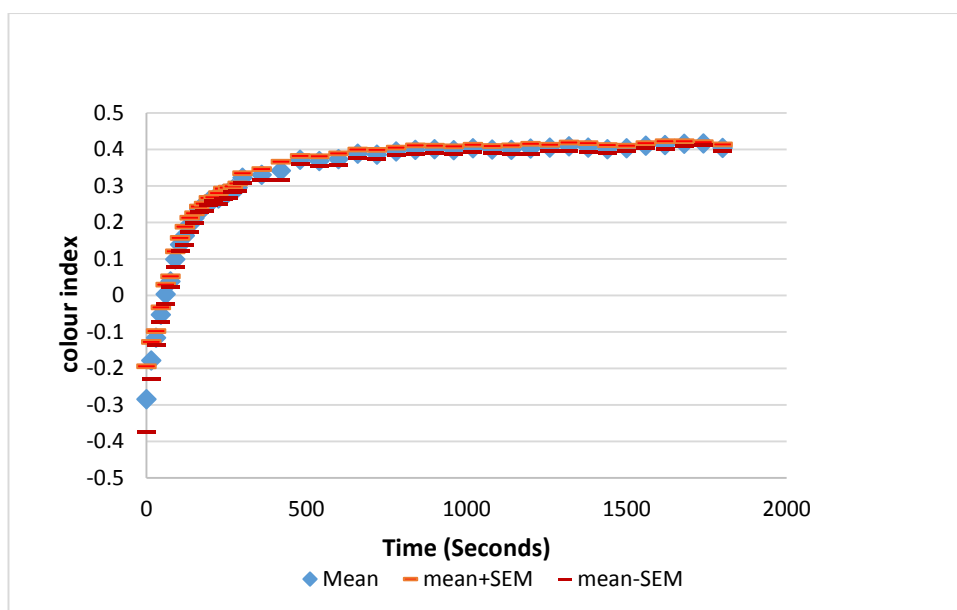


Figure 4.25: Response time with Nytran membrane and increased dye+ counter ion content, SEM= standard error of mean.

Figure 4.25 shows that the membrane equilibrates at about 15 minutes where the error bars are small and in the beginning where the change takes place, the error bars are bigger. This is probably due to the uncertainty in accurately timing the start of the experiment as the pH is switched, leading to larger variations where the response is changing rapidly.

Time constant of a sensor is 2.5 minutes which was calculated by using the formula given in the figure 4.26. Five times the time constant gives 99% of the final value of response time i.e. 12.5 minutes. It takes 7.9 minutes for a response time to reach its 63.2% of initial value.

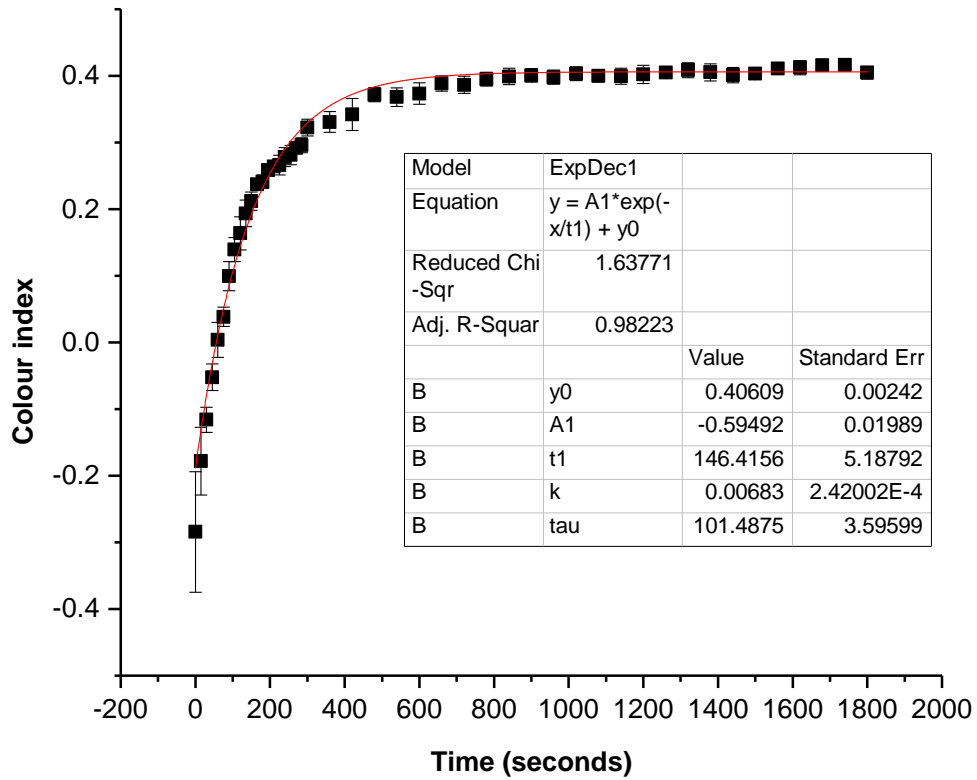


Figure 4.26: Response time curve showing the equation used to calculate the time constant.

4.4.8 Effect of temperature on membrane

The effect of temperature on sensing membrane was studied and the red green and blue values were extracted using ImageJ.

Serial Number	Temperature	pH	Image Number	Red	Green	Blue	(R-B)/G
1	25 °C	7.31	714	110	133	122	-0.09023
2	26 °C	7.31	715	95	116	106	-0.09483
3	27 °C	7.31	718	95	116	106	-0.09483
4	28 °C	7.31	719	93	115	105	-0.10435
5	29 °C	7.30	720	101	125	114	-0.104
6	30 °C	7.30	721	93	114	105	-0.10526
7	31 °C	7.30	722	97	118	108	-0.09322
8	32 °C	7.30	723	94	115	105	-0.09565
9	33 °C	7.29	724	97	118	108	-0.09322
10	34 °C	7.29	725	92	116	106	-0.12069

Table 4.6: RGB values at different temperatures. pH changed by changing temperature.

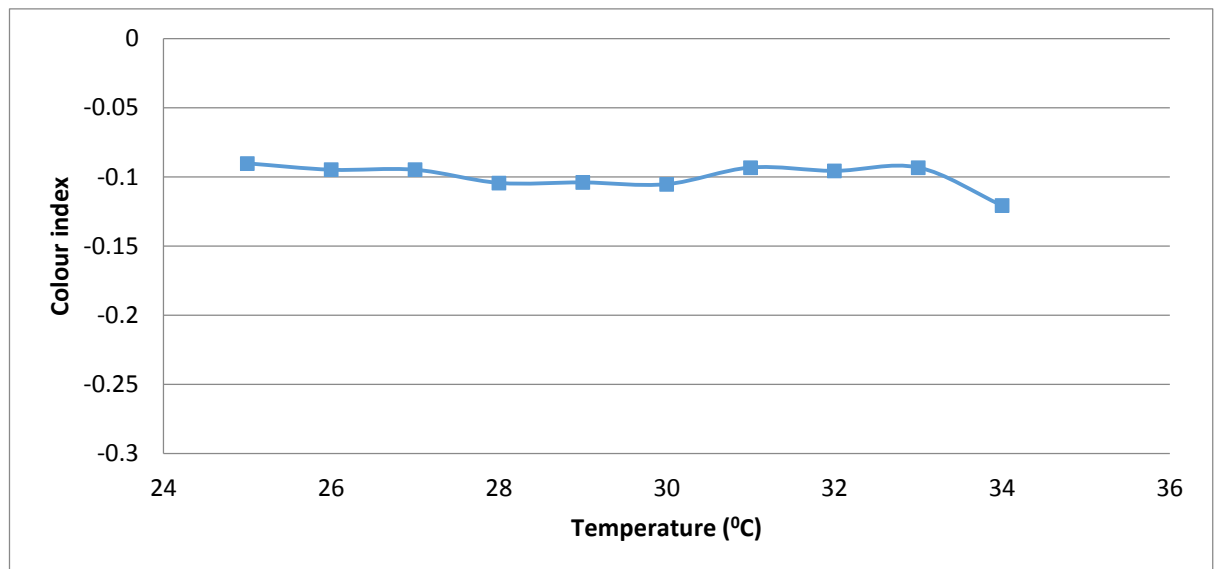


Figure 4.27: change in colour index values with temperature increase.

The colour index values don't show any trend but there is a degree of variation. This could be because of the following reasons.

1. pH of buffer solution is changing by changing the temperature. This would be a gradual change.
2. Lighting is not consistent throughout the experiment. It is bright in the morning and can possibly change in the evening. The inconsistency of clouds and sun can make more difference in the lighting conditions.
3. The camera moves while photographing and the position of the camera varies each time the photograph is taken.
4. The colour of the membrane is pale in the photographs.

The light should be controlled as much as possible. This could be done by photographing in the dark room. The camera should be fixed so it does not move. A consistent light source should be used during photography. The intensity of camera's flash light or a separate flash add on may vary depending on the battery power resulting in bright photographs in the beginning and dark photographs at the end of the experiment so a mains lamp should be used instead. The colour of the membrane can be enhanced by increasing the amount of the dye in the membrane solution.

All the above factors were addressed before repeating the experiment over a wider temperature range. The following results were obtained when the lighting and position of the camera was controlled. The sensor was also modified by increasing the amount of dye and adding a white Nytran membrane.

S. No	Temperature of water bath	Temperature of buffer	pH	Photo No	R	G	B	(R-B)/G
1	4.0 °C	5.2 °C	7.15	2160	171	119	41	1.092437
2	5.5 °C	6.0 °C	7.14	2161	177	123	43	1.089431
3	8.3 °C	8.0 °C	7.13	2162	170	120	43	1.058333
4	10.4 °C	10.0 °C	7.11	2163	161	117	40	1.034188
5	12.0 °C	12.0 °C	7.10	2164	157	116	40	1.008621
6	14.0 °C	14.0 °C	7.07	2165	159	117	42	1
7	16.0 °C	16.0 °C	7.06	2166	153	117	41	0.957265
8	18.0 °C	18.0 °C	7.04	2167	153	117	41	0.957265
9	18.7 °C	20.0 °C	7.03	2168	150	116	41	0.939655
10	24.0 °C	22.0 °C	7.01	2169	148	116	41	0.922414
11	26.0 °C	24.0 °C	7.00	2170	146	116	41	0.905172
12	28.0 °C	26.0 °C	6.99	2171	143	116	41	0.87931
13	30.0 °C	28.0 °C	6.99	2172	145	117	42	0.880342
14	32.0 °C	30.0 °C	6.98	2174	141	116	42	0.853448
15	34.0 °C	32.0 °C	6.98	2175	131	114	40	0.798246
16	36.0 °C	34.0 °C	6.97	2176	133	114	41	0.807018
17	38.0 °C	36.0 °C	6.97	2177	132	113	41	0.80531
18	40.0 °C	38.0 °C	6.97	2178	128	114	41	0.763158
19	42.0 °C	40.0 °C	6.96	2179	124	113	40	0.743363

Table 4.7: pH and colour index values at different temperatures.

It is evident from table 4.7 that the pH of phosphate buffer changes with change in temperature. The pH decreases by increasing temperature, so it is not clear whether the recorded decrease in the colour index is due to a temperature response or due to the pH change associated with the temperature change.

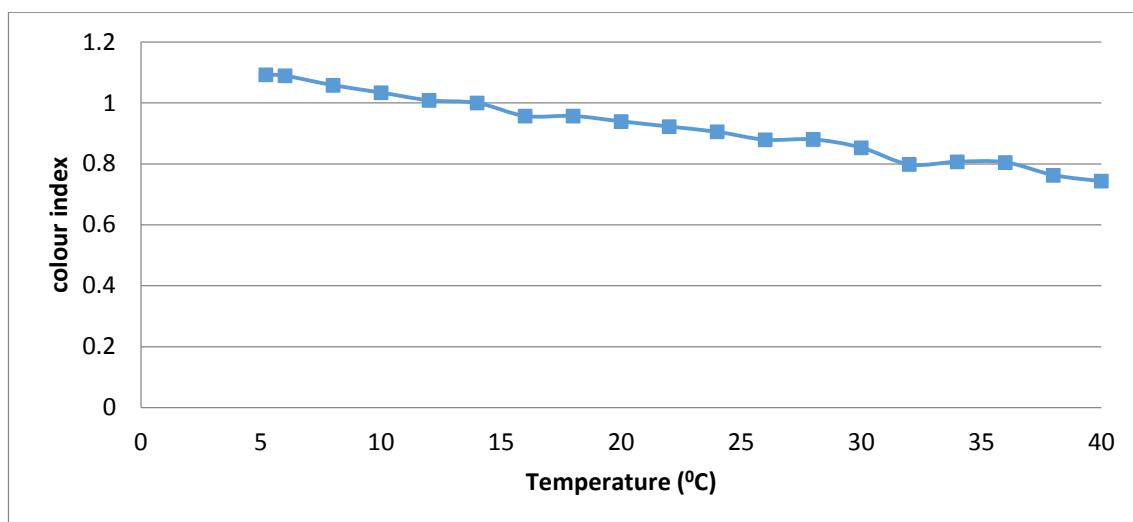


Figure 4.28: change in colour index values with temperature. pH was changing.

To test this, 1 M NaOH was used to maintain the pH of buffer at each temperature. At first attempt, there was a visual change of colour due to addition of NaOH. This was because the membrane got disturbed and couldn't equilibrate as there was no stirring. The sodium hydroxide concentration reduced to 0.5 M to prevent the disturbance.

Using dilute NaOH to maintain the pH of buffer

The following results were obtained when the experiment was repeated using dilute NaOH (0.5 M) and a magnetic stirrer to ensure rapid equilibrium.

Serial Number	Temperature of water bath	Temperature of buffer	pH	Photo number	(R-B)/G
1	3.2 °C	5.2 °C	7.27	2188	0.895522
2	12.9 °C	12.8 °C	7.27	2189	0.775194
3	18.3 °C	18.7 °C	7.27	2190	0.645161
4	24.5 °C	24.2 °C	7.27	2191	0.587719
5	34.3 °C	33.3 °C	7.27	2193	0.463636

Table 4.8: pH and colour index values at different temperatures.

This time there was no visual change of colour on addition of NaOH as the membrane equilibrated quickly.

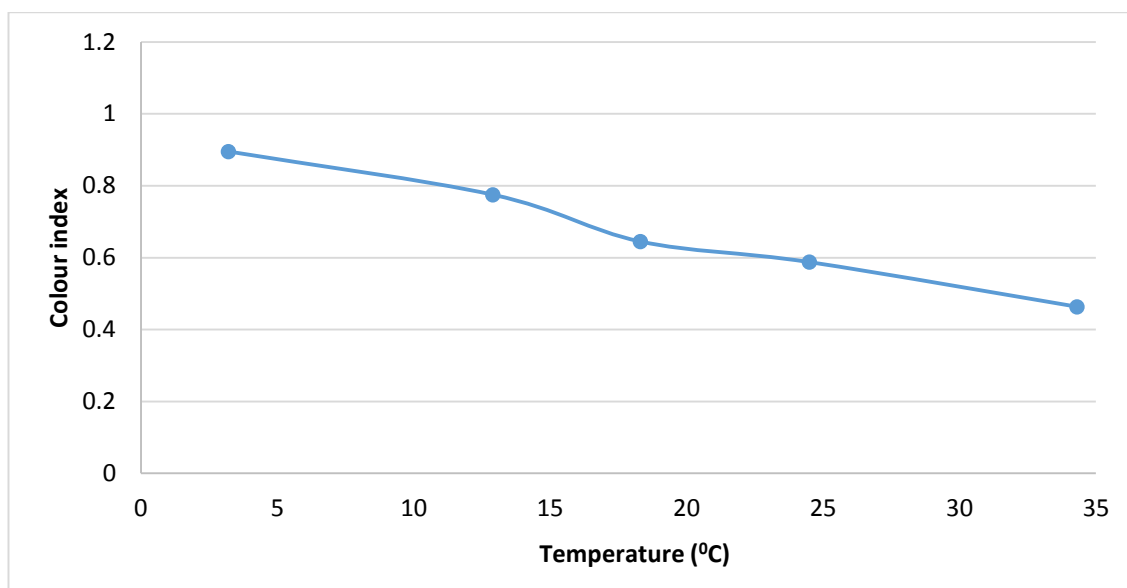


Figure 4.29: change in colour index values with temperature at pH 7.27

The graphs show that there is still a variability in the colour of the membrane which can be the property of the membrane to change its colour with temperature. This was further investigated by repeating the experiment at high temperature and using HCl to adjust the pH to see if the same kind of graph was obtained after analysing the photos in ImageJ.

Using HCl to maintain the pH of buffer

When 0.5M HCl was used to control the pH of buffer while reducing the temperature, the following results were obtained.

Serial Number	Temperature of water bath	Temperature of buffer	pH	Photo number	(R-B)/G
1	40 °C	40.5 °C	7.27	2195	0.52381
2	29.9 °C	33.8 °C	7.27	2196	0.613497
3	25 °C	27.1 °C	7.27	2197	0.695122
4	15 °C	18.5 °C	7.27	2198	0.803681
5	6.6 °C	7.5 °C	7.27	2199	0.975
6	3.9 °C	5.5 °C	7.27	2200	1.006

Table 4.9: pH and colour index values at different temperatures.

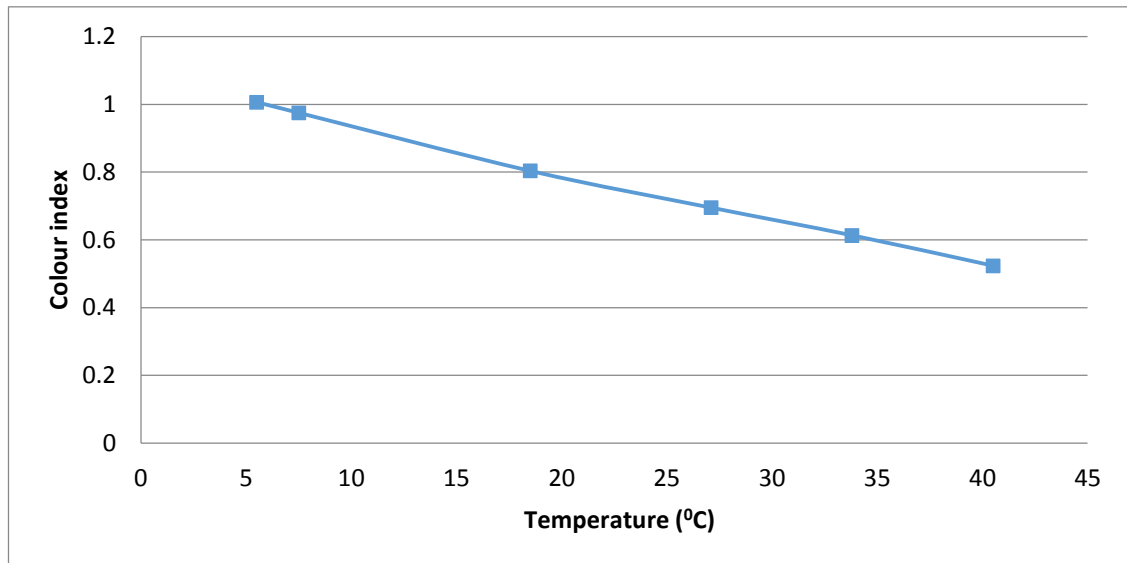


Figure 4.30: change in colour index values with temperature at pH 7.27

The graph shows the similar trend as it was when NaOH was added to adjust the pH which makes it obvious that there is some effect of temperature on membrane.

Using sea water

The effect of temperature was studied on membranes using seawater. The pH of seawater changed gradually from 7.78 to 8.2 by changing the temperature from 4.4 °C to 44.8 °C. Figure 4.30 shows the colour index values plotted against temperature when the experiment was repeated thrice but this could be due to change in pH.

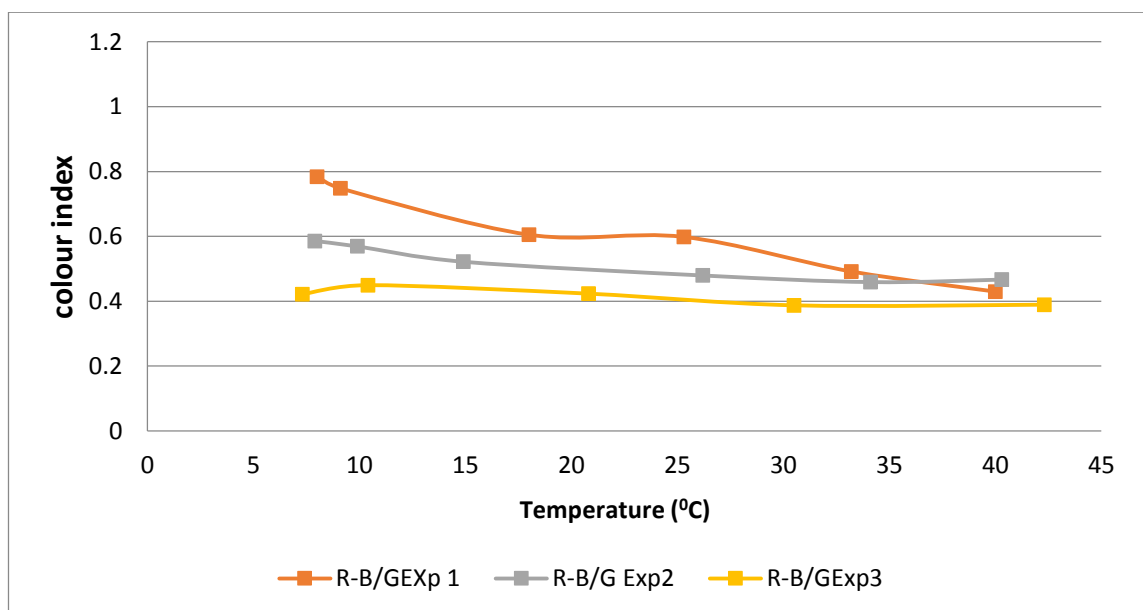


Figure 4.31: Effect of temperature on membrane colour while pH was changing.

The behaviour of membrane in the first and second experiment looks more or less similar except a slight drop down of the RGB values in the beginning which can be because of dye bleaching due to the tungsten light source. The third experiment was done next day with the same membrane used in the first and second experiment which had been left in the buffer. This membrane therefore shows slightly different behaviour. The experiment was repeated by maintaining the pH using NaOH and HCl.

Using NaOH to maintain the pH of seawater

The experiment was repeated with sea water. The pH was adjusted with 0.125 M NaOH solution at each new temperature before taking the photograph. The pH was initially adjusted using 0.5 M NaOH but it was observed that the pH of sea water increased too much with a single drop of NaOH. This is because the buffering capacity of the sea water is very low. 0.125 M NaOH was used to adjust the pH instead.

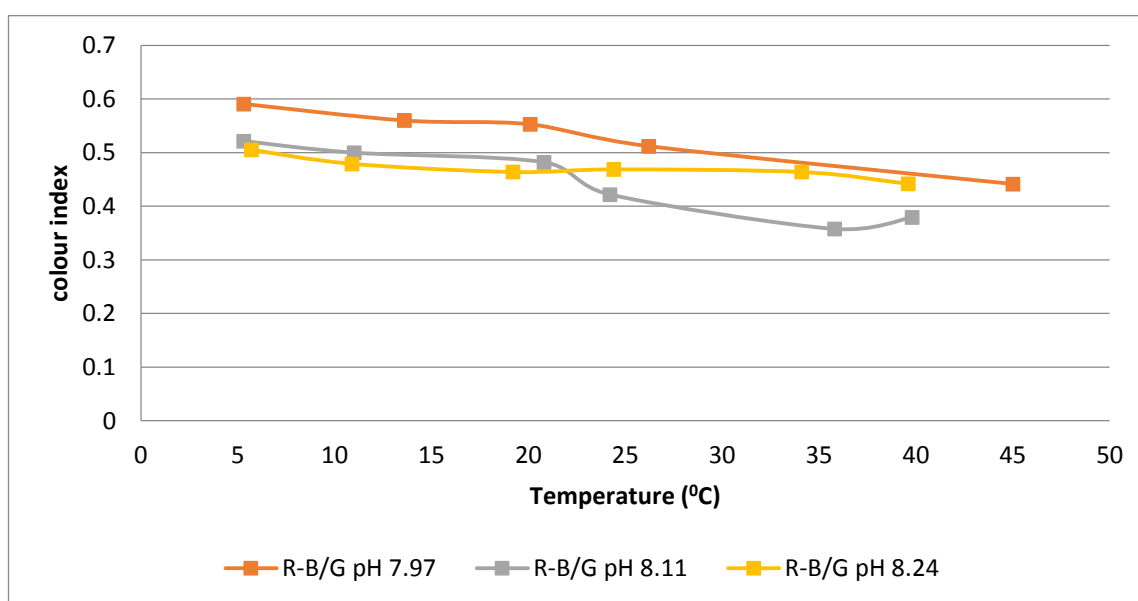


Figure 4.32: colour index vs. Temperature. pH was controlled using NaOH: at pH 7.97 .

From literature it is known that acid sensitive indicators like bromothymol blue shift their colour to the acid side at boiling hot temperature (Kolthof, 1937) but as the temperature change is not too large and the properties of the indicator change when it is not a plasticised membrane therefore, from the graph above, it can be concluded that the colour index values decrease as the temperature increases over the 40 °C

range tested. This decrease is about the 0.2 on the colour index scale in sea water and can lead to an error. In figure 4.24, changing colourpH from 5.9 to 7.7 changes colour inP by approximately 0.4. The error therefore could be 0.9 pH units over 40 °C . HCl was used to maintain the pH to see if the same behaviour was observed.

Using HCl to maintain the pH of sea water

The same behaviour of dropping down of colour index is observed. The experiment was repeated three times to see the trend. The following results were obtained (figure 4.32).

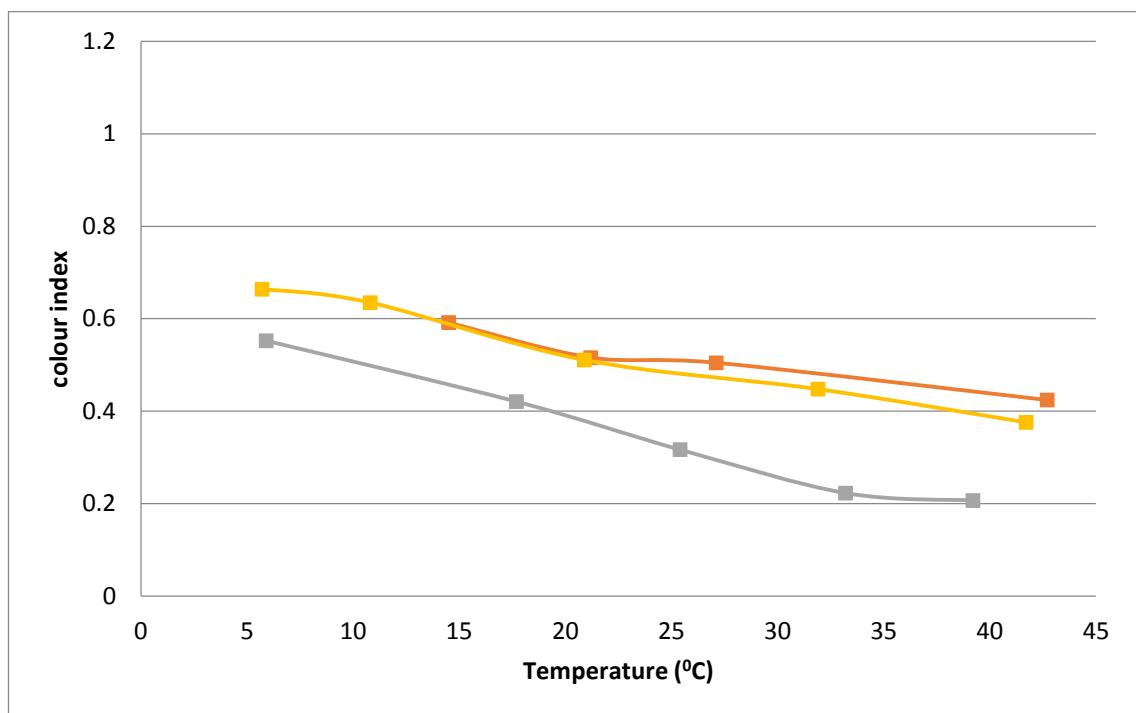


Figure 4.33:(R-B)/G vs. Temperature. pH was controlled using HCl: at pH 7.85(red),7.72(grey),7.47(yellow)

The graph obtained is similar to the one obtained when NaOH was used to adjust the pH. The overall behaviour of the membrane is clear and it tends to a slightly greener shade from blue when the temperature is increased. The colour change is not drastic and the change is barely visible to the naked eye but the photos and colour index values show the change. It can be concluded that temperature affects the sensing membrane and drops the colour index value by about 0.3 over the temperature interval studied.

This can be controlled by calibrating the sensing membrane at different temperatures or at a specific temperature near to the expected temperature of the sample environment providing the calibration temperature matches the sample within a few degrees (about 15 °C), the error should be small.

4.4.9 Effect of Salt on membrane

The sensing membrane film responded as expected in the presence of high concentrations of NaCl without a pK_a shift. At very low concentration of salt (0.05 M-0.15 M), the pK_a shifts. There is little effect of salt at the concentrations ranging from 0.2 M to 0.5 M. All the samples responded similarly except one or two which was because of the difference in the thickness of the membrane that was visible in water too. The UV spectra (figure 4.35) also suggest that there is a slight difference in the absorbance at different salt concentrations which should be considered while calibrating the sensor. The sensor should be calibrated at the salt concentration that matches the sea water before applying it to the sea sediments or should be calibrated in seawater itself. The Images below show the response in different concentrations of NaCl at pH 7.3 and 5.8.

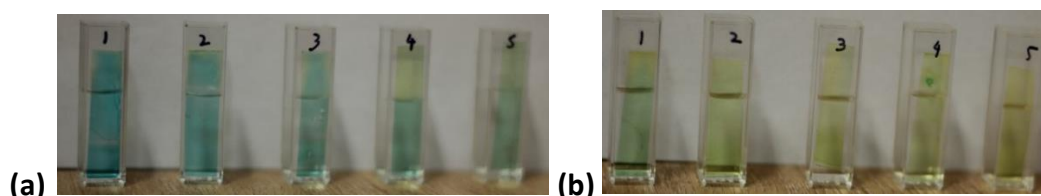


Figure 4.34: The colour response of membrane at salt concentrations 0.05 M, 0.15 M, 0.25 M, 0.35 M and 0.45 M (from left to right) (a) at pH 7.3, (b) at pH 5.8.

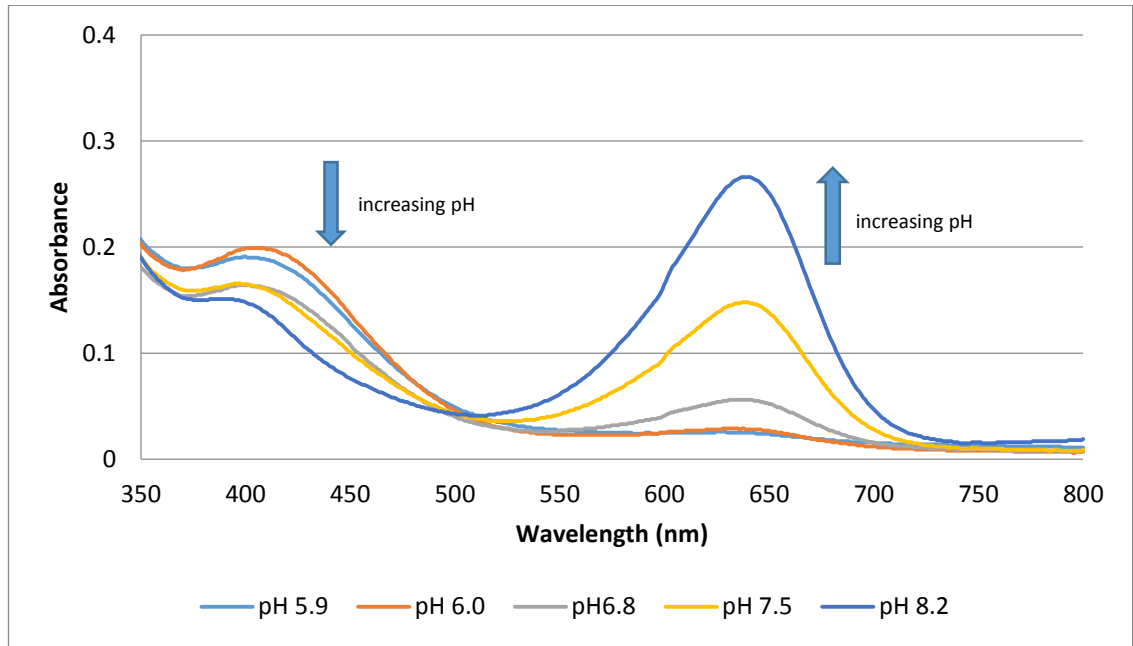


Figure 4.35: UV visible spectrum of BTB membrane in 1:1 phosphate buffer and 1 M NaCl solution (similar ionic strength to seawater).

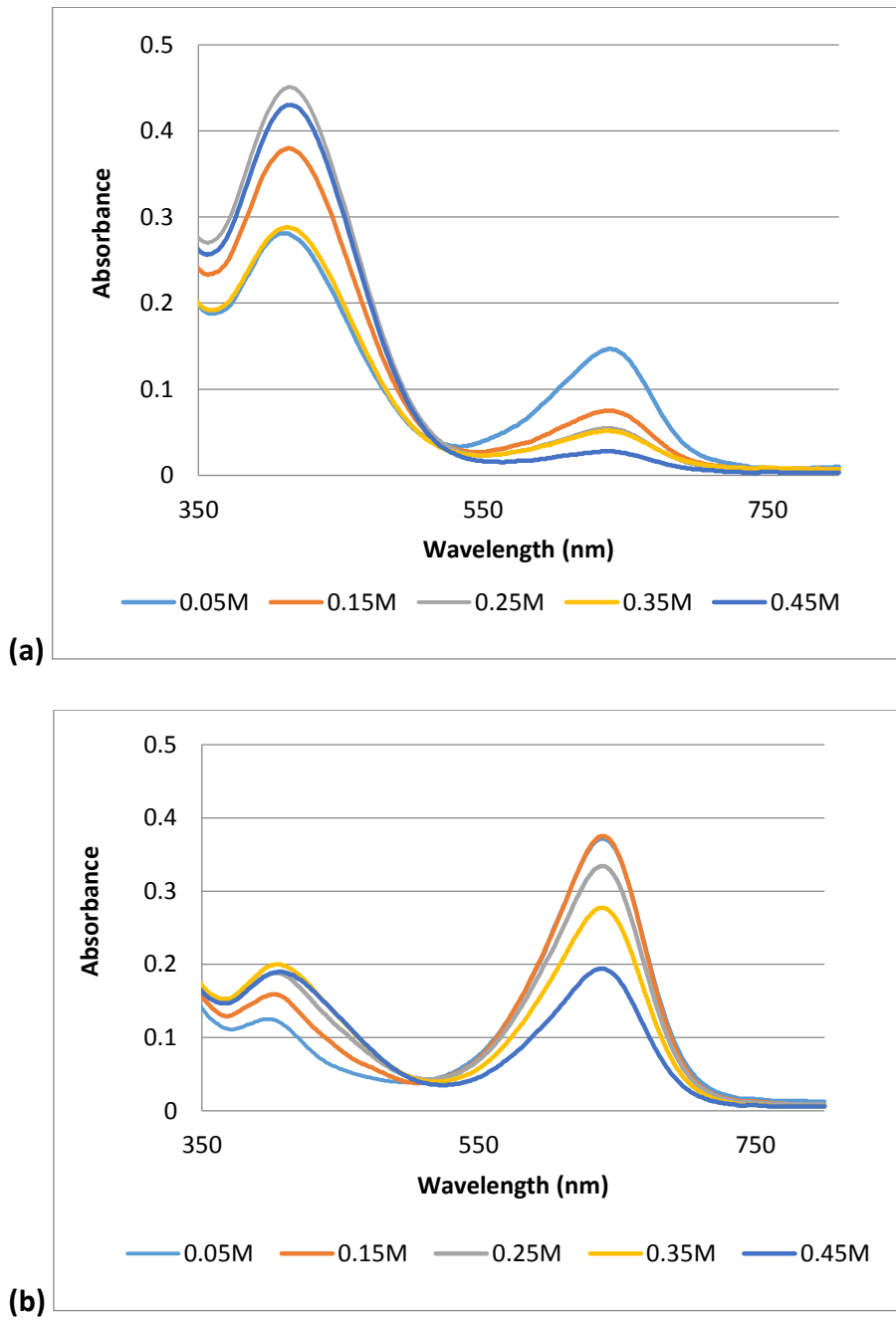


Figure 4.36: Effect of salt on membrane at (a) pH 5.8, (b) pH 7.3.

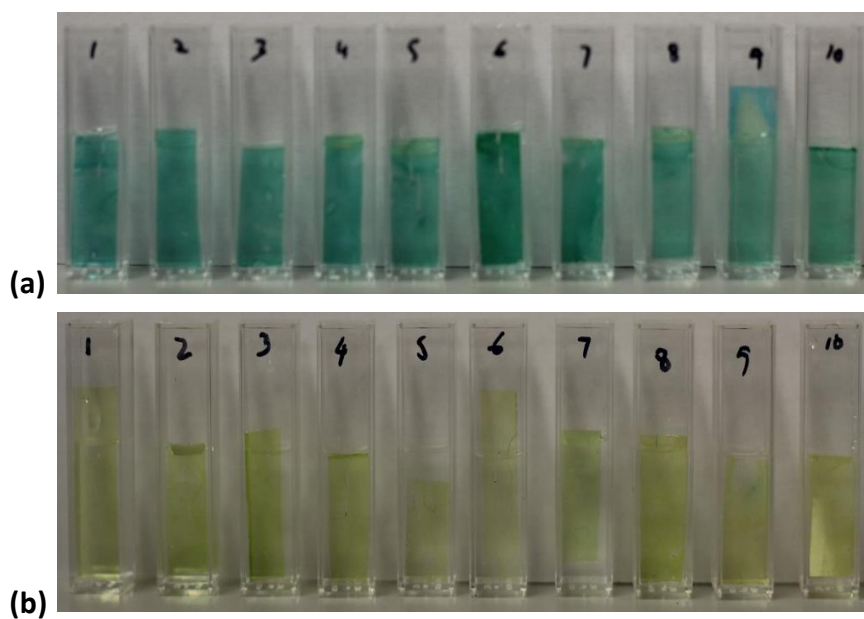


Figure 4.37: The colour response of BTB membrane at different salt concentrations from left to right: 0.20 M, 0.21 M, 0.22 M, 0.23 M, 0.24 M, 0.26 M, 0.27 M, 0.28 M, 0.29 M, 0.30 M (a) at pH 7.3 and (b) at pH 5.8.

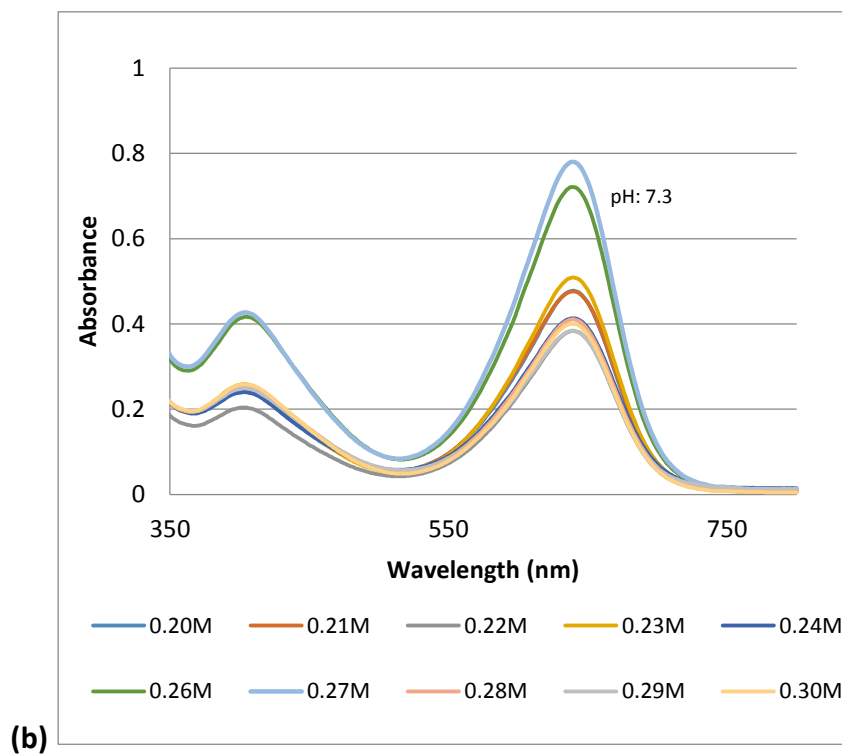
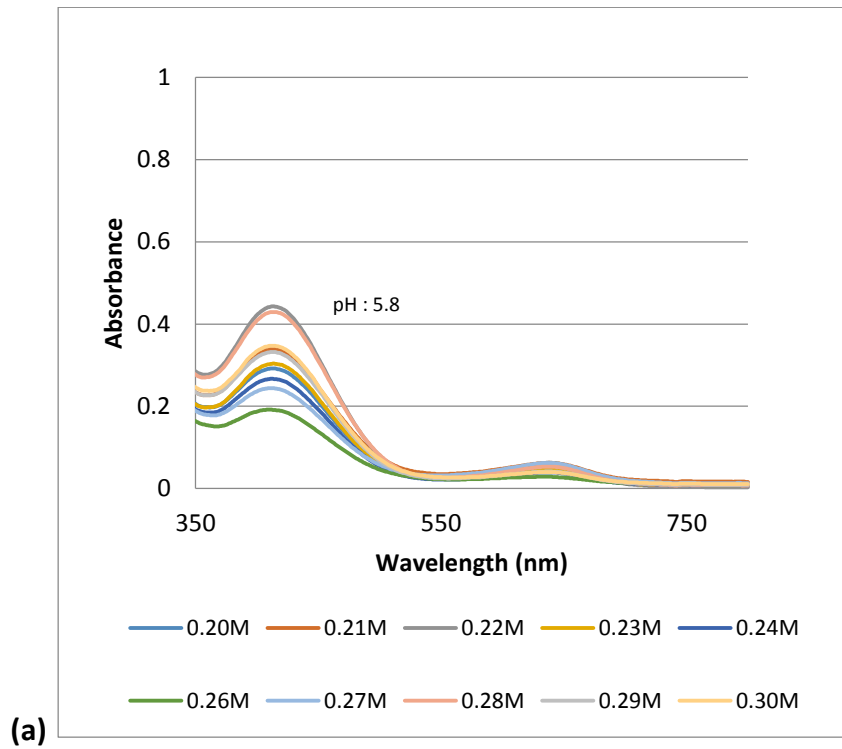


Figure 4.38: Effect of salt on membrane at (a) pH 5.8 (b) pH 7.3

The spectra (figure 4.35, 4.37) showed that there was a slight effect of salt on membrane that changed the absorbance slightly. The experiment was repeated again as some effect of salt was observed. The concentration of NaCl in seawater is about 0.5 M, therefore phosphate buffer solutions were made that contained the amount of NaCl close to sea water (0.40 M, 0.42 M, 0.44 M, 0.50M, 0.54 M, 0.56 M, 0.58 M and 0.60 M). The pH was adjusted to 6.69 while making buffer with the salt.

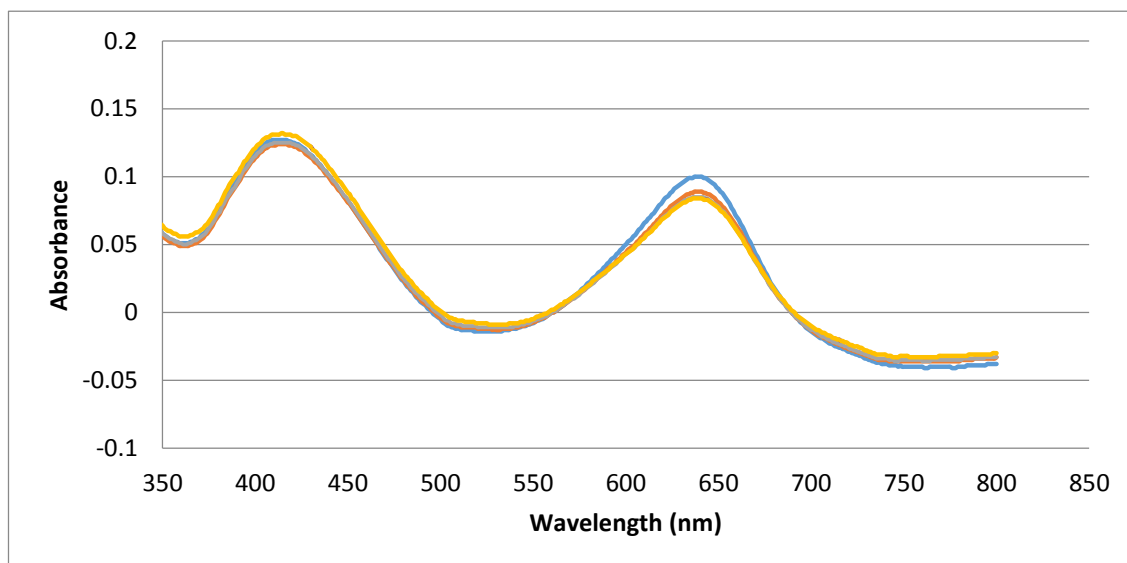


Figure 4.39: UV-visible spectrum of membrane at pH 6.69, blue: 0.40 M, red: 0.46 M, grey: 0.48 M, and yellow: 0.52 M.

The required amount of salt for 50 mL was first taken in 25 mL buffer (0.1 M) solution, then the volume was increased to 40 mL by adding water. The pH was adjusted using the buffer stock solutions and the volume was finally made up to 50 mL.

As it can be seen from the spectra in figure 4.38 that the spectrum does not change much for the concentrations from 0.46 M-0.52 M but in low concentration such as 0.40 M, There is some effect of salt which should be considered during calibration.

The same experiment was repeated using a photographic approach. The sensing probes were made and the response was photographed in a light box that contained the camera in a fixed position and LED lights inside.

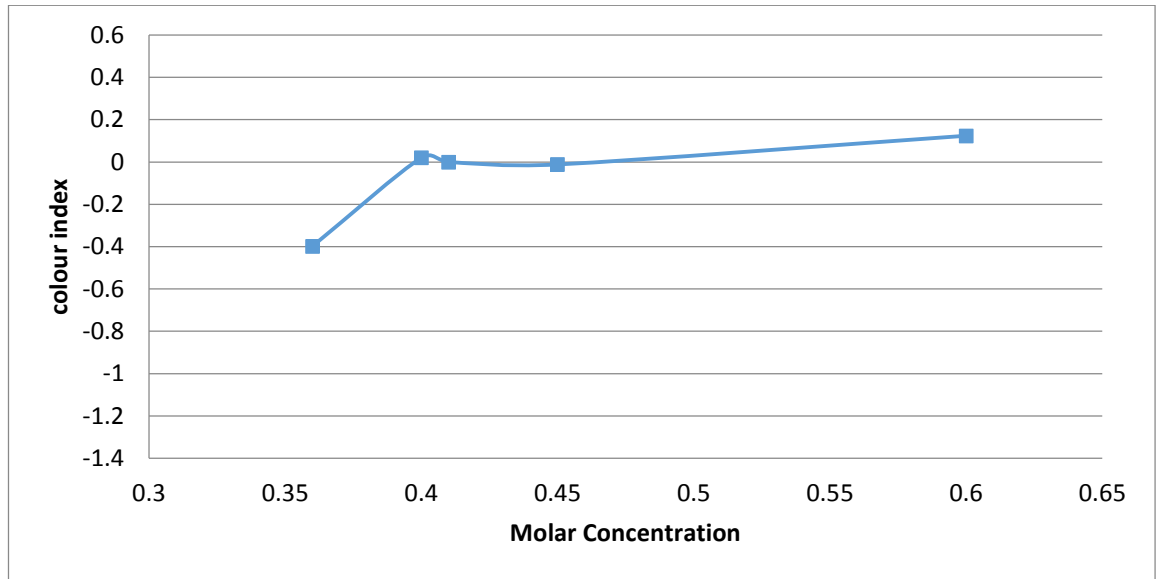


Figure 4.40: colour index values at different salt concentrations.

There is also some effect of salt when evaluated by the photo analysis. The colour index range in figure 4.39 is the range that is normally observed during calibration. The graph was plotted at this range to observe the error salt concentration may induce at the full range of calibration. The effect of salt was also tested in sea water (taken from Lowestoft) by diluting it 10 percent and increasing the NaCl salt by 10 percent. The pH of sea water was 8.09 which slightly changed by both addition of salt and water. 0.007M NaOH and HCl were used to adjust the pH. In the case of dilution 2 drops of HCl were added which dropped the pH down so 2 drops of NaOH were added to bring the pH back to 8.09. In case of addition of salt, 1 drop of NaOH was added to adjust the pH. These very small additions will have a negligible effect on the salt concentration.

The response was analysed in the spectrometer (Hitachi 3010) and photographed in the light box.

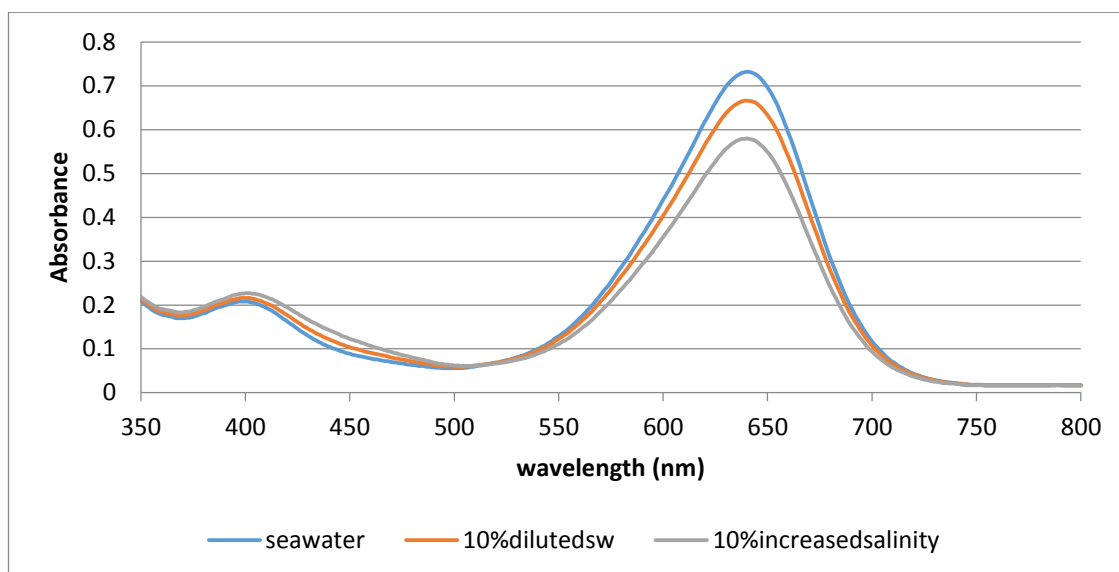


Figure 4.41: UV visible spectrum of membrane in seawater. Blue: original seawater, red: 10% diluted sea water and green: 10% increased salt in seawater.

The colour index values of original seawater, 10% diluted seawater and 10% increased salt in seawater were -0.211, -0.318 and -0.307 respectively. The colour index values change by 0.1 when diluted or by addition of salt. Figure 4.40 suggests that both dilution and increased salinity change the absorbance. The experiment was repeated by diluting the sea water 2%, 4%, 6%, 8%, 9% and 10%. The temperature of the sea water was 21 °C and the pH was adjusted to 7.97 by using 0.0035 M HCl as the pH increased both by dilution and addition of salt. The membrane used for this experiment had the composition dye: 25 mg, counter ion: 88 mg, PVC: 74 mg, Plasticizer: 250 mg, THF: 1.5 mg. The 12 µm metering bar was used to spread the solution by taking 350 µL.

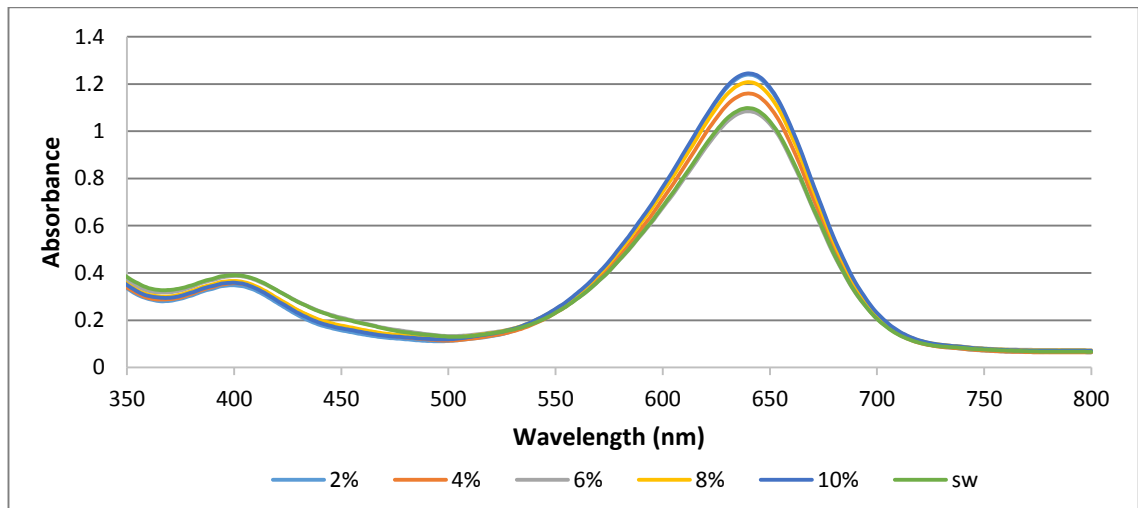


Figure 4.42: UV-vis spectrum at different dilutions.

As seen in the spectrum, the dilution changes the absorbance slightly ranging from 1.08 to 1.24. The photographs were analysed and the colour index values were plotted against the dilution.

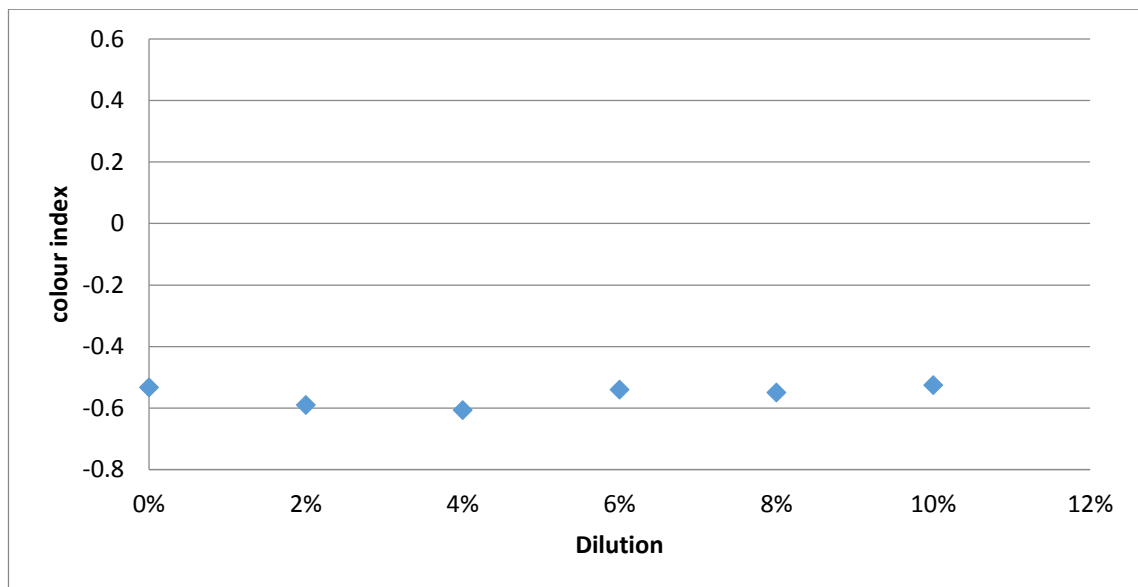


Figure 4.43: Effect of dilution at pH 7.97 and temperature 22.1°C on the extracted colour index values.

As shown in the figure 4.42, the dilution has a very small effect on the colour index values. The maximum variation occurs at 2% and 4% dilution which have variation ranging from -0.53 to -0.60 on the colour Index $((R-B)/G)$, however 6-10% dilution brings the colour index values back to the original seawater value. The SD is 0.03 which is 2% of the total index units in the calibration range. This was deemed to be an

acceptable uncertainty due to possible small variations in salinity. This error is about 0.06 pH units (chapter 5, figure 5.7).

It was concluded that the change in salt concentration can affect the colour response therefore the sensors should be calibrated at the salinity that is expected at the study site or a sample from the study site should be taken to calibrate the sensors. As long as, the salinity is not drastically changing like in Estuaries, the sensors will be reliable but may not be reliable at the sites where the salinity is constantly changing.

4.4.10 Effect of light

During an attempt to take the reflection spectrum of the sensor with a nytran membrane in place using a fibre optic spectrophotometer, it was observed that the dye was completely bleached by the high intensity light. The effect of light was studied by keeping one probe in sunlight stored in buffer (pH 7.7) and one in the dark stored in the same buffer by keeping it in a box. Each day, the probes were photographed and their response in the buffer (pH 6) was observed

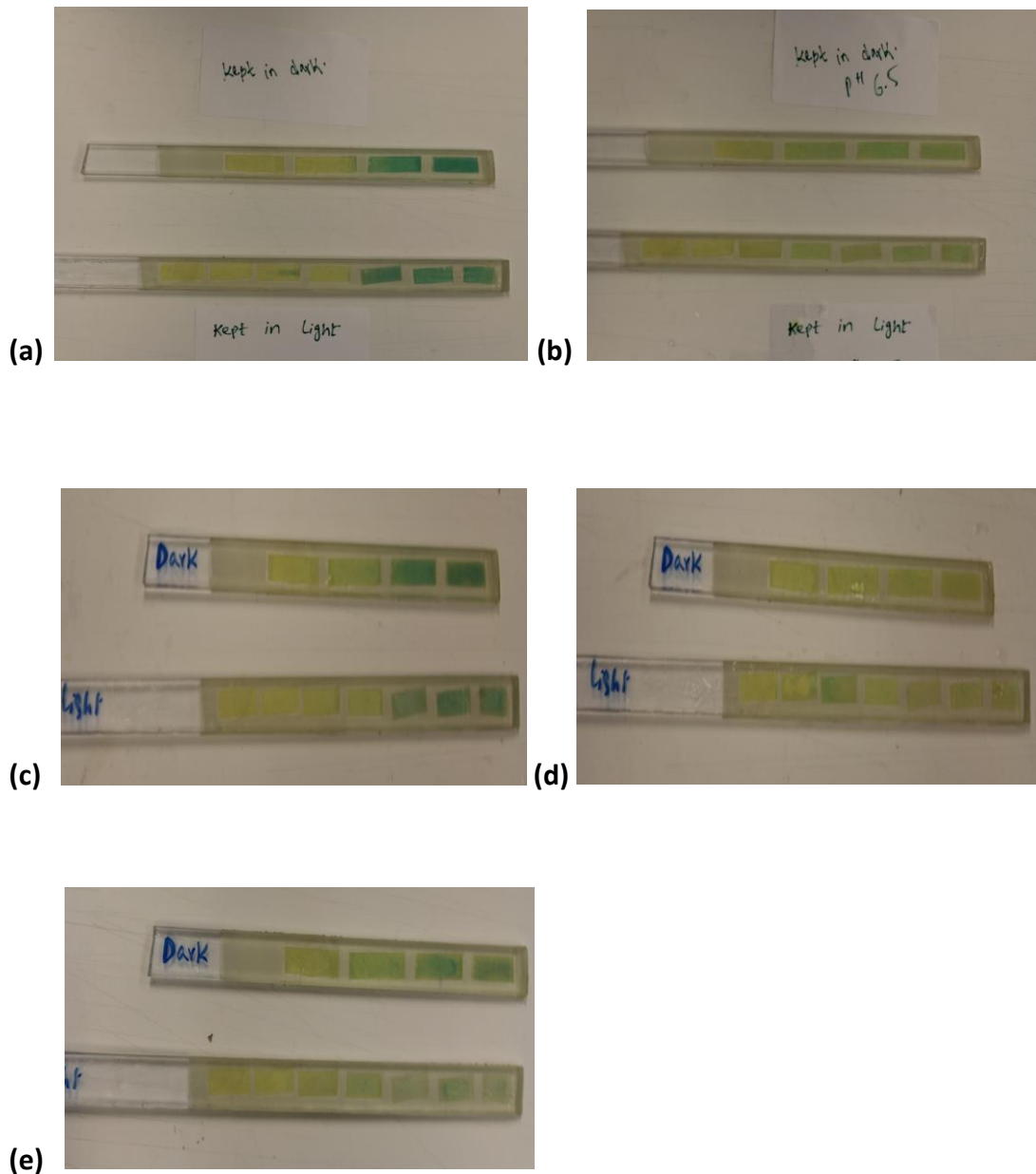


Figure 4.44: Effect of light on the sensor. (a) Day 2: response in the buffer (pH 7.7) in which probes were kept.(b) Day 2: Response in buffer 6.5 (c) Day 3: response in buffer pH 7.7 in which they were kept (d) : Day 3: response in buffer pH 6 (e) Day 4: Response in the buffer pH 7.7 in which they were kept, clear bleaching of dye.

Figure 4.43 suggests that light affects the colour response. The colour becomes lighter if it is left longer in sun light and in aqueous medium. It is suggested that the sensors should be kept dry in the dark. Figure 4.43 a, c and e shows the slow bleaching of dye from day 2 to day 4.

4.4.11 Effect of flash

There was no evident change in the colour of the dry probe. The RGB values were taken only from the dry probe as it was noticed that the probe that was inserted in the basic buffer and then taken out and photographed became green from blue which is because the probe was no longer in the basic condition so its colour changed as it dried out.

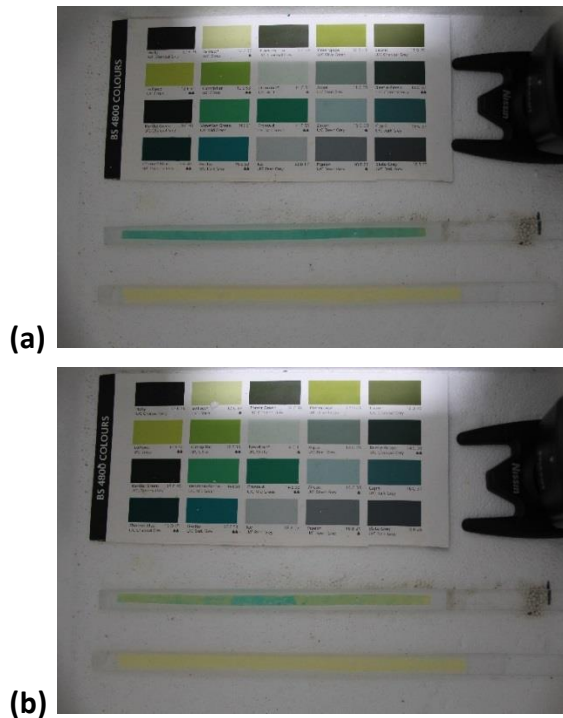


Figure 4.45 (a): Image taken at the start of the experiment. (b): Image taken at the end of the experiment.

Figure 4.45 shows the colour index values plotted against time to see if the colour bleaches with flash or not.

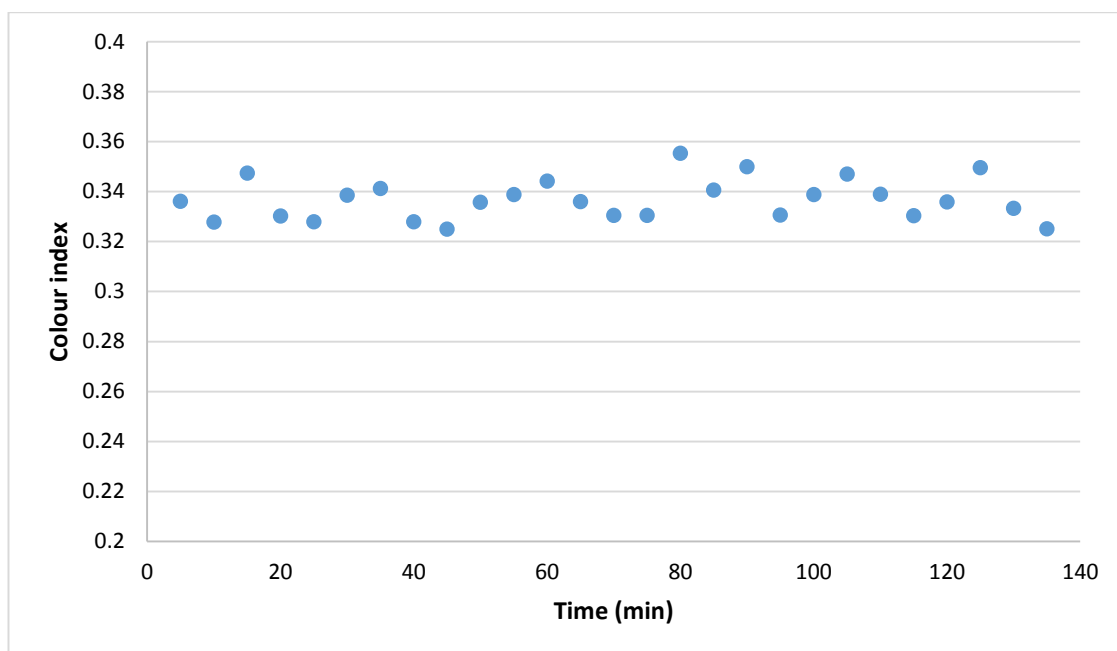


Figure 4.46: colour index vs time in minutes.

The colour index values show small but significant variations. This may be because the lighting in the polystyrene box is not very consistent and the camera positioning is not controlled either. The movement of the camera can bring error in the colour index values but the overall pattern seems to be the same over 140 minutes and there is no apparent bleaching of the dye due to the camera flash.

4.4.12 Storing preference

The probe stored in 0.5 M NaOH took longer to respond subsequently so the probes should not be stored in base. The one stored in phosphate buffer pH 7 and the one kept dry responded equally but the one kept in 0.5 M HCl seemed to respond faster but that could be human observation error as it changes colour from yellow to blue very quickly and the difference is very clear so it looks like it changed quickly, while changing from blue to green is less observable. It seemed that leaving the sensors in aqueous solution for a long time bleaches the dye as when the one left in buffer in the dark was observed next day, the colour had bleached slightly and therefore it should be kept dry in the dark.

4.4.13 Reusability

Figure 4.46 shows the response of a membrane kept in acidic buffer pH 4.7. The response was measured every hour for five hours.

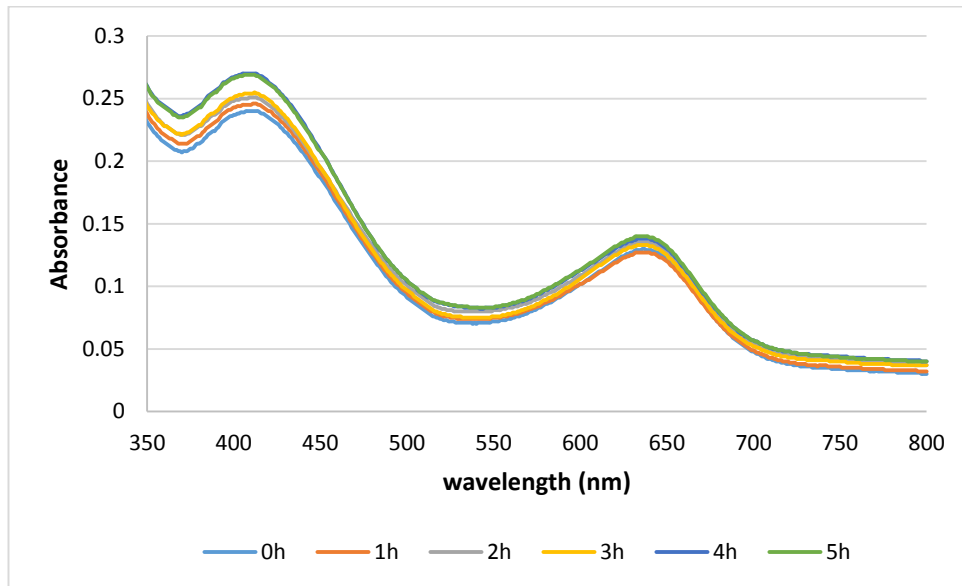


Figure 4.47: The reusability of the sensing membrane kept in the acidic buffer pH 4.7 in a cuvette and wrapped with foil.

Figure 4.47 shows the response of a membrane kept in basic buffer pH 7.8. The response was measured every hour for five hours.

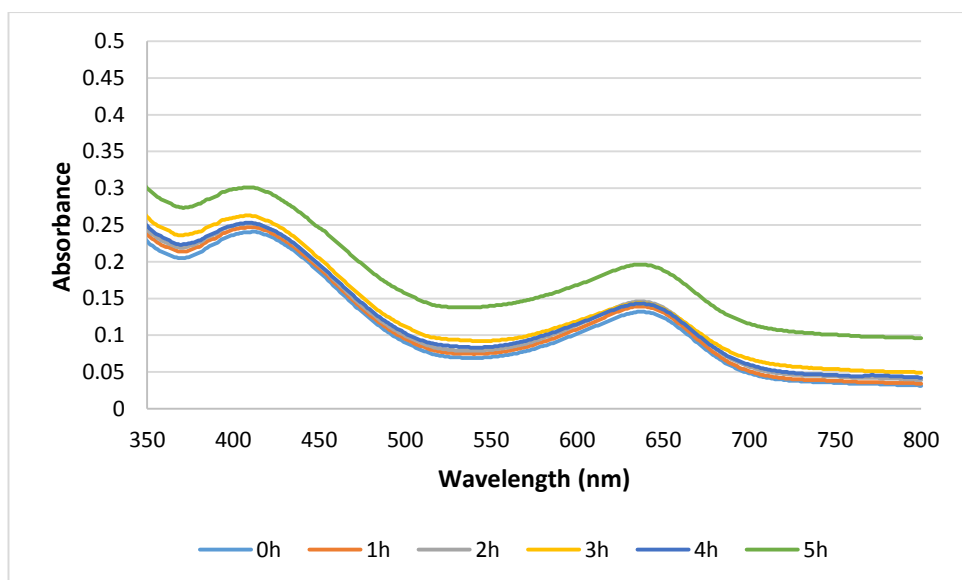


Figure 4.48: The reusability of the sensing membrane kept in basic buffer pH 7.8 in a cuvette and wrapped with foil.

In figure 4.47, the spectrum is more or less the same as the spectrum of the membrane stored in the acidic buffer. There is a slight increase in the absorbance with time. In the spectrum taken at 5 h, the light might have scattered from the cuvette surface. Since it is parallel all the way, this suggests a zero error of the experimental cuvette. In figure 4.46 the peak at 640 remains almost the same while the second peak slightly changes. The small change in absorbance demonstrates the reusability but, as the sensors are inexpensive, single use is recommended to avoid any potential complications from the sensor's history. The overall response shows that if left in aqueous medium for a longer time, the dye does not bleach or leach which favours the SPI application as it takes time to settle down the SPI before it photographs in the sediments and the probe itself needs to be in the sediments for at least fifteen minutes to equilibrate.

4.5 Conclusions

The following conclusions can be drawn from the experiments presented in this chapter.

- The sensor equilibrates in seconds without Nytran membrane and in 15 minutes with a Nytran membrane attached. This presumably represents the time taken for H^+ to diffuse through the relatively thick (0.45 μm) Nytran membrane.
- Temperature has an effect on the sensor and should be considered while using it in the field. The sensors should be calibrated at the temperature expected in the marine sediments.
- There is some salt effect on the sensor, which should be considered when constructing the calibration. This is unlikely to be a major problem in vast marine environments where salt concentration is quite consistent but it could be problematic in environments where salinity changes, such as estuaries.
- Light bleaches the dye from the sensor so the sensing probes should be kept in the dark, i.e. wrapped in kitchen foil until used.
- The sensors should be stored dry. Prolonged exposure to an aqueous environment bleaches the dye, however the sensor is robust for up to four

hours in an aqueous medium which is good as the SPI can be left in the sediment and it takes some time to settle down in the sediments. For every new station however, using a fresh probe is recommended.

4.6 References

<http://www.rkprint.co.uk/wp-content/uploads/2011/01/KControlCoater.pdf>

Kolthoff,IM (1937). *Acid-base indicators*. The Macmillan Company, New York, p189

Chapter 5

Device calibration and first tests on a cruise

5.1 Introduction

A working pH sensing probe for marine sediments had been developed and the characteristics had been studied. The next step was to calibrate the sensor and apply it in the marine sediments. This chapter discusses different methods used in an attempt to calibrate the sensor. Attempts were made to make calibration simple, easy and reliable. Development of a software that automated the process of measuring pH values vs depth, sensor's response and certain issues observed during the first test of the sensors on a cruise have been discussed.

5.2 Materials and Methods

5.2.1 Calibration using phosphate buffers

For this work, membranes were made with the following composition:

Component	Amount
Bromothymol blue	50 mg
Tetraoctyl ammonium bromide	176 mg
PVC	148 mg
Bis-2(ethylhexyl)sebacate	500 mg
THF	3 mL

Table 5.1: Composition of sensing membrane used for calibration.

Phosphate buffers of pH 6.8, 6.94, 7.0, 7.1, 7.21, 7.34, 7.4, 7.52, 7.62, 7.72, 7.81, 7.91 were made as discussed in chapter 2 with 0.5 M NaCl salt in the buffer. The 6 μm metering bar was used to spread 0.5 mL membrane solution on a transparency sheet. Three pH probes were made and the probes were conditioned before calibration by inserting them twice in buffer of pH 7.91 and 6.8. While conditioning, the probes were pressed using a rubber roller which removed any air bubbles trapped between the membrane and the sensing layer. The probes were dipped in each buffer to a depth of 8cm, left to equilibrate and then removed and photographed. The RGB values were

extracted using ImageJ software and a plot of colour index values against the pH was constructed. After calibration, a sediment core collected by Ms Alida Rosales was analysed using the same probes. The core was collected from the Wash but it had been in the lab for a few days so was only used as a representative sample of a likely marine sediment and no site-specific relevance should be attached to the results.

5.2.2 Calibration using agarose gel

20 % w/v (2 g in 10 mL) agarose gel was made using buffers of pH 6.5, 6.6, 6.7, 6.8, 6.9, 7.0, 7.1, 7.2, 7.3, 7.4, 7.5, 7.6, 7.7, 7.8, 7.9, and 8.0 to dissolve the agarose powder. A calibration stick made of plastic with holes drilled through it was specially designed to calibrate the sensor by filling the holes with the agarose gel. The calibration sticks are shown in figure 5.1 b. This method if successful, will make the calibration fast and will give an easy way to calibrate the sensor using SPI. The calibration stick was taken. The base of the calibration stick was covered with sticky tape. The holes were filled with 200 μ L of the agarose buffer solutions. The stick was kept on ice to solidify the gel. The sticky tape was peeled off and the stick placed on the sensor probe. It was left for 10 minutes, after which the stick was removed and the probe photographed.



Figure 5.1: (a) Figure of calibration stick showing the general design (b) photograph of the calibration sticks with different spacing and hole sizes.

Alternative approaches were used to improve calibration:

1. Using the calibration stick (8 mm holes @15 mm spacing as a mould only), gel was taken out from each hole and placed on the sensing probe. This gave a direct contact and the response could be seen clearly and the probe could be pressed on the gel if required.
2. Using a calibration stick (5 mm holes @10 mm spacing), the holes were filled with the agarose solution leaving two holes empty in between each gel to avoid cross contamination. The gel stick and the sensing probe were stuck together using sticky tape to maximise contact.
3. A 7 mm holes @15 mm spacing calibration stick was taken and the sensor was kept on it (rather than keeping calibration stick on the sensor) and a heavy glass plate was put on it to improve the contact.
4. 6mm holes @10 mm spacing and 6mm holes@15 mm spacing calibration sticks were kept on the sensors and a heavy glass plate was used above them to exert downward pressure.
5. Putting the probe on the calibration stick and wrapping both with sticky tape to ensure good contact.
6. Filling the buffer gels into the aluminium apparatus shown in figure 5.2 and screwing it together. Once the gel solidified, the apparatus was unscrewed and the plastic block containing the gel was pressed firmly onto the probe. The rubber "O" rings should help prevent creep and cross contamination.

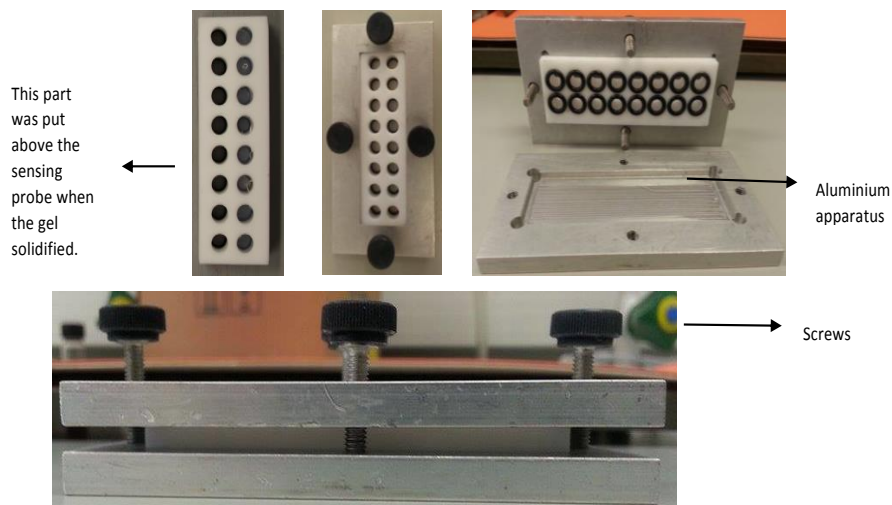


Figure 5.2: Apparatus used for calibration.

7. Using the aluminium apparatus and using a sticky tape beneath rather than screwing it to its base.
8. Rectangles of gel were cast by taking two slides and sticking them at the bottom with sticky tape, leaving a space between the two slides by putting plastic spacers in between, clamped with spring clips. The space was filled with the buffer gel and kept on ice to cool down. When the gel was formed, the apparatus was dismantled and the gel was cut into pieces and placed on the probe. The set up is shown in figure 5.3.



Figure 5.3: glass slides stuck together with agarose gel inside.

Three probes were taken and on two of them gel pieces of pH 6.24, 6.44 and 6.65 were placed. These two probes were photographed after they had equilibrated and were compared. A third probe was taken and gel pieces of the same pH (6.2) were placed on it and the probe was photographed after it had equilibrated to make sure all the pieces gave the same colour index values.

5.2.3 Investigating the variability of probe response in calibration

The following variables were investigated

- Probe to probe variability
- Photo to photo variability
- Within a probe variability

Three probes were made to study probe to probe variability. Each probe was equilibrated in one buffer and photographed five times in the light box to study photo to photo variability. Different areas were selected within a probe photograph in ImageJ

to get RGB values to study the variability within a probe. The calibration graph was plotted by taking the mean of the means.

5.2.4 Calibration in seawater

As the probes will be used in marine sediments, therefore it is important to calibrate the probes in seawater. The probes were made using a thicker (12 μm) metering bar and the amount of solvent was also reduced to half (1.5 mL) in this experiment. Two probes were calibrated in fresh sea water taken from Lowestoft (Cefas). The rig used is shown in figure 5.4. The pH of the seawater was increased and decreased by bubbling nitrogen gas and CO_2 gas respectively and magnetic stirrer was used for proper mixing. Response was photographed at each pH (monitored by a glass membrane pH electrode Fisher scientific AB15). The temperature of the seawater was measured by a temperature probe, Fisher Scientific Platinum sensor (Pt-100 Ω).

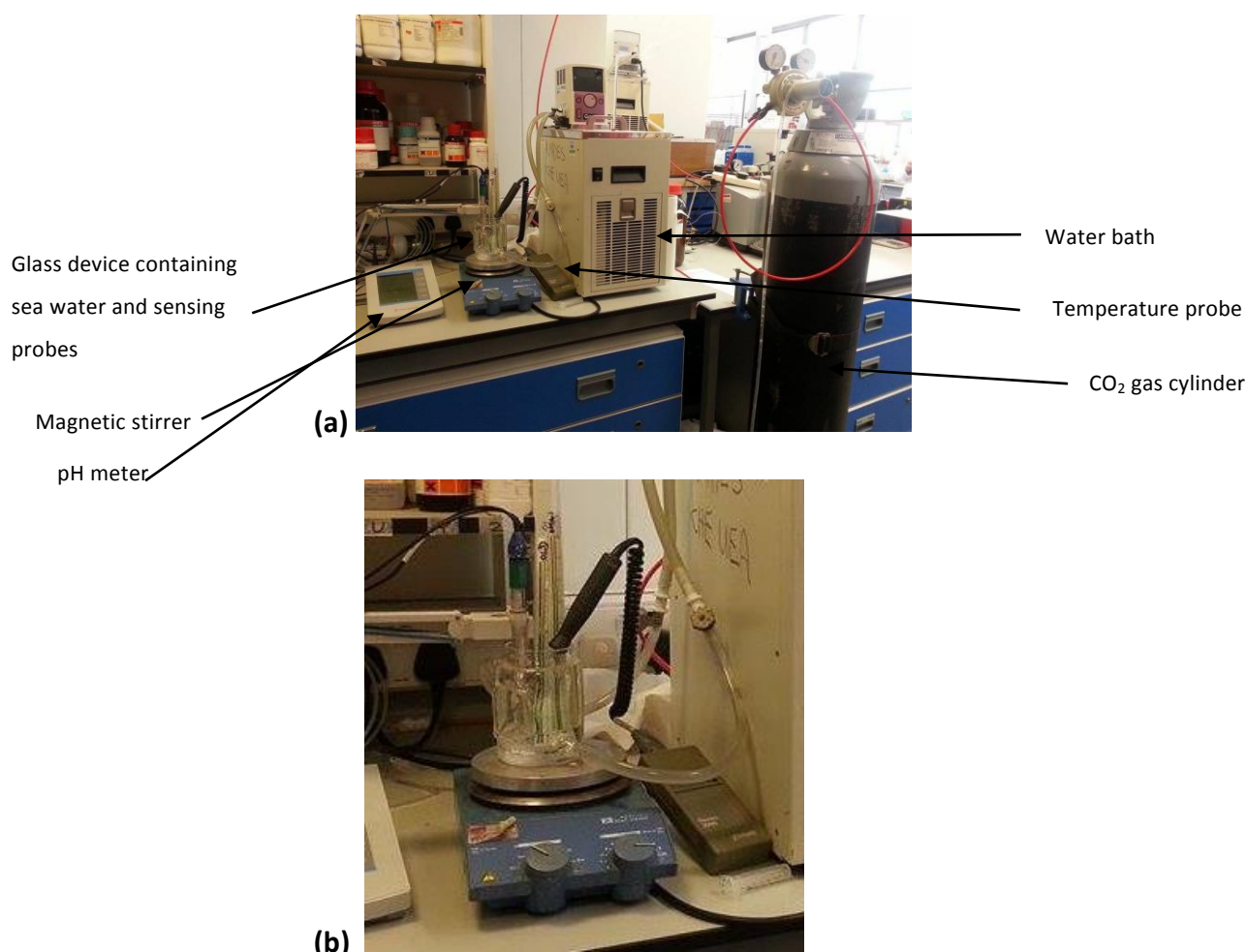


Figure 5.4: (a) Experimental set up for calibration. (b) A closer view of glass device.

Calibration at different temperatures

The temperature has some effect on the sensor so three probes were calibrated at 7.4 °C, 11 °C and 15 °C. The calibration was done as explained in the previous experiment and temperature was controlled using a circulating water bath and monitored by a temperature probe.

5.2.6 Automation of pH measuring technique

An R script was developed by David Stephens (Cefas) which automated the whole process of measuring the pH with depth from the photos. The Image is opened in the R studio. The starting point and the ending point are selected on the image for analysis. The script then measures pixel by pixel RGB values on the sensor strip along the height and the length by cropping the strip and masking irrelevant areas. It then converts the values into colour index values and plots a pH vs depth plot using the user input calibration equation. The start and end points in mm and calibration equation can be changed in the script. Figure 5.5 is an example of the output.

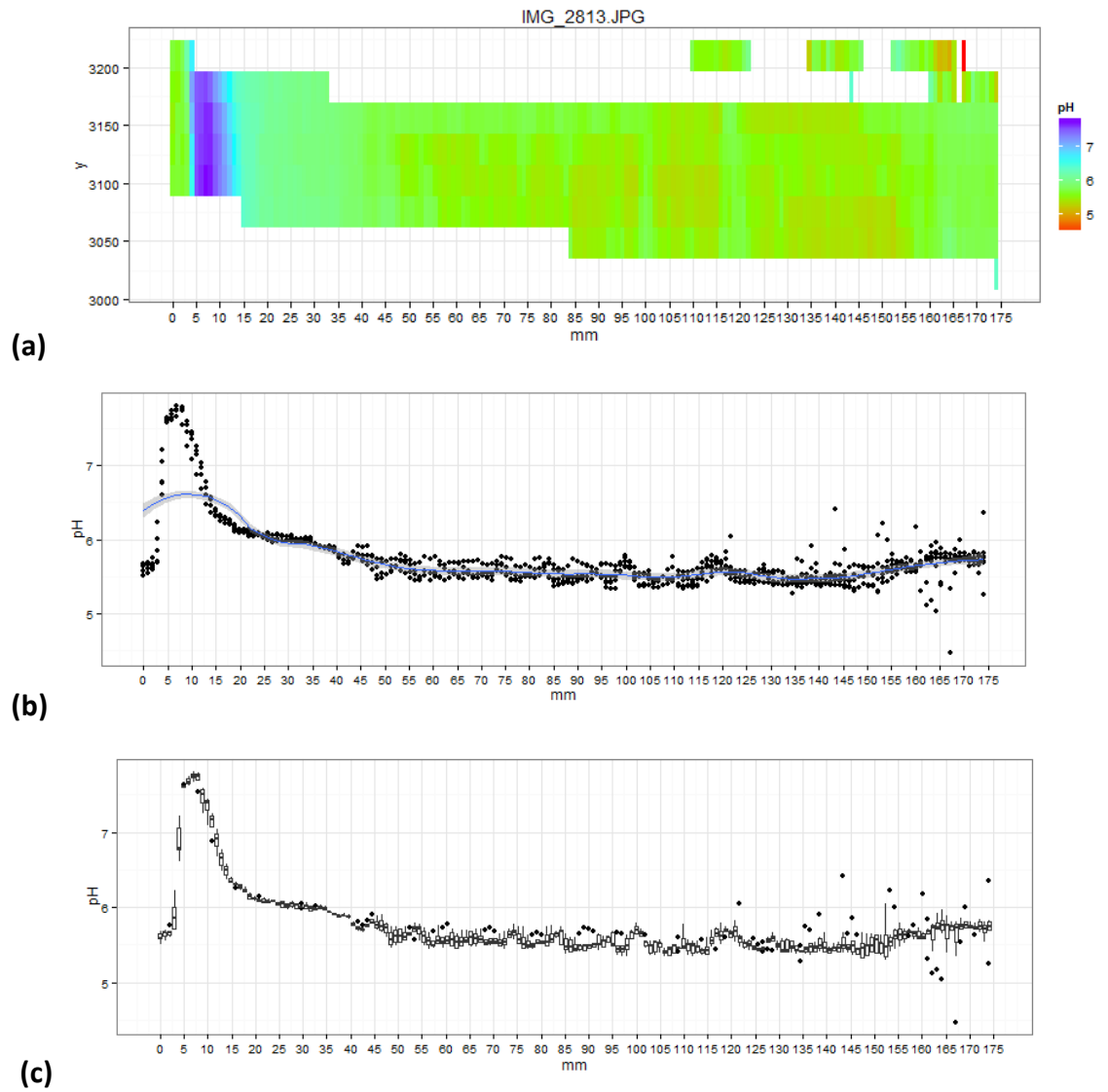


Figure 5.5: Result output from the R script showing the data as (a) a false colour pH map generated by the software for the sensor area (b) an average pH value across the strip (c) box plot- white box: interquartile range (iqr), horizontal line: median value, vertical line: range of the data, individual points: potential outliers, which are identified as >2.5 iqr from the median.

5.2.7 Application of the pH sensors in sediment cores during the Cefas Endeavor cruise

The sensor probes were tested during the Cefas Endeavor cruise 'CEND 15113' by a colleague Alida Rosales. Some microelectrode profile data was measured at the same time as the probe data allowing the results to be compared. The probes were used to measure the pH profiles of the sediment cores during the cruise. The same membrane composition as given in table 5.1 was used for both calibration and the probes taken for the cruise. The 6 μm metering bar was used to spread the solution by taking 500 μL . One of the probes from sheet 1 was calibrated in phosphate buffers by photographing and taking the RGB values using ImageJ. The photographic conditions at this time were not optimised. The probes were photographed in the polystyrene box containing an external flash.

5.3 Results and Discussions

5.3.1 Calibration with phosphate buffers

Figure 5.6 shows the three different designs used in the calibration. The probes were photographed in day light. The 'brick like' design was tested because it was thought that having small pieces of sensor membrane stuck down might reduce problems of bubbles being trapped between membranes and sensing strip. It was observed however, that the probe with the brick like design got a lot of air bubbles trapped inside slowing down the response and they had nowhere to escape to. The other two designs were equally good and showed for fewer problems with trapped bubbles.

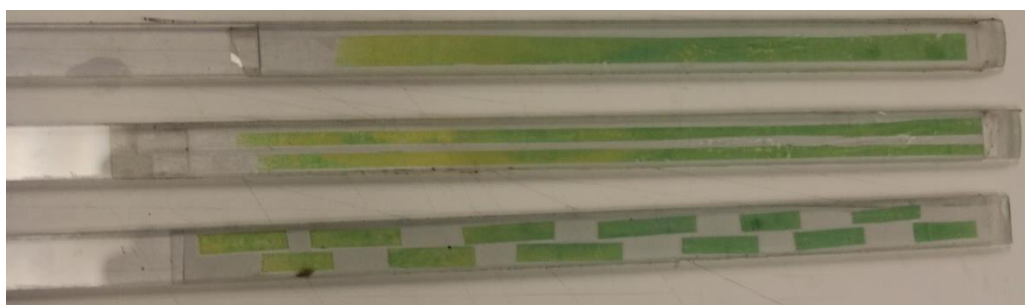


Figure 5.6: Probes of three different designs.

The RGB values of the striped probe (middle one in figure 5.6) were obtained using ImageJ and the colour index was calculated using the formula $(R-B)/G$. The following calibration graph was obtained.

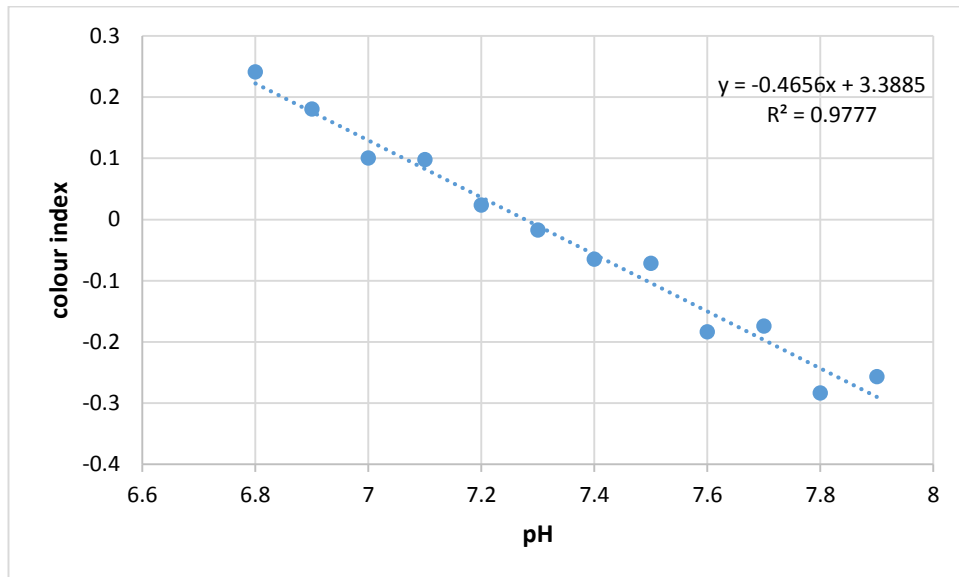


Figure 5.7: Calibration graph of striped probe showing equation and R^2 value.

The RGB values of the top probe (single wider sensing probe) in figure 5.6 were obtained using ImageJ and the colour index was calculated using the formula $(R-B)/G$. The following calibration graph was obtained.

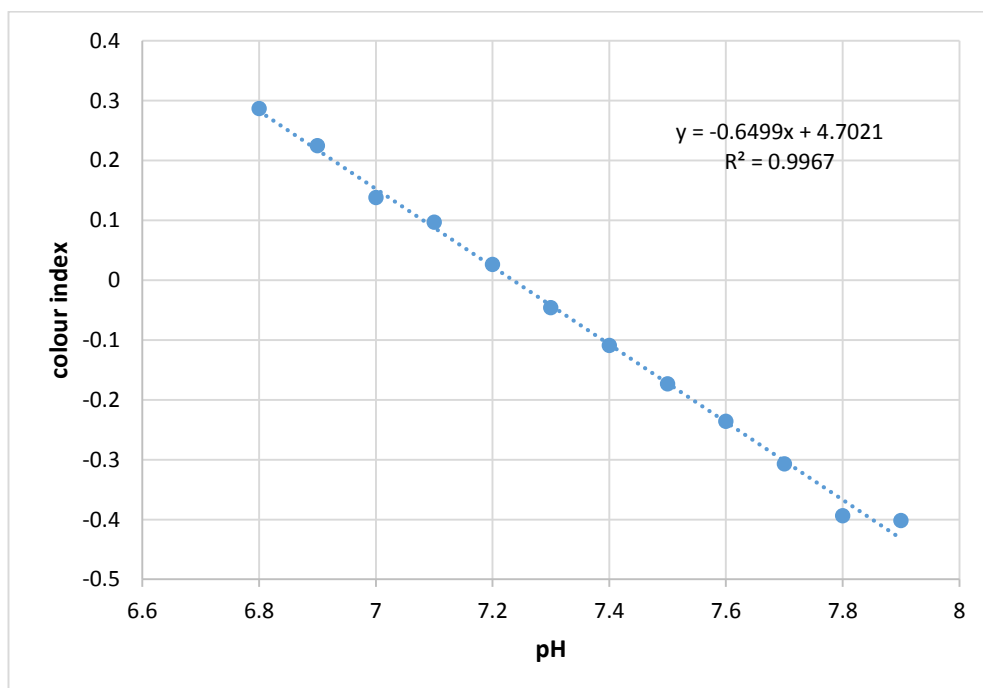


Figure 5.8: Calibration graph of normal probe showing linear equation and R² value.

If we compare both the graphs, it is evident that the normal design gives a better calibration graph with lower scatter and a higher R² value than the one that contains two strips of sensor. The brick like design was rejected because air bubbles were entrapped in the probe and were difficult to remove, thus affecting the response.

5.3.2 Sediment core analysis

A sea sediment core was taken from Alida Rosales (collected from the Wash) and analysed. The three probes were inserted in the sediment for 30 minutes as shown in figure 5.9. A few centimetres were soft but then a rubber mallet was used to force the probes down into the harder sediment layer. The probes did not break so they are very robust and can be inserted with force into compacted sediments when required.

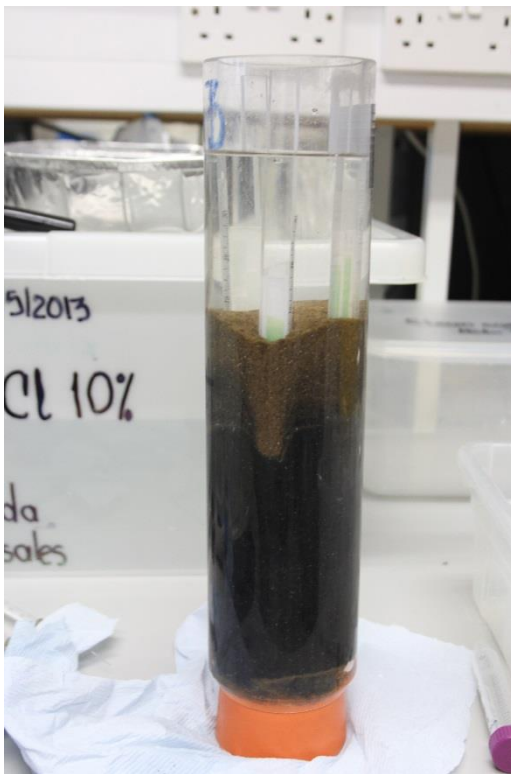


Figure 5.9: Probes in the sediment core.

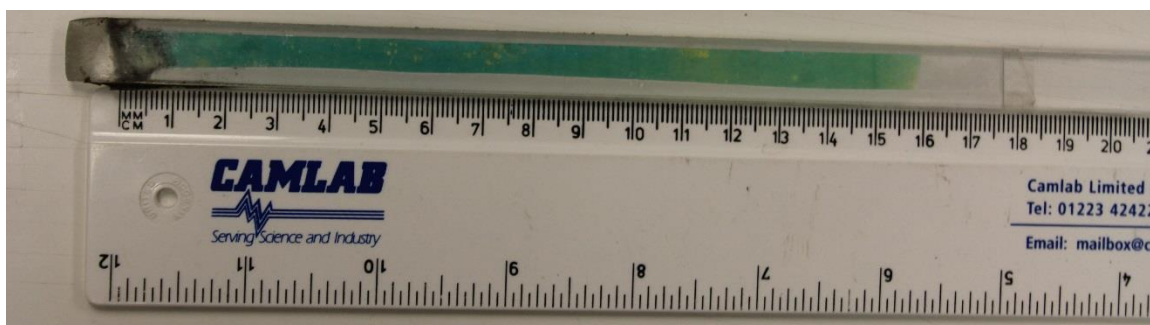


Figure 5.10: Photograph of the probe response taken in the lab without controlling light conditions.

The equation from the calibration graph was used to calculate the pH manually at every centimetre.

Depth in cm	Red	Green	Blue	(R-B)/G	pH
1	88	115	83	0.043478	7.17
2	64	104	73	-0.08654	7.37
3	62	103	72	-0.09709	7.38
4	62	100	68	-0.06	7.33
5	67	99	66	0.010101	7.22
6	48	91	66	-0.1978	7.54
7	40	85	65	-0.29412	7.69
8	37	83	66	-0.3494	7.77
9	40	81	62	-0.2716	7.65
10	33	77	62	-0.37662	7.81
11	34	77	61	-0.35065	7.77
12	33	78	62	-0.37179	7.81
13	33	78	62	-0.37179	7.81
14	36	79	64	-0.35443	7.78
15	40	81	64	-0.2963	7.69

Table 5.2: Calculation of pH using the equation from the calibration graph.

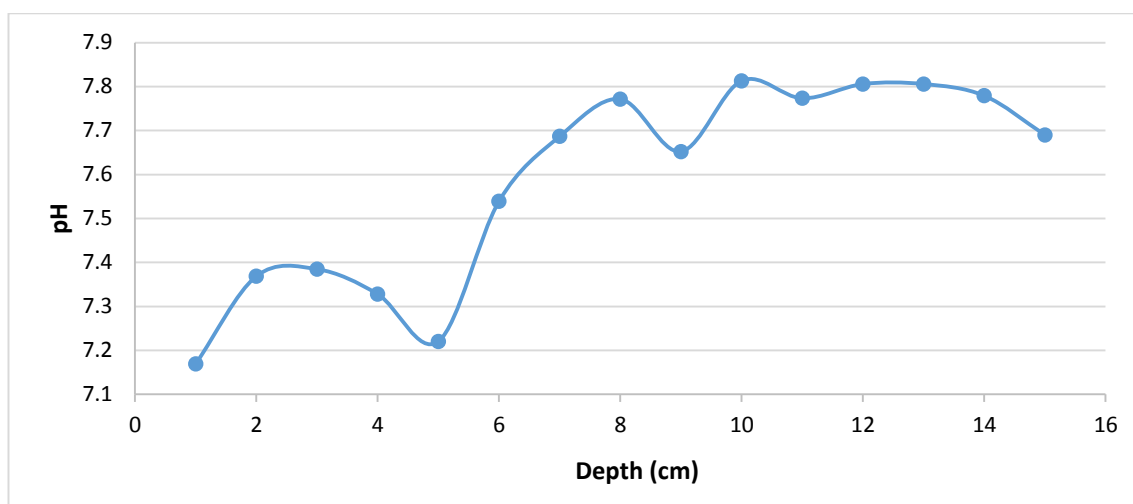


Figure 5.11: pH vs depth profile of the sediment core.

The probe was photographed in daylight on the bench in the lab. Figure 5.11 shows that the pH at the first cm of the probe was 7.16 which was the interface. The pH was higher in the sediments as compared with water. At 5 cm, pH is 7.3 and at 8 cm, pH reaches a maximum value of 7.7 but pH decreases at 9cm to 7.3. At 10 cm, it is 7.8 and stays fairly constant beyond that depth.

5.3.3 Improving the photographic conditions

To make the calibration and measurement more reliable, the photographing conditions were improved and a scale was added to the probe by printing the scale on transparency sheet and attaching it to the probe beside the sensing strip. The experiment was repeated by photographing the probe in a dark polystyrene box using remote flash gun. The flash gun was kept in the box. The camera settings were changed to get decent photos. The following settings were used:

Shutter priority mode (TV), Shutter speed: 1/200, ISO: 400, internal flash: 0, external flash: 1.5, channel: 1. Focused manually.

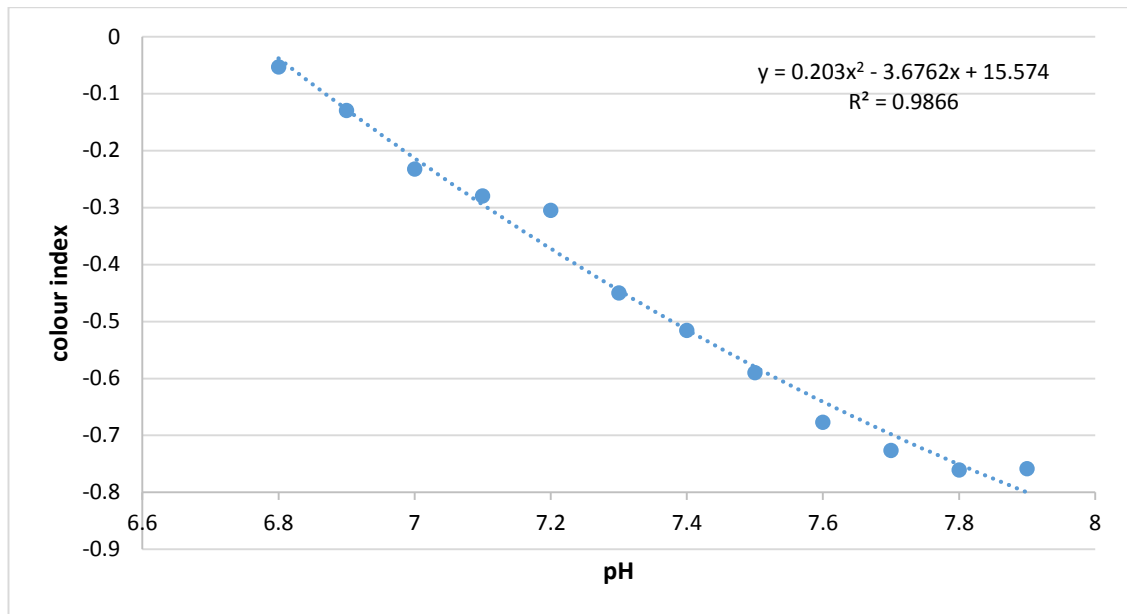


Figure 5.12: Calibration graph after photographing in the polystyrene box.

Although the equation of best fit has changed from linear to quadratic, it will probably give more reliable results because of improvements in the photographic conditions. A randomly chosen pH 7.2 buffer was taken and the probe was inserted in it to see if it relates to the calibration graph.

pH of buffer	Red	Green	Blue	(R-B)/G	Calculated pH $Y=0.4628*x^2 - 1.0126x+6.7647$
7.2	78	144	122	-0.30556	7.11

Table 5.3: Validation of pH calculation.

The calculated pH from the equation is 7.11, compared with an expected value of 7.20. Interestingly, the trend line has missed exactly the same calibration point so may be the measured pH of the buffer was slightly erroneous. Otherwise if we look at the calibration graph, pH 7.2 is at x value of -0.3 which is exactly the same as calculated for the buffer. This validates the sensor's response within 0.09 pH units.

Sediment core analysis with improved photographic conditions

The same sediment core was again analysed with the improved photographic conditions (polystyrene box and remote flash) and the following results were obtained. The probe was kept in the sediment for 20 minutes.

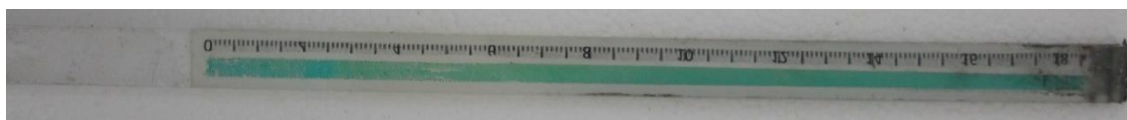


Figure 5.13: Photo of probe after response taken in polystyrene box with an external flash inside.

The interface was at 2.5 cm and the first centimetre represents the pH in the seawater and after that the sediment pH.

Depth in cm	Red	Green	Blue	(R-B)/G	pH
1	72	122	110	-0.31148	7.12
2	65	125	108	-0.344	7.17
3	85	127	105	-0.15748	6.94
4	100	132	111	-0.08333	6.85
5	86	130	105	-0.14615	6.92
6	76	127	102	-0.20472	6.99
7	69	125	101	-0.256	7.05
8	72	124	104	-0.25806	7.06
9	64	120	101	-0.30833	7.12
10	65	118	103	-0.32203	7.14
11	65	117	100	-0.29915	7.11
12	58	115	97	-0.33913	7.16
13	58	115	101	-0.37391	7.21
14	60	113	100	-0.35398	7.18
15	52	101	91	-0.38614	7.22
16	53	103	92	-0.37864	7.21

Table 5.4 : Calculation of pH with depth in the sediment core from probe photo.

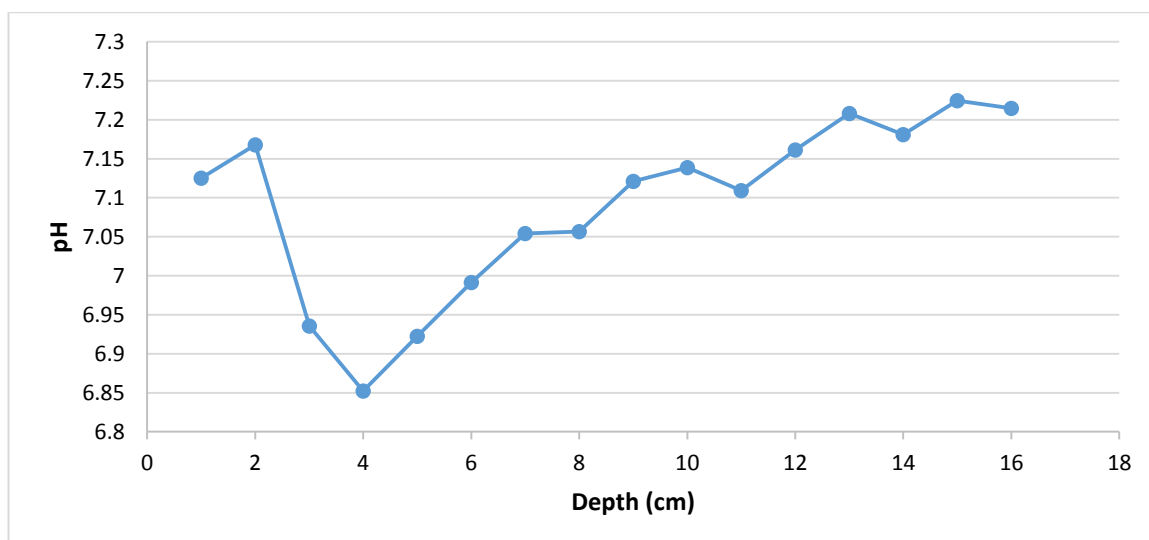


Figure 5.14: pH vs depth profile of sediment core.

Figure 5.14 suggests that the pH of water was 7.1 and in the first centimetre of the sediment, the pH was 7.16 which dropped down quickly to 6.6 and 6.8 in the 2 centimetres below. This is possibly due to the re-oxidation of Fe and Mn along with oxalic mineralisation. (Revsbech *et al.*, 1983, Archer *et al.*, 1989, cai *et al.*, 1999, Luff *et al.*, 2001, Wenzhofer *et al.*, 2001, Stahl *et al.*, 2006) The pH then gradually increased to 7.2 which is possibly due to the Mn and Fe reduction that increase the pH. (Wenzhofer *et al.*, 2001, Stahl *et al.*, 2006).

5.3.4 Calibration using agarose gel

The calibration sticks were used in an expectation that the calibration would be easy and fast. However, the liquid diffuses from one hole to the other, resulting in a pH gradient rather than distinct colours. There should be more space between the holes, so the experiment was repeated by filling every second hole with buffers 6.5, 6.6, 6.8, 7.0, 7.2, 7.4, 7.5, 7.8, and 8.0 and this time there were clear distinct colours. Calibration sticks with different hole sizes and different spacings were made. (8 mm holes at 15 mm, 6 mm at 10 mm, 6 mm at 15 mm, 5 mm at 10 mm and 7 mm at 15 mm). The response was continuous because there was not a good contact between the sensor and the calibration stick. Photos were taken in a wooden dark box with a flash in it (example photograph shown in figure 5.15). The comparison is shown in figure 5.16. The pH of the buffers were 6.24, 6.44, 6.65, 6.83, 7.03, 7.23, 7.42, 7.62, and 7.83.

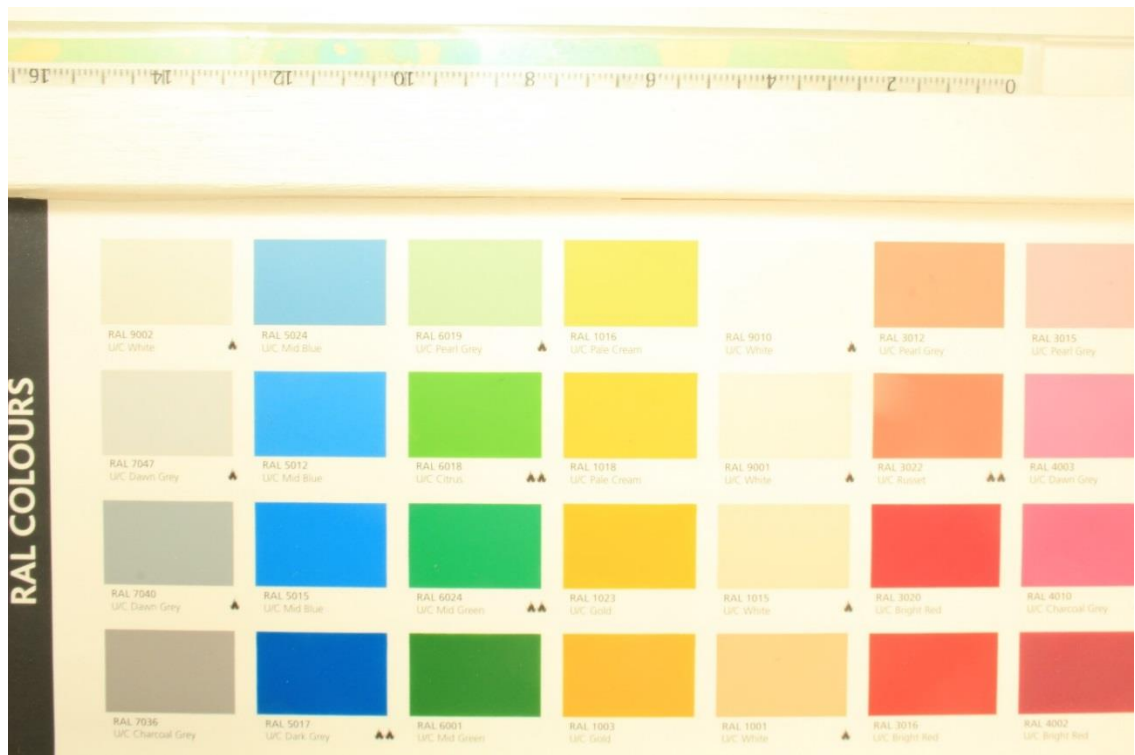


Figure 5.15: photo of probe used for calibration in a light box containing flash.

The photos taken in the dark box were very bright. There was not good contact between the gels and the sensor and there was no clear distinction among the colour response at the same stick. A comparison is shown in the figure 5.16.



Figure 5.16: Calibration sticks and probes used for calibration.

The experiment was repeated by changing the camera settings: ISO was reduced and f number was increased to get darker photos. The calibration was done in a similar way but this time some weight was put on the calibration stick, both the devices were stuck together using a sticky tape and after taking the calibration probe out from the ice, it was wiped.

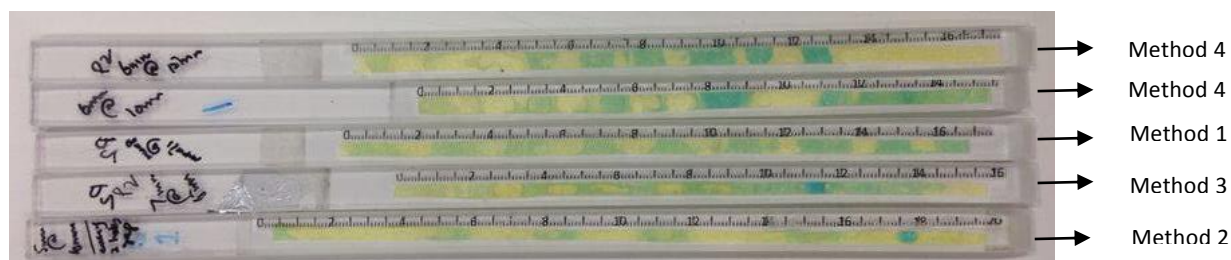


Figure 5.17: comparison of probes used in calibration by using different methods. (For description of methods see pp173-175).

Out of methods 1 to 4, it was noticed that method 1 and 2 improved the calibration. Out of methods 5 to 7, None of the methods worked well and there was not good contact between the sensor and the gel and there was no distinct response useful for calibration. Figure 5.18 shows the result from the device with “o” rings used to calibrate. The results were poor so this approach was not pursued any further.

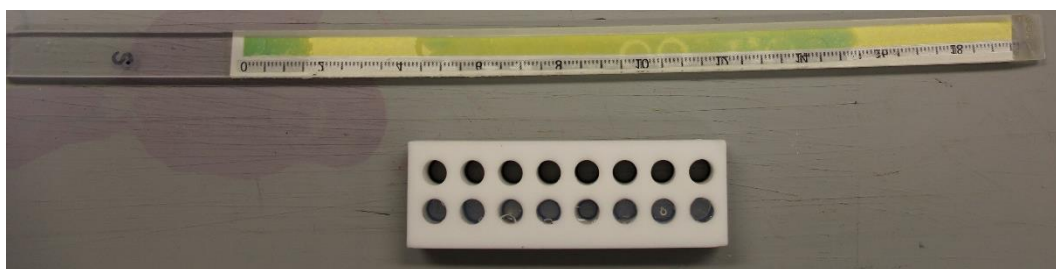


Figure 5.18: photo of probe calibrated using the aluminium apparatus.

Figure 5.19 shows the results obtained from method 8. The probe with the pieces of the same pH (6.2), which appeared green when it was wet and photographed, became blue after drying. This could be because of the white membrane used in this experiment which was Protran.

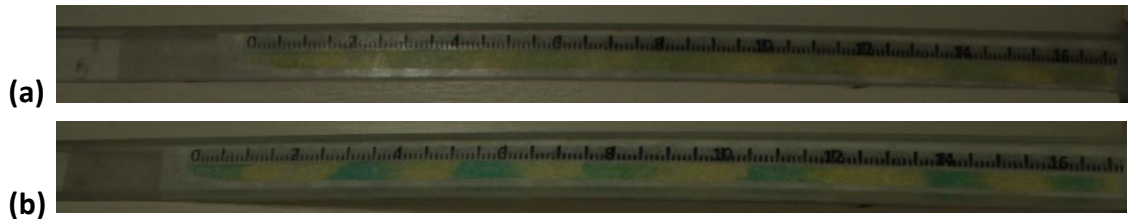


Figure 5.19: Calibration probes showing the variability of colour wet or dry when protran is used. (a) Photographed wet (b) photographed dry.

pH	Colour index
6.2	0.40
6.2	0.41
6.2	0.42
6.2	0.42

Table 5.5: Colour index values at same pH on a calibration probe.

The table 5.5 shows some variability at the same pH which means that the calibration method is not very precise. This difference could also be because of the lighting inconsistency which was not optimised here and an external flash was used as a light source. Due to the contact problem, a few pieces couldn't equilibrate as efficiently therefore there is a difference in the colour index values. Two probes were taken and the gels of three different pHs were kept on them to compare if both probes give the same colour index values at the same pH values. One of the probes had a Nytran overlay and the other had a protran overlay. Table 5.6 shows the calibration values of the two probes.



Figure 5.20: comparison of two probes (a) Protran (b) Nytran

pH	Probe 1				Probe 2			
	Red	Green	Blue	Colour index (R-B)/G	Red	Green	Blue	Colour index (R-B)/G
6.24	48	67	39	0.134	47	70	45	0.029
6.44	57	70	43	0.200	52	68	42	0.147
6.65	68	80	49	0.238	61	74	44	0.229

Table 5.6: comparison of probes at same pH for calibration.

The colour index values of both the calibration probes were plotted on the graph.

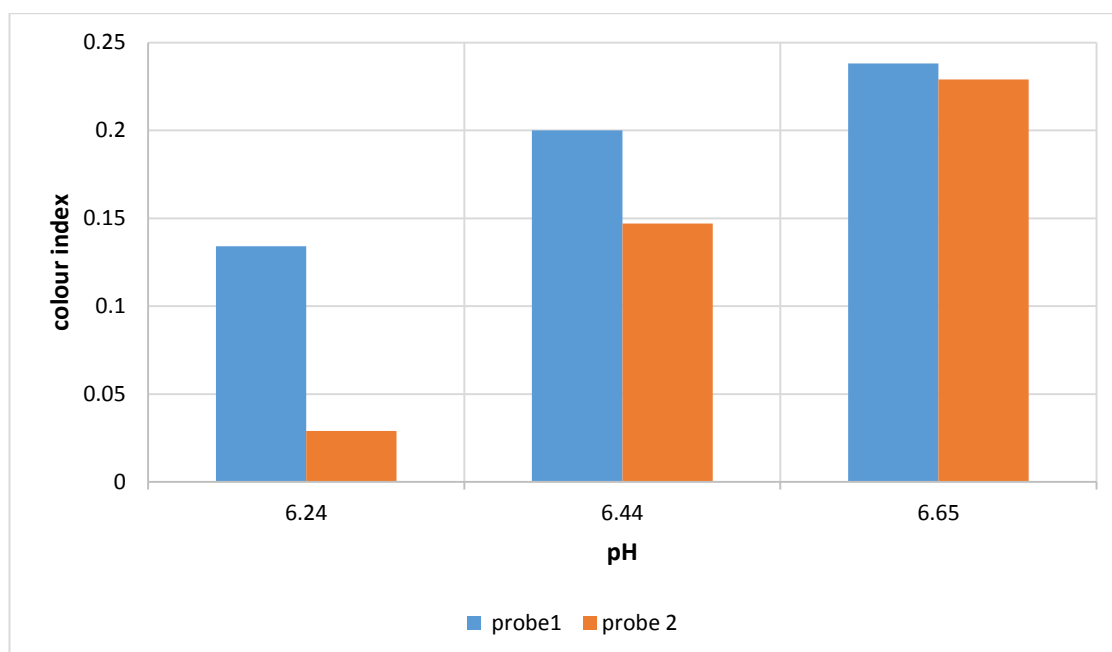


Figure 5.21: Calibration graph of two probes.

The results of this experiment indicate that either there is some probe to probe variability or the calibration method is not appropriate. The white membrane used in two sensing probes was different. This was further investigated. Two calibration sticks (6 mm@15 mm and 8 mm @15 mm) were taken, sticky tape was stuck on the bottom and the buffer gels were filled in them . Then they were kept on ice to allow the gel

to solidify. When the gel solidified, the sensing probes, which were made using a protran white membrane in this experiment, were kept above the sticks and left to equilibrate. The sensing probes were photographed after they had equilibrated and their colour index values were compared. Two more probes were made and were calibrated in phosphate buffer and the results were compared with the ones obtained from using agarose gel.

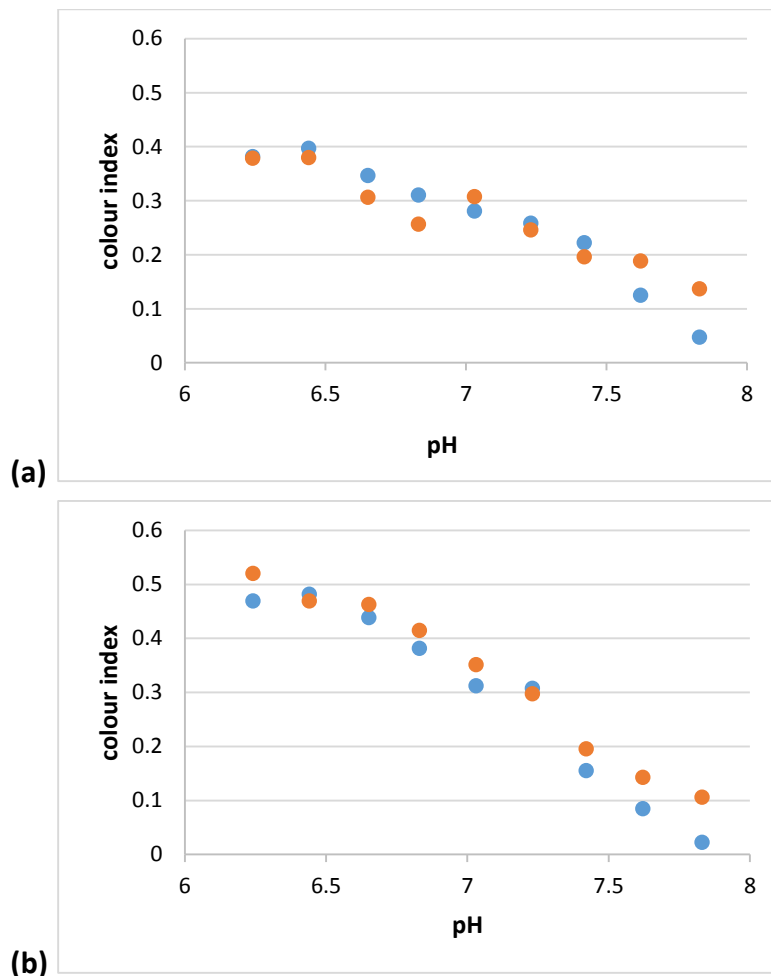


Figure 5.22: Calibration of two probes using (a) gel and (b) buffer solutions.

The agarose gel method might have been helpful to calibrate using the SPI faceplate later in this work. This would allow calibration in a single attempt and a single photograph which would be very convenient. Diffusion of buffer from the gel pieces leads to a continuous response on the probe rather than a distinct response (figure 5.16) which was controlled by using a calibration stick that has holes drilled at larger

distance (figure 5.17, 5.18). It was observed that due to a contact problem of gel with the sensing probe, gels with the same pH value gave different colour index values (figure 5.20).

Figure 5.22 suggests that there is some difference between using gels and free solution buffers. The calibration in the free phosphate buffer shows a clear trend and less probe to probe variability. As the calibration in the phosphate buffer solutions containing sodium chloride salt is easy, fast and reliable, therefore it was chosen as a better method to calibrate while calibrating with the agarose gel is more complex and less reliable. At this point the flash was not replaced by LEDs, therefore the colour index values are different for the two probes used for calibration in phosphate buffer solutions. Lighting was improved after this experiment.

5.3.5 Investigating the variabilities

The probe variability, photo to photo variability and within a photo variability were tested. Three probes were made to study probe to probe variability. Each probe was equilibrated in one buffer and photographed five times in the light box to study photo to photo variability and different areas were selected within a probe photograph in ImageJ to get RGB values to study the variability within a probe. The calibration graph was plotted by taking the mean of the means.

pH	Photo graph /secti on	Probe 1				Probe 2				Probe 3			
		R	G	B	(R- B)/G	R	G	B	(R- B)/G	R	G	B	(R- B)/G
5.8 3	1/1	226	210	108	0.562	209	192	96	0.588	199	182	94	0.577
	1/2	228	212	111	0.552	213	196	95	0.602	202	186	92	0.591
	2/1	223	208	106	0.563	207	190	96	0.584	199	182	94	0.577
	2/2	225	210	109	0.552	210	194	93	0.603	203	187	94	0.583
	3/1	222	207	105	0.565	209	193	96	0.585	198	182	94	0.571
	3/2	224	209	109	0.550	213	196	95	0.602	202	186	92	0.591
	4/1	221	207	106	0.556	208	191	97	0.581	200	183	94	0.579
	4/2	223	208	108	0.553	211	195	94	0.6	203	187	93	0.588
	5/1	218	204	102	0.569	207	191	96	0.581	202	186	92	0.591
	5/2	220	206	106	0.553	210	194	93	0.603	199	182	94	0.577

Table 5.7: RGB values and colour index values for three probes at pH 5.8 including values with in a photograph and in five different photographs

pH	mean probe1	mean probe2	mean probe3	mean of means	Std error of mean
5.83	0.557	0.593	0.583	0.578	0.011
6.03	0.636	0.599	0.565	0.6	0.021
6.22	0.58	0.555	0.524	0.553	0.016
6.44	0.504	0.485	0.478	0.489	0.008
6.65	0.425	0.412	0.411	0.416	0.005
6.83	0.382	0.369	0.384	0.378	0.005
7.01	0.346	0.347	0.361	0.351	0.005
7.21	0.242	0.271	0.285	0.266	0.013
7.41	0.135	0.181	0.213	0.176	0.023
7.61	0.031	0.088	0.12	0.08	0.026
7.81	-0.074	0.009	0.095	0.01	0.049
8	-0.171	-0.074	-0.02	-0.088	0.044

Table 5.8: Mean colour index values of three probes at pH different pH values, standard deviations and standard error of means.

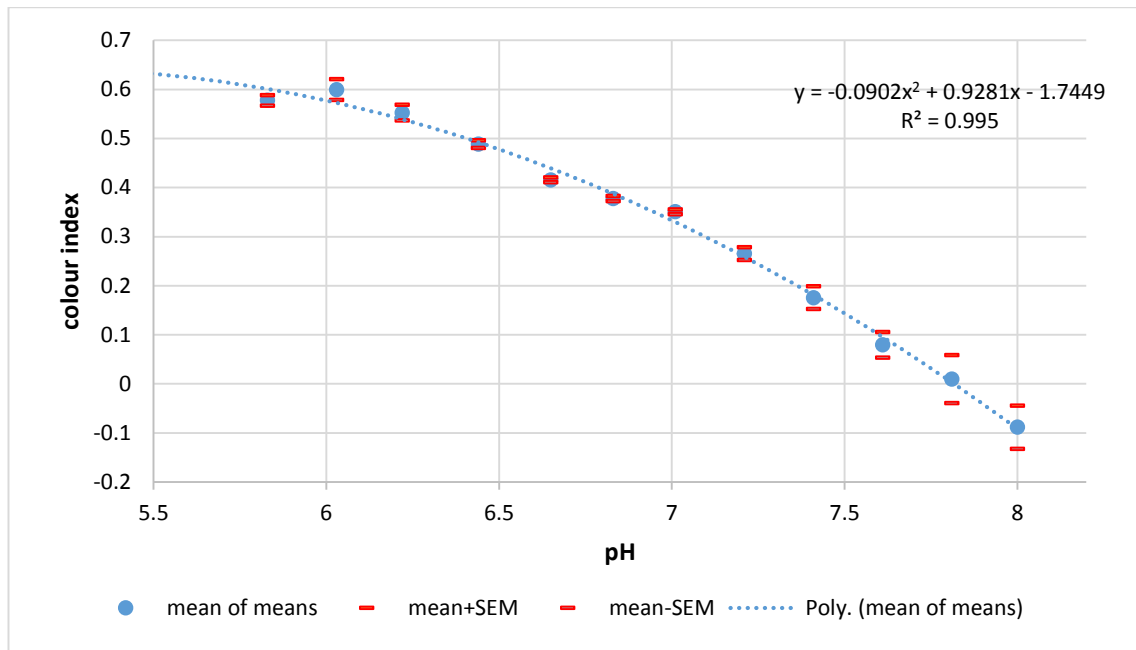


Figure 5.23: Calibration graph for three probes.

In figure 5.23, the means of means (including the mean of colour index values within a probe, mean of five photos of the same probe and mean of three different probes at the same pH value) were plotted. There was variability of ± 0.01 colour index unit from photo to photo and within a photo. The error bars are mainly due to probe to probe variability (± 0.1) as observed by the colour index values. Table 5.7 shows the variation within the photo, from photo to photo and probe to probe only for pH 5.8, further probe to probe variation can be seen in table 5.8 which shows the mean values taken at each pH value. The calibration graph is well fitted with a quadratic equation, with an R^2 value > 0.99 .

5.3.6 Calibration using seawater

Calibration was done in seawater by bubbling nitrogen gas and carbon dioxide gas into the seawater to establish the required pH value and the probes were photographed after they equilibrated at each pH value set. The following calibration graph was obtained using seawater.

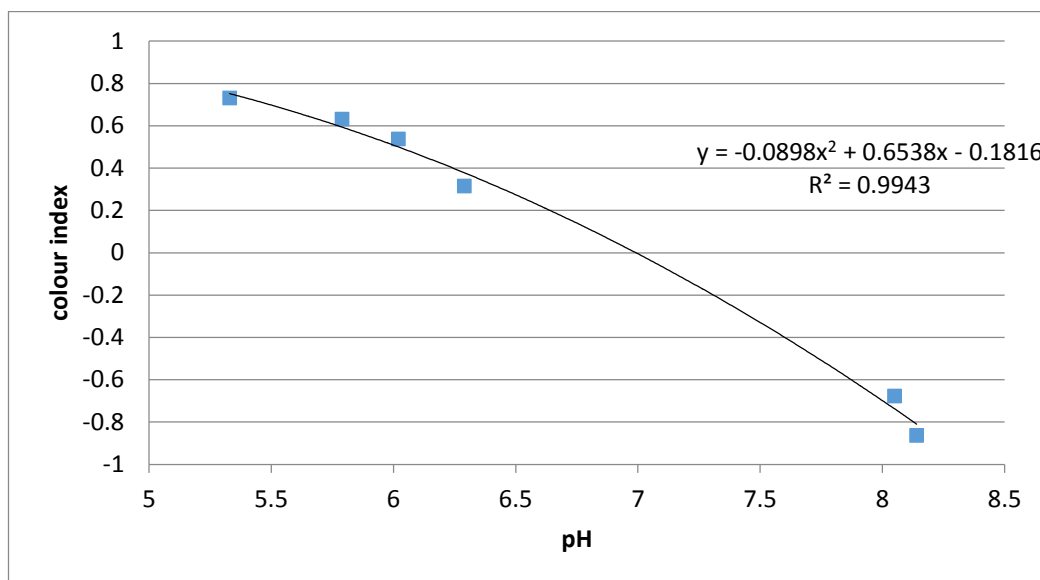


Figure 5.24: calibration in seawater.

The temperature changed by 1.1 °C during calibration. The general response characteristics have not changed in the seawater. The overall trend is the same but the composition of the membrane was different from the one used while calibrating in the phosphate buffer. The experiment was repeated and the same composition was used this time. In addition, N₂ gas was used to carefully reverse the rapid pH drop generated by even small additions of CO₂ at more alkaline pH values. This allowed more pH values in the mid range to be measured, giving a more detailed and more accurate calibration. The temperature was noted. Three probes were calibrated and the mean colour index was plotted.

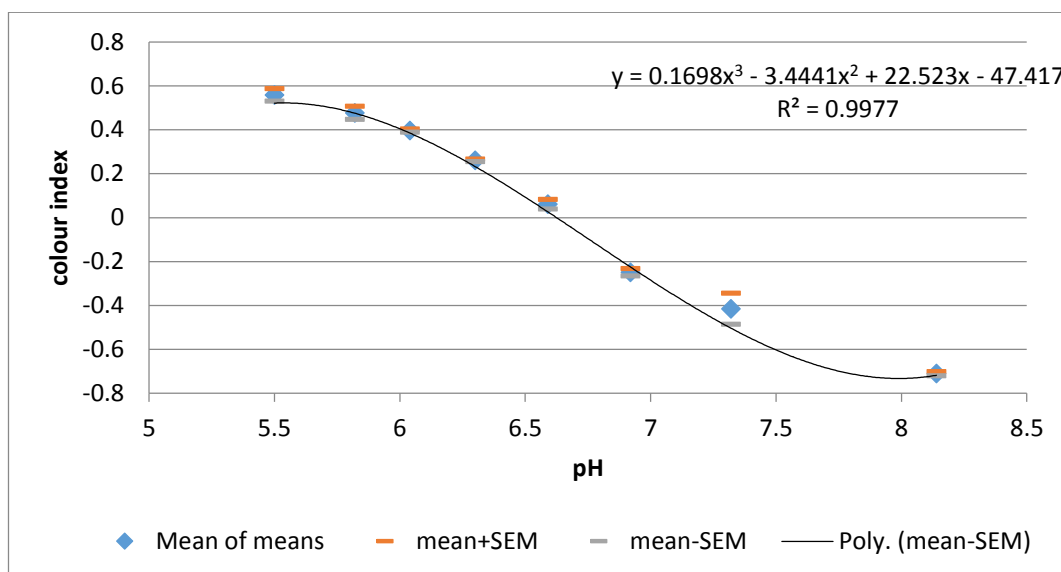


Figure 5.25: Calibration of probes in seawater using the same composition of membrane which was used for calibration in phosphate buffer.

Temperature changed by 1.3 °C during calibration. The equation of best fit has changed to cubic due to the plateau values now being visible at the high and low extremes of calibration range although the property of the dye ionisation should better be described by sigmoid function as the colour of the dye does not change any more below or above the pH sensing range of (5.5-8) i.e. it reaches a plateau at these values.

5.3.7 Calibration at different temperatures

As the temperature has some effect on sensor, therefore the probes were calibrated at different temperatures to see the difference. Nine probes were made and three fresh probes were used to calibrate at each temperature: 8.5 °C, 11 °C and 15 °C.

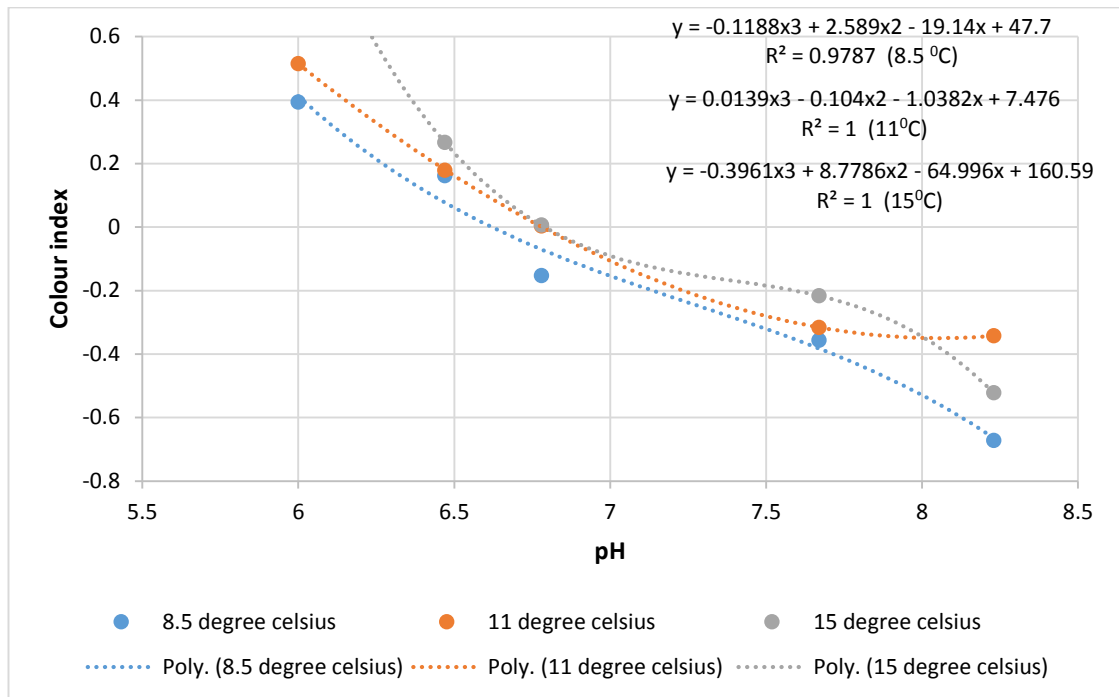


Figure 5.26: Calibration at three different temperatures.

There is not large difference in the calibration lines at different temperatures, although the equation changes. This is because of the difference in the values at very basic pH. This may be probe to probe difference rather than a temperature effect. In order to account for any temperature variation, it is worth calibrating at the temperature which is expected in the field when/where the sensors are applied.

5.3.8 Cruise Trial (Cefas Endeavor cruise 'CEND 15113')

The following calibration graph was obtained for the batch of probes sent on the cruise and the equation was used in the R script for the analysis of the photographs obtained from the cruise. The calibration was done at the room temperature using phosphate buffer solutions (Since the seawater calibration method and temperature effects discussed above had not been established at this stage).

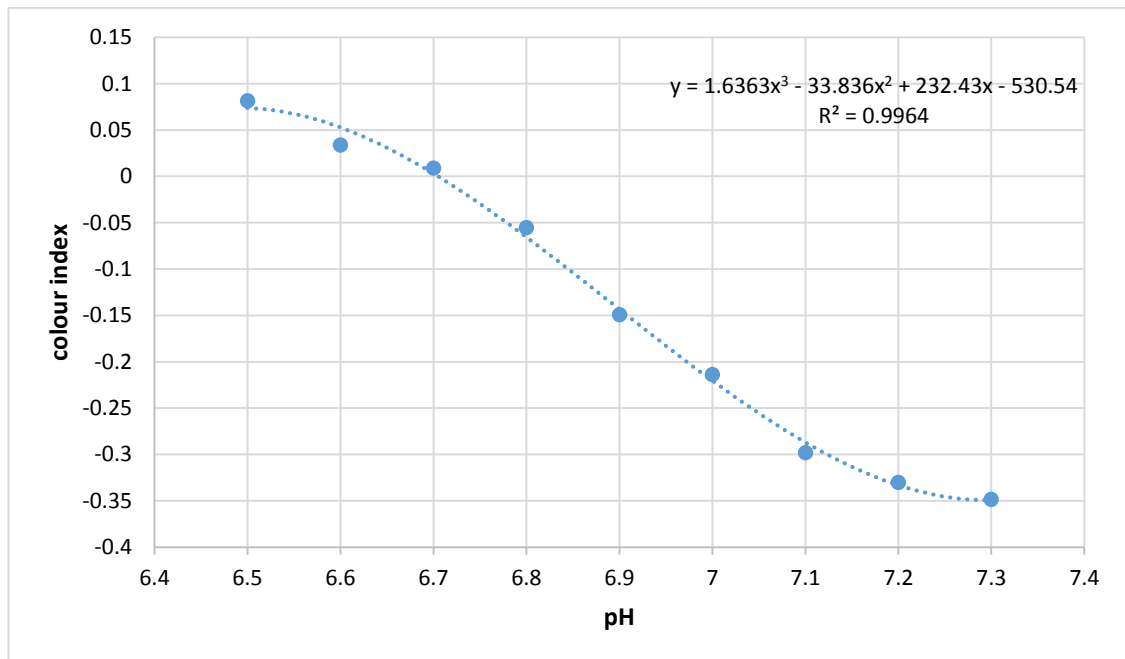


Figure 5.27: Calibration for the cruise trial.

The trend line is a cubic, giving a very high R^2 value (> 0.99). The results below show the pH profiles of the sediment cores collected and analysed during the cruise.

Station	Latitude	Longitude	Time of coring	Date	Temperature	Salinity	Depth of sediment
30	53 ⁰ 50.941'	005 ⁰ 14.229' E	22:42	7-8- 13	Not recorded	Not recorded	36.3 m
43	54 ⁰ 58.277'	007 ⁰ 19.141E	21:00- 22:00	7-8- 13	17.84 °C	31.42	27.8 m
60	55 ⁰ 14.799'N	002 ⁰ 55.509'E	21:00- 22:00	9-8- 13	14.5 °C	35	31.5 m
68	54 ⁰ 08.475'N	001 ⁰ 12.2757'E	21:00- 22:00	10- 8-13	16.4 °C At bottom: 12.9	34.67	56.9 m
81	55 ⁰ 35.135'N	002 ⁰ 52.571'E	21:00- 22:00	12- 8-13	17.4 °C on sea	34.68	97.5 m
101	56 ⁰ 51.222'N	000 18.290'E	21:00- 22:00	14- 8-13	19.69 °C At bottom:	34.95	110 m
19 (119 on	52 ⁰ 52.694'N	002 40.106'E	21:00- 22:00	5-8- 13	17 °C	34.5	40 m
127	57 49.977'N	000 25.639'W	22:00	16- 8-13	15.54 °C At bottom:8 °C	34.88	116 m

Table 5.9: Important measurements during the cruise (source: Alida Rosales Villa) Salinity is defined as 'The total amount of solid material in grams contained in one kilogram of seawater when all the carbonate has been converted to oxide, the bromine and iodine replaced by chlorine, and all organic matter completely oxidised' (As cited in: Williams and Sherwood, 1994).

Some of the microelectrode data (kindly supplied by Alida Rosales) has been compared with the probe data but unfortunately the microelectrodes broke so the comparison could only be done at a few stations. Figure 5.28 shows the probe profile at station 30. The microelectrode data was taken in a separate subcore and probes were used in a separate subcore both taken from the same station. The probes were completely inserted in the sediments so there is no interface whereas the pH was measured in water and sediments using the microelectrode and the negative values of depth represent the pH in the water. The comparison of the microelectrode and probe data is shown in figure 5.29.

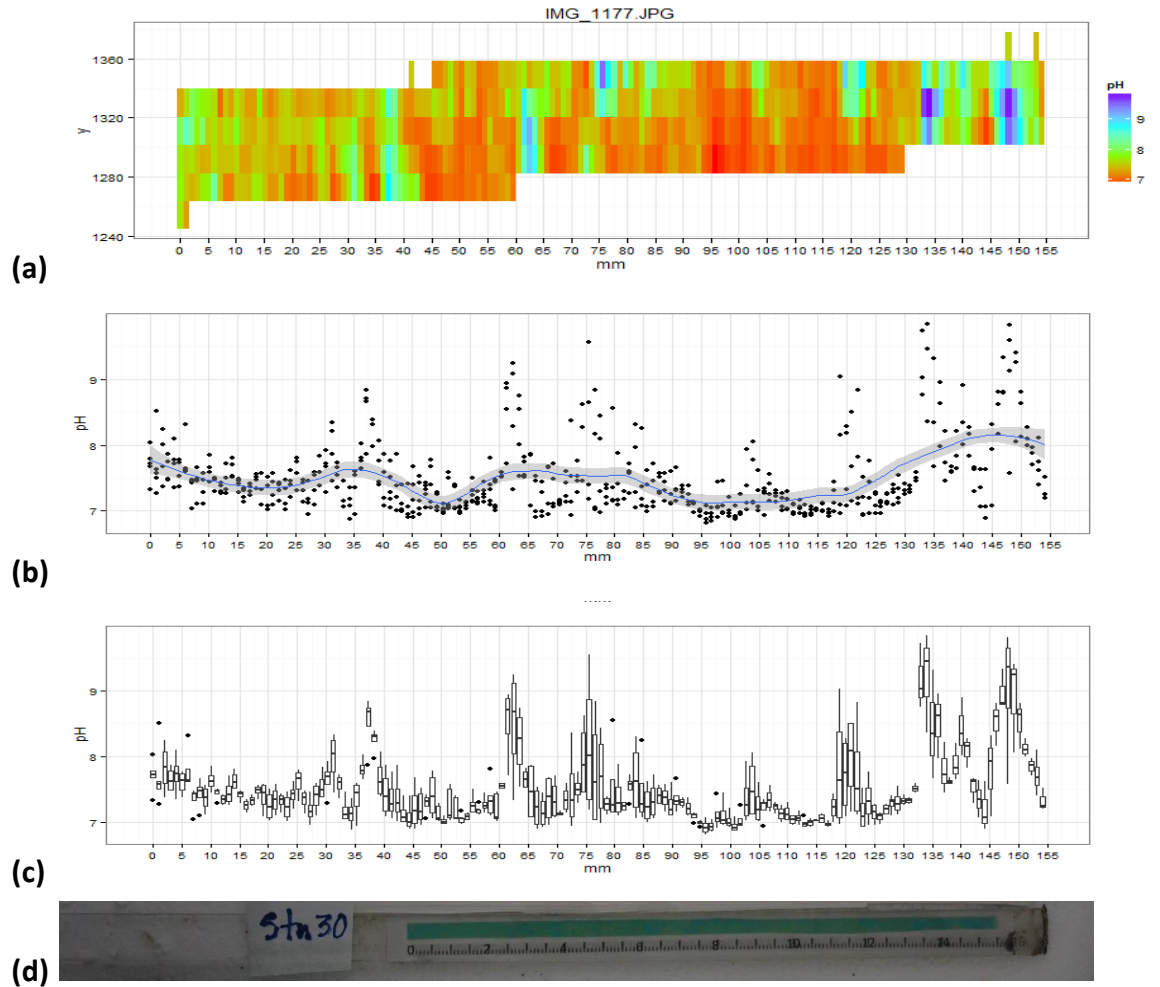


Figure 5.28: The pH profile at station 30 measured by probe. (a) a false colour pH map generated by the software for the sensor area (b) an average pH value across the strip (c) box plot- white box: interquartile range (iqr), horizontal line: median value, vertical line: range of the data, individual points: potential outliers, which are identified as >2.5 iqr from the median. (d) The actual probe.

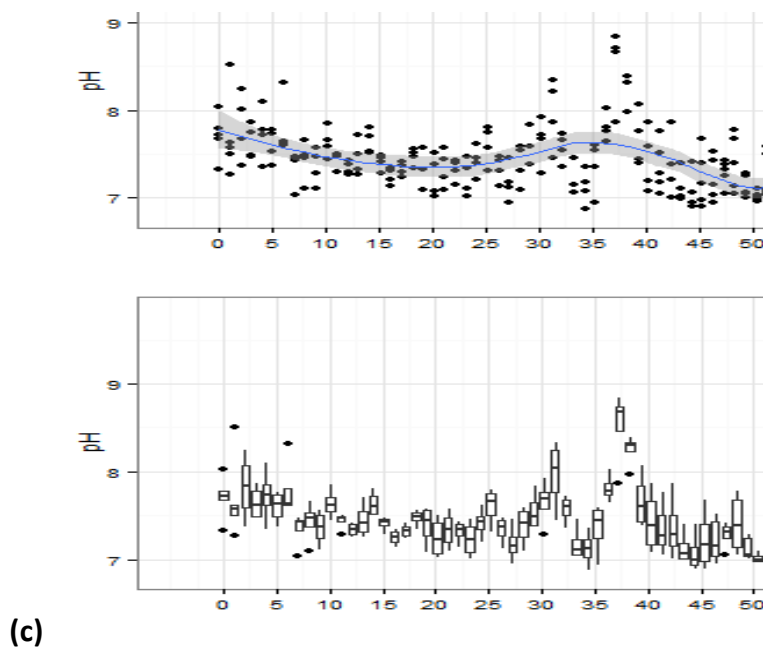
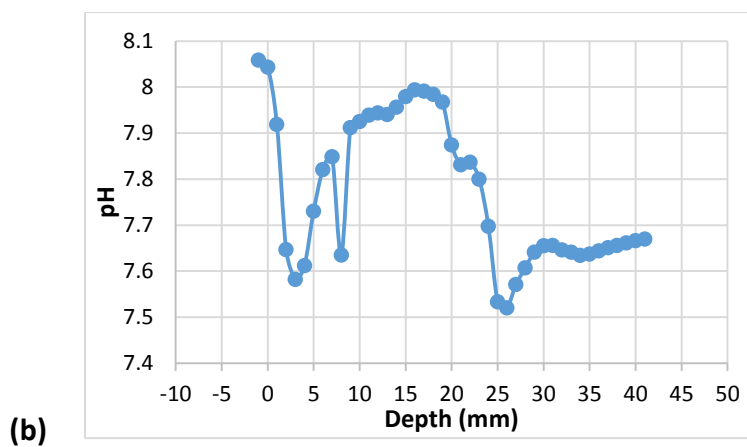
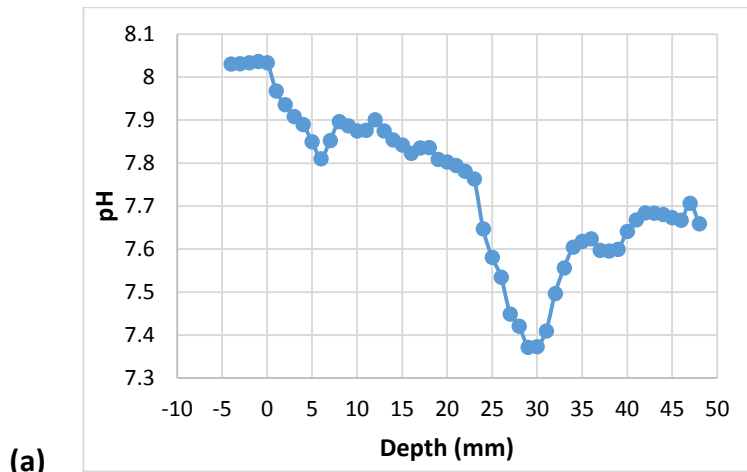


Figure 5.29: (a) and (b) pH profile measured by microelectrode at station 30(profile1). (Source: Alida Rosales Villa), (c) pH vs depth profile measured by probe.

The pH values measured by the probe are reasonably comparable with the microelectrode data. In the first 5 mm, the pH drops down to about 7.6 measured by probe while it drops down to 7.8 according to the microelectrode data. Then it increases up to 0.1 unit in microelectrode data but it keeps decreasing in the probe data and reaches to 7.5 and only starts increasing at 25 mm to 30 mm, it increases to 7.8 from 7.5 and then drops again to as low as 7 at 60 mm. At 30 mm in the microelectrode data there is a sharp decrease in pH and goes down to less than 7.4 and increases again slowly and gets to 7.7 at 48 mm. The second microelectrode profile from the same core is broadly similar but shows quite a lot of differences in detail. This indicates the likely heterogeneity of the sample, suggesting that direct comparisons for the purpose of probe data variation should only be made if the probe and microelectrode are used to measure close together in the same sub-core. It should also be noted that the microelectrode approach, while more established than our new optical approach is still very little used in such samples, so care should be taken when considering it as the definitive reference data against which our approach is “ground truthed”.

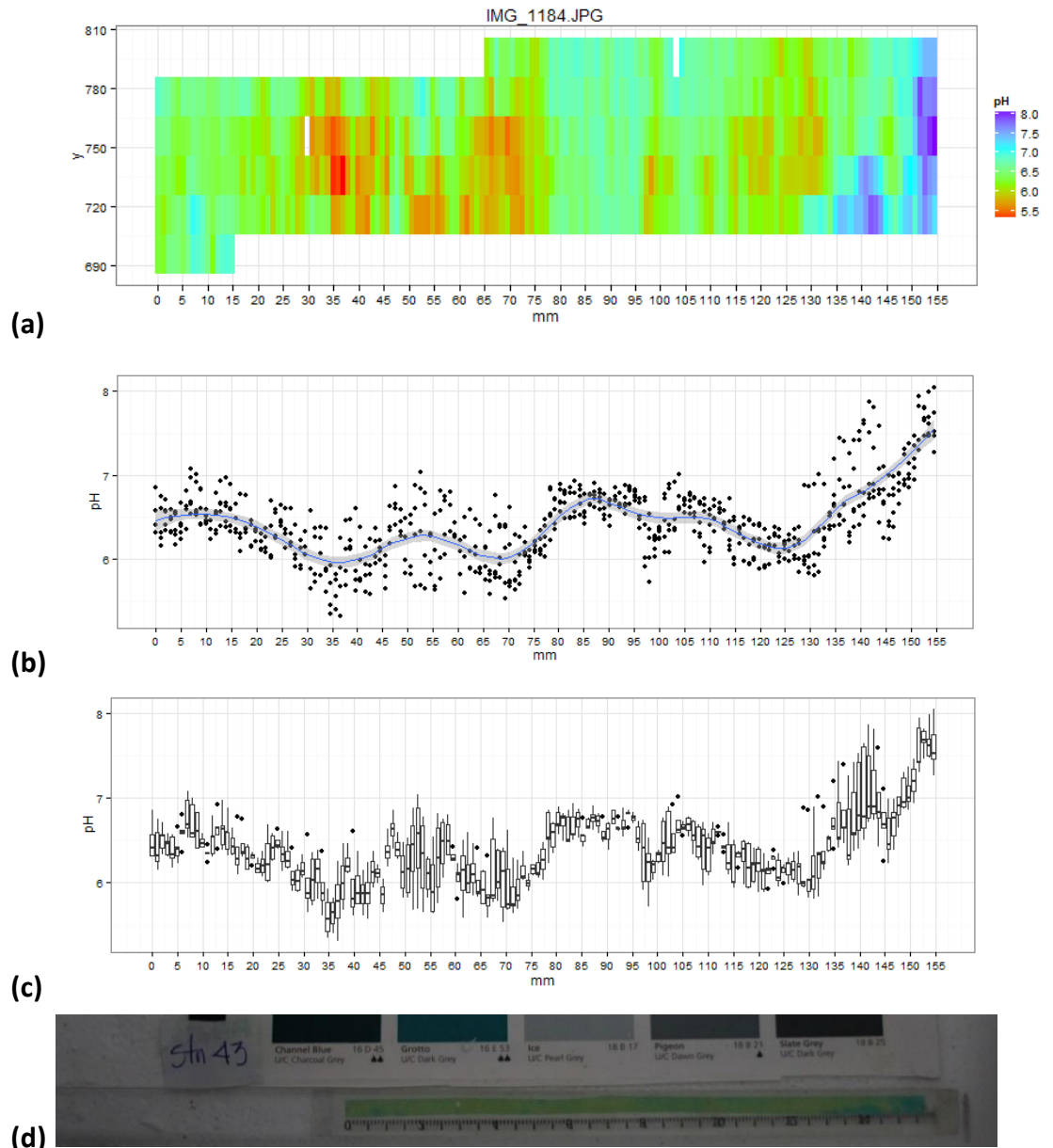


Figure 5.30: pH profile measured by probe at station 43. (a) a false colour pH map generated by the software for the sensor area (b) an average pH value across the strip (c) box plot- white box: interquartile range (iqr), horizontal line: median value, vertical line: range of the data, individual points: potential outliers, which are identified as >2.5 iqr from the median. (d) The actual probe.

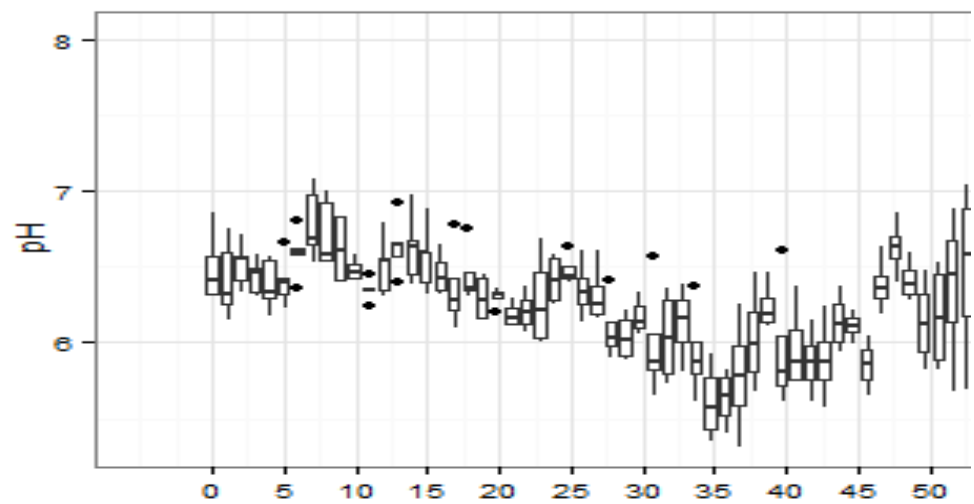
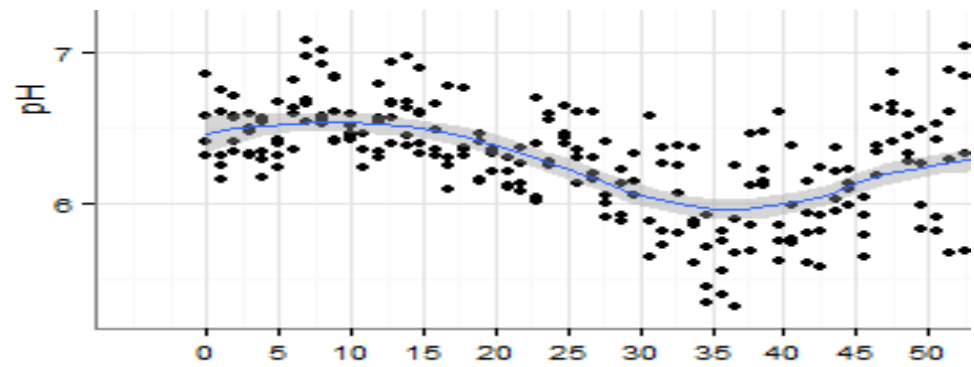
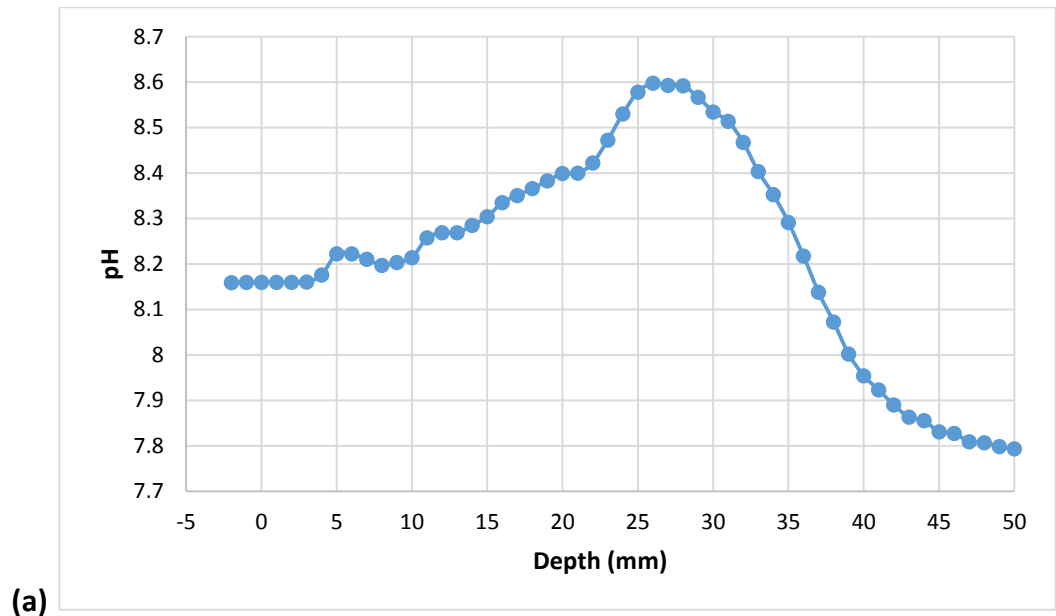


Figure 5.31: (a) pH profile measured by microelectrode at station 43. (Source: Alida Rosales Villa). (b) pH profile measured by probe at station 43.

The probe data and microelectrode data for station 43 is quite different. The microelectrode data shows an increase in pH from 8.15 to 8.6 at 25mm then keeps dropping down and reaches pH 7.8 at 50 mm. According to the probe data, the pH in the top sediment is about 6.5 and drops down to 5.8 at 35 mm, then increases again to about 6.2 and is more or less the same until 70 mm where it increases again to 6.9 at 60 mm. The probe measurement gives some additional pH data at greater depth and pH drops down to 6.3 again at 125 mm and then keeps increasing up to 155 mm. The following reasons may be responsible for the variability of the microelectrode data compared with the probe data.

- The core used for the microelectrode data was different from the core in which probes were used although both cores came from the same large NEOS core and from the same station. As discussed before there can be variability within a core so the data might be regarded as the real data in two different cores.
- It may be the microelectrode data that is at fault, as well as or instead of the probe e.g. it seems unlikely that a pH as high as 8.6 would be present in a sediment. Equally, a pH as low as 5.8 for a marine sediment (measured by probe) also seems unusual, though such values have been measured at Stiffkey (Chapter 6).
- The photographic conditions were rather crude and the position of the camera changed each time the probe was photographed in the polystyrene box. The lighting was not consistent either and an external flash was used to light up the dark box. This would be more likely to affect the absolute pH values rather than the trends and behaviour recorded but is certainly a source of variation and uncertainty.
- Calibration was not done in the seawater and at the temperature as it was at the sites, however the salinity for the calibration was very close to the salinity observed. Again, this is more likely to affect absolute pH values rather than trends.

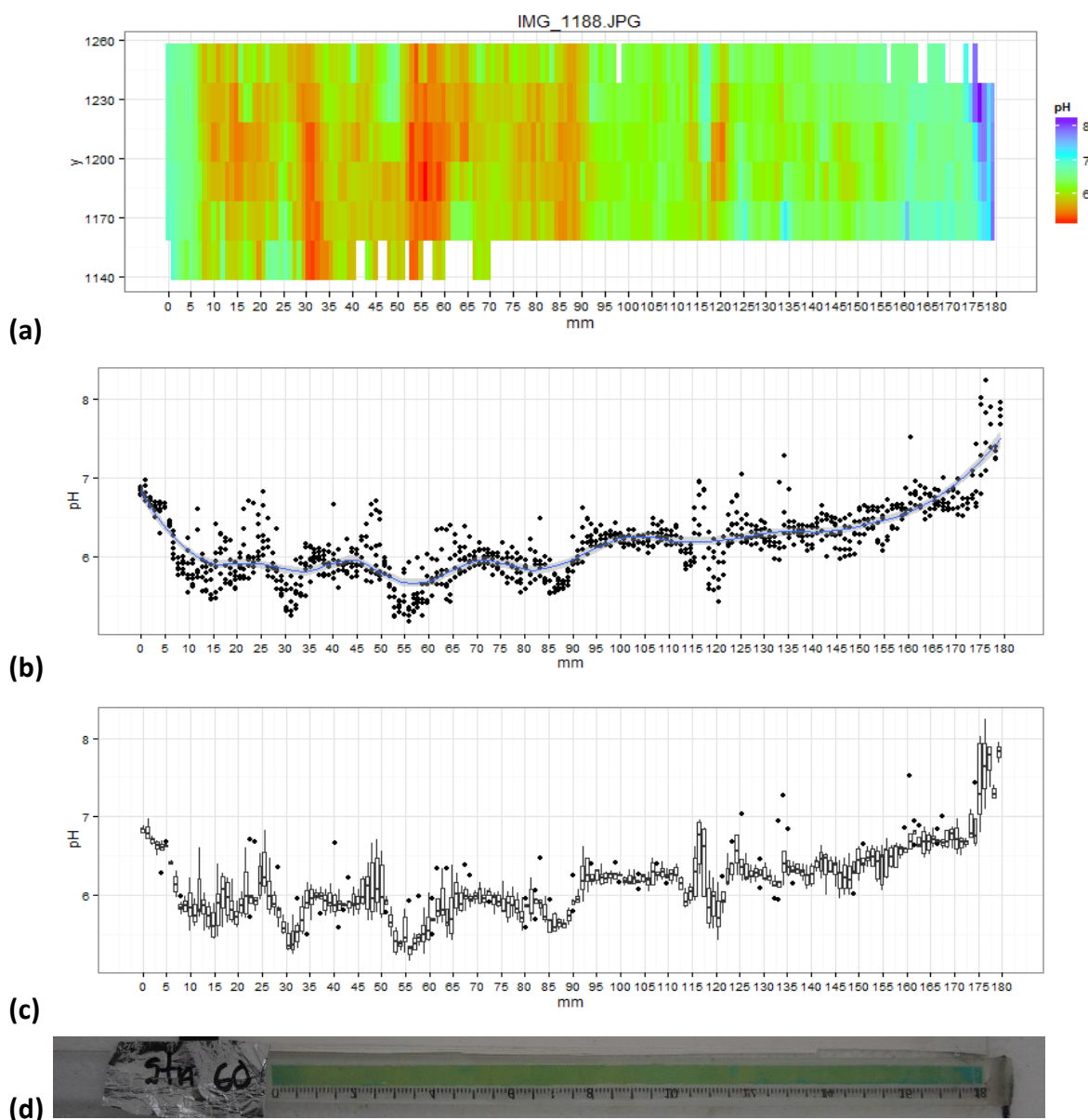


Figure 5.32: pH profile measured by probe at station 60. (a) a false colour pH map generated by the software for the sensor area (b) an average pH value across the strip (c) box plot- white box: interquartile range (iqr), horizontal line: median value, vertical line: range of the data, individual points: potential outliers, which are identified as >2.5 iqr from the median. (d) The actual probe.

At station 60, the pH drops down from 7 to 6 in the first few millimetres then there are a few drops in pH until 90mm which can be clearly spotted as yellow areas on the probe. This is possibly due to the re-oxidation of Fe and Mn along with oxic mineralisation. (Revsbech *et al.*, 1983, Archer *et al.*, 1989, Wenzhofer *et al.*, 2001, Stahl

et al., 2006). At 90 mm, however, the pH starts increasing again and rises to 7 which is likely due to Fe and Mn reduction. (Wenzhofer *et al.*, 2001 and Stahl *et al.*, 2006). At the very end it is quite basic and the pH is about 7.9. If the probe is seen closely, there were some yellow patches which may be because of the biological activity and the pH was low at these sites. These are not air bubbles as they tend to appear bright yellow and can be detected very easily. A piece of membrane containing the yellow patch and the piece of a dark membrane were selected in ImageJ and the RGB values were taken for comparison.

section of probe	Red	Green	Blue	(R-B)/G (colour index)
dark patch	72	93	56	0.172
yellow patch	79	99	53	0.26

Table 5.10: RGB values of dark and yellow patches on the sensing probe.

There is a clear difference in the colour index values and therefore many ups and downs can be seen in the pH profiles due to the yellow patches. In effect, the probe is providing a detailed 2D map of small scale variation across its small but significant (a 3 mm) width. Analysing this could be of considerable interest if it can be established that this is real variation rather than probe artefact, though it is not easy to design an appropriate experiment to test this.

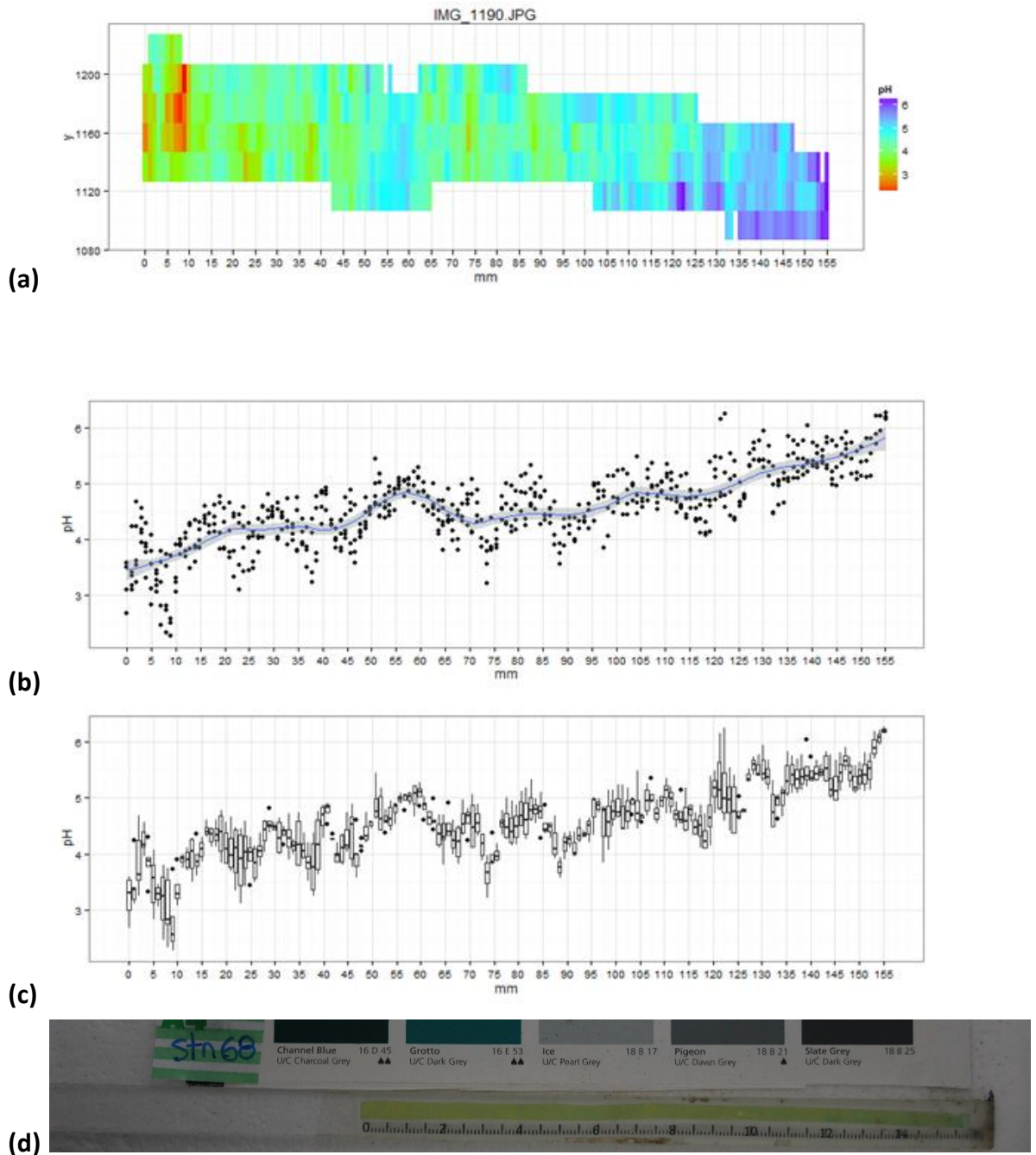


Figure 5.33: pH profile measured by probe at station 68. (a) a false colour pH map generated by the software for the sensor area (b) an average pH value across the strip (c) box plot- white box: interquartile range (iqr), horizontal line: median value, vertical line: range of the data, individual points: potential outliers, which are identified as >2.5 iqr from the median. (d) The actual probe.

At station 68, the pH is very low and about 4.5 in the top sediments and then keeps increasing and reaches close to 6 at 155mm. The membrane strip is not upside down, as a few green areas can be detected on the photo indicating water content or variation. pH was quite low at this station. There is no microelectrode data to compare

with at this station but the very low values seem unlikely, suggesting there was a problem with the probe.

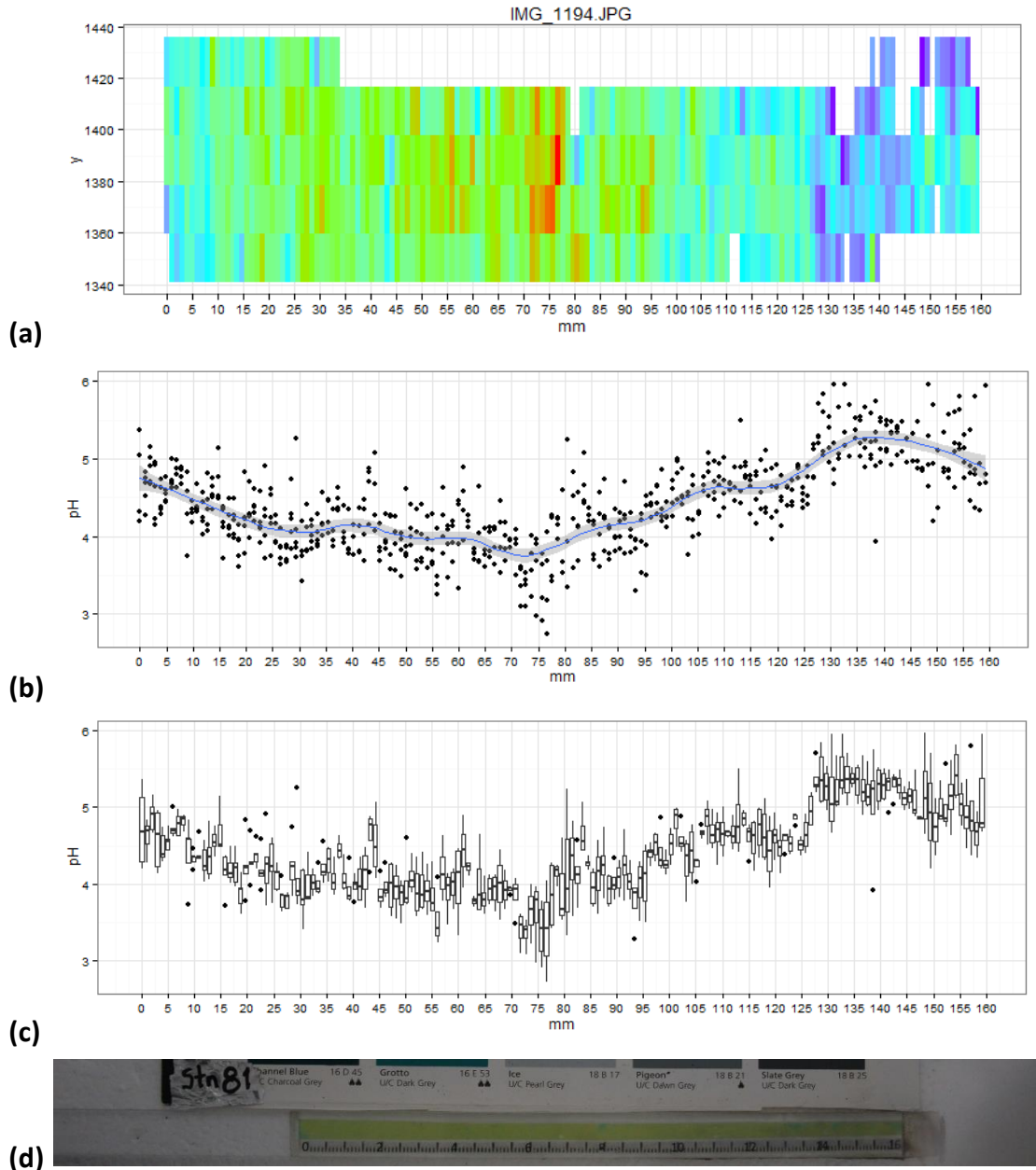


Figure 5.34: pH profile measured by probe at station 81. (a) a false colour pH map generated by the software for the sensor area (b) an average pH value across the strip (c) box plot- white box: interquartile range (iqr), horizontal line: median value, vertical line: range of the data, individual points: potential outliers, which are identified as >2.5 iqr from the median. (d) The actual probe.

At station 81, the pH is again very low and drops down from 5 to 4 in the top millimetres and stays 4 until 65 mm. After that, it starts increasing and reaches up to 5.2 in the depth at 145-150 mm. The sediments were muddy here and there were many burrows and the sediments had an anoxic zone. The faunal activity and burrow ventilation by polychaets enhances the hydrogen ion production which drops down the pH of the surroundings where the burrows are present (Hulth *et al.*, 2002), but even so, this seems a surprisingly low pH.

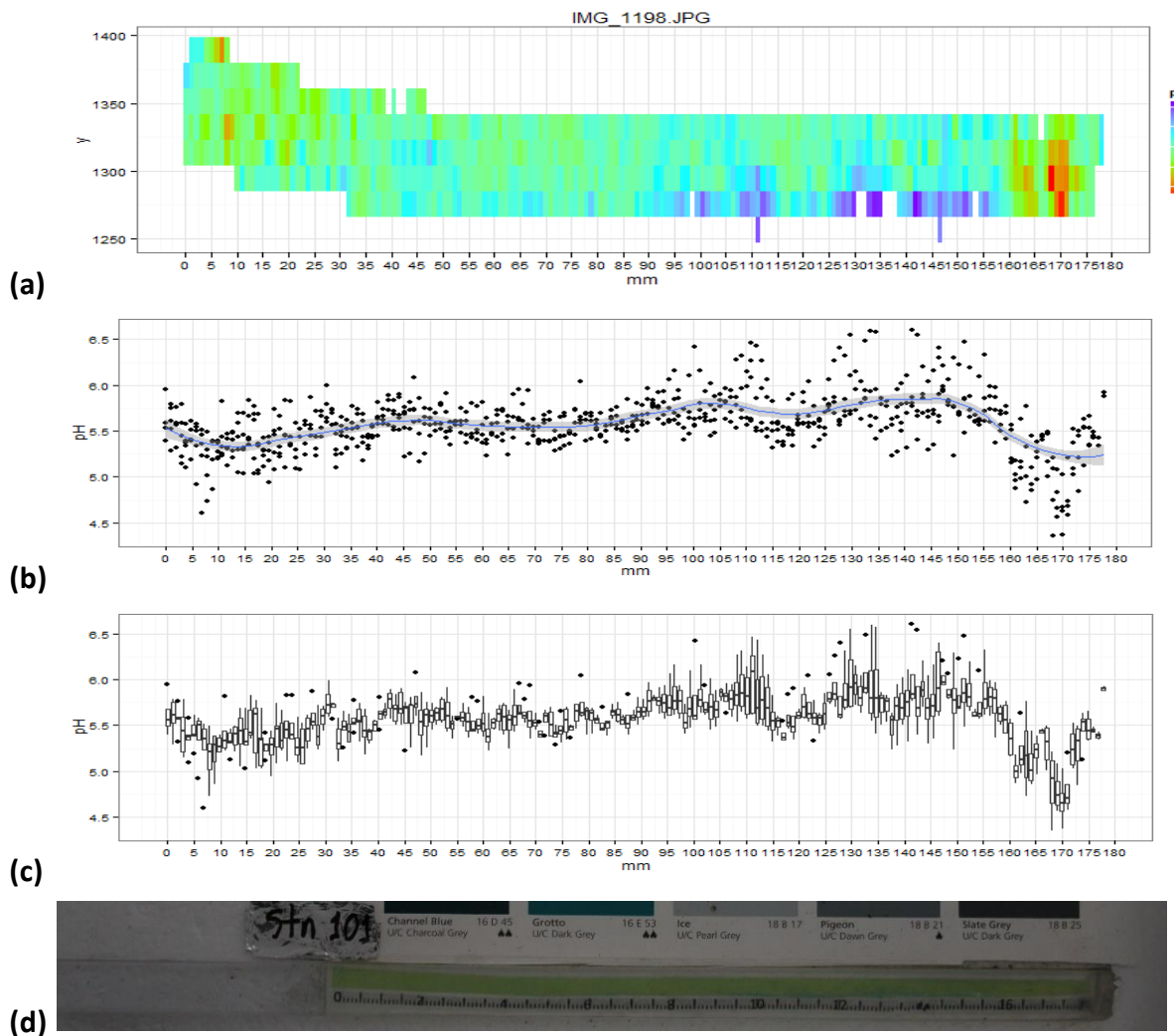
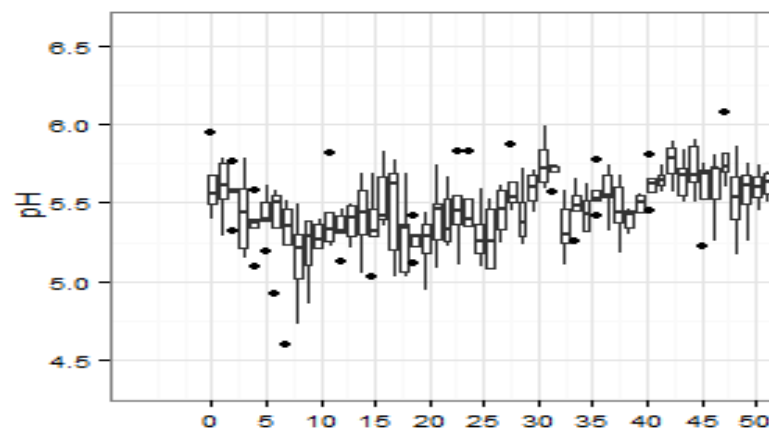
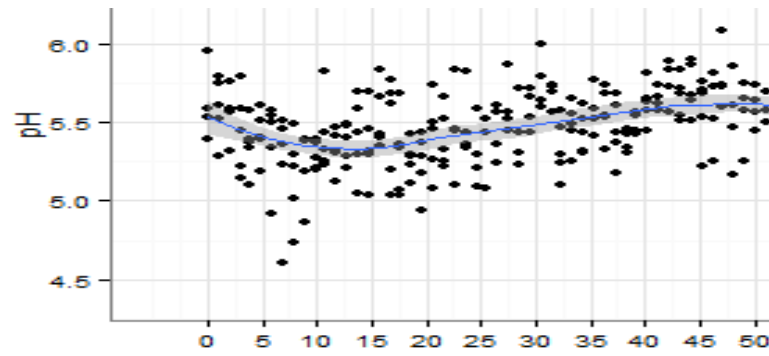
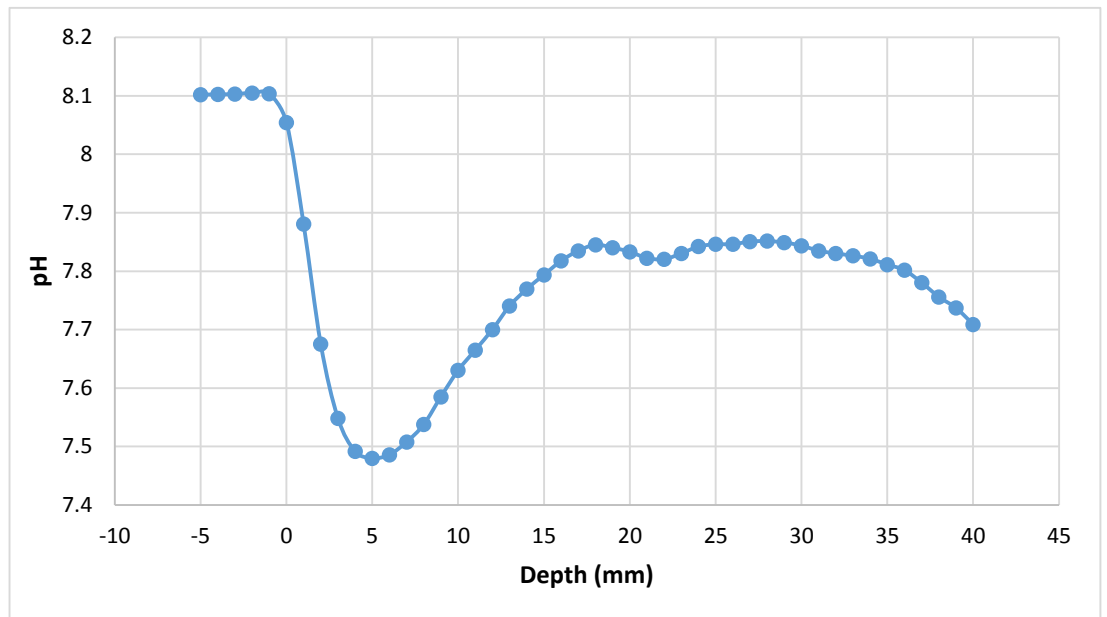


Figure 5.35: pH profile measured by probe at station 101. (a) a false colour pH map generated by the software for the sensor area (b) an average pH value across the strip (c) box plot- white box: interquartile range (iqr), horizontal line: median value, vertical line: range of the data, individual points: potential outliers, which are identified as >2.5 iqr from the median. (d) The actual probe.

(a)



(b)

Figure 5.36: pH profile measured at station 101 by microelectrode (source: Alida Rosales Villa). (b) pH profile measured at station 101 by probe.

At station 101, according to microelectrode data, the pH drops from 8.05 to 7.48 in first 5 mm depth in the sediments and then starts increasing and reaches to 7.8 at 18 mm. At 34 mm, it starts dropping again and is 7.7 at 40 mm but according to probe measurement, it is 5.5 and stays fairly constant from 40 mm. The difference may be because the photo is dark, producing erroneous colours or the measurements may be actual and the pH may be low here, although the microelectrode data indicated otherwise.

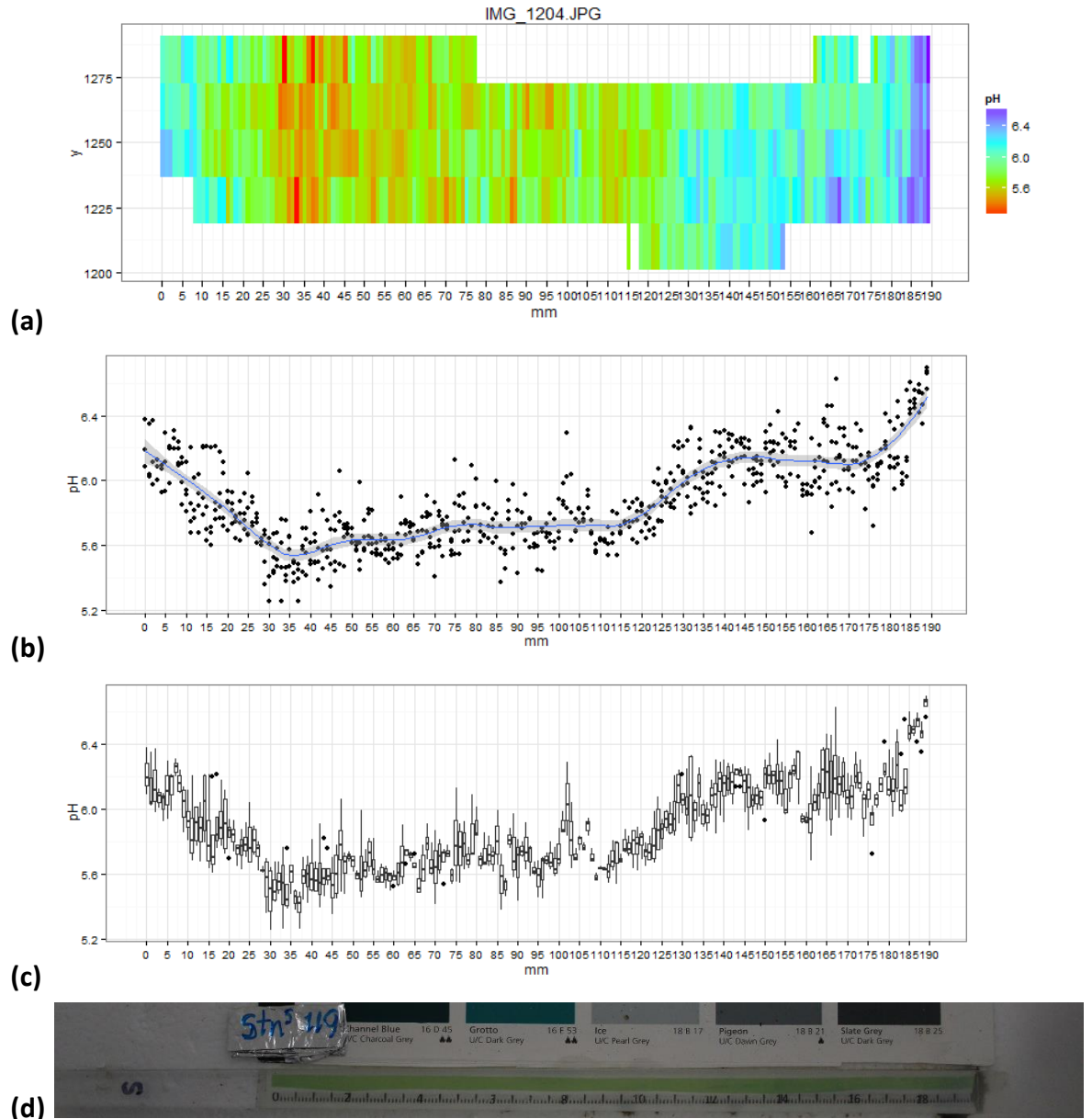


Figure 5.37: pH profile measured by probe at station 119. (a) a false colour pH map generated by the software for the sensor area (b) an average pH value across the strip (c) box plot- white box: interquartile range (iqr), horizontal line: median value, vertical line: range of the data, individual points: potential outliers, which are identified as >2.5 iqr from the median. (d) The actual probe.

At station 119, the pH drops from 6.3 to 5.5 at 30mm and remains more or less the same until starts increasing again at 120mm and reaches 6.3 at 140mm.

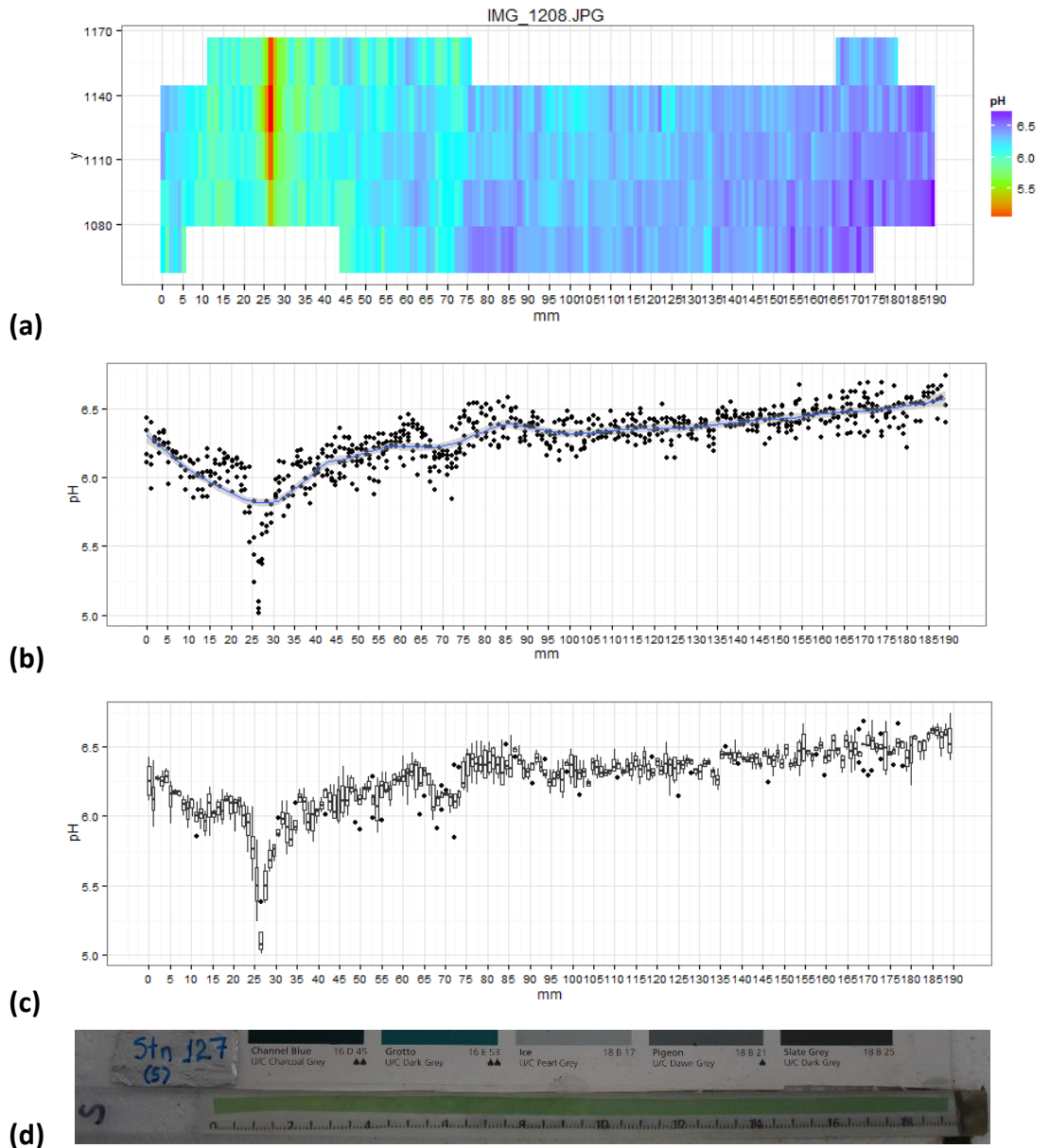


Figure 5.38: pH profile measured by probe at station 127. (a) a false colour pH map generated by the software for the sensor area (b) an average pH value across the strip (c) box plot- white box: interquartile range (iqr), horizontal line: median value, vertical line: range of the data, individual points: potential outliers, which are identified as >2.5 iqr from the median. (d) The actual probe.

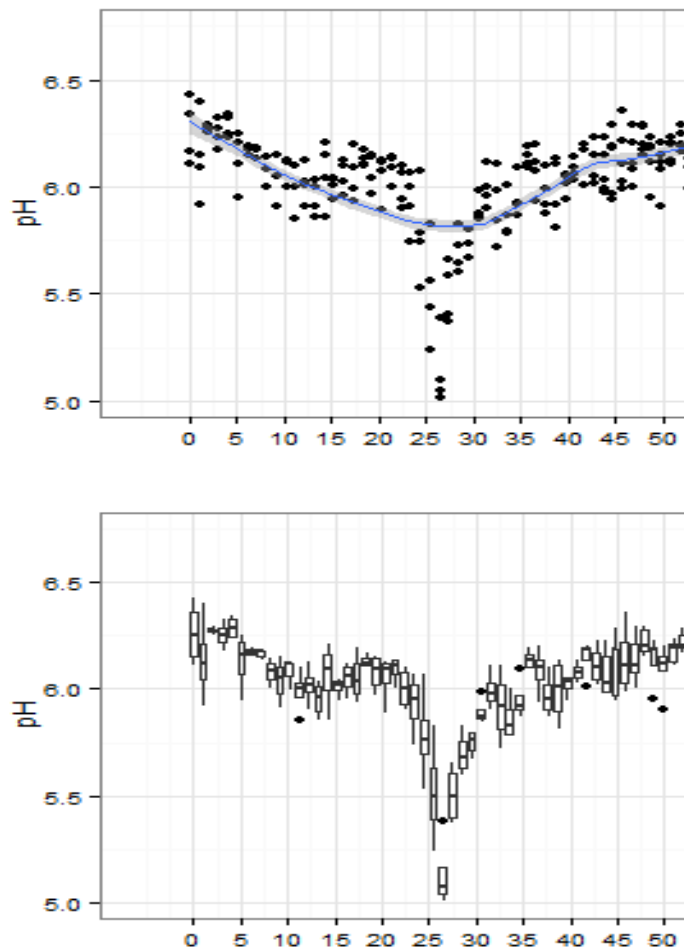
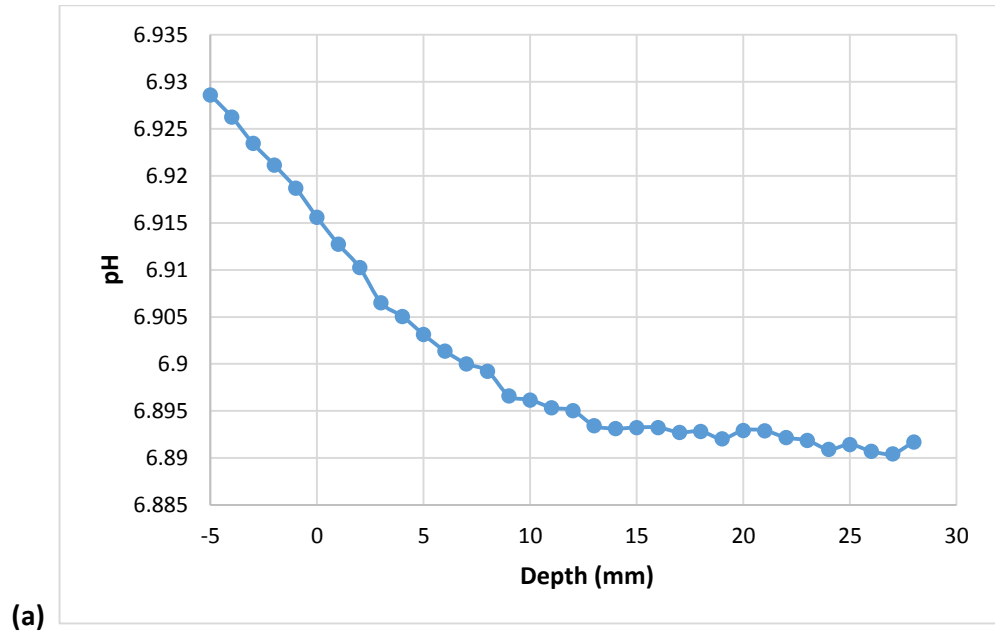


Figure 5.39: pH profile measured at station 127 by microelectrode (source: Alida Rosales Villa). (b) pH profile measured at station 127 by probe.

At station 127, according to microelectrode data, the pH changed little from 6.9 to 6.8 until 27 mm but according to probe measurements, pH changed little, then dropped sharply at about 27 mm-the exact point where the microelectrode profile ended. The values are close to the microelectrode data and at this station the pH was quite low according to both measurements. The probe gives some additional pH information at depth, where it starts increasing again and reaches 6.5. This part could not be measured by microelectrodes.

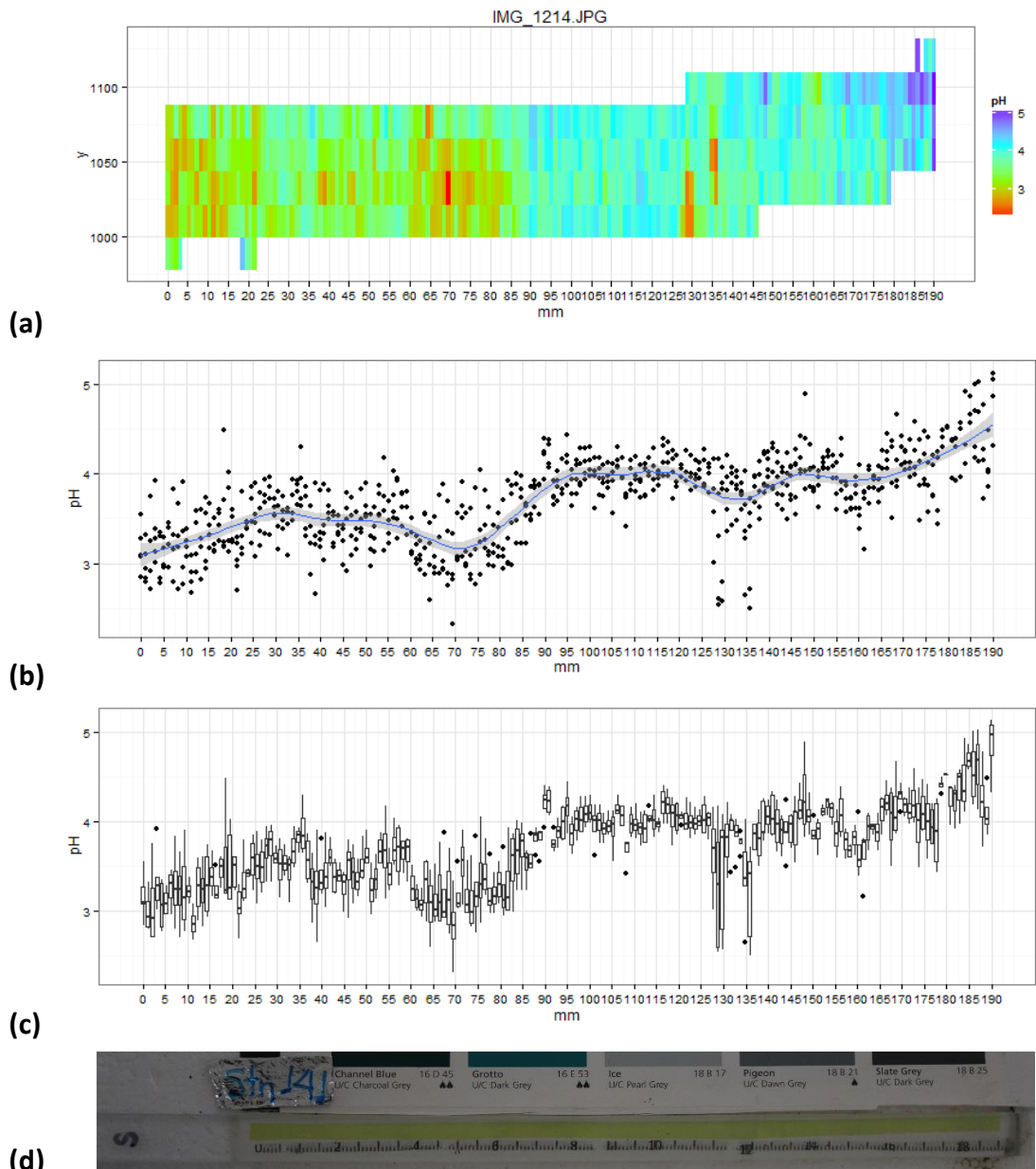


Figure 5.40: pH profile measured by probe at station 141. (a) a false colour pH map generated by the software for the sensor area (b) an average pH value across the strip (c) box plot- white box: interquartile range (iqr), horizontal line: median value, vertical line: range of the data, individual points: potential outliers, which are identified as >2.5 iqr from the median. (d) The actual probe.

The pH at station 141 is very low. It is possible that the sensing membrane was mistakenly put upside down while manufacturing the probe and therefore it stayed yellow. The pH is 3 at the top sediments and then gradually increases to 4 and above at the bottom which is unlikely if it changed at all. This may rather be variation due to colour inconsistency with the photographic setup used.

5.4 Conclusions

- An effective calibration method has been developed by bubbling CO₂ and N₂ into seawater to adjust the pH to desired values. The data can be fitted to produce an equation to calculate the pH from an unknown sea sample.
- Calibration at different temperature has shown slight variations. This can be controlled by calibrating at the temperature that is expected at the site of interest.
- Obtaining pH vs depth profiles from photos has been made simple and rapid by automation of the process using a routine in the statistical program 'R'.
- In general, the probes gave lower pH indications than the microelectrodes. This suggests that there may have been a calibration issue.
- Photographing conditions were inadequate at the first trial. This needed to be improved for the next application of sensors, in order to obtain more reliable results. The photographic conditions have been improved (discussed in chapter 4).

5.5 References

Archer, D., S. Emerson and C. Reimers, 1989 Dissolution of calcite in deep-sea sediments: pH and O₂, microelectrode results. *Geochimica Cosmochimica Acta* **53**, 2831-2845.

Hulth, S., Aller, R. C., Engstrom, P. & Selander, E. 2002, A pH plate fluorosensor (optode) for early diagenetic studies of marine sediments. *Limnology and Oceanography* **47**, 212-220.

Revsbech, N. P. & Ward, D. M. 1983 Oxygen microelectrode that is insensitive to medium chemical composition: use in an acidic microbial mat dominated by *Cyanidium caldarium*. *Applied and Environmental Biology* **45**, 755-759.

Stahl, H., Glud, A., Schroder, C. R., Kliment, I., Tengberg, A. & Glud, R. N. 2006 Time resolved pH imaging in marine sediments using luminescent planar optode. *Limnology and Oceanography: Methods* **4**, 336–345.

Wenzhöfer, F., Adler, M., Kohls, O., Hensen, C., Strotmann, B., Boehme, S., & Schulz H. D. 2001 Calcite dissolution driven by benthic mineralization in the deep sea: In situ measurements of Ca²⁺, pH, pCO₂, O₂. *Geochimica Cosmochimica Acta* **65**, 2677–2690.

Williams, W.,D. & Sherwood, J. E. 1994 Definition and measurement of salinity in salt lakes. *International journal of salt lake research* **3**, 53-63.

Chapter 6

Seasonal pH profiles from Stiffkey salt marsh

6.1 Introduction

Intertidal areas of fine sediment transported by water and stabilised by vegetation are called saltmarshes (Boorman, 1995). The vegetation present here can survive in the salt water for long periods. Salt marshes have the following zones, out of which one or more may be absent at a given site. The zoning is done considering the tide and vegetation. The 'pioneer zone' is covered by all the tides except the lowest ones and has open communities (spread randomly) of one or more of *Spartina spp*, *Salicornia spp* and *Aster tripolium*. The 'low marsh' zone is covered by most of the tides and has closed communities (having boundaries) of at least *Puccinellia maritime* and *Atriplex portulacoides* and also the pioneer zone species. The 'Middle marsh' zone is only covered by the spring tides and contains the closed communities of one or more of *Limonium spp.* and/or *Plantago* and also the species from the previous two zones. The 'High marsh' zone is only covered by the highest spring tides and contains closed communities of *Festuca rubra*, *Armeria maritime*, *Elytrigia spp.* and also the species from previous zones. The 'Transition zone' is covered occasionally by tides in the event of strong storms (Boorman, 2003). Understanding salt marsh biogeochemistry is important as they are major stores of organic carbon, the cycling of which can contribute to the global carbon cycle and climate change. Our reason for studying it was much more pragmatic, however. It represented an interesting and accessible habitat where (hyper) saline sediments could be reached on foot, allowing us to test pH probes under real field conditions without the complications of going to sea.

6.1.1 Study Site

For the seasonal pH profiles, Stiffkey saltmarshes at the Norfolk Coast were selected as a study site. This is easily accessible and is about an hour and a half drive from Norwich. The map below shows the location of the site. The two study sites (pond and creek) are both present at the “lower marsh” zone.



Figure 6.1: (a) Map showing the location of the site. (b) Photos of the study sites: creek and pond.

There are many different types of plants present at Stiffkey of which the major species are *Antriplex portulacoides*, *Limonium vulgare*, *Spartina anglica*, *Puccinellia maritime* and *Elytrigia aetherica*. The study site is in the low marsh zone which is dominated by the vegetation recognised as *Antriplex portulacoides* and *Limonium vulgare* close to the pond where the pH profiles in the vegetation were recorded. Figure 6.2 shows images of the vegetation taken in summer.

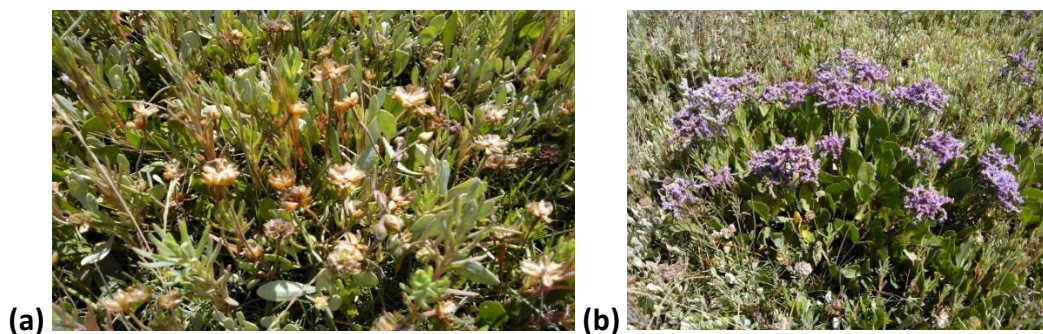


Figure 6.2: Vegetation at the study site mainly found close to the pond. (a) *Antriplex portulacoides*, (b) *Limonium vulgare*

6.2 Material and Methods

The seasonal pH profiles of the mud were measured from the Stiffkey salt marshes by taking measurements in summer, autumn, winter and spring. The final composition of the sensing membrane that gives bright colours and does not slow down the response was used throughout all the seasonal pH data collection. The composition was: BTB (50 mg), TOAB (176 mg), PVC (74 mg), Plasticizer (250 mg), THF (1.5 mL). The yellow (6 μm) metering bar was used to spread 250 μL of the solution on the transparency sheet and probes were made as discussed before. Summer data was collected in mid-July 2014 (14-4-2014). Three experiments were carried out.

- Five probes were inserted in the pond and one probe was taken out and photographed at 5 minutes, second at 10 minutes, third at 15 minutes, fourth at 30 minutes and fifth at 60 minutes to check the response time in the mud. One of the probes was inserted back and re-equilibrated three times to check the reproducibility.
- The pH profiles were measured in the mud starting from the edge of the pond in the vegetation, edge of the pond and under the water in the pond using the probes.
- The pH profiles were measured at the creek in a row down the side of the creek from the top level to the permanent stream at the bottom.

In summer, the pH as a rough guide, was measured using a portable pH meter (Hanna instruments HI9025 with polymer body electrode) and the conductivity was measured using a conductivity meter (Fisher Scientific Acumet AP75 with conductivity probe).

The temperature was measured using a temperature probe (Fisher Scientific Platinum sensor (Pt-100 Ω)). The calibration was done in seawater taken from Lowestoft at 20 °C because the lowest and the highest temperature observed at Stiffkey was 18.3 °C and 22.3°C respectively. Calibration was completed using a pH meter (Fisher scientific AB15), conductivity meter (Jenway 4320) and temperature probe (Fisher Scientific Platinum sensor (Pt-100 Ω)).

Autumn data was collected in mid-September (18-9-2014). The probes were prepared in a similar way but the black lines were printed on the transparency sheet and then the solution was spread on it. These lines help with cutting the membrane straight and can easily be recognised by the software as the edges during data analysis. The following experiments were carried out.

- The pH profiles at the creek.
- The pH profiles in the pond starting from the vegetation close to the pond. Two probes were used in the vegetation away from the pond.

The temperature, pH and conductivity were measured. The calibration was done separately for the two sites due to a large difference in the conductivity. Water samples from each sites were taken back to the lab for calibration using the procedure discussed in chapter 5.

Winter data was taken on 9th December 2014. A pH meter (Hanna instruments HI 9025) and a conductivity meter (Fisher Scientific Acumet AP75) was used during the field work. Long probes were tried along with the usual ones. The pH profiles were taken only in the vegetation and the pond. Six normal probes were used at three posts in the vegetation and two big probes were used in the vegetation. Eight probes were used in the pond and in the edge of the pond in the vegetation. The calibration was done in the water sample taken from the pond.

6.3 Results and discussions

6.3.1 Calibration for the summer pH profiles

The conductivity of seawater which was used for calibration of the probes used at both sites was 48 mS cm^{-1} . The same camera and zoom settings were used for calibration as at Stiffkey. Calibration was done at $20 \text{ }^\circ\text{C}$ after collecting data from the field and measuring the temperature during the field work. The temperature at Stiffkey was $22.3 \text{ }^\circ\text{C}$ in the pond water, $21.6 \text{ }^\circ\text{C}$ on the surface of the sediments and $18.3 \text{ }^\circ\text{C}$ in the sediments. The conductivity of water was 50 mS cm^{-1} and average pH was 8.0. The pH of sediments in the pond was 7.16 and in the vegetation, it was 7.39. The conductivity at the creek was 50.9 mS cm^{-1} which was more than the seawater conductivity which was used for calibration due to the fact that the saltmarshes have more salt concentration than seawater due to evaporation.

The following calibration graph was obtained.

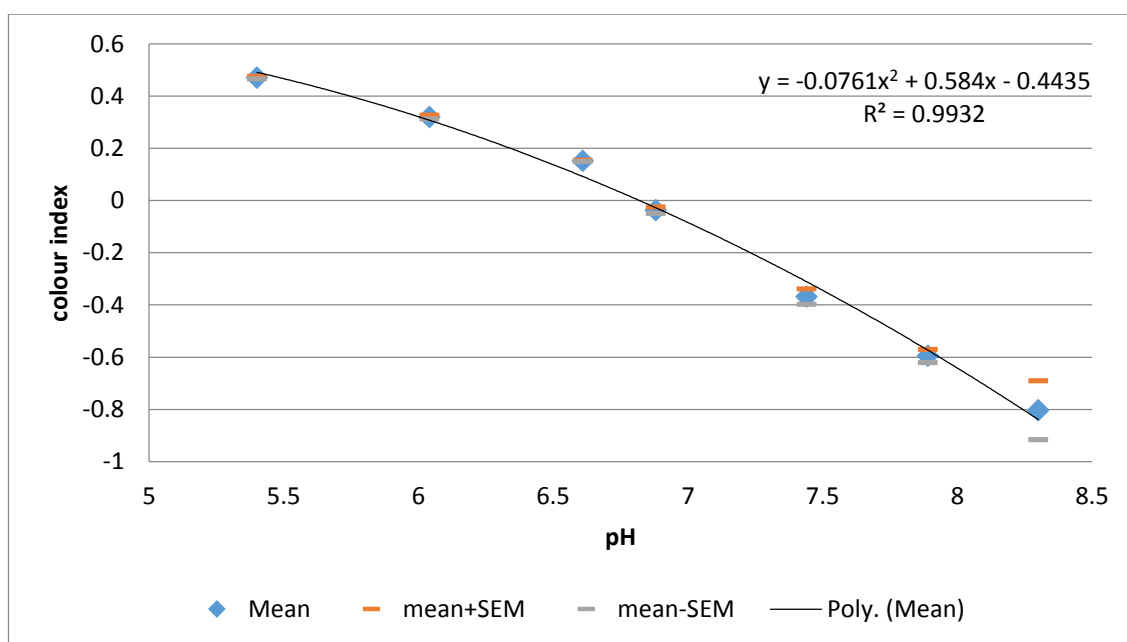


Figure 6.3: Calibration graph for the probes used to collect the summer data (n=3).

The inverse of the equation from the graph above was used in the R script to calculate the pH.

6.3.2 Calibration for the autumn pH profiles

The calibration for the probes made from sheet A and C was done in the water sample taken from the pond using two probes coming from sheet A and B as the probes made from these sheets were used there. The calibration for the probes made from sheet B was done in the water sample taken from the creek as these probes were used there. The calibration was done at 18 °C for the pond and at 21 °C for the creek. The conductivity of the pond water measured in the lab was 53.8 mS cm⁻¹ and that of creek water was 36.8 mS cm⁻¹ and the pH of the water sample was 8.33 at the creek and 8.11 in the pond water. The following calibration curves were used for the two sites.

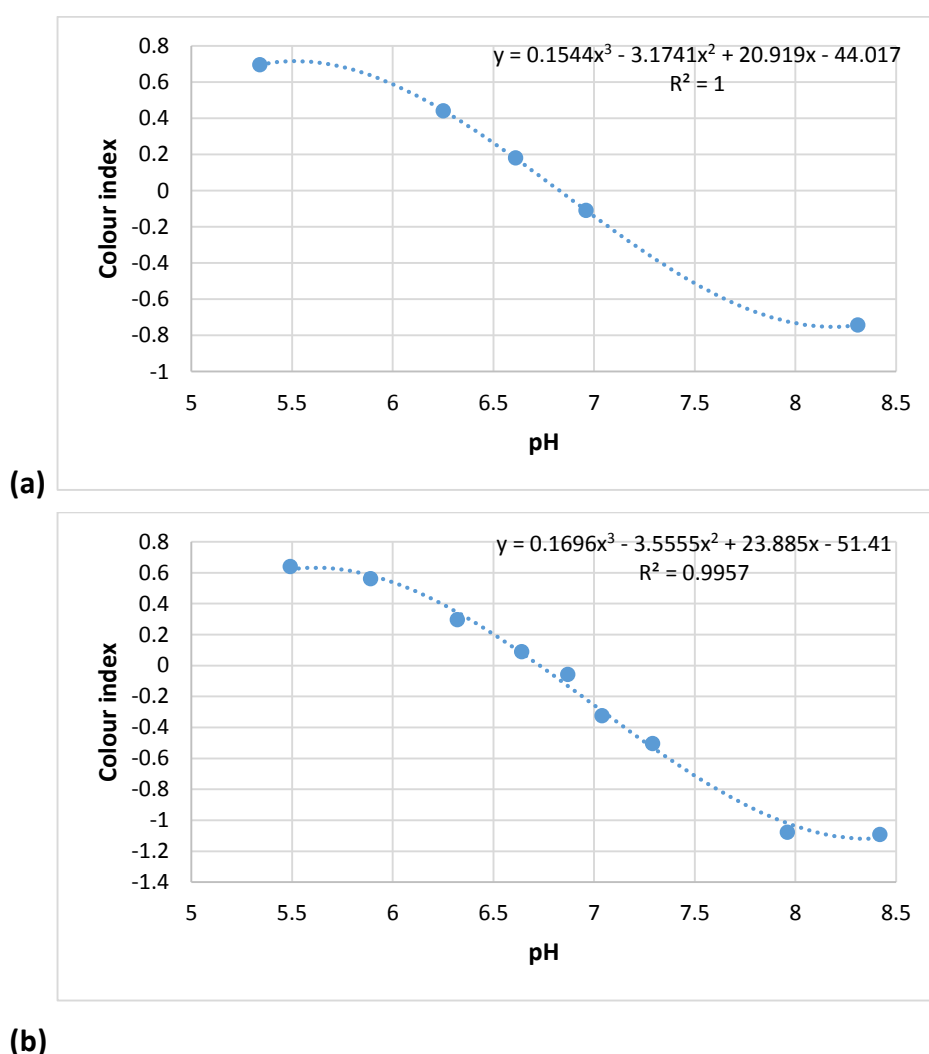


Figure 6.4: (a) Calibration graph for the probes used in the pond (b) Calibration graph for the probes used at the creek.

6.3.3 Calibration for the winter pH profiles

The air temperature was 1.3 °C and the pond temperature was 1.4 °C. The mud temperature in the pond was 5.2 °C and the temperature at the vegetation in the mud was 4.8 °C. The pH of the water was 7.98. The conductivity was 58.5mS cm⁻¹ in the pond. Calibration was done at 5 °C. The conductivity measured in the water sample taken from the pond in the lab at 5.6 °C was 51 mS cm⁻¹ and the pH was 8.19. The calibration graph is given in figure 6.5.

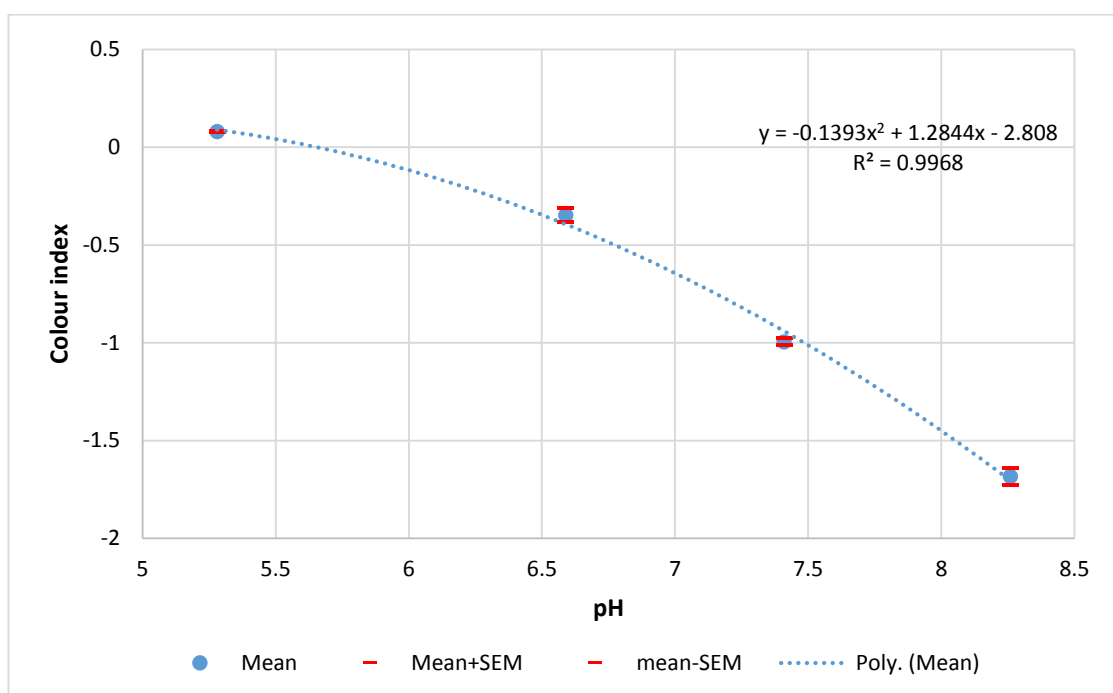


Figure 6.5: Calibration graph for the probes used in the pond and vegetation (n=3).

The response time and the reproducibility of the probe was checked during the summer visit to stiffkey. The results obtained are presented below.

6.3.4 Response Time of probe in the mud

Figure 6.6 shows the pH profiles plotted at 5, 10, 15, 30 and 60 minutes time intervals to check the response time in the mud. The sediment water interface is at 0 mm and negative values represent the pH in the water above the pond mud.

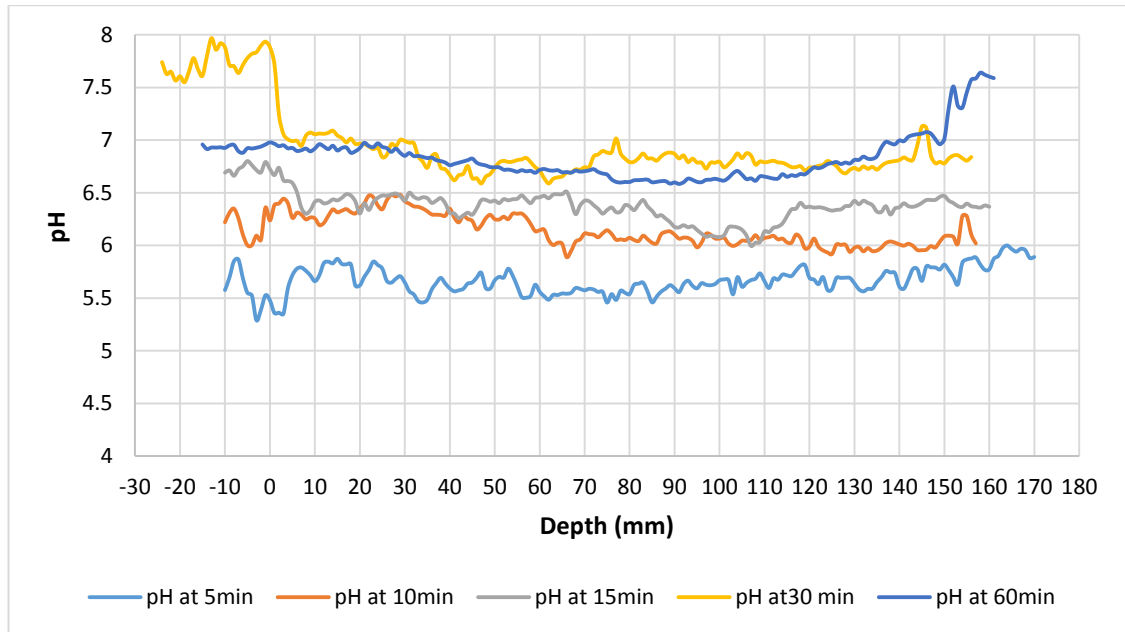


Figure 6.6: Apparent pH plotted after different equilibration time intervals where 0 mm is the interface.



Figure 6.7: Actual probes taken at (a) 5min, (b) 10min, (c) 15min, (d) 30min, and (e) 60min.

In figure 6.6 pH profile of the probe taken out and photographed after 5 minutes, 10 minutes, 15 minutes, 30 minutes and 60 minutes can be seen. At 5 minutes, the interface in figure 6.7a was still not very clear. The probe seemed to be still equilibrating as the pH of the water measured in the pond by the pH glass electrode was 7.85-8.06 measured at different locations within the pond. The probe colour corresponded with a pH of about 6 in the water at 5 minutes. In figure 6.7b the probe taken out after 10 minutes is shown. As seen in figure 6.6, the probe colour corresponded to pH 6.4 in the water but the sensor might still be equilibrating. In figure 6.7c the probe taken out and photographed after 15 minutes is shown. As seen

in figure 6.6, the colour corresponded to the pH of 6.8 in water. It was still equilibrating as a clear interface still couldn't be judged by eye in the probe photo and a rough pH guide from the pH meter has shown the pH of water close to 8 so a pH profile at 30 minutes may reflect an equilibrated probe.

In figure 6.7d pH probe taken out and photographed after 30 minutes is shown. Interface was at 3.5cm in the probe photograph which can clearly be judged optically. As seen in figure 6.6, the maximum pH in the water was close to 7.8 and 7.0 in first 20 mm and drops down further to 6.5 in the depth of 45mm. The probe looked equilibrated at this point except a few yellow patches which could be due to the contact problem. In figure 6.7e pH probe taken out and photographed after 60 minutes is shown. The interface was at 1.5cm in the probe photograph. The pH was about 7.0 and the same in the top mm of the sediments however dropped to 6.7 at 65 mm. The pH seen in the sediment at 60 minutes was more or less the same as compared with the profile taken at 30 minutes except that the pH of water measured by the probe taken out at 60 minutes was less. This could be a probe to probe variability or because of the probe inhomogeneity seen in the probe photograph in figure 6.7e. In the figure 6.6, less inhomogeneity is seen in the profiles from 20 mm to 140 mm so the profiles at each time were averaged for this depth and pH was plotted against time to see the equilibration time.

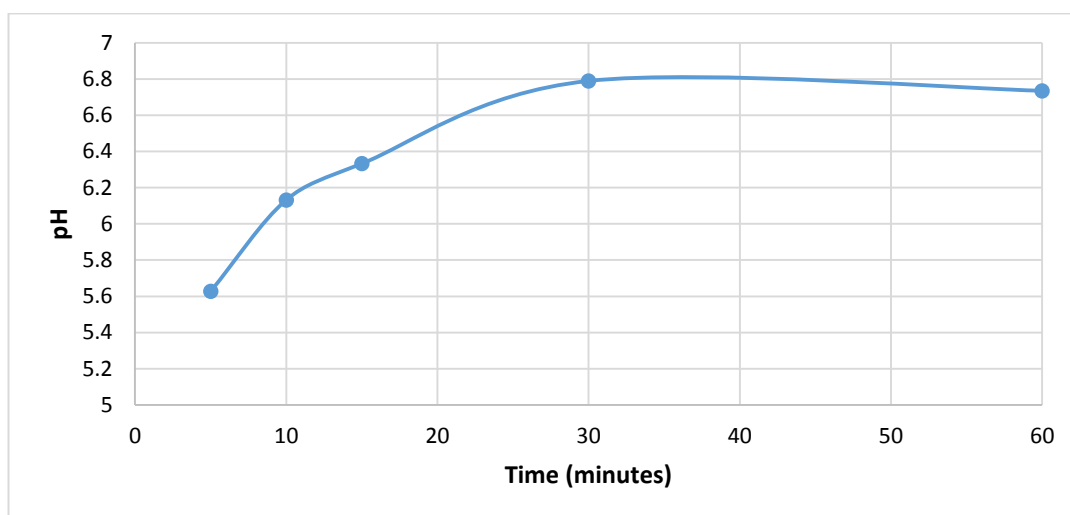


Figure 6.8: Response time curve plotted by averaging the pH values from 40mm to 150mm in the profile given in figure 6.6 for the given time.

Thus it was concluded that the probes equilibrate in about 30 minutes. This response time may be faster in harder sediments. The mud where the probes were used was very soft. If the sediments are hard, the contact between sediments and probe becomes better and probes respond faster. A multiple use of the same probe or conditioning the probe before it is used can also speed up the response.

6.3.5 Reproducibility of the probe

The probe was used three times in the mud and left to equilibrate for fifteen minutes each time. The same probe was again inserted more or less at the same position in the pond for 15 minutes. The results in the figure 6.8 show the profiles from the pond.

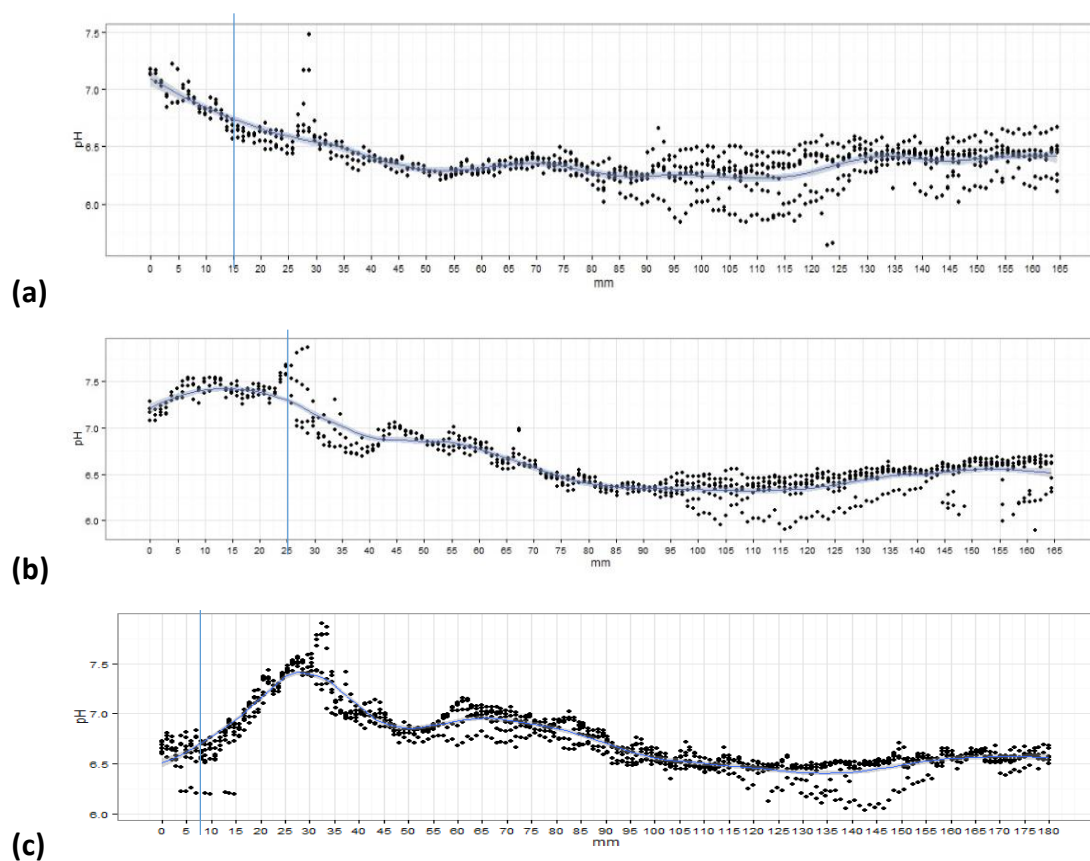


Figure 6.9: pH profiles from the same site using the same probe multiple times illustrating that the probe is reusable. The interface is marked as a blue line on each profile (a) Profile at first use, (b) profile at second use, (c) profile at third use.

The interface in figure 6.8a was at 15 mm, in figure 6.8b, it was at 25 mm and in figure 6.8c it was at 7 mm. According to figure 6.8b and 8c, the pH of water was 7.4, which

was different from that measured by electrode which was 7.8-8 but the reading was not reliable as the electrode was fluctuating a lot. It dropped to 7 in the sediments and further dropped to 6.5 in the depth. The trend is the same in figure 6.8a but the pH values were slightly lower and the pH of water was 7.2 and in the sediments it dropped to 6.5 and in the depth to 6.3. The bottom profiles are quite similar but there are tiny differences on the top of the mud profile. The main purpose was to check if the probe can be used multiple times and it seems it can be used multiple times, at least during one hour, but it is better to use a new probe each time to be on the safe side as while doing the storing preference it was observed that if kept in aqueous conditions for hours and days, the dye bleaches. The probe has been reused and there have been no technical issues like damage etc. and there was no bleaching obviously evident from the results. The slight difference in the position of the probe each time has probably changed the profile slightly that is why the profile in figure 6.8a is slightly different from the profile in figure 6.8b and 6.8c. Rising pH can be observed in the first 15mm in figure 6.8c and a dropping of pH can be seen in 6.8a and 6.8b. In figure 6.8a the values are dropping for about 30mm and in b for about 50mm. However the overall trend is the same.

6.3.6 Seasonal pH profiles

Seasonal pH profiles were measured at Stiffkey salt marsh at the pond, vegetation near the pond and at the creek. Table 6.1 summarises some of the parameters measured during the study.

Season/post	pH		Temperature		Conductivity
	Water	Surface	Water	Surface	
Summer/Pon	8.00	7.16	22.30	21.60 °C	50.4 mS cm ⁻¹
Vegetation	-	7.39	-	20.50 °C	-
Creek post 1	-	-	-	19.20 °C	-
Creek post 2	-	-	-	19.50 °C	-
Creek post 3	-	-	-	19.10 °C	-
Creek post 4	-	-	-	18.30 °C	-
Creek post 5	-	-	-	18.40 °C	-
Creek post 6	-	-	-	18.40 °C	-
Creek post 7	-	-	-	18.40 °C	50.9 mS cm ⁻¹
Autumn/pond	8.11	-	22.50	18.50 °C	52 mS cm ⁻¹
Vegetation	-	-	-	17.30 °C	-
Creek post 1	-	-	-	20.50 °C	-
Creek post 2	-	-	-	17.11 °C	-
Creek post 3	-	-	-	17.15 °C	-
Creek post 4	-	-	-	17.19 °C	-
Creek post 5	-	-	-	17.29 °C	-
Creek post 6	-	-	-	17.39 °C	-
Creek post 7	-	-	20.85	17.33 °C	35.5 mS cm ⁻¹
Winter/pond	7.90	-	1.40 °C	5.20 °C	58.5 mS cm ⁻¹
Vegetation	-	-	1.40 °C	4.80 °C	-

Table 6.1: pH, temperature and conductivity measured at pond, creek and vegetation in Stiffkey salt marsh.

6.3.7 Seasonal pH profiles from the vegetation

Three probes were inserted in the vegetation in a row as shown in figure 6.9.



Figure 6.10: Probes and pH meter in the vegetation near the pond.

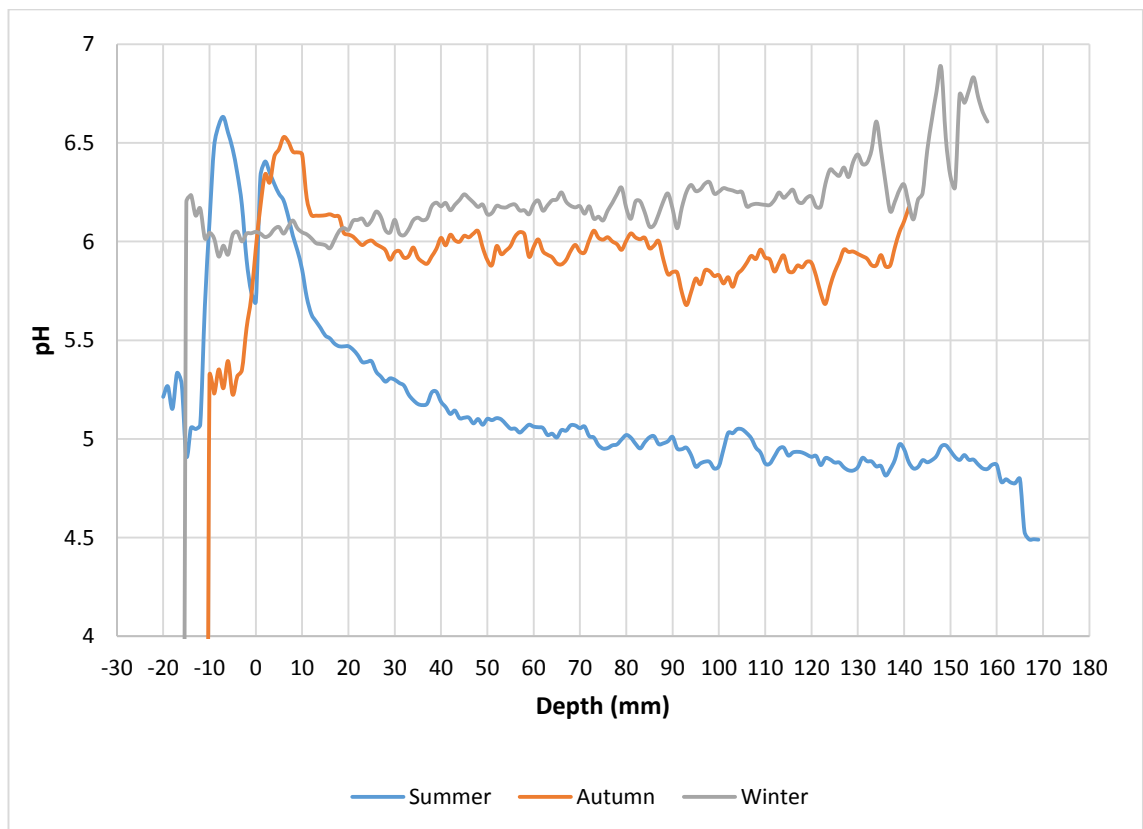


Figure 6.11: Mean seasonal pH profiles in the vegetation near the pond at Stiffkey salt marshes (n=3, 4 and 6 for summer, autumn and winter).

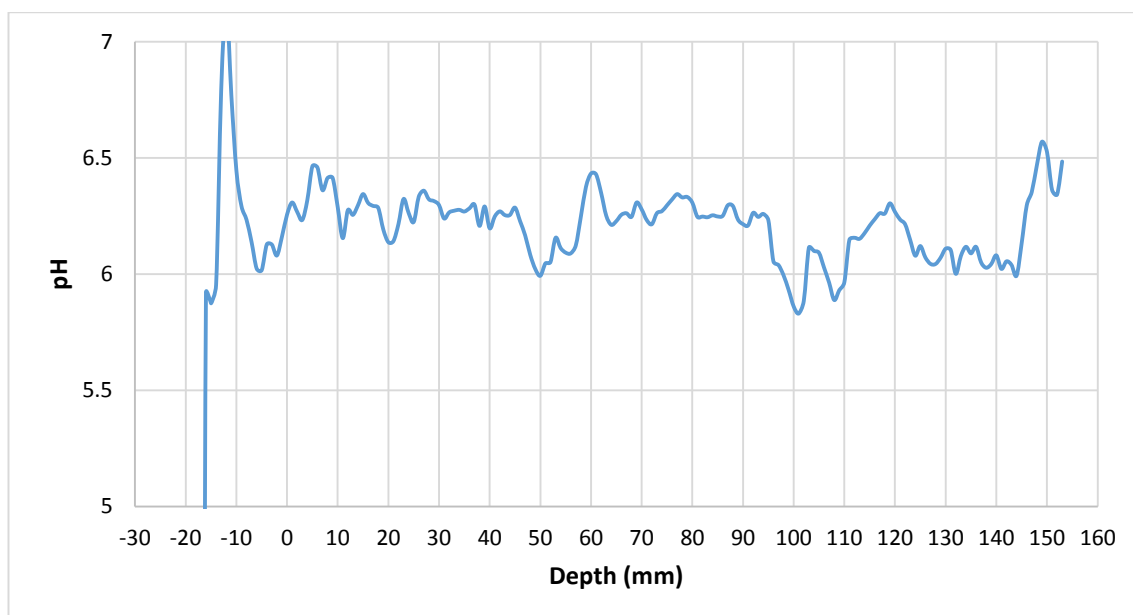


Figure 6.12: Mean pH in vegetation in autumn at 1m distance from the pond.

The profiles above the interface are variable because the probe was not in contact with sediments and the amount of water present here was not enough for the probes to be soaked in. The profiles above the surface therefore are not the real measurements. An interesting seasonal pH change was observed in the vegetation below the interface. In summer, at 50 mm depth where the pH in the mud reaches its minimum value, the mean pH (measured by three probes) was 5. In autumn, the pH was relatively higher in the sediments than in summer. The highest pH observed was 6 and the lowest was 5.7. In winter, the pH was relatively higher (6.1) in the sediments than observed in summer and autumn. Thus there was a seasonal variation in pH profiles. However, the pH of vegetation was always less than observed in the pond. Such results have been previously stated for the pH in the saltmarshes of the Mundaka-Gemika (Bay of Biscay, N. Spain) by I. Benito *et al.* (1990) where a pH as low as 5.5 had been observed in the vegetation of saltmarshes. And this is because of the dead organic matter and roots which form humic acids making the mud rich in H^+ (Benito *et al.*, 1990).

In autumn, at 1 m away from the pond, the pH profile was slightly different than measured at the vegetation close to the pond. The average profile from two probes is given in figure 6.11. The pH values are relatively higher at 1m distance from the pond.

The overall trend is the same however. Below 90 mm pH dropped as seen in both profiles (figure 6.10 and 6.11).

In winter, two long probes were tried in the vegetation to measure the pH at greater depth. Although the light box was designed for the small probes, long probes were photographed by moving the probe on the shelf and photographing in parts. These photographs were then analysed and the profiles combined to give the full depth profile. The data from two probes was averaged and the mean pH profile is given in figure 6.12.

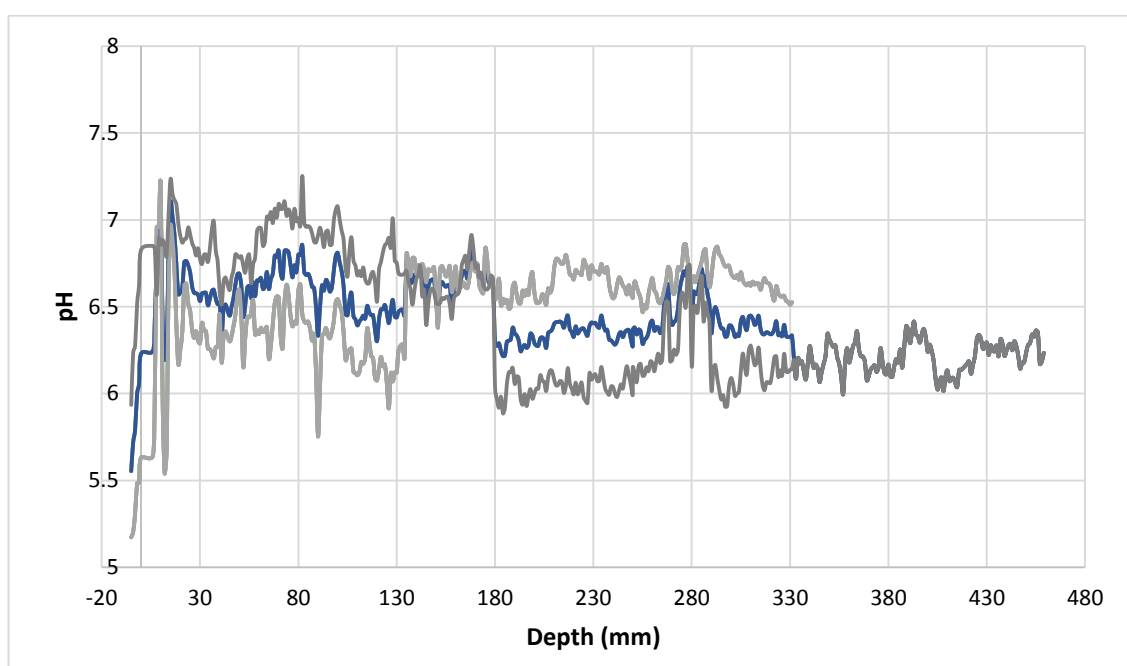


Figure 6.13: Average pH profile of vegetation in winter measured by long probes (blue) and individual profiles (grey).

The pH in the top of the vegetation is higher (figure 6.12) than measured by small probes (figure 6.10). For example at 30mm, the pH measured by small probes was 6 and pH measured by long probes was 6.5. In the depth, the pH decreased to 6. The long probes came out to be very patchy. The results were sufficient to demonstrate that long probes can be manufactured and applied if required, at sites where it is desired to measure pH profiles to much greater depths.

6.3.8 Seasonal pH profiles from the pond

In summer five probes were used to measure the pond profiles. Two in the vegetation at the edge of the pond and three in the pond.



Figure 6.14: Probes in the pond showing probe insertion, probe in-situ under the pond surface and probe removed and wiped ready for photography.

In autumn, two probes were used at each post covering the eight posts. In winter, similar experiment was repeated. Figure 6.14 shows the average seasonal pH profiles from the edge of the pond.

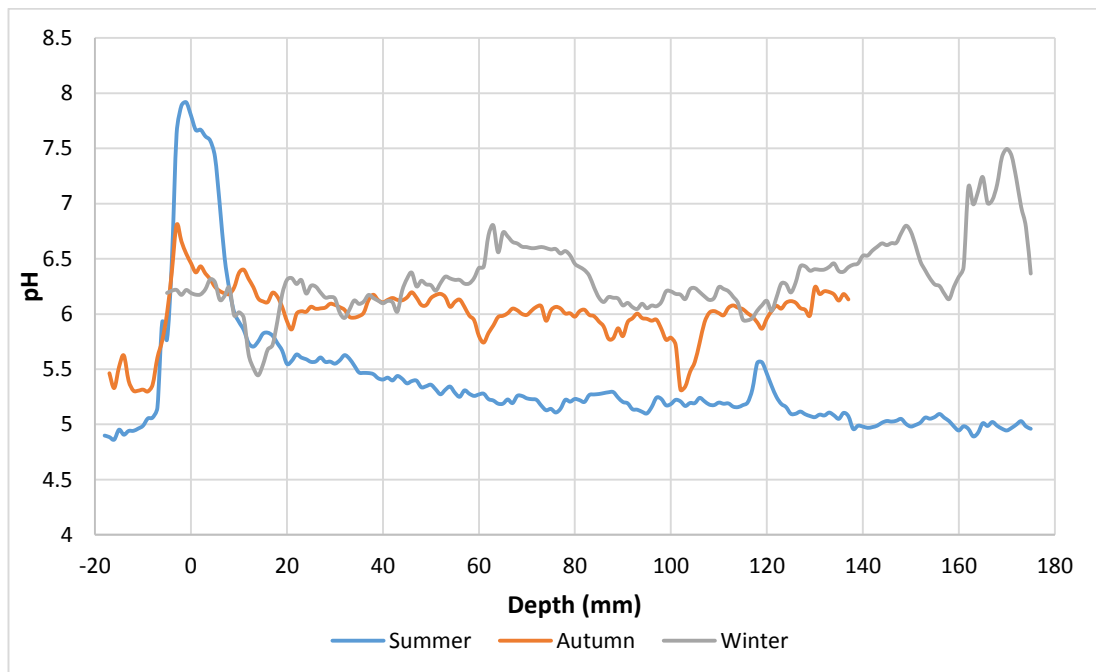


Figure 6.15: Seasonal pH profiles at the edge of the pond at Stiffkey saltmarshes showing mean pH profiles (n=3 for autumn and winter, n=2 for summer).

Since there was vegetation at the edge of the pond, a similar pattern is seen in Figure 6.14 as compared with the pH profiles in the vegetation shown in figure 6.10 and a very low pH was observed. A similar seasonal change was observed. The pH was lower in summer than in autumn and lower in autumn than in winter. In figure 6.14, the summer data shows that the pH at the interface (0 mm) was 7.9 dropped to 5.2 at 60 mm, it was even lower at the depth of 140 mm and reached to 5. In autumn, the maximum pH on the top of the vegetation was 6.8 and dropped to 6.3 at the interface (0 mm). The pH was 5.9 at 20 mm depth. The lowest pH observed was 5.3 in autumn and it was higher than measured in summer. In winter, the pH at the interface was 6.1 and dropped to 5.4 in the mud which was the lowest pH observed. pH increased to 6.8 at 62 mm. A maximum pH of 7.4 was seen in the depth of 171 mm. The noticeable rise in pH at greater depths in autumn and winter suggests that there may be processes occurring here that slowdown in colder conditions reducing the H^+ generation compared with the rates in summer which drive down and maintain the pH at the low (~ 5) value.

It is interesting to note the smaller scale variations in the profiles showing heterogeneity. This may be due to buried material, burrows or other causes. The pH probes alone cannot provide information on this, highlighting an advantage of the SPI system (See chapter 7).

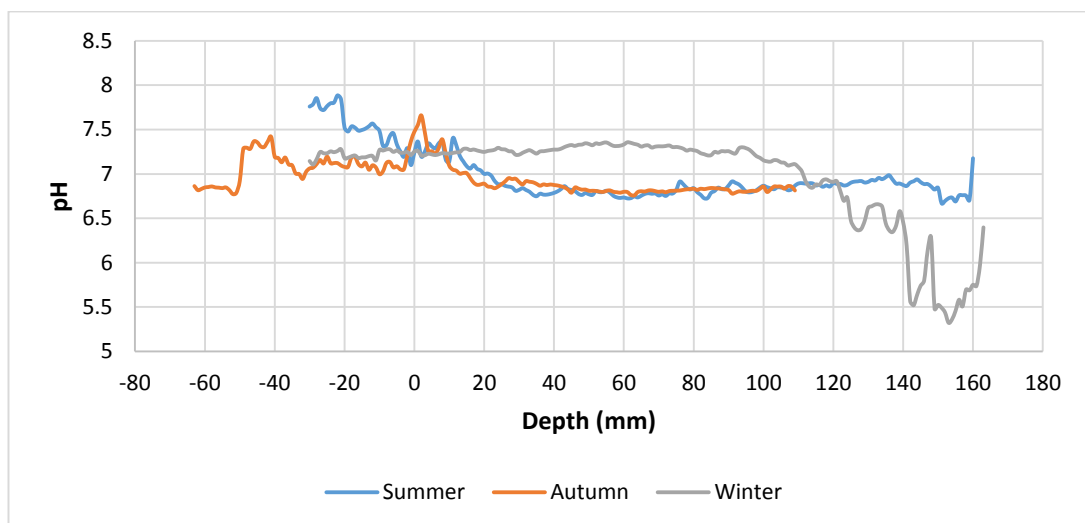


Figure 6.16: Seasonal pH profiles of pond at Stiffkey saltmarshes ($n= 3, 13$ and 5 for summer, autumn and winter where n is the number of profiles averaged).

Figure 6.15 shows the seasonal pH profiles of the pond. In summer, the maximum pH in the water was 7.6. At the interface, it dropped to 7.2 and in the mud it was as low as 6.7 at 33 mm. At 102 mm, a higher pH 6.9 was measured. In autumn, the maximum pH in the water was 7.4 reaching to 7.6 at the interface and dropped to 6.8 at 30 mm and stayed constant in the depth. In winter, the maximum pH of 7.2 was measured by the probes and remained the same until 92 mm. In the depth, pH decreases to 5.5. This very low pH was measured by two probes out of five and is a real measurement as there was no obvious issue observed with the probe. In the sediments, the pH increased from summer to winter. In water, the maximum pH was observed in summer and lower pHs in autumn and winter.

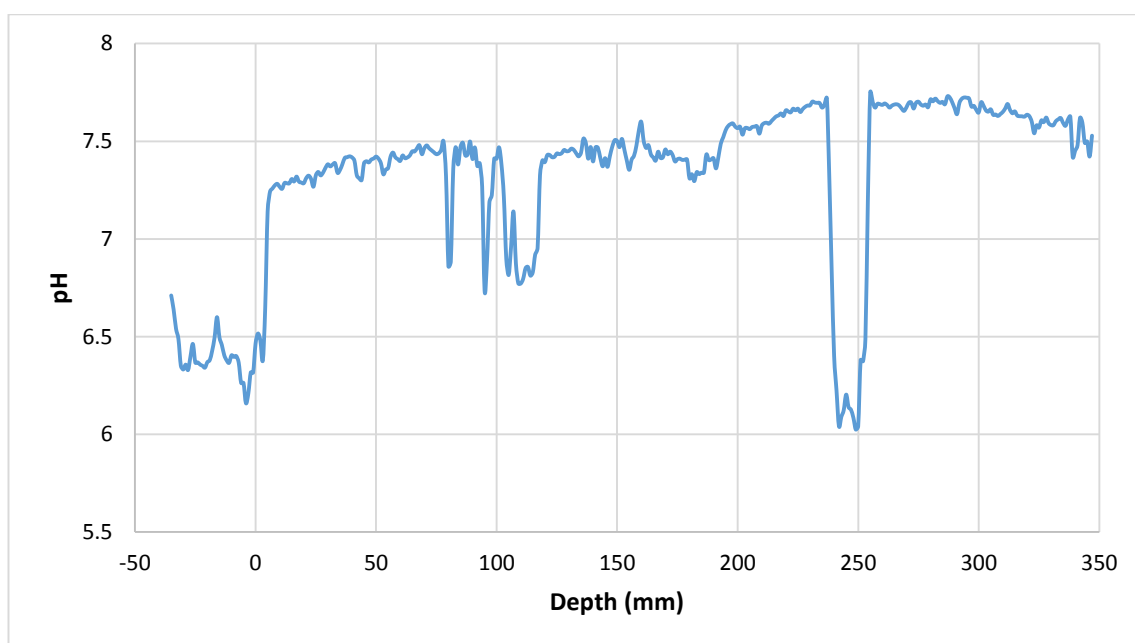


Figure 6.17: pH profile of pond taken from long probe in winter.

From 0 mm to 50 mm, the pH is about 7.2 exactly as measured with the small probes. However it was slightly higher from 68 mm to 100 mm and raised to 7.4. At 110 mm, a low pH (6.8) was measured by both long and small probes. The pH remained 7.4 from 119 mm to 200 mm and from 225 mm to 343 mm, it reached to 7.6. This depth was measured by only long probes. A very low apparent pH at 250 mm in figure 6.16 appeared due to an air bubble trapped in the probe and should be neglected. This was very clear in the image of the probe.

6.3.9 pH profiles at the creek in summer

The pH profiles were taken down the creek at Stiffkey salt marshes where station 1 was opposite to the second support of the bridge, station 2 was between the two supports, station 3 was opposite to the third support and so on. During the measurements taken at the creek, it was observed that the probes came out very patchy due to the mud/sand being dry and low in the pore water. Probes were homogeneous close to station 7 and especially at station 7 where there was overlying water, allowing the hydrogen ions to move freely into the sensing probe. The conductivity of the water was 50.9 mS at station 7 in the creek bed (flowing stream).

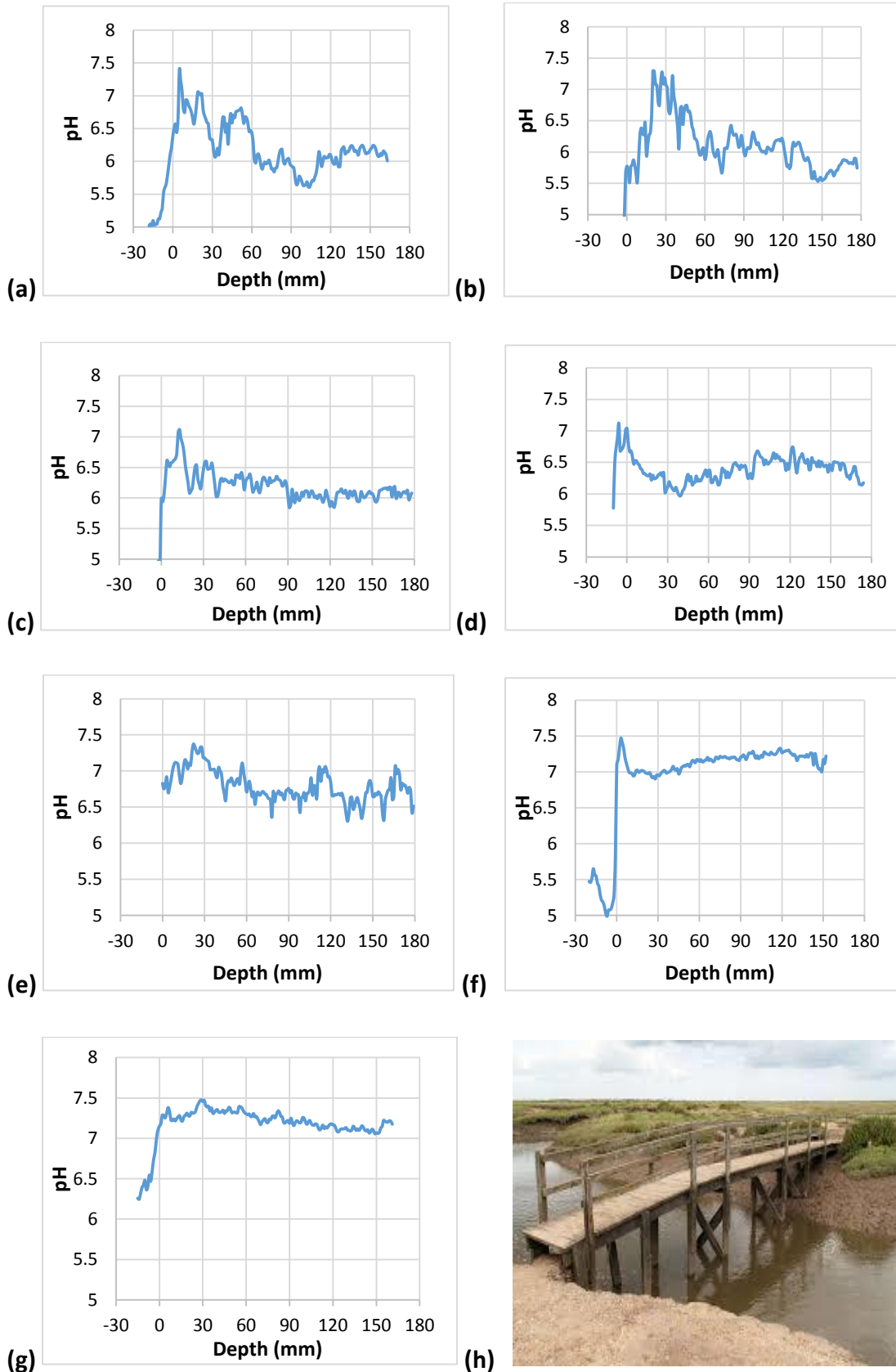


Figure 6.18: Mean pH profiles at the creek at station (a) 1, (b) 2, (c) 3, (d) 4, (e) 5, (f) 6 and (g) 7. (n=2) (h) Photograph of the creek.

Figure 6.17 shows the pH profiles from different stations at the creek. The profiles at station 1 and 2 showed lower pH values at intervals due to the patches observed on the probes at these stations which appeared due to the lack of pore water because the stations were very dry. At station 3, the maximum pH in the sediment was about 6.8 below the interface that dropped to 6 at 70 mm. At station 4, the pH was 6.8 at the interface and dropped to 6 at 40mm. At 120 mm, it increased to 6.5. At station 5, the pH at the interface was 6.8. It increased to 7.2 at 20 mm. The pH dropped to 6.7 at 70 mm and remained the same in the depth. At station 6, the pH at the interface was 7.5 and dropped to 7 at 20 mm. It increased to 7.2 at 120 mm. At station 7, the pH at the interface was 7.2, pH increased to 7.5 at 30 mm and dropped to 7 at 120 mm. A quick comparison of all the profiles at 7 stations shows that the pH in the sediments increased from 6 to 7 from station 1 to station 7.

6.3.10 pH profiles at the creek in autumn

The pH profiles were measured again in the autumn at the same stations and the following results were obtained. Figure 6.18 shows the pH profiles measured in autumn at 7 stations at the creek.

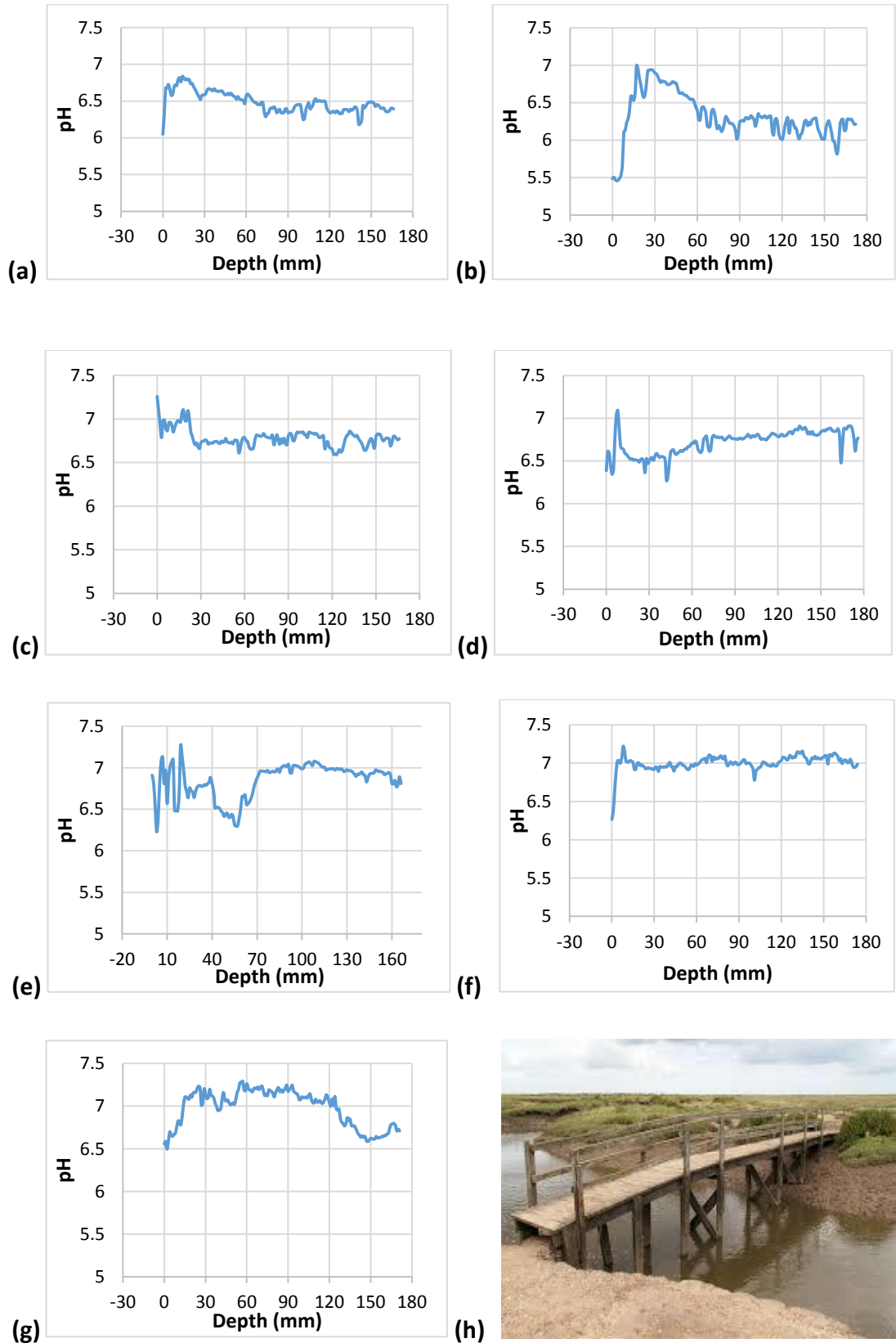


Figure 6.19: Mean pH profiles at the creek at station (a) 1, (b) 2, (c) 3, (d) 4, (e) 5, (f) 6 and (g) 7. (n=2) (h) Photograph of the creek.

Figure 6.18 shows the pH profiles from different stations at the creek measured in autumn. The same problem of patchy probes was observed due to less water at station 1 and 2. The profile at station 1 in figure 6.18a shows that the pH at the interface was 6.6 and in the sediments it dropped to 6.3 at 80 mm. At station 2, the probes were dry on the top explaining why a very low apparent pH has been measured however at 30 mm the pH was 6.8 and dropped to 6.1 at 80 mm and on average remained the same in the depth. At station 3, the pH at the interface was 7.2 and dropped to 7 just below the interface. At 30 mm, pH as low as 6.6 was observed and in the depth it remained almost the same. At station 4, the pH was 6.4 at the interface and 7 below the interface which might be because of the sediments dragging down due to the probe insertion. pH was 6.4 at 30 mm and increased to 6.8 at 80 mm and remained the same in the depth. At station 5, an average pH of 6.7 was observed in the top 30 mm. The pH decreased to 6.2 at 52 mm and increased to 6.9 at 80 mm and remained the same in the depth. At station 6, a constant pH of 7 was observed in the depth of 174 mm. At station 7, from 30 mm to 93 mm, a pH of 7.2 was observed. At 41 mm pH of 6.9 was observed. pH dropped to 6.5 at 149 mm. This is the only profile in the group where a relatively steep change on pH was observed with depth.

A quick comparison of all the stations shows that as we moved towards the water, the pH in the sediments at 30 mm increased from 6.5 to 7. If we compare the profiles of station 6 and 7 (where there was water and the probes did not come out patchy and dry) in figure 6.17 and 6.18, the pH in the sediments was higher in the summer than in autumn. If the profiles at station 7 (figure 6.17g, 6.18g) are compared with the profiles of pond in summer and autumn (figure 6.15), both the profiles below the interface have a maximum pH value 7.3 but in the depth the minimum pH value of 6.8 was observed in the pond and 7.1 in the creek in summer. The autumn profiles at both sites are very similar.

6.4 Conclusions

The response time of the probes in the soft mud was 30 minutes without conditioning the probes beforehand. The probes can be reused multiple times as no bleaching of dye or damage was observed by reusing the old probes but in these studies a new probe was used for each measurement. The probes came out patchy at most of the stations at the creek because there was not enough pore water in the sediments. Any such issues can be easily detected optically. The probes were robust and never broke during any of the measurements although a rubber mallet was used to push the probes down the vegetation mud. Longer probes can be manufactured if required to take deeper profiles.

At Stiffkey salt marsh, a seasonal change in pH profiles have been observed. In summer, the pH in the vegetation decreased to 5 within a few centimetres. In autumn, it decreased to 5.8 and in winter it decreased to 6.2. In the pond, pH was around 6.7 in summer, 6.8 in autumn and 7.2 in winter. Higher pH of 7.3 was observed at the creek in summer and lower 7.1 in autumn. Denitrification occurs at low pH and increases the pH of the sediments (Soetaert *et al.*, 2007). Denitrification takes place mostly in the upper few cm where nitrate is produced by ammonium oxidation. In summer, denitrification slows down because the role of nitrate as an oxidant is depressed in highly reducing sediment. During winter, denitrification is stimulated because the suboxic zone expands (Bender *et al.*, 1977; Vanderborght *et al.*, 1977; Froelich *et al.*, 1979). Therefore the pH of sediments in the summer is low and in the winter it increases at Stiffkey salt marshes. Lower pH in the vegetation compared with the pond is a result of accumulation of roots and dead organic matter which forms humic acids and the mud is thus more acidic. (Ranwell, 1972; Gray and Bunce, 1972; Bassett, 1978).

6.4 References

- Bassetp, A. 1978 The vegetation of a Camargue pasture. *Journal of Ecology* **66**, 803-827.
- Bender, M. L., Fanning, K. A., Froelich, P. N., Heath, G. R. & Maynard, V. 1977. Interstitial nitrate profiles and oxidation of sedimentary organic matter in the eastern equatorial atlantic. *Science* **198**, 605-609.
- Boorman, L. A. 2003 Saltmarsh Review. An overview of coastal saltmarshes, their dynamic and sensitivity characteristics for conservation and management. JNCC Report, No. 334
- Froelich, P. N., Klinkhammer, G. P., Bender, M. L., Luedtke, N. A., Heath, G. R., Cullen, D., Daulphin, P., Hammond, D., Hartman, B., Maynard, V. 1979 Early oxidation of organic matter in pelagic sediments of the equatorial atlantic: suboxic diagenesis. *Geochimica Acta*. **43**, 1075-1090.
- Gray, A. J. & Scott. R. 1977 The ecology of Morecambe Bay. VII. The distribution of *Puccinellia Maritima*, *Festuca ruhra* and *Agrostis stolonifera* in the salt marshes. *Journal of Applied Ecology* **14**, 229-241.
- Ranwell, D. S. (1972). *Ecology of salt marshes and sand dunes*. London : Chapman and Hall.
- Soetaert. K., Hoffmann, A. F., Middelburg, J. J., Meysman, F. J. R. & Greenwood, J. 2007 The effect of biogeochemical processes on pH. *Marine Chemistry* **105**, 30-51.
- Vanderborght, J. P., Wollast, R. & Billen, G. 1977. Kinetic models of diagenesis in disturbed sediments Part I Mass transfer properties and silica diagenesis. *Limnology and Oceanography* **22**, 787-793.

Chapter 7

pH profiles from recovered cores and SPI trials

7.1 Introduction

The first trials of pH sensors discussed in chapter 5 raised some issues that were resolved and having better photographic conditions and better calibration, some seasonal pH profiles were obtained from Stiffkey salt marshes Norfolk. Keeping the same composition of the membrane solution and using the same photographic kit as discussed in chapter 6, the sensor's performance was further tested in different cruises by using the sensors in recovered sediment cores and pH profiles were obtained. The sensors were also adapted for SPI and pH profiles were measured during different cruises *in-situ*. The results are discussed in this chapter.

7.2 Materials and Methods

pH probes were manufactured as described previously in chapter 6 and applied in recovered cores collected during the research cruises. pH probes were also attached to the SPI for *in-situ* pH profiling during different cruises. A slot was milled on the SPI faceplate to slide the probe into. The SPI probes were manufactured on Perspex strips cut to the exact size of the faceplate slot (15 mm by 5 mm deep). The top end of the strip was reduced to <1mm thick and contoured so that it could be placed under the rubber seating strip of the SPI faceplate and held in place by a removable stainless steel strip that formed part of the frame surrounding the faceplate. This was fixed by flush fitting bolts. The bottom end of the strip had a chisel tip that pushed down tightly into the edge of the rubber seal to hold it in place tightly once the top part was clamped by stainless steel strip. Figure 7.1 shows a probe attached to the SPI faceplate.

The probes were used in the sediment cores and SPI data was collected by Claire Powel (Cefas) during the Prince Madog cruise in July 2014 and by Briony Silburn (Cefas) during the Discovery cruise in March 2015 and May 2015. The calibration for the Prince Madog cruise was done at 15 °C using three probes. The method for calibration has been discussed before in chapter 6. An *in-situ* calibration was done repeating the same

calibration method discussed before but using the SPI at Cefas for the discovery cruise. A bucket full of seawater taken from Lowestoft (Cefas) was used for calibration and CO₂ and Ar were used to change the pH of the water. A pump was used for stirring the water to help the seawater equilibrate. The temperature was controlled by using a water bath that was connected to copper coils that were immersed in the seawater (Figure 7.1). Probe calibration for recovered sediment cores was done as discussed previously in chapter 6 using seawater at 10.5 °C.

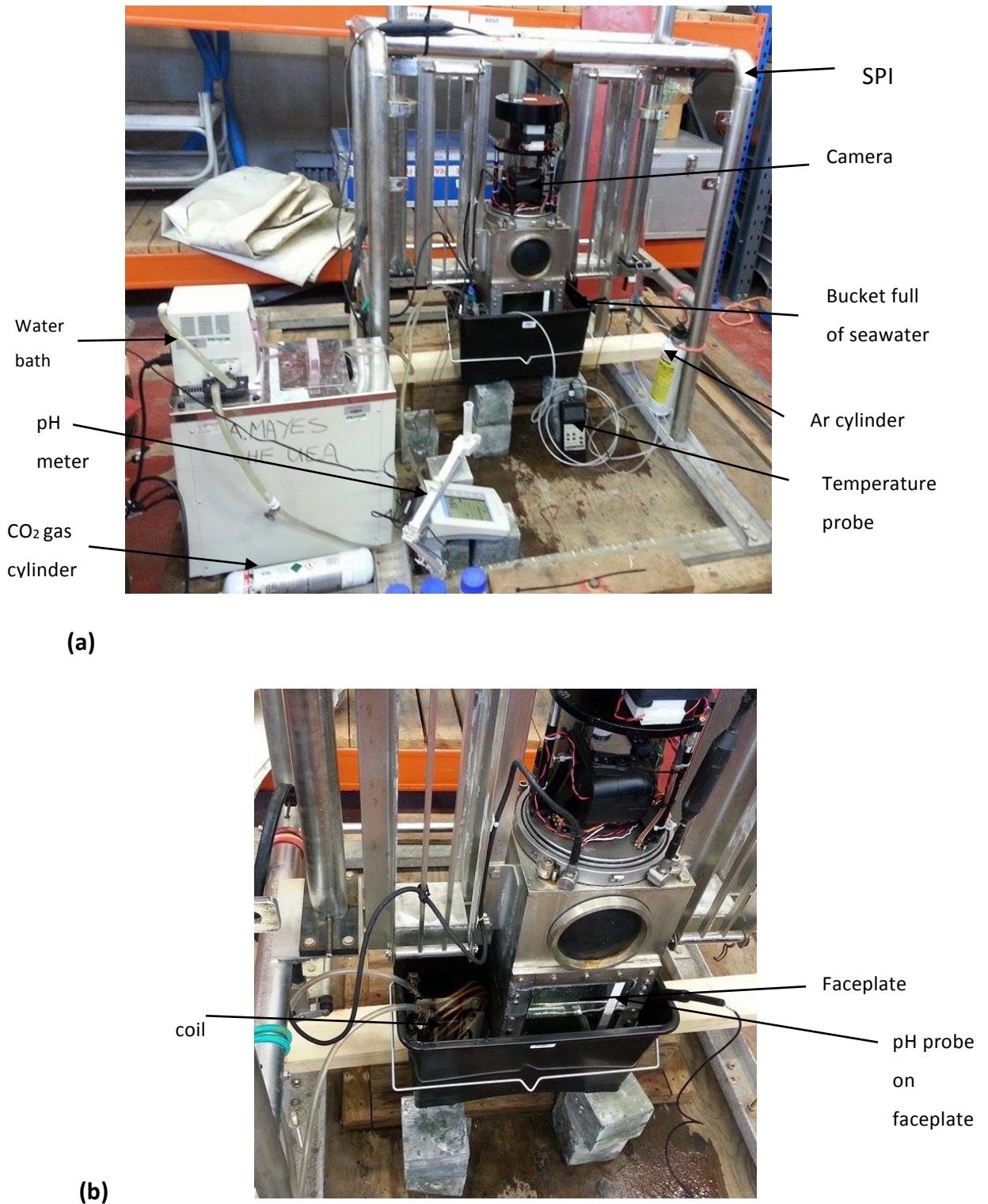


Figure 7.1: (a) Experimental set up for SPI probe calibration, (b) closer view of bucket.

7.3 Results and discussions

7.3.1 pH profiles of sediment cores from the Prince Madog cruise

Calibration was done in the lab as discussed in chapter 5 at 15 °C and 11 °C in seawater taken from Lowestoft and the resulting graphs are shown in figure 7.2 and 7.3. The inverse of the equation was used for analysing the photographs taken during the cruise.

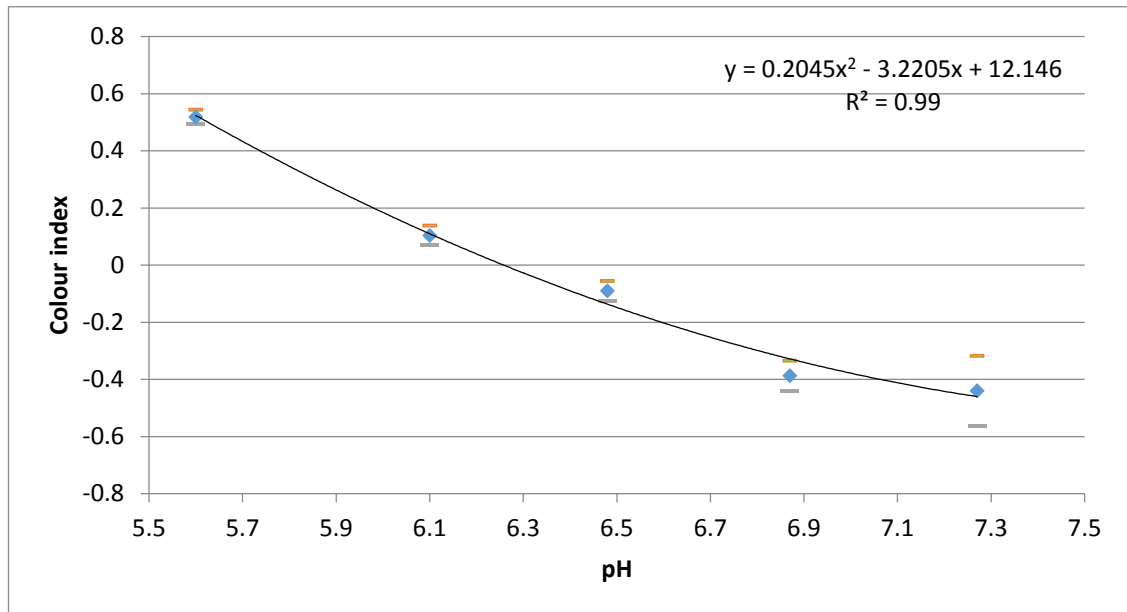


Figure 7.2: Calibration at 15 C° graph for the probes used in the Prince Madog cruise.

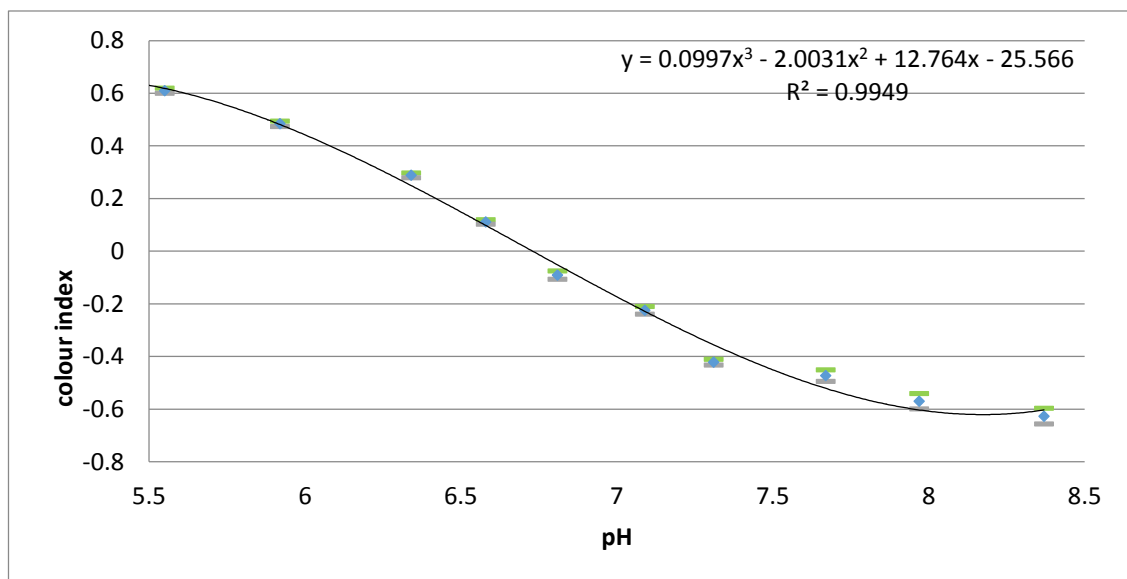


Figure 7.3: Calibration at 11 C° graph for the probes used in the Prince Madog cruise.

The calibration equation obtained from figure 7.2 was used to measure the pH profiles from the photographs taken at stations 32, 34, 35 and 37 where temperature is close to 15 °C and the calibration equation obtained from figure 7.3 was used to measure the pH profiles from the photographs taken at station A6 and its cores where the temperature was 13 °C. The temperature observed at different stations where probes were used in the recovered cores are listed in table 7.1. The stations were located in the North Irish Sea between the Isle of Man and the Coast of Cumbria (between 4°20' and 3° 30' west and 54 °10' and 54 ° 30' North).

Date	Station	Temperature when inserted	Temperature when taken out	Comments
01-07-14	32	14.5 °C	15.4 °C	Water was being dragged down from surface.
	33			Core was too shallow for pH probe
	34	15.4 °C	15.9 °C	Tube of water was covered with foil. Completely equilibrated in 50 minutes
	35	15.2 °C	16 °C	Water was being dragged down by the stick.
	37	16 °C	16.5 °C	Stick was not conditioned in the sea water before using
03-07-14	A6 core2	13.9 °C	14.5 °C	
	A6 core3	13 °C	13.9 °C	Massive burrow
	A6 core4	13.5 °C	13.8 °C	

Table 7.1: Temperature observed at different stations. (Source: Claire Powel, Cefas)

The pH profiles obtained from different stations are given below.

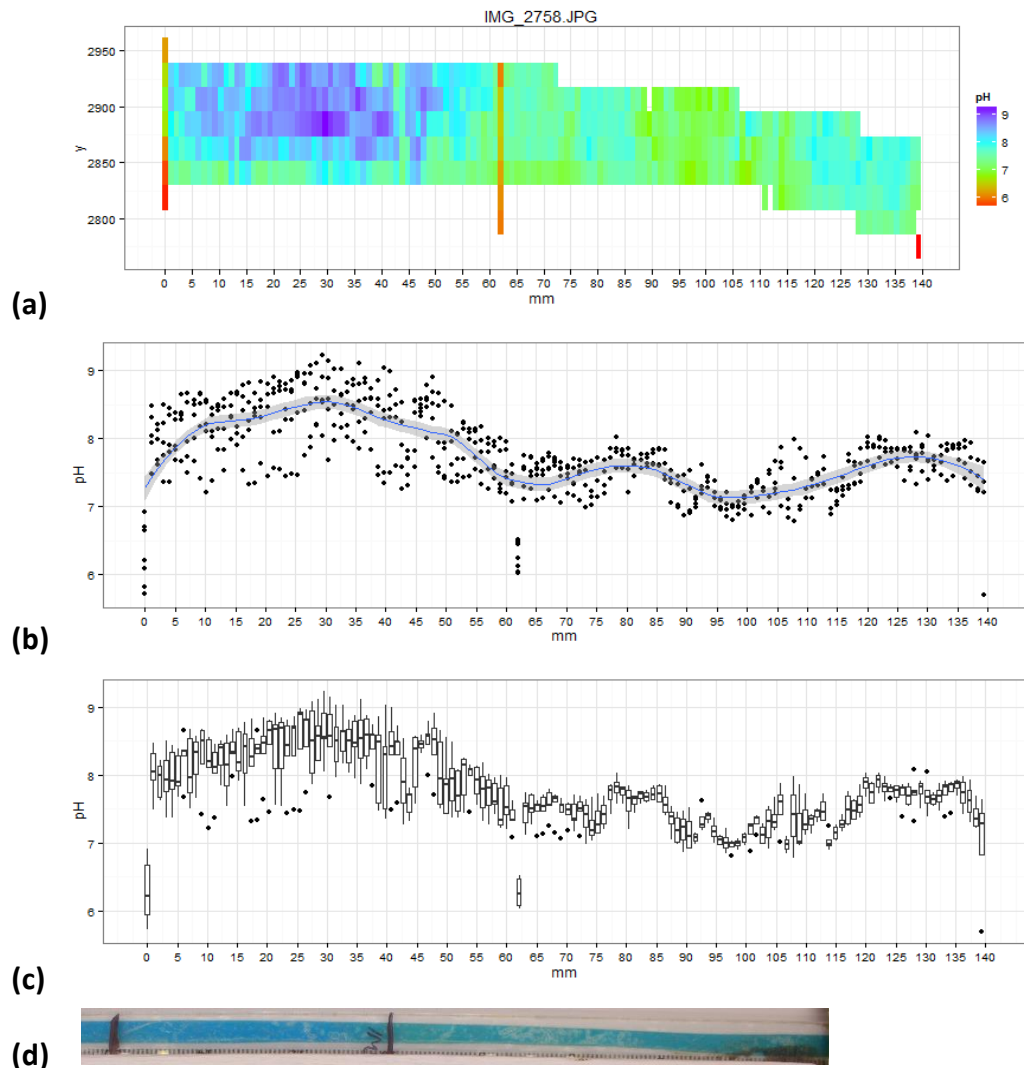


Figure 7.4: pH profile at station 32 (a) a false colour pH map generated by the software for the sensor area (b) an average pH value across the strip (c) box plot- white box: interquartile range (iqr), horizontal line: median value, vertical line: range of the data, individual points: potential outliers, which are identified as >2.5 iqr from the median. (d) The actual probe.

Figure 7.4 shows the pH profile at station 32. On the probe, the first mark shows how far the probe was in the core and the second mark shows the sediment water interface. In figure 7.4 b, the pH of the seawater was 8 which fell down at the sediment water interface to 7.5. The probe had white patches which were due to the damage caused to the sensing membrane due to pressing hard while manufacturing it. The lowest pH in the sediment was 7.0. The coloured lines in the figure 7.4a were the marks made on the probe that were picked by the software as a separate line.

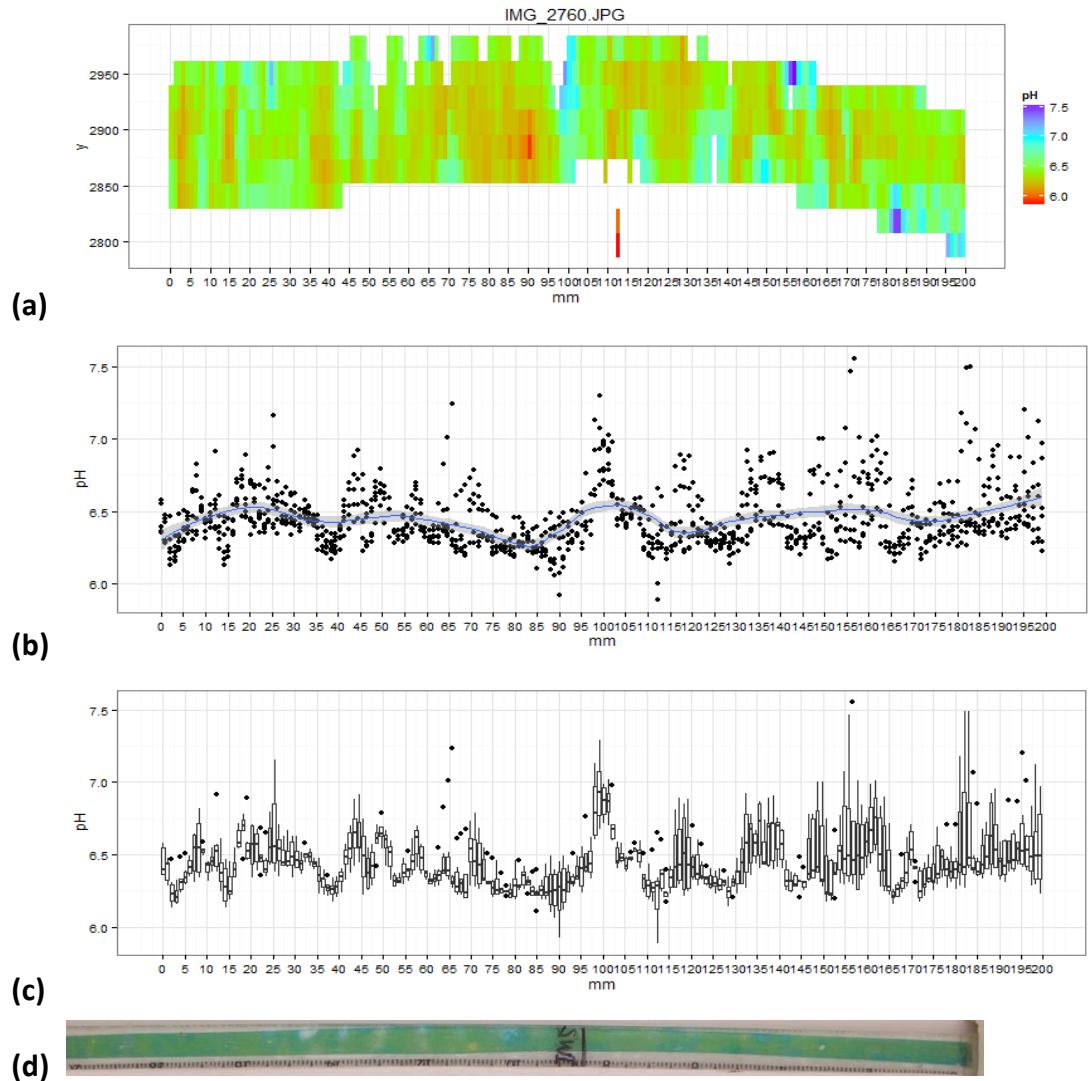


Figure 7.5: pH profile at station 34 and the actual probe (a) a false colour pH map generated by the software for the sensor area (b) an average pH value across the strip (c) box plot- white box: interquartile range (iqr), horizontal line: median value, vertical line: range of the data, individual points: potential outliers, which are identified as >2.5 iqr from the median. (d) The actual probe.

Figure 7.5 shows the pH profile at station 34. The apparent pH of seawater measured by this probe was very low. This could be because of the poor contact between the nytran membrane and sensing membrane. The pH was about 6.5.

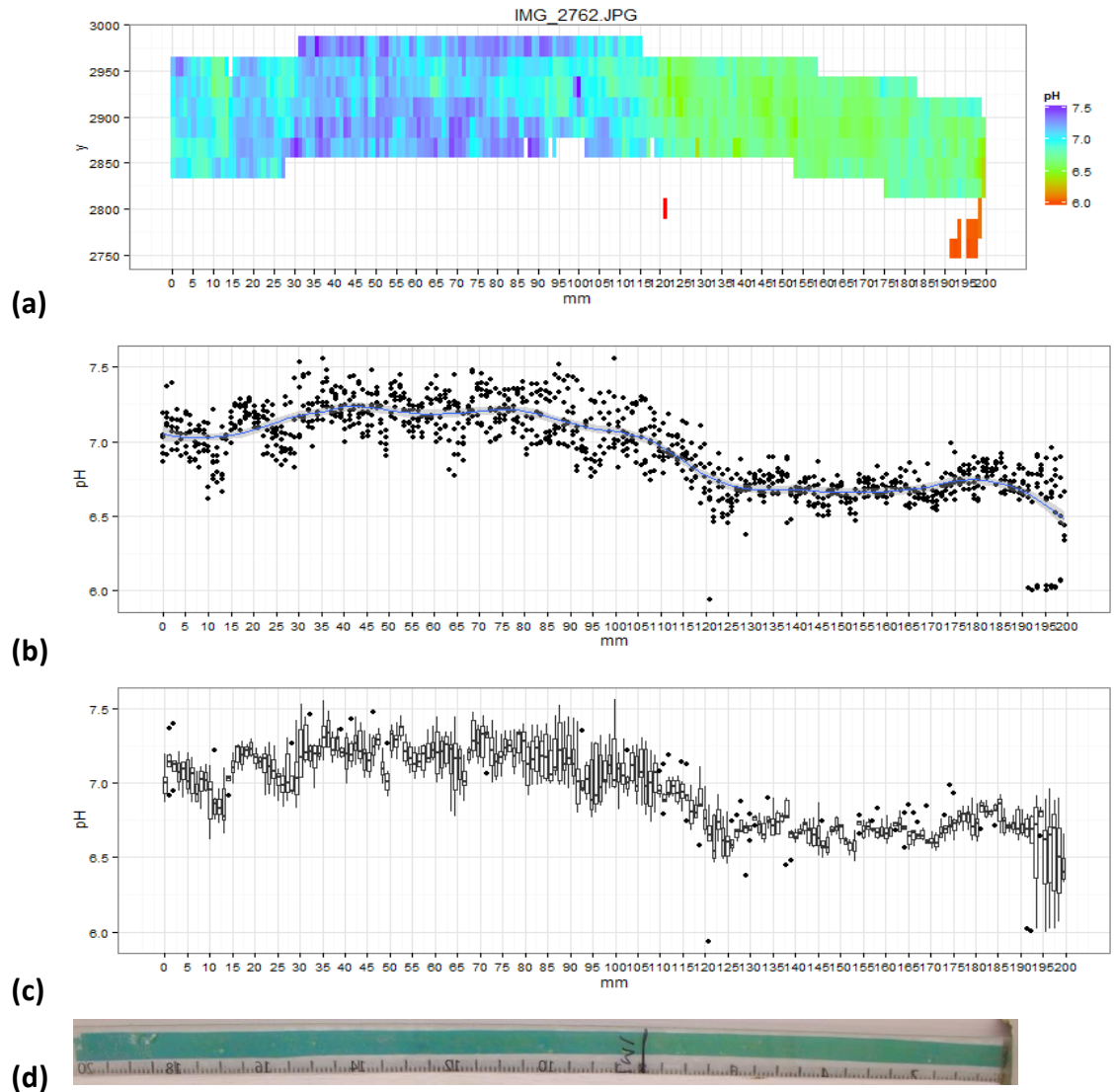


Figure 7.6: pH profile at station 33 and the actual probe (a) a false colour pH map generated by the software for the sensor area (b) an average pH value across the strip (c) box plot- white box: interquartile range (iqr), horizontal line: median value, vertical line: range of the data, individual points: potential outliers, which are identified as >2.5 iqr from the median. (d) The actual probe.

Figure 7.6 shows the pH profile at station 33. At station 33, pH of seawater was about 7.3 which dropped at the interface to 6.7. The interface was at 120 mm. The probe was very homogeneous and the colour change could be detected optically.

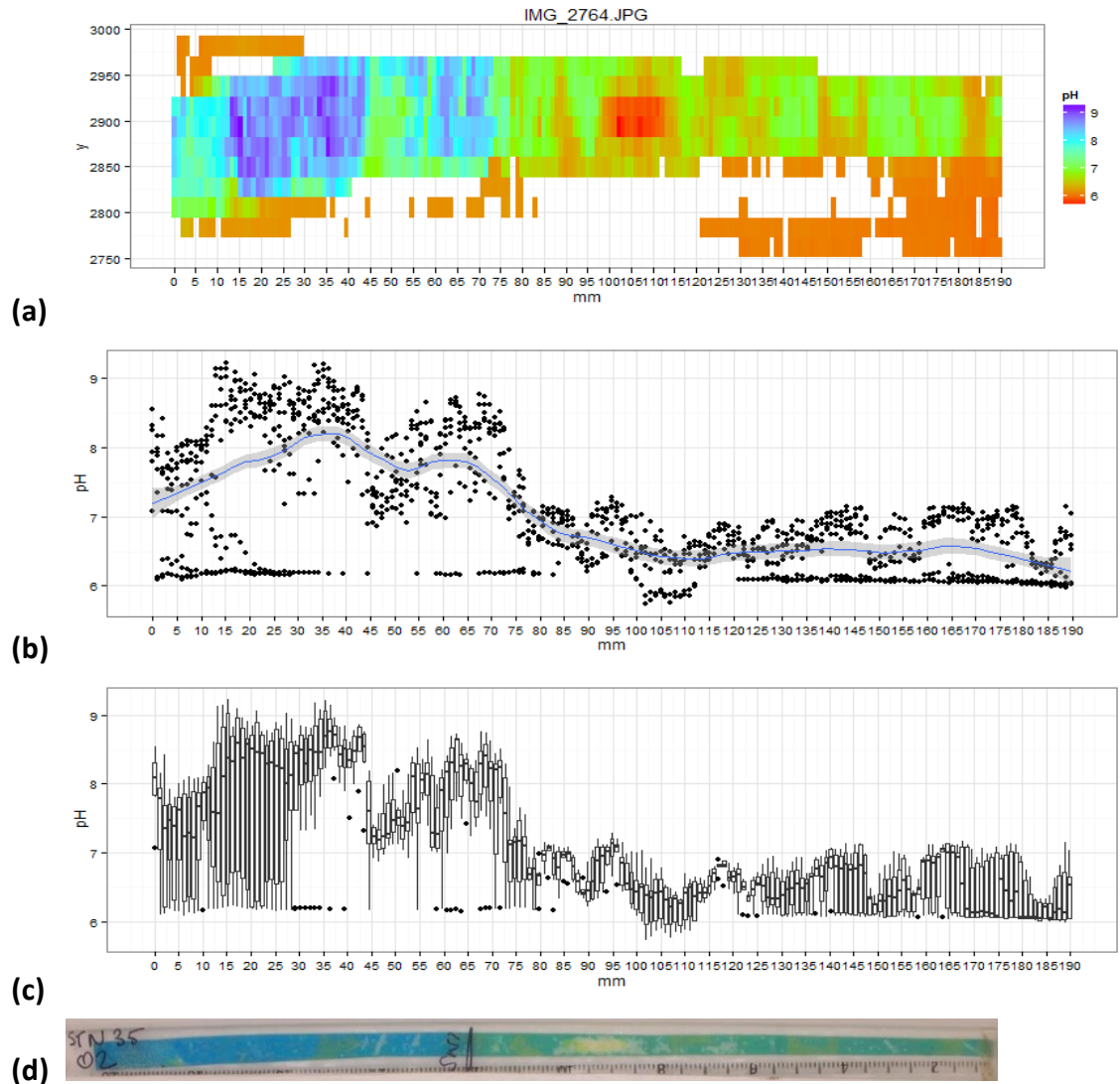


Figure 7.7: pH profile at station 35 and the actual probe (a) a false colour pH map generated by the software for the sensor area (b) an average pH value across the strip (c) box plot- white box: interquartile range (iqr), horizontal line: median value, vertical line: range of the data, individual points: potential outliers, which are identified as >2.5 iqr from the median. (d) The actual probe.

Figure 7.7b shows the pH profile taken at station 35. The pH of seawater at station 35 is 8.9 which dropped down to 7 at the sediment water interface (90 mm). There was a huge yellow section on the probe where the apparent pH was below 7 (about 6.5) at 105mm. This could be an air bubble or could be a response to the actual low pH.

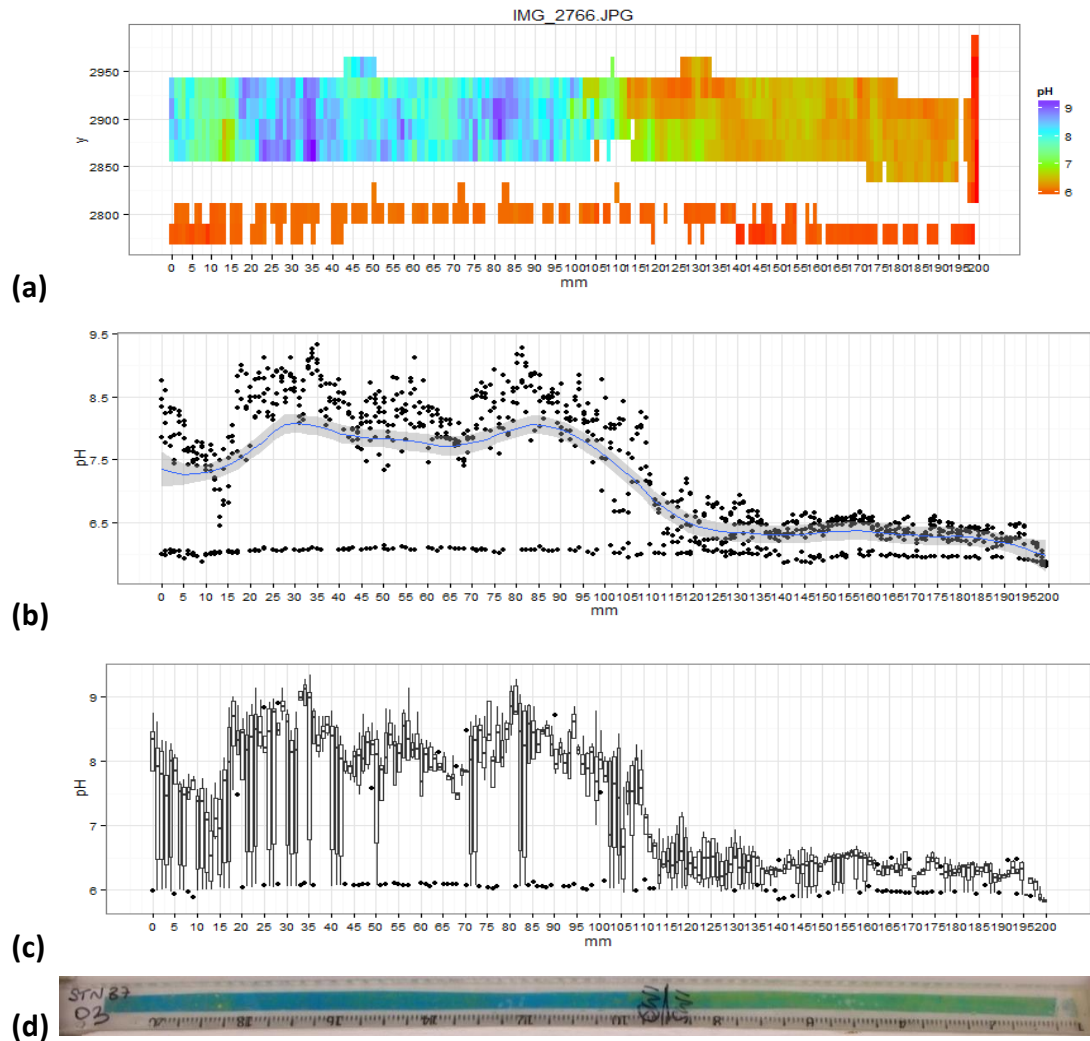


Figure 7.8: pH profile at station 37 and the actual probe (a) a false colour pH map generated by the software for the sensor area (b) an average pH value across the strip (c) box plot- white box: interquartile range (iqr), horizontal line: median value, vertical line: range of the data, individual points: potential outliers, which are identified as >2.5 iqr from the median. (d) The actual probe.

Figure 7.8 shows the pH profile taken at station 37. At station 37, the pH of water was about 8 which dropped down to 6.5 at 115 mm where the interface was marked and stayed the same at greater depth.

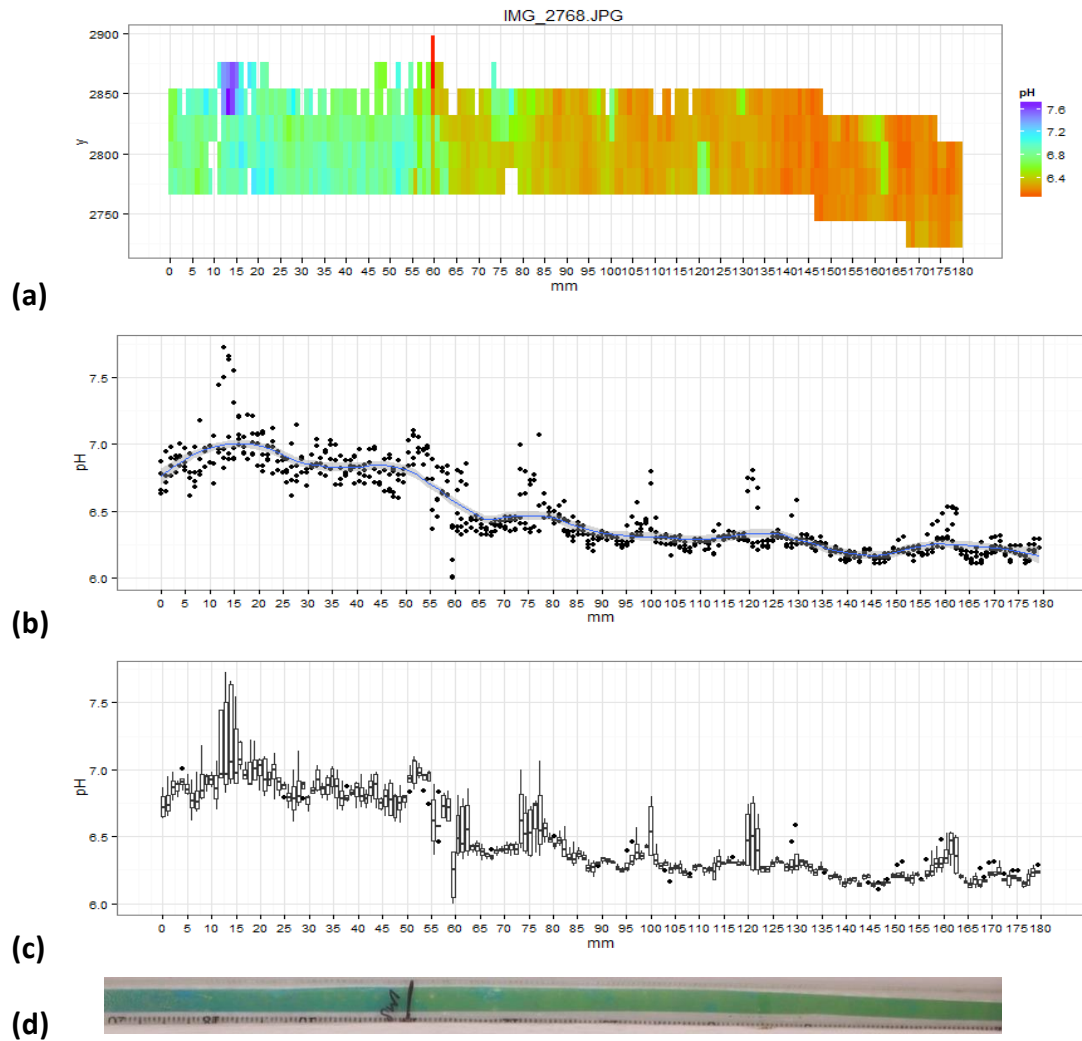


Figure 7.9: pH profile at station A6 core2 subcore2 and the actual probe (a) a false colour pH map generated by the software for the sensor area (b) an average pH value across the strip (c) box plot- white box: interquartile range (iqr), horizontal line: median value, vertical line: range of the data, individual points: potential outliers, which are identified as >2.5 iqr from the median. (d) The actual probe.

Figure 7.9 shows the pH profile taken at the station A6 from core 2 subcore 2. The pH of the water was 7 and dropped down to 6.5 at the interface which was at 60 mm at station A6 in the core 2 sub core 2. The pH dropped down further in the sediment to 6.3 at 85 mm. There was another drop in pH at 140 mm where the pH was 6.2.

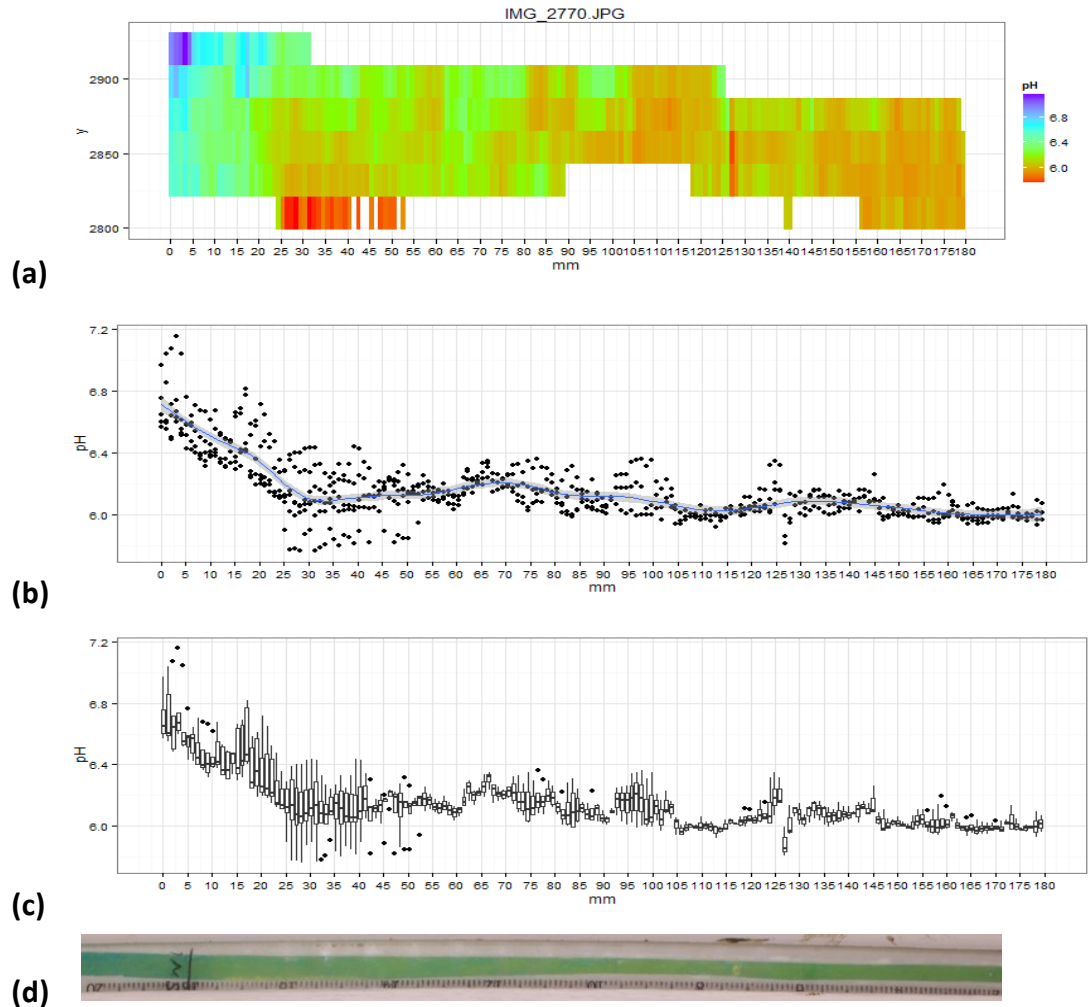


Figure 7.10: pH profile at station A6 core 3 sub core 2 and the actual probe (a) a false colour pH map generated by the software for the sensor area (b) an average pH value across the strip (c) box plot- white box: interquartile range (iqr), horizontal line: median value, vertical line: range of the data, individual points: potential outliers, which are identified as >2.5 iqr from the median. (d) The actual probe.

At station A6 core 3 sub core 2 the pH of the water was about 6.5 but it can be seen on the actual probe that the probe had not completely equilibrated but a little blue section can be detected on the photograph. In figure 7.10, a few data points are seen close to pH 7.2 which represent the pH of sea water. At the interface, which is marked at 20 mm, the pH was 6.3. However pH dropped further in the depth at 45 mm to 6.2. A sharp decrease in pH was seen at 105 mm where pH dropped down to 6. In this core, a massive burrow was seen, therefore a pH as low as 6 might be a realistic possibility due to potential oxygenation of the sediment by this biological activity.

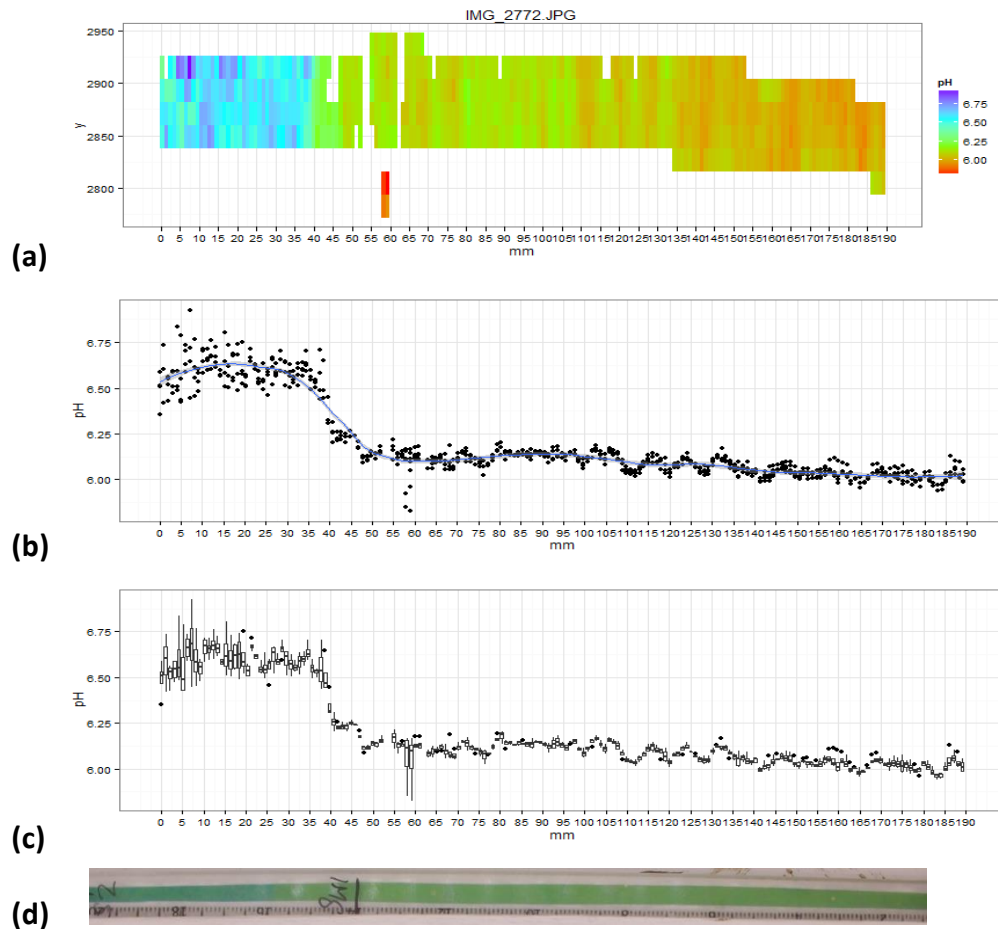


Figure 7.11: pH profile at station A6 core4 subcore2 and the actual probe (a) a false colour pH map generated by the software for the sensor area (b) an average pH value across the strip (c) box plot- white box: interquartile range (iqr), horizontal line: median value, vertical line: range of the data, individual points: potential outliers, which are identified as >2.5 iqr from the median. (d) The actual probe.

Figure 7.11 shows the pH profile at station A6 core4 subcore2. The pH of water in this core was about 6.6 which dropped to 6.1 at 50 mm which was close to the interface (60 mm). There was a further decrease of pH in the depth where it reached pH 6 at 135 mm.

7.3.2 SPI Trial from Prince Madog

The Prince Madog research vessel was not suitable for leaving the SPI in the sediments for longer period due to its limitations on its positioning system. The probes needed to be in the sediments for at least 15 minutes to completely equilibrate but during the cruise, the probes were in contact with sediments only for a few seconds, due to which no meaningful profiles could be obtained. However, the preliminary SPI trial

demonstrated that the probes are robust and survive the insertion without any visible damage. They could be used multiple times. No problems were observed during their use with membrane splitting, adhesive peeling or other issues that might have caused problems. This was very encouraging for future use.

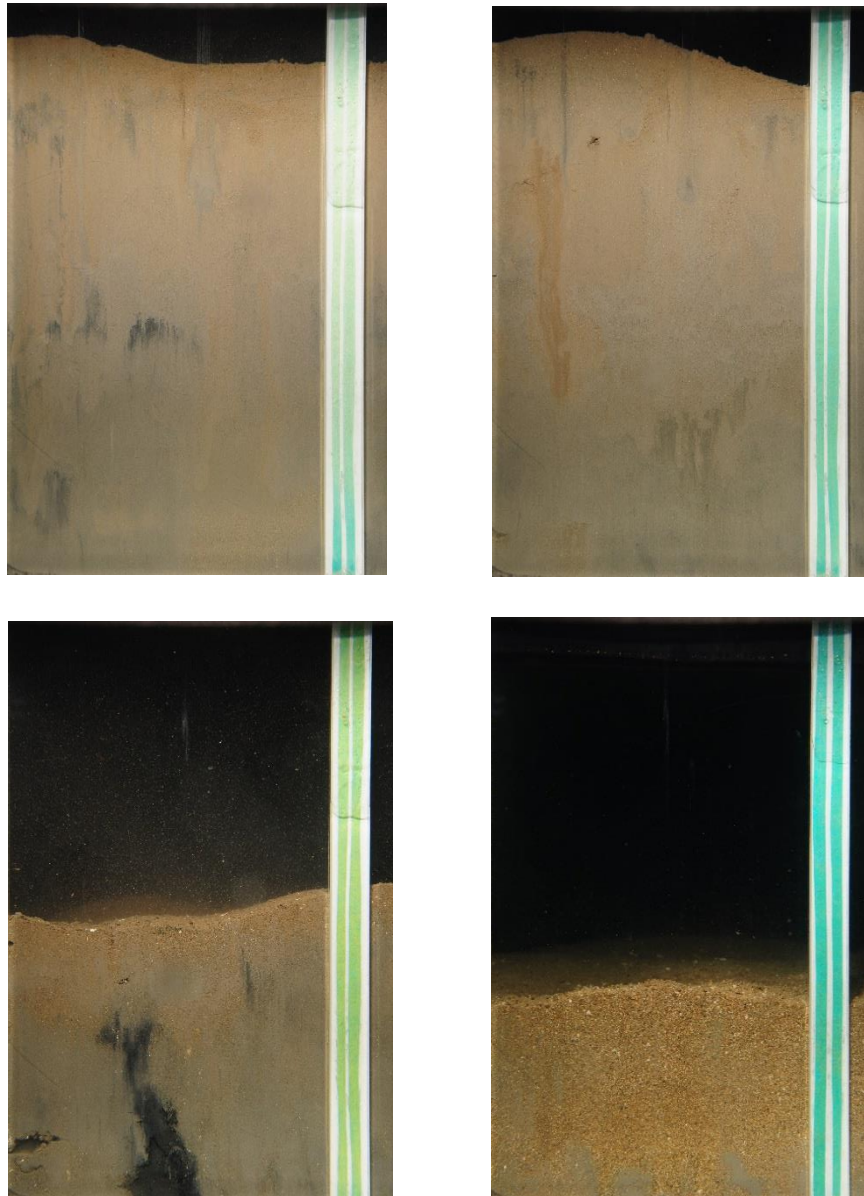


Figure 7.12: SPI images with the attached pH probes from brief sediment insertion during the Prince Madog cruise.

7.3.3 pH profiles from Cefas March 2015 cruise (DY021):

The probe calibration was done at 10.5 °C using five probes (one from each batch) as discussed previously in chapter 6. The mean colour index values were plotted and the inverse of the equation obtained (figure 7.13) was used to analyse the photographs obtained from the cruise.

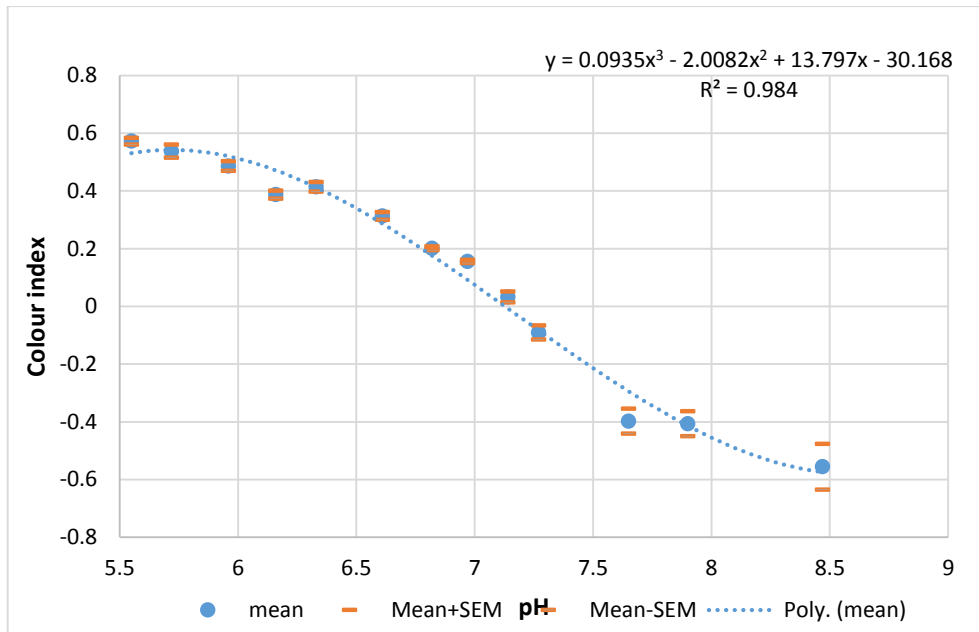


Figure 7.13: calibration graph for probes used in the recovered sediment cores.

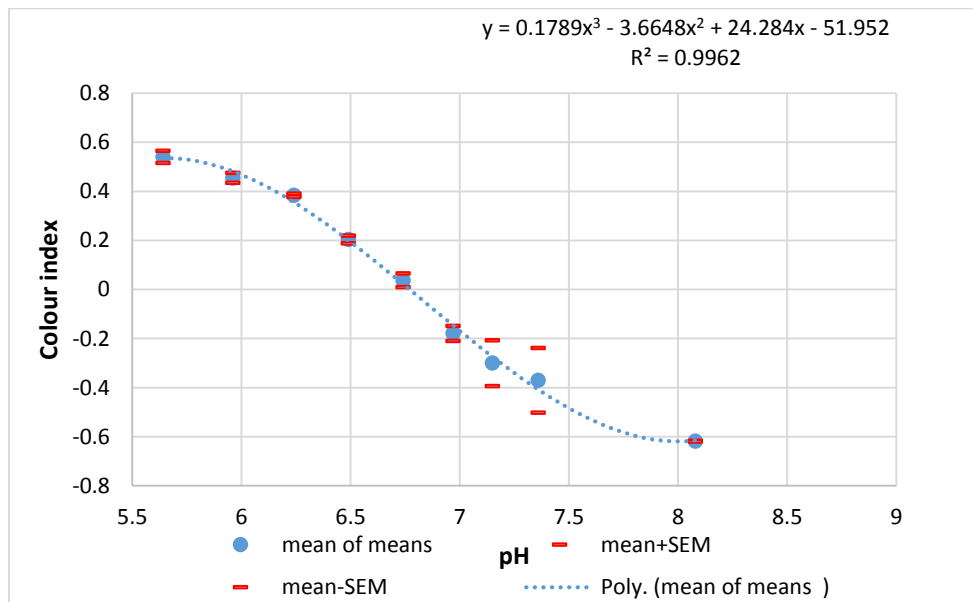


Figure 7.14: SPI calibration graph from in-situ calibration using SPI system.

Figure 7.14 shows the calibration graph obtained by doing calibration using the SPI system. The colour index values of top, middle and bottom sections of the probe taken from the probe photographs at each pH value were averaged and the means were plotted against pH. If we compare figure 7.13 with figure 7.14, the overall trend looks similar. However, in the SPI calibration graph bigger error bars between pH 7 and 7.5 can be because of the fact that it takes longer for a bucket full of sea water to equilibrate when the CO₂ gas is bubbled and thus there is variation in colour at the top, middle and bottom sections of the probe. An additional time is required for the probe to equilibrate in the equilibrated seawater before it is photographed at a certain pH value. Some differences in the RGB values and calibration would also be expected due to the different camera and lighting on the SPI compared with the light box.

The map in figure 7.15 was provided by Cefas and shows the location of the stations from where the cores were collected. The manuscript of map has not been published yet but has been submitted. (Stephens D, Diesing M (submitted)). The data used to create the mud layer on the map has been published previously by Stephens. (Stephens. D, 2015). The GPS location and temperature of different sites are listed in table2 (source: Briony Silburn).

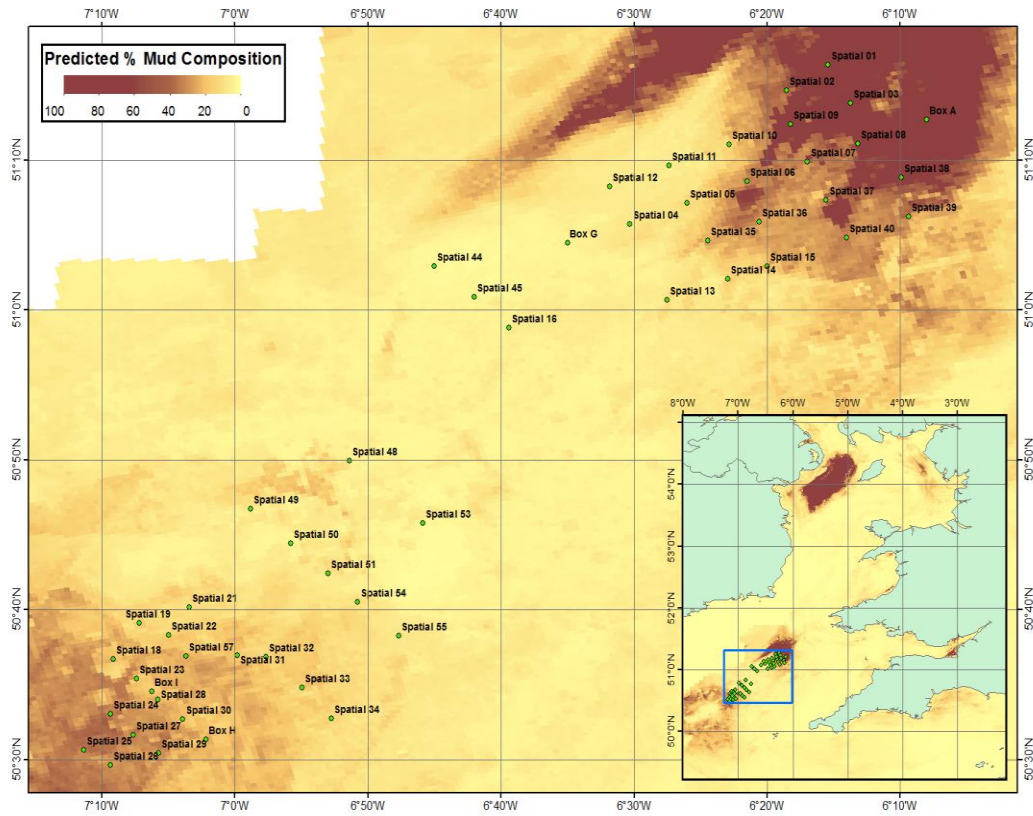


Figure 7.15: Map showing the location of the sites covered during the cruise.

Latitude	Longitude	Station ID	Temp (°C ± 0.5)
51.21	-6.13	Box A	10.4
51.07	-6.58	Box G	10.3
50.52	-7.04	Box H	10.1
50.58	-7.10	Box I	10.3
51.27	-6.26	Spatial 01	10.6
51.24	-6.31	Spatial 02	10.3
51.23	-6.23	Spatial 03	10.8
51.10	-6.51	Spatial 04	10.8
51.12	-6.43	Spatial 05	10.8
51.14	-6.36	Spatial 06	10.8
51.17	-6.28	Spatial 07	10.8
51.19	-6.22	Spatial 08	10.8
51.21	-6.30	Spatial 09	11.1
51.18	-6.38	Spatial 10	10.8
51.16	-6.46	Spatial 11	10.8
51.14	-6.53	Spatial 12	10.8
51.01	-6.46	Spatial 13	10.8
51.03	-6.38	Spatial 14	11
51.05	-6.33	Spatial 15	10.8
50.98	-6.66	Spatial 16	10.5
50.61	-7.15	Spatial 18	10.5
50.65	-7.12	Spatial 19	10.8
50.67	-7.06	Spatial 21	10.8
50.64	-7.08	Spatial 22	10.2
50.59	-7.12	Spatial 23	10.5
50.55	-7.16	Spatial 24	10.2
50.51	-7.19	Spatial 25	10.2
50.49	-7.16	Spatial 26	10.5
50.53	-7.13	Spatial 27	10.8
50.57	-7.10	Spatial 28	10.5
50.51	-7.10	Spatial 29	10.8
50.54	-7.07	Spatial 30	10.2
50.62	-7.00	Spatial 31	10.2
50.61	-6.96	Spatial 32	10
50.58	-6.92	Spatial 33	10.2
50.55	-6.88	Spatial 34	10.8
51.08	-6.41	Spatial 35	10.6
51.10	-6.34	Spatial 36	10
51.12	-6.26	Spatial 37	10
51.15	-6.17	Spatial 38	10.2
51.10	-6.16	Spatial 39	9.5
51.09	-6.23	Spatial 40	9.8
51.05	-6.75	Spatial 44	10.4
51.01	-6.70	Spatial 45	10.2
50.83	-6.86	Spatial 48	10
50.78	-6.98	Spatial 49	10.4
50.74	-6.93	Spatial 50	10.2
50.71	-6.88	Spatial 51	10
50.76	-6.77	Spatial 53	
50.67	-6.85	Spatial 54	10.6
50.64	-6.79	Spatial 55	10
50.61	-7.06	Spatial 57	

Table 7.2: Location of stations and their temperature (Source: Briony Silburn, Cefas).

pH profiles within the same cores are compared in figure 7.16, 7.17 and 7.18.

Differences in the pH profiles within the same core

Some of the profiles in the same core looked very similar but some of them were very different. Examples are given below.

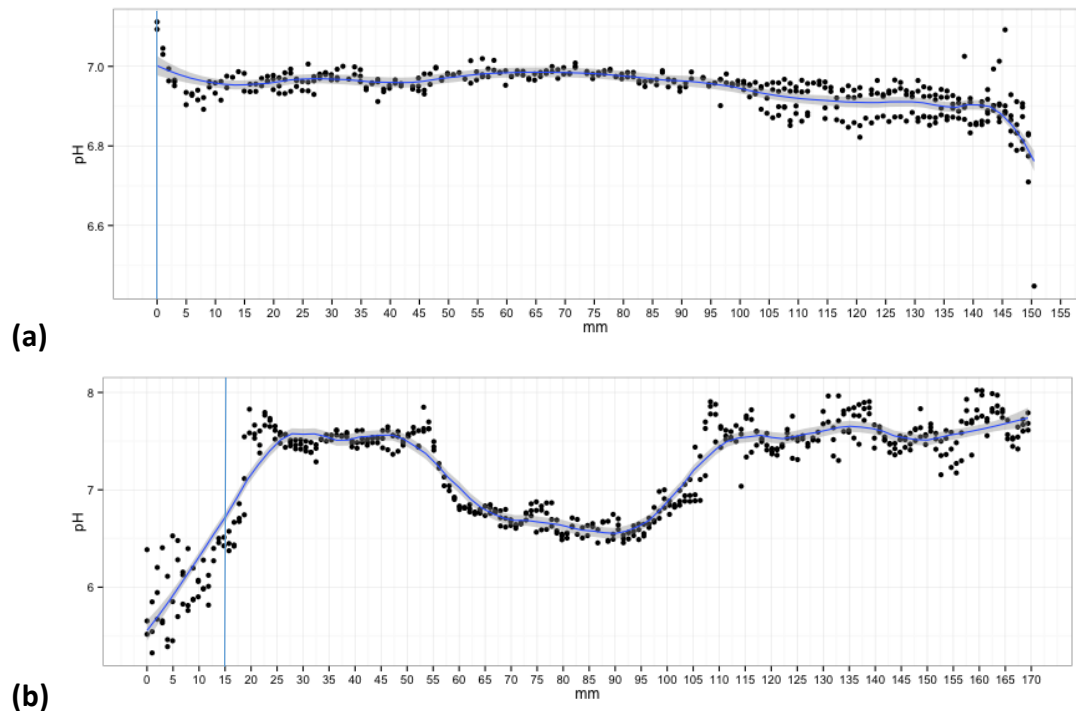


Figure 7.16: Two pH profiles of station Box H taken from the same core using two probes. Blue line represents the sediment water interface.

In figure 7.16a, the interface was at 0 mm. The pH in the sediments was about 6.95. At 55 mm, the pH was 7 and dropped down to 6.9 at 105 mm. In figure 7.16b, the interface was at 15 mm, where the pH was 7.5. There was an air bubble on the top of the probe i.e. from 0 mm to 20 mm. There was a drop in pH at 70 mm where the pH was 6.8. An increase in pH was seen from 105 mm and onwards where the pH was 7.5. The two pH profiles obtained from the same core are quite different from each other demonstrating local heterogeneity.

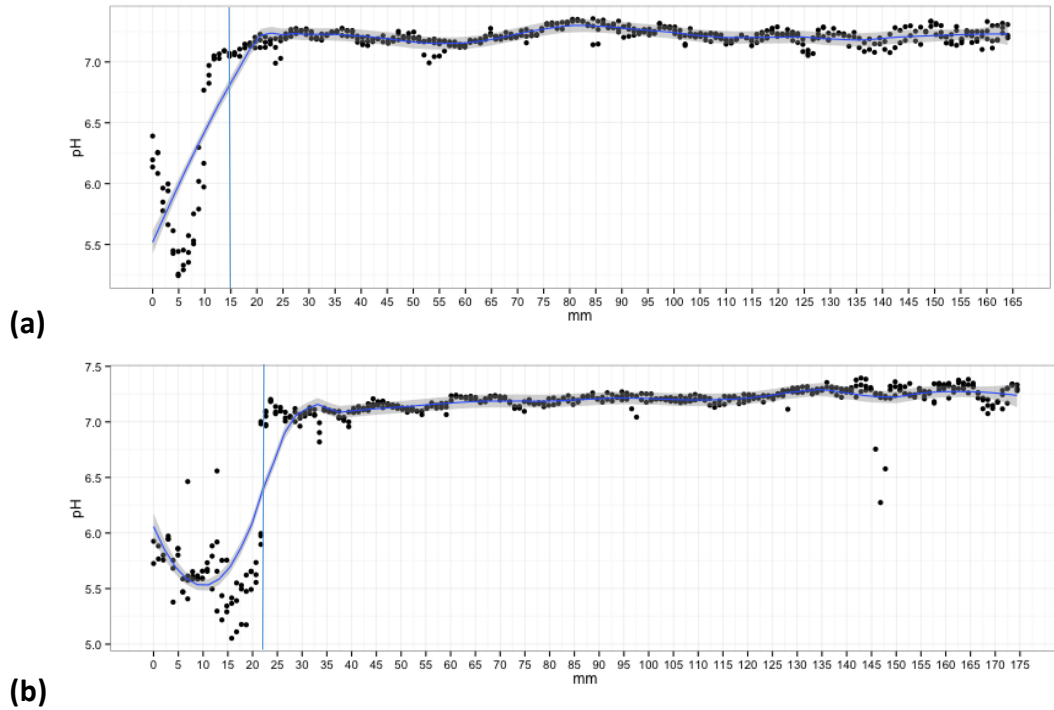


Figure 7.17: Two pH profiles of station spatial 031 taken from the same core using two probes.

In figure 7.17, the profiles from the same core at station spatial 031 are shown. The interface in figure 7.17a was at 15mm and in figure 17.5b was at 22 mm. The pH is about 7.3 in both the profiles with a very slight increase with depth. In this case the duplicate probes showed an almost identical response.

Most of the profiles in the sandy mud looked very different from each other within a core.

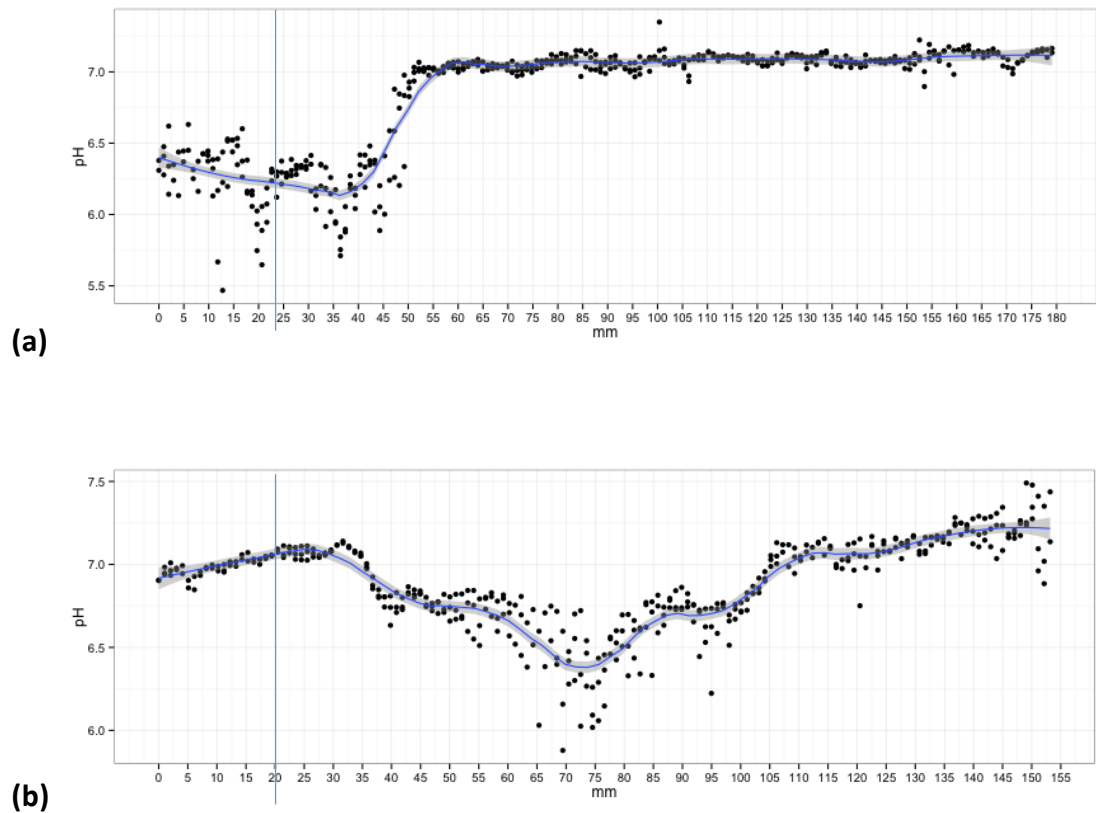


Figure 7.18: Two pH profiles of station spatial 035 taken from the same core using two probes

In figure 7.18a and 7.18b, the profiles from the same core at station spatial035 are shown. In figure 7.18a, the pH in the sediments was 7. The second profile taken from the same core is different. The interface was at 20 mm and the pH dropped to 6.4 as seen in figure 7.18b at 70 mm. It increased to 7.4 at 140 mm. This feature might be caused by some perturbation e.g. a burrow.

Depending on the type of the sediments, the profiles for mud, sand, sandy mud and muddy sand are compared in the same graph in figure 7.19 after averaging the data taken from the sites that had similar type of sediments. No interface was marked for any of the profiles taken from the mud, therefore it has not been averaged so it is difficult to align different probe results. However, a single profile as a representative of mud is given in figure 7.20. A comparison of pH profiles of different types of sediments is given in figure 7.19. An average pH profile for sand is obtained by

averaging the profiles at stations spatial 16, 23, 27, 45, and 49. An average profile of sandy mud is obtained by averaging the profiles at the stations spatial 26, 36 and 37 and an average profile of muddy sand is obtained by averaging the profiles at station Box H, spatial 35, 28 and 31.

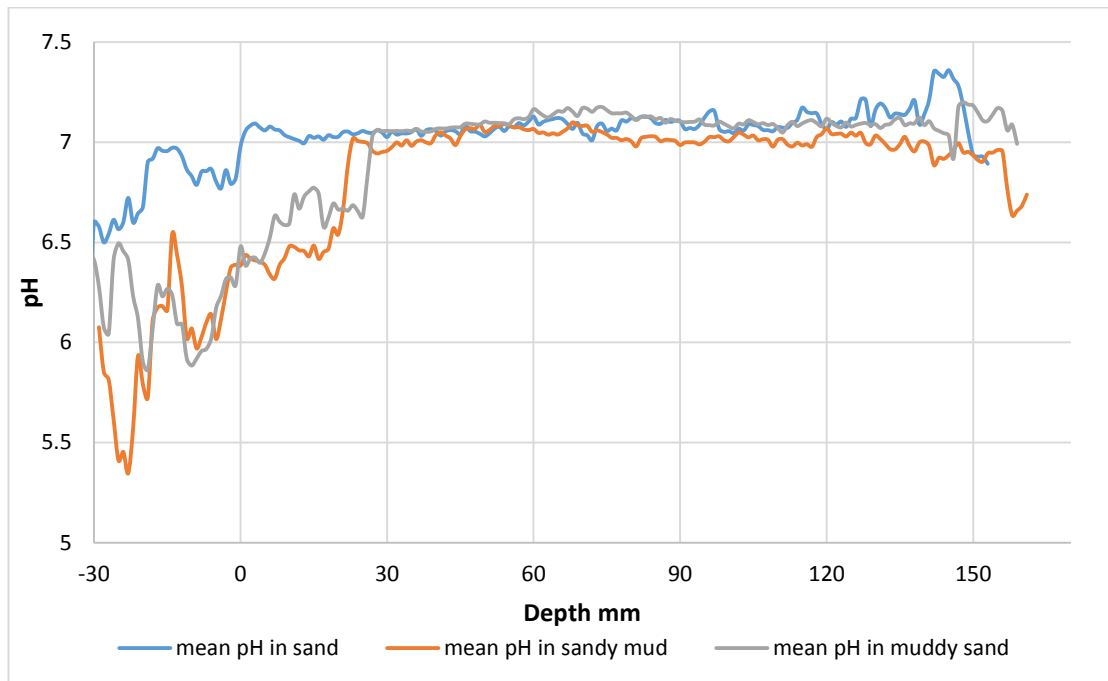


Figure 7.19: Average pH profiles of sand, sandy mud and muddy sand.

The pH in the sand remained almost the same in the depth. In sandy mud, the pH just below the interface (0 mm) was about 6.6 and increased to 7 at 30 mm. The same pattern was observed for muddy sand.

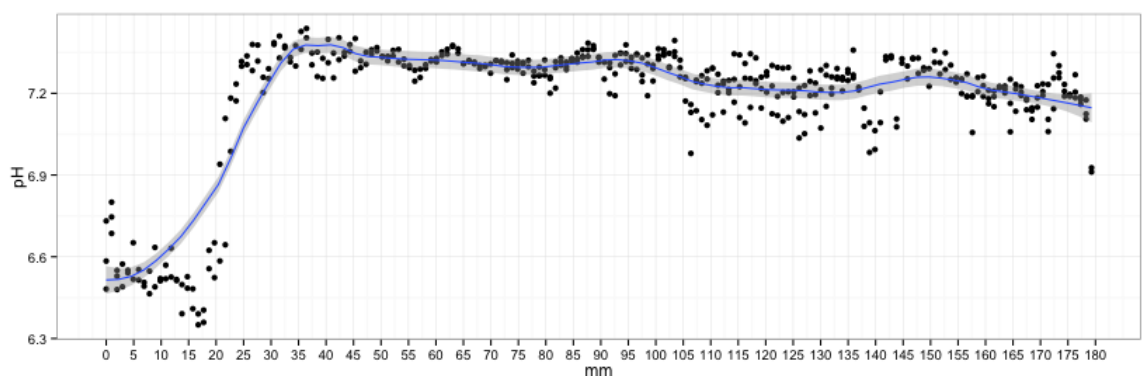


Figure 7.20: pH profile of mud at station spatial 001.

A pH profile of mud is given in figure 7.20. Although the interface was not marked (which is important because at interface, the pH changes), however, in the sediments the pH mostly remained 7.3.

7.3.4 Sediment Profile Imagery (SPI)

The probes were attached to the SPI camera and the probe was photographed every 5 minutes for 15 minutes in the sandy sediments at station Box G. Figure 7.21a represent the apparent pH profiles at 5 minutes intervals and shows the equilibration process of a fresh probe at station Box G (A). The probes require at least 15 minutes to equilibrate. Figure 7.21b represents the equilibrium process of a used probe at station Box G (B). Where Box G (B) was 5 m apart from Box G (A).

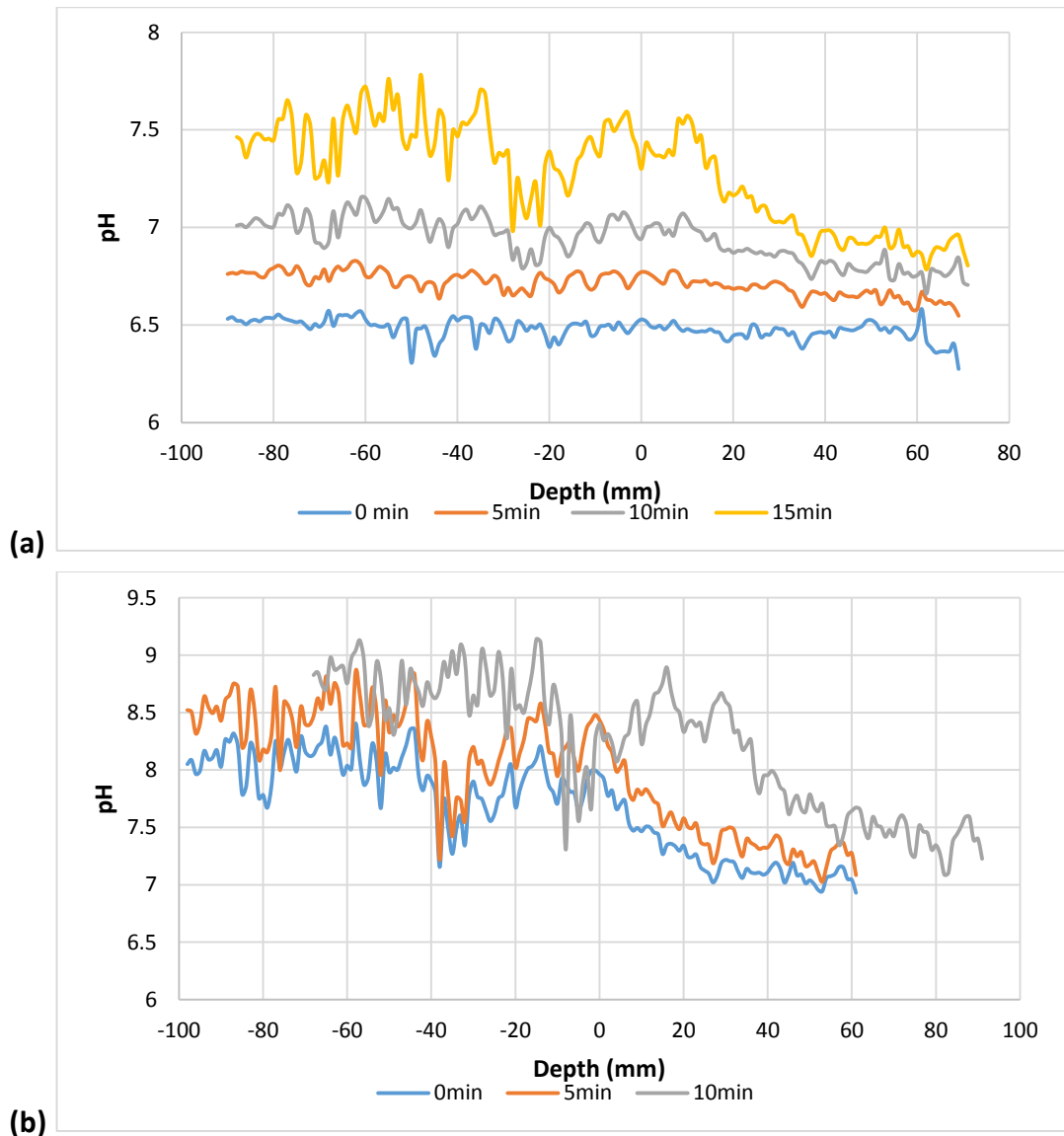


Figure 7.21: Equilibration time series of (a) fresh probe and (b) used probe using SPI.

Since the probe had equilibrated once so at 5 minutes, the probe seems almost equilibrated but at 10 minutes, the position of probe changed (it sank) hence the profile has become displaced by about 30 mm.

pH profiles of different kinds of marine sediments measured using the SPI are shown in figure 7.22.

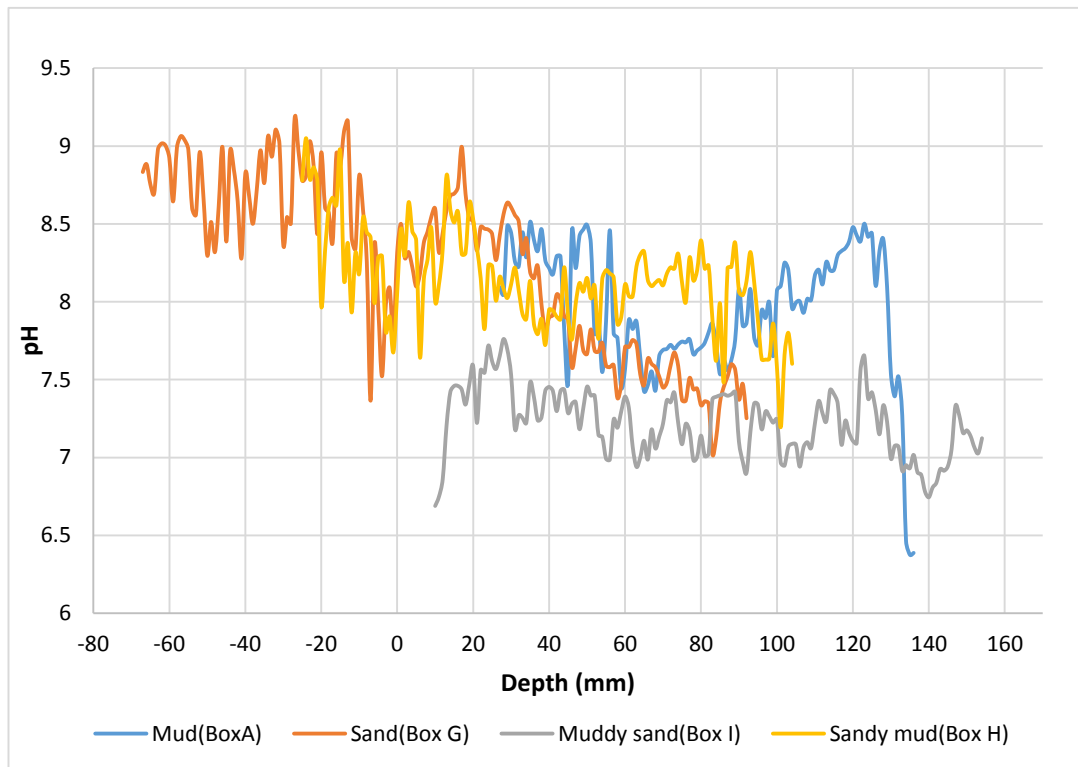


Figure 7.22: pH profiles at different stations using SPI.

In the mud, due to sinking, the interface and water pH could not be measured, however a pH profile from 30 mm to 130 mm is given in figure 7.22. The pH at 30 mm was 8.5 and dropped to 7.5 at 70 mm. It increased again to 8.5 at 123 mm. A similar trend can be seen for the sand at depth. The pH in the water was about 8.6 when the profile for sand was taken. An interesting profile for sandy mud and muddy sand can be seen in figure 7.22. In sandy mud, the pH at the interface dropped to 8.2 from 8.6 at 2 mm depth. At 15 mm depth, it increased to 8.5 again and dropped to 8.0 at 30 mm and remained more or less the same in the depth. In the muddy sand pH as low as 6.6 at 11 mm was measured. It increased to 7.4 at 30 mm and on average remained the same in the depth.

If the profiles measured in the sediment cores in figure 7.19 are compared with the *in situ* profiles measured using SPI in figure 7.22, in the mud, the sediment core profile is more reliable than the profile measured by SPI due to the sinking problem. In the sand, and sandy mud, higher pH was measured by SPI probes than measured in the sediment

cores by normal probes. The profiles of muddy sand were very similar measured by both SPI (*in situ*) and in the sediment cores.

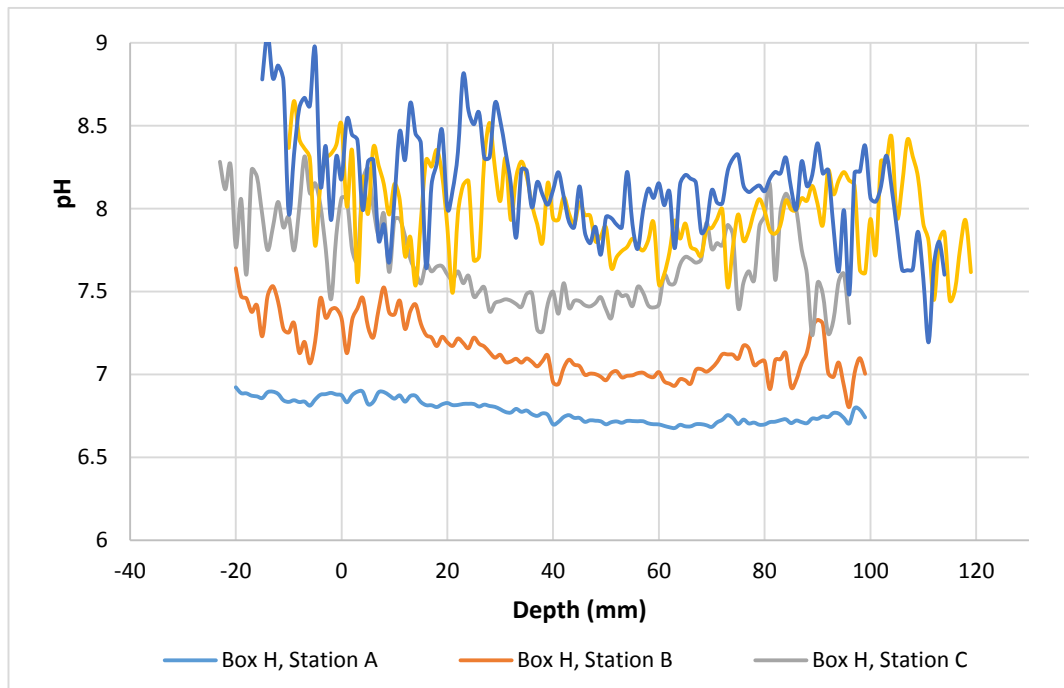


Figure 7.23: pH profiles at the same station where station B was at 5m distance, C at 10m, D at 15m and E at 20m from A taken by SPI.

In figure 7.23, profiles at the same station but different substations (A to E where B was 5 m apart from A, C was 5 m apart from B and so on) are given. Some variations in the profiles are observed at 5 m spacing. These variations can be real as it was a sandy mud or this could be an equilibration problem caused by sinking. Profiles at station D and E look very similar. However profiles at station A, B and C are quite different.

7.3.5 Issues observed

During the cruise, when the probes were unwrapped, some of them appeared patchy as shown in figure 7.24. Either the dye had bleached or during manufacturing, a non-homogeneous part of the sheet was taken. This was, however, not observed during calibration when the probes were fresh so it is much more likely to be an ageing problem. If probes are kept longer (a month), this problem can be observed. In

previous work (e.g. at Stiffkey) probes were manufactured just before the trips, so this ageing problem was not observed and was much more apparent on the probes used later in the cruise.

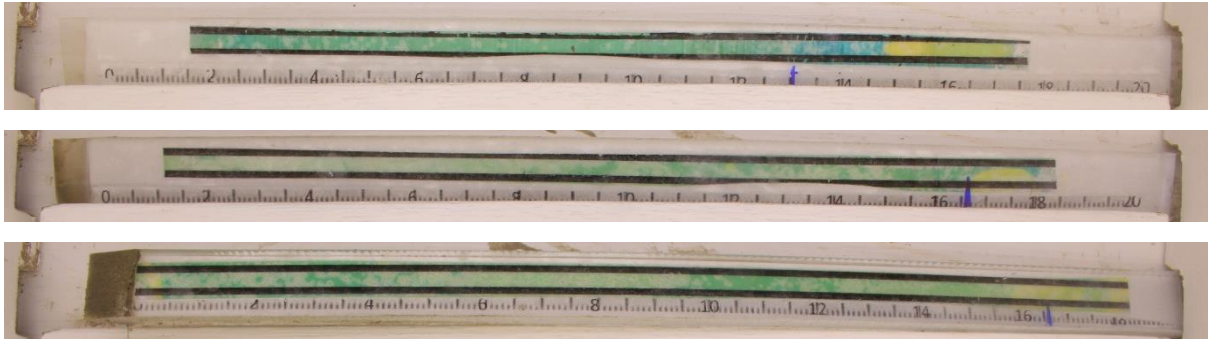


Figure 7.24: Images of the used probes showing the white patches due to aging.

One of the unused probes was observed under the microscope and it appeared that the dye had crystallised in the membrane leaving the surroundings appearing as white patches. This might have occurred due to ageing. However, useful data can still be obtained from the probes because when the photographs were analysed in the software, useful profiles with consistent data points were still obtained from the unaffected regions of the probes.

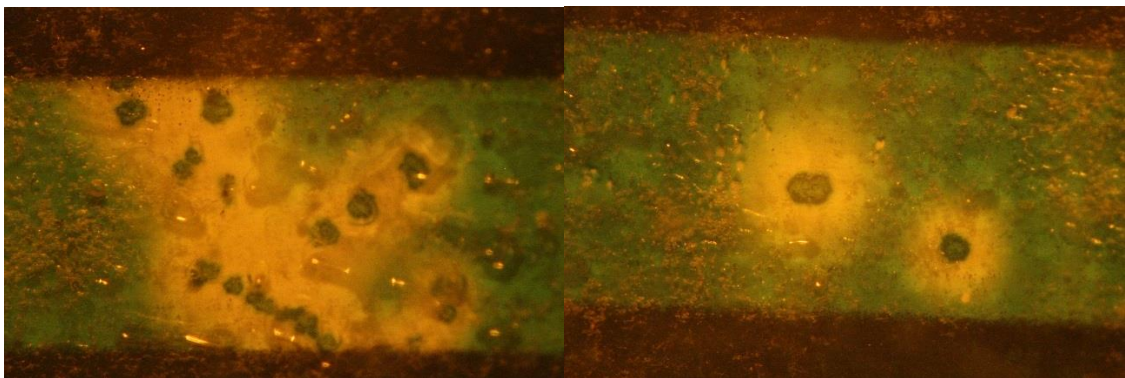


Figure 7.25: A closer view of the probe in the microscope.

Closer observation of the white areas under a binocular microscope (figure 7.25) suggested that the dye crystallised. This could be because of nucleation, e.g. on dust particles. According to the literature, the dye properties depend on the stability of the polymer and the environment around the sensor molecule. The long term instability of sensor can be caused by crystallization, crosslinking, cracking, plasticizer migration

and sensor migration (Geddes and Lakowicz, 2005). The membrane solution was filtered before spreading it on the transparency sheet for the probes made for the next cruise to try to avoid dye crystallisation due to any dust particles.

In the soft mud, the SPI keeps on sinking and makes the profiling slightly complicated. From the results shown in this chapter, however, it is clear that the SPI stays at least for ten minutes in the soft mud at the same position. It appeared that the probes were not inserted tightly enough into the faceplate and that fine mud could penetrate around the back of the probe towards the bottom of the plate. The sensing membrane was not destroyed but the mud covered the front side of the probe which is photographed (figure 7.26). This problem can probably be solved mechanically by cutting the probes to give a tighter fit and clamping with the SPI faceplate firmly so that there is no chance for the mud to drag into the probe. Some modification of the stainless steel frame at the bottom may be required to clamp the strips more tightly and keep good contact to the SPI faceplate to prevent this problem.

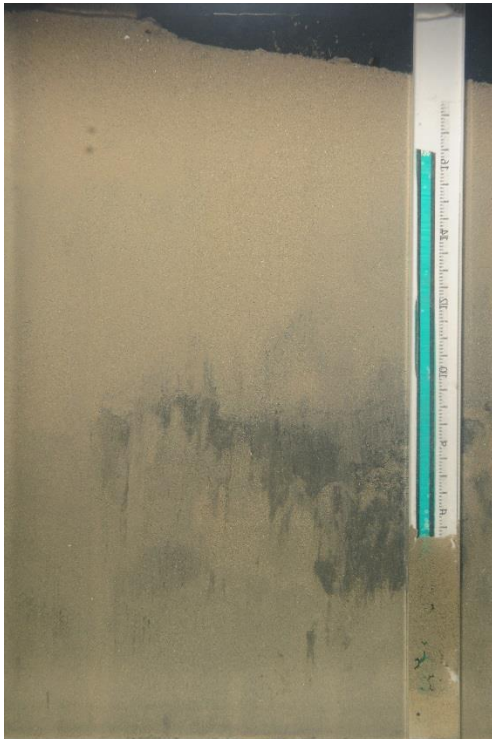


Figure 7.26: SPI-image, showing the mud dragged into the probe slot and hid the probe.

7.4 Conclusions

The probes were successfully used in recovered sediment cores and profiles from different types of sediments have been obtained. The SPI trials have shown that the probes are robust and can survive multiple insertion without any damage caused to the sensors. Mud entered the probe slot at some sites and hid the probe which can be controlled if the SPI faceplate and probe are attached firmly in future to stop the mud from dragging in the probe slot. Some mechanical engineering can solve the problem.

In the sand and mud, the pH remained at 7 and 7.2 in the depth respectively. In the muddy sand and sandy mud, the pH below the interface dropped to 6.5 and gradually increased until 30 mm where it reached its maximum value of 7 and stayed the same in the depth. The profiles measured using SPI show similar results for muddy sand. In the sand, mud and sandy mud, higher pH was measured by SPI probes than measured in the sediment cores by normal probes. It is not currently clear what might cause this discrepancy. If the probes are kept for longer than a month, some crystallisation of dye occurs, but useful profiles can still be measured.

No attempt has been made here to analyse the profiles obtained in detail or to ascribe any detailed meaning of them in terms of possible sedimentary processes-the focus has rather been on the technical aspects of the measurements themselves. A large number of pH microelectrode profiles were also recorded on the March cruise by Briony Silburn, however, once this data is worked up it is hoped that side by side comparisons of profiles can be made (at least for the top 50-70 mm-the reach of the microelectrodes) to provide some independent validation of the values and trends obtained by the optical probes. Such a study will potentially give much greater confidence to the values determined by the optical method and will pave the way for their routine use on future cruises. Plans are currently being made to send probes on a further cruise in August as part of the ongoing future development of the technology and its embedding into routine monitoring programmes.

7.5 References

Geddes, C. D. & Lakowicz, J.R. (Eds.) (2005). *Reviews in fluorescence*. U.S.A : Springer science+business media Inc. p144.

Stephens, D. & Diesing, M. (submitted) Towards quantitative spatial models of seabed sediment composition. PLoS One.

Stephens, D. 2015 North Sea and UK shelf substrate composition predictions, with links to GeoTIFFs. *Centre for Environment, Fisheries and Aquaculture Science* doi:10.1594/PANGAEA.84546.

Chapter 8

Summary and future work

8.1 Summary

A PVC based plasticised pH sensor has been successfully developed for use in marine sediments by immobilising bromothymol blue. The sensor has a response range from about 5.5 to 8.5 and is ideal for application in the marine environment. The sensor responds in 15 minutes. The dye does not leach. The sensor is robust and can be used in harsh environments where other pH sensors like pH microelectrodes and macro electrodes break. The technique includes photographing the sensor's response using a light box that contains LED lights that give consistent light on the shelf where the probe rests and is photographed. The position of the camera on the light box is fixed and the movement is controlled to avoid any variations that usually occur due to camera positioning, position of probe and lighting inconsistency. The photographs obtained can be analysed using an automated R script, specially developed for getting the pH profiles from the photographs of the sensors, to get the pH vs depth profiles of the sediments using the equation obtained from calibration. The technique is very easy and the light box is portable. The sensor has been successfully calibrated in the lab using seawater. An *in situ* calibration using the SPI system has been successfully carried out for application of the sensor in combination with the SPI system. The sensor has been applied to record the seasonal pH profiles from Stiffkey salt marshes Norfolk. The profiles show an interesting seasonal change. The sensor has also been applied in recovered sediment cores during different cruises and a large amount of information has been obtained. Successful SPI trials have been made.

In Chapter 1, an overall introduction to the work and important concepts were discussed. The presently used techniques, their drawbacks and a relevant literature review were presented to form the basis of the project and explain the need for development of this robust optical sensor. The importance of pH of marine sediments and its relevance to the key processes occurring in the marine sediments (early diagenesis) was discussed in some detail based on the published literature.

In chapter 2, the work included the selection of suitable dyes and their spectral properties. The first attempt at immobilising the dyes in a cellulose acetate membrane was made. The dye was successfully immobilised by making a solution of dye in THF that contained cellulose acetate as a polymer, a counter ion, a plasticizer and a wetting agent. The solution was spread on a transparency sheet and after it dried, the sheet was cut into pieces. The time scans showed that the sensor needed to be optimised for fast reversibility and for controlling the leaching of the dye. ImageJ was used to take the RGB values from the photographs and the values were plotted against the pH.

In chapter 3, the focus of the work was to optimise the sensor. Different ratios of the components of the membrane solutions were tried to optimise the response of the BTB and neutral red sensing membranes. Cellulose acetate was replaced by PVC which solved the problem of leaching of dye, and decreased the response time. However it also introduced a problem of pK_a shift of bromothymol blue. The dye was changed to cresol red and cresol purple. Initial trials in salt water showed that the pK_a again shifted back to the original value, therefore bromothymol blue was chosen as a final dye to be used in the marine environment in this work where the presence of salt can maintain the pK_a value of the dye. However, for other applications, cresol red and cresol purple based sensors, developed and discussed in this chapter, can be used. These dyes, after being immobilised, had a pK_a value of about 7 and would be suitable for low-salt environment. They responded fast, were reversible and the dye did not leach out. The BTB sensors responded in 100 seconds after being conditioned once.

Chapter 4 discussed the development of a sediment probe from the sensing membrane and the characteristics of the sensor. The thickness of the sensor was controlled by using metering bars. A sediment probe was developed by sticking the membrane on a plastic stick using double-sided sticky tape. Different white membranes were tried and nytran membranes were finally chosen as a background to stop any colour interferences from the sediment colour. A scale was added next to the sensor for better pH profiling. Photographic conditions were improved by developing a light box and the lighting consistency was ensured. Response time with a nytran membrane measured by photographing the change was 15 minutes. The sensor

composition was changed by increasing the amount of dye and counter ion to get clearer colours in the photographs and decreasing the thickness of the membrane to keep the response fast. The effect of temperature, salt and light on the sensor was studied. The sensor bleached in sunlight. There was a small effect of salt and temperature on the sensor. It was concluded that the sensors should be kept dry and kept in the dark by wrapping them in kitchen foil after manufacturing them. The effect of salt and temperature can be reduced by calibrating the sensors in a water sample taken from the site and at a temperature similar to the site where they are deployed. The salinity of seawater does not change a lot except in estuaries where differences in salinity may affect the response of the sensor. Cresol red or cresol purple based sensors discussed in chapter 3 may be used at such sites but responses would need to be corrected for salinity (measured independently in some way). However in this work, the effect of temperature and salt on these sensing membranes was not studied.

In chapter 5, different methods were used to calibrate the sensors such as

1. Calibrating using phosphate buffers.
2. Solidifying the phosphate buffers in agarose gel and using the gels to calibrate the probes and
3. Using seawater for calibration by bubbling nitrogen and carbon dioxide gas into it to adjust the pH. This approach proved to be effective and reproducible for application in the marine environment and was chosen as an effective method to calibrate sensors for marine application.

The sensors were tried in sediment cores during a cruise for the first time using preliminary photographic conditions which included a polystyrene dark box with a hole on the lid where the camera lens was adjusted to photograph the probe. An external flash was kept in the box. The profiles obtained from the first trial and their comparison with the microelectrode results showed that they were very different from the profiles measured using the microelectrodes. The profiles were measured by a colleague Alida Rosales during this cruise. This difference was due to bad photographic conditions where the settings of the camera were different from the camera settings used during the calibration. The temperature and salinity was not considered during

the calibration. The camera moved each time the lid was taken off from the dark box to put the probe in. The external flash was operated by batteries that after being used for some time did not produce a consistent light in the box. The analysis of photographs was automated in collaboration with Cefas by David Stephens who created an R script for a quick analysis of the photographic data.

In chapter 6, better calibration and photographic conditions were established, which made better and reliable pH profiling possible. A seasonal change in pH profiles of pond, creek and under the vegetation was measured at Stiffkey salt marsh. The results showed that the overall pH in the sediments gradually increased from summer to winter. The experiments showed that the probes could be used multiple times and the equilibration time in soft mud was 30 minutes. The response is faster in hard sediments where the contact between the sediments and the sensing probes is better. Some long probes were manufactured and the profiles were measured which illustrated that longer probes could be manufactured if required for profiling to greater depths.

Chapter 7 included the results from various cruises in collaboration with Cefas. The sensors were tried by Cefas (Claire Powell and Briony Silburn) in recovered sediment cores along with the pH microelectrodes during three different cruises. The pH profiles measured by Cefas during the March cruise are the biggest ever data collected till date. The sensors were adapted for attaching them to the SPI faceplate. The photographs obtained from Cefas were analysed to get the pH profiles. The results showed that the sensors were robust and could be used in combination with the SPI for pH profiling. This is the first time that the SPI has been used in combination with optical pH sensors during the cruise to measure *in-situ* pH profiles at four different sites at the water depths greater than 100 m. In soft mud, the SPI keeps on sinking and thus does not allow the sensor to equilibrate, however, in hard sediments, some interesting information has been obtained. Some of the sensors, when used after a month, showed crystallisation of the dye in the membrane which can be an ageing problem. However, this was never observed before when the sensors were manufactured shortly before use.

8.2 Future work

Future work should include a better and faster manufacturing technique for pH sensors that may include fast spreading of the solution on the transparency sheets using machinery (e.g. inkjet printing). The ageing problem of the probes can be studied to investigate what causes the dye to crystallise and how it could be controlled. This may necessitate further optimisation of the membrane composition and adjustments to the nature and amounts of counter-ion and plasticizer. The successful development of a robust optical pH sensor and its successful application in the marine environment provides a basis for development of optical sensors for other parameters such as redox or free iron. Initial trials were made to develop a redox sensor. The same technique was used to immobilise methylene blue in a PVC membrane. However, the dye could not be immobilised effectively in this way. Future work should include attempts to immobilise a redox dye effectively and still allow it to respond to the redox potential. Several dyes with different potentials might be needed side by side to cover the required potential range.

A possible future work could be the detection and quantification of iron using a colourimetric method based on the photographic technique. Iron in a blood serum, wine and water has been previously detected optically and quantified using a photographic technique by Vallejos *et al.* A film like sensing membrane was obtained by transforming an organic iron chelator into an acrylic monomer and copolymerising it with hydrophilic co-monomers. The film was cut and immersed into the samples, where iron (Fe^{2+} and Fe^{3+}) was detected by a colour change. The film Images were used to quantify iron. (Vallejos *et al.*, 2013). This can be a starting point to detect and quantify iron in marine sediments and would form an interesting extension of the strategies developed in this work for pH sensing.

8.3 References

Vallejos, S., Muñoz, A., Ibeas, S., Serna, F., García, F. C. & Garcia, M. 2013 Solid sensory polymer substrate for the quantification of iron in blood, wine and water by scalable RGB technique. *Journals of Material Chemistry* **1**, 15435-15441.